Phosphorylation of the PTCH1 C-terminal domain: profiling and significance

Felix Charles Cross

Submitted in accordance with the requirements for the degree of Doctor of Philosophy

The University of Leeds

School of Molecular and Cellular Biology

Faculty of Biological Sciences

The candidate confirms that the work submitted is his own and that appropriate credit has been given where reference has been made to the work of others.

Acknowledgements

Firstly, and most importantly I would like to thank my supervisor Dr Natalia Riobo-Del Galdo for all her support and guidance over the last 4 years, for allowing me to work in such a welcoming and helpful environment, and for making my PhD experience an enjoyable one. I extend my appreciation to my co-supervisor Professor Richard Bayliss for his support and for allowing me to explore another facet of biology.

I would especially like to thank Dr Matthew Batchelor for all his knowledge and guidance with my NMR work, especially during my final year. I will forever be grateful for all the time you have sacrificed for me.

I would like to thank Hattie, Danai, and Esther for making the lab such an enjoyable place to be, and for making my whole PhD experience so much more entertaining. I will miss you all so much and I can't thank you enough for your, love and support.

Thanks also to my friends Kane, Meg C, Meg F, Scott, Claire, Fay and Julia. I couldn't have wished for a better group of people to share my PhD journey with and I'm so glad we've all made it!

Thank you to my family for their support and encouragement, I always know you have belief in me in everything that I do, and that has been so important to me throughout my PhD, so, thank you.

Finally, I would like to thank my girlfriend, Abbie, for her patience with me whilst I've been writing this thesis. I'm glad we will finally have our evenings back! Thank you for always being there for me during the frustrating times and for always believing in me.

Abstract

The Hedgehog (HH) signalling pathway is a well-established signalling cascade, and aberrant activity of the pathway is associated with the development of many cancer types. Much of the pathway hyperactivity stems from mutations within the primary HH receptor protein, PTCH1, a transmembrane protein with a long cytoplasmic C-terminal domain (CTD). Within the CTD are several proline-rich motifs, and within the first one is a TPSP motif which is a hotspot site for mutation within various cancers. The TPSP motif is the primary focus of this thesis, in Chapter 1, I show the changing phosphorylation states of the TPSP motif between wild-type (WT) and disease-associated mutants by mass spectrometry. In Chapter 4, I investigate the structure of the proximal region of the PTCH1 CTD by nuclear magnetic resonance, confirming its intrinsically disordered nature and single phosphorylation of T1195 in the TPSP motif by in vitro phosphorylation assays with a S/T-P directed kinase, ERK2. In Chapter 5, I investigate the functional role of the TPSP motif, showing that mutations within the TPSP motif increase the levels of phosphorylated ERK1/2 and increased cell proliferation compared to PTCH1, indicating that the TPSP motif regulates Erk1/2 phosphorylation, which could explain the role of TPSP mutations in cancer.

In Chapter 6, I describe a novel interaction between PTCH proteins and the peptidyl prolyl isomerase Pin1. The findings point towards a complex interaction which requires multiple binding sites within each PTCH protein but do not confirm a role of the TPSP motif in the interaction. In Chapter 7, I describe my contribution to a side project that demonstrated the ability of PTCH1 and PTCH2 to form heterodimers. In this project I demonstrated that heterodimers are equally responsive to rSHH than homodimers of PTCH1 or PTCH2, and that the

difference in activity observed between PTCH1 and PTCH2 is not due to the lack of conservation of the CTD.

In summary, this thesis improves the understanding of the structure and functionality of the first proline-rich motif of the PTCH1 CTD and uncovers a novel interaction between PTCH proteins and Pin1, adding of the complex nature of PTCH1.

Table of Contents

List of Figures

List of Tables

List of Abbreviations

ATG	Autophagy related protein
ATP	Adenosine triphosphate
BCC	Basal cell carcinoma
BSCC	basal squamous cell carcinoma
BCS	Bovine calf serum
cAMP	Cyclic adenosine monophosphate
CD	Circular dichroism
CK2	Casein kinase 2
CNS	Central nervous system
Co-IP	Co-immunoprecipitation
CRD	Cysteine-rich domain
Cryo-EM	Cryo-electron microscopy
CTD	C-terminal domain
DHH	Desert hedgehog
DISP1	Dispatched
DMEM	Dulbecco’s modified eagle medium
DMSO	Dimethyl sulfoxide
DNA	Deoxyribose nucleic acid
eGFP	Enhance green fluorescent protein
EM	Electron microscopy
FBS	Foetal bovine serum
FRAP	Fluorescence recovery after photobleaching
Fu	Fused
GAPDH	Glyceraldehyde-3-phosphate dehydrogenase

GLI	Glioma-associated oncogene
GPCR	G protein-coupled receptor
GSK-3β	Glycogen synthase kinase 3β
HECT E3	Homologous to E6AP C-terminus E3
HH	Hedgehog
HHAT	Hedgehog acetyl transferase
His	Histidine tag
IFT	Intraflagellar transport
IHH	Indian hedgehog
IP	Immunoprecipitation
KCOT	Keratocystic odontogenic tumour
Kif7	Kinesin family member 7
MCS	Multiple cloning site
MEFs	Mouse embryonic fibroblasts
ML	Middle loop
MS	Mass spectrometry
mL	Millilitres
mM	Milimolar
μL	Microlitre
μM	Micromolar
NBCCS	Nevoid Basal Cell Carcinoma
nL	Nanolitre
nM	Nanomolar
NMR	Nuclear magnetic resonance
NPC1	Neimann-Pick C1
N-SHH	Recombinant N-terminal fragment of SHH

NTD	N-terminal domain
PCR	Polymerase chain reaction
PDK1	Phophoinositide-dependent kinase 1
PKA	Protein kinase A
PMF	Proton motive force
PPIase	Peptidyl prolyl isomerase
PPII	Polyproline II
PRM	Proline-rich motif
Ptc1	Mouse Patched 1
PTCH1	Human Patched 1
PTCH2	Human Patched 2
PTCHD1	Patched domain-containing protein 1
PtdIns(3,4,5)P3	Phosphatidylinositol (3,4,5)-triphosphate
PtdIns(4,5)P2	Phosphatidylinositol 4,5-biphosphate
RLUs	Relative luciferase units
RNA	Ribonucleic acid
RND	Resistance nodulation division
RPM	Revolutions per minute
SAG	Smoothened Agonist
SCC	Squamous cell carcinoma
SCO	Side-chain oxysterol
SDS	Sodium dodecyl sulphate
SDS-PAGE	Sodium dodecyl sulphate polyacrylamide gel electrophoresis
SEC	Size exclusion chromatography
SHH	Sonic hedgehog

Smad3	Mothers against decapentaplegic homolog 3
SMO	Smoothened
SSD	Sterol-sensing domain
STK36	Serine/threonine kinase 36
SuFu	Suppressor of Fused
TGFβ	Transforming growth factor β
TM	Transmembrane
ULK1	Unc-51-like kinase 1
vdW	van der Waal
WCL	Whole cell lysate

Chapter 1

Introduction

Chapter 1

Introduction

1.1 The Canonical Hedgehog Signalling Pathway

1.1.1 Brief Introduction to the Hedgehog Signalling Pathway

The Hedgehog (HH) pathway is a key signalling pathway for central nervous system (CNS) and limb patterning, and limb development during embryogenesis (Briscoe and Therond, 2013; Yang, C. et al., 2021). Moreover, it governs cell maintenance and differentiation in adult organisms (Chapouly et al., 2019).

The HH pathway is a key signalling pathway for the CNS, promoting the formation of the blood-brain barrier which is essential for the regulation of the CNS homeostasis (Alvarez et al., 2011). The HH pathway also plays an important role in mammalian limb development in species such as *Drosophilla melanogaster* (Jiang and Struhl, 1995) and mammals (Chiang et al., 2001). The pathway is essential for neural tube development, regulating the proliferation of precursor cells to maintain a balance of proliferation and differentiation (Yang, C. et al., 2021). The HH pathway has been shown to promote the promote proliferation of adult stem cells from various tissue types (Zhao et al., 2009). An example of this pathway activation in mammalian adults is the activation of the pathway in hair follicles to promote hair growth (Lim et al., 2018).

The pathway operates through receptor-mediated downstream signalling, initiated when a ligand binds to a membrane-bound receptor protein (Pedersen et al., 2016). In the ‘off’ state of the pathway, the receptor protein represses downstream signalling, thereby inhibiting the transcription of target genes (Hanna

and Shevde, 2016). Conversely, ligand binding alleviates this repression in the 'on' state, triggering a signalling cascade that leads to the upregulation of target gene transcription (Rubin and de Sauvage, 2006) (**Figure 1.1**).

1.1.2 Human Hedgehog ligands

The primary function of the HH ligands is to bind to the HH receptor, thereby facilitating the upregulation of gene transcription (Shin et al., 2011). The human genome encodes three HH ligands, namely Sonic HH (SHH), Desert HH (DHH) and Indian HH (IHH) (Hanna and Shevde, 2016) located at positions 7q36, 12q12-q13.1 and 2q35 respectively (Yuksel-Apak et al., 2012; Linhares et al., 2014; Mehta et al., 2021). Among these ligands, SHH exhibits the broadest expression pattern and plays a pivotal role in various developmental processes, including CNS patterning and limb development, as well as numerous other biological functions, whereas DHH is restricted to gonadal development and IHH is mainly restricted to bone and skin development (Cohen, 2010), as well as being the primary HH ligand expressed in the small intestine and colon. Buller et al (2012) found that IHH is responsible for the negative regulation of the size of the intestinal crypt compartment size, negatively regulating stem cells at the base of the crypt. IHH helps to balance crypt growth formation and replacement of damaged epithelial cells (Buller et al., 2012).

1.1.3 GLI transcription factors

There are three isoforms of mammalian GLI proteins: GLI1 functions solely as a transcriptional activator, whereas GLI2 and GLI3 can function as both transcriptional activators and repressors (Hui and Angers, 2011). This dual role is determined by the proteolytic cleavage of GLI2 and GLI3, facilitated by a

protein called Suppressor of Fused (SuFu) (Dunaeva et al., 2003; Humke et al., 2010). GLI proteins remain inactive due to phosphorylation by protein kinase A (PKA), this phosphorylation is lost upon pathway activation (Niewiadomski et al., 2014).

1.1.4 PTCH protein isoforms

There are two isoforms of the PTCH1 receptor: PTCH1 and PTCH2, encoded in different genes at chromosome positions 9q22 and 1p32 respectively. Both of these proteins act as negative regulators of the signalling pathway through the inhibition of the membrane-bound effector protein, Smoothened (SMO) (Skoda et al., 2018). A microdeletion at the 9q22.3 location leads to patients being heterozygous for PTCH1, these patients exhibit the phenotypes associated with Gorlin Syndrome, also known as Nevoid Basal Cell Carcinoma syndrome (NBCCS) (Spadari et al., 2022). In the absence of ligand, PTCH1 and PTCH2 localise to the primary cilium (Liem et al., 2009).

The primary role of PTCH1 is to function as a cholesterol transporter, mobilising cholesterol to the inner lamella of the plasma membrane (Radhakrishnan et al., 2020; Kinnebrew et al., 2021). As a result, this activity leads to the inhibition of the membrane-bound effector protein SMO in the absence of ligand. When SMO is inactive, GLI proteins are retained at the base and tip of the primary cilium, bound to SuFu, Fu, and Kif7, consequently, full-length GLI2 and GLI3 proteins are proteolytically processed into their repressor forms (GLI2R and GLI3R) through partial proteasomal degradation (Pan et al., 2006). Formation of GLI2R and GLI3R requires phosphorylation from one of a collection of kinases including proteins kinase A (PKA), glycogen synthase kinase 3 (GSK3) and casein kinase

1 (CK1) (Tempé et al., 2006). Repressor forms of GLI are translocated to the nucleus, where they block transcription of HH target genes.

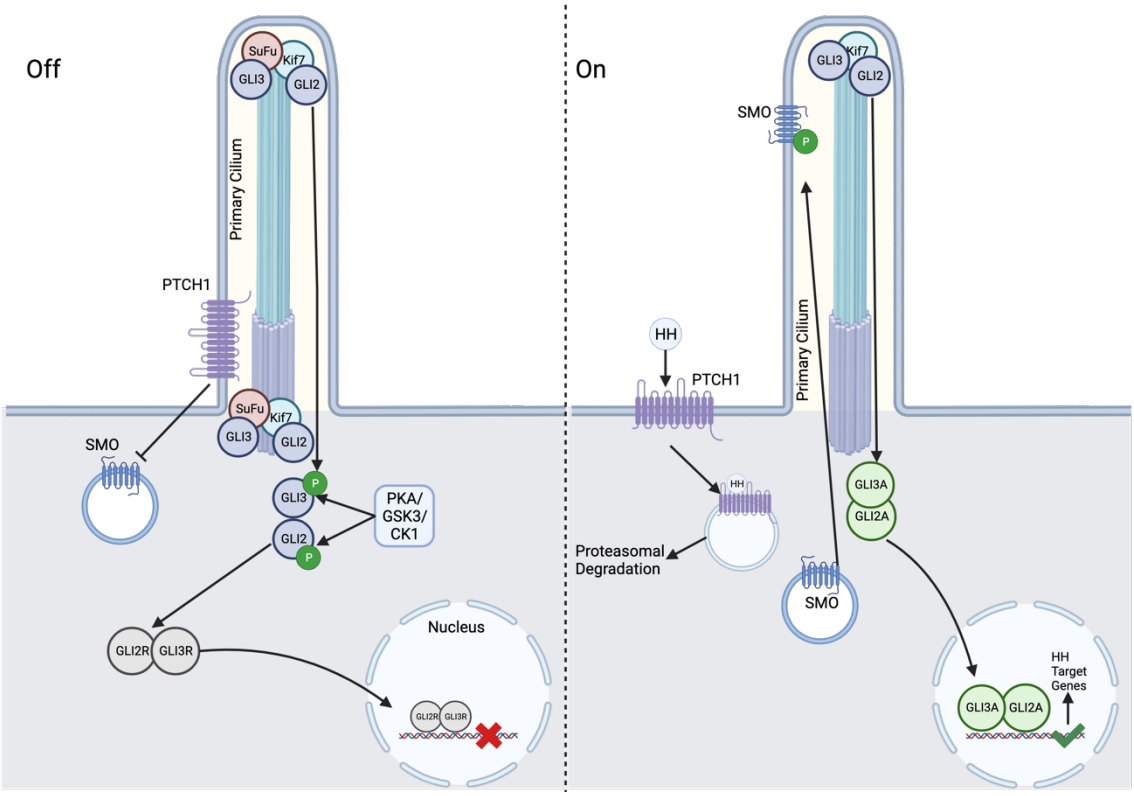

Figure 1. 1 Simplified representation of canonical Hedgehog Signalling

In the absence of any HH ligand, the pathway exists in its off, inactive state. PTCH1 is positioned at the primary cilium where it blocks the activation of SMO. GLI2 and GLI3 proteins are sequestered and held at the base and the tip of the primary cilium by Kif7 and SuFu, after which they are phosphorylated by a range of kinases including PKA, GSK3 and CK1. This is followed by proteolytic processing of the GLI proteins into their repressor forms, GLI2R and GLI3R, after which they translocate to the nucleus and block the activation of target genes.

When HH ligands are present, they bind to PTCH1, causing it to become internalised and degraded, allowing SMO to become activated by cholesterol molecules and migrate to the tip of the primary cilium where it activates GLI2 and GLI3 (forming GLI2A and GLI3A), which can translocate to the nucleus and activate the transcription of HH target genes.

Figure created using BioRender.com

Upon HH ligand binding to PTCH1, the receptor-ligand complex becomes internalised and targeted for degradation through the endolysosomal pathway (Yue et al., 2014). The absence of active PTCH1 causes the local ciliary levels of cholesterol to increase, consequently, activating SMO through cholesterol binding (Luchetti et al., 2016). SMO becomes activated through multiple phosphorylation events by CK1α and G protein-coupled receptor kinase 2 (GRK2), promoting its translocation to the primary cilium (Basler et al., 2011). When at the primary cilium, SMO inhibits the activation of PKA by two mechanisms: inhibiting cAMP production by coupling to Gi proteins and directly binding to the catalytic PKA subunits (Arveseth et al., 2021; Happ et al., 2022), blocking the conversion of GLI2 and GLI3 into their repressor forms, as well as sequestering SuFu. Once SMO is activated, SuFu/GLI2-3 complexes traffic to the ciliary tip, where the full-length GLI proteins are phosphorylated by STK36 and ULK3 to achieve maximal activation (Han et al., 2019). Activated GLI proteins migrate to the nucleus to induce expression of target genes (Humke et al., 2010).

1.1.4 Dysregulation of the Hedgehog Pathway

Dysregulation of the HH pathway has been associated with the development of several cancer types, such dysregulation can stem from mutations within pathway components or changes in their expression profiles (Briscoe and Therond, 2013; Chen, H. et al., 2016).

Many HH functions are mediated by upregulating the transcription of specific genes, including *GLI1, CCND1* and *MYCN* (Mastrangelo and Milani, 2018; Sabol et al., 2018). This transcriptional activation contributes to the promotion of stemness, proliferation, survival, and angiogenesis (Di Mauro et al., 2017). The

downstream effects of HH signalling are complex and context dependent. In general, HH signalling promotes cell survival, proliferation, and differentiation, while concurrently inhibiting apoptosis (Pasca di Magliano and Hebrok, 2003; Jenkins, 2009). Moreover, it regulates essential cellular processes such as cell migration, adhesion, and the secretion of extracellular matrix components (Alman, 2015; Hanna and Shevde, 2016). Loss of function of PTCH1 during embryogenesis results in premature death as the embryo cannot survive the gestation period and exhibits exencephaly, open neural tube and cardiac arrest (Holtz et al., 2013). Loss of function of PTCH1 during adulthood is associated with the development of diseases. Contrary to this, PTCH2 is non-essential for development and primarily serves to support the function of PTCH1 (Nieuwenhuis et al., 2006).

1.1.5 Smoothened

SMO is a 7 transmembrane (7TM) domain protein belonging to the GPCR superfamily that contains an extracellular cysteine-rich N-terminal domain (CRD), a linker domain, an α-helical bundle and a long intracellular CTD (Byrne et al., 2016). Smoothened activity is regulated by the presence of cholesterol, the availability of which is regulated by PTCH1 (Luchetti et al., 2016). The role of PTCH1 causes free cholesterol levels to reduce in the outer lamella of the plasma membrane, therefore, PTCH1 can influence SMO activity by reducing the cholesterol levels available for SMO activation (Zhong and Wang, 2022). Within SMO there are two sterol ligand binding motifs, one of these sits in a cavity generated by the structure of the SMO transmembrane domains and the other sits within the CRD. Both oxysterols and cholesterols can bind to the CRD which leads to SMO activation (Radhakrishnan et al., 2020) Agonists such as

Smoothened agonist (SAG) have the capacity to bind to the cavity within the 7TM domains (Radhakrishnan et al., 2020). Notably, mutations within the 7TM cavity appear to have minimal impact on the canonical HH signalling pathway (Radhakrishnan et al., 2020).

Activation of SMO by sterols triggers a conformational shift that, when blocked by negative regulators, is locked and unable to occur. Binding of SHH to PTCH1, elevates the local levels of cholesterol at the primary cilium, increasing the activation of SMO (Radhakrishnan et al., 2020). Inhibitors that target cholesterol synthesis have been linked with an increase in the incidence of holoprosencephaly which is similar to what is seen in disorders associated with a deficiency in HH ligands (Radhakrishnan et al., 2020). Side-chain oxysterols (SCOs) are derivatives of cholesterol, marked by the presence of oxygenated functional groups such as hydroxyl or epoxy groups (Radhakrishnan et al., 2020). These components have a major impact on the activation of HH signalling and the stimulation of SMO activity at the primary cilia (Radhakrishnan et al., 2020). Importantly, a reduction in oxysterol biosynthesis has not been associated with developmental diseases that are linked to decreases in HH ligand levels.

1.1.6 Hedgehog Ligand Processing

HH ligands undergo several different types of proteolytic processing. To begin with, a 46 kDa protein is produced in the endoplasmic reticulum that contains an N-terminal signalling domain and a C-terminal auto-processing domain (Ramsbottom and Pownall, 2016). Immediately post-translation, the precursor HH ligands are cleaved into N and C-terminal fragments by an autoproteolytic reaction that involves addition of cholesterol to the newly formed C-terminus of

the N-fragment (Porter et al., 1996). The HH-N fragment is further processed with the addition of a palmitate molecule at the N-terminal domain by HH acetyl transferase (HHAT) (Buglino and Resh, 2008). Meanwhile, the HH-C fragment is degraded (Yang, J. et al., 2015) (**Figure 1.2**). The processed active ligand (palmitoyl, cholesteroyl-N-HH, abbreviated throughout the results chapter as "SHH") is release from the producing cell by the transporter function of Dispatched (Disp1) (Hall et al., 2019). Disp1 contains an SSD that is thought to accommodate the cholesterol modification of SHH to aid its release from the membrane (Stewart et al., 2018).

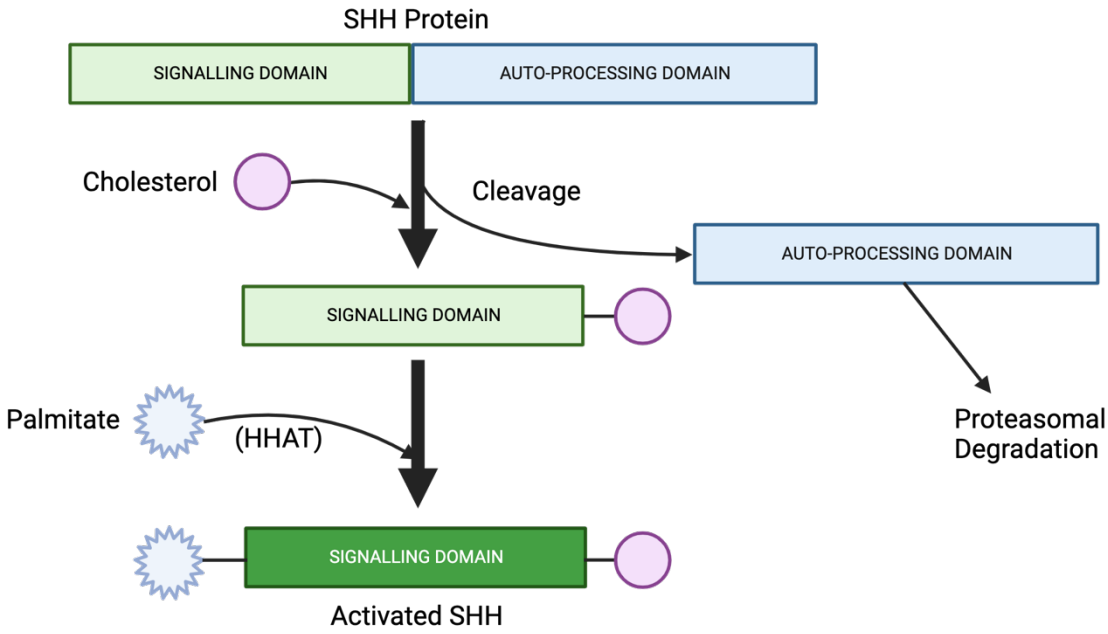

Figure 1. 2 Sonic HH ligand processing

Figure depicting the cleavage of the SHH protein, followed by the addition of palmitate and cholesterol molecules to the N- and C-terminals respectively, forming a dually-lipidated, active SHH protein. The palmitate molecule is added by HH acetyl transferase (HHAT).

Figure created using BioRender.com

1.2 The Primary Cilium

1.2.1 Introduction to the Primary Cilium

The primary cilium is a long, thin sensory organelle which is present in most cell types (Hoey et al., 2012), with one primary cilium per cell (Wheway et al., 2018). Their presence fluctuates throughout the cell cycle, with the assembly of the primary cilium, known as ciliogenesis taking place between the G0 and G1 phases of the cell cycle (Plotnikova et al., 2009), and disassembly of the cilium occuring before mitosis (Plotnikova et al., 2009). After mitosis, each cell inherits a pair of centrioles which migrate to opposite poles of the cell, after which, ciliogenesis can take place again from the mother centriole. The main role of the primary cilium is to sense extracellular signals and regulate intracellular signal transduction cascades, they can detect slight chemical changes in their local environment (Christensen et al., 2007; Kiprilov et al., 2008).

1.2.2 Structure of the Primary Cilium

The main body of the primary cilium, known as the anexome, consists of a bundle of microtubules arranged in a 9 + 0 arrangement, whereby the microtubules are arranged in 9 microtubule doublets (Hoey et al., 2012). This is different to a 9 + 2 arrangement of microtubules in motile cilia, where the microtubules link with protein spokes to provide movement to the cilium (Kiesel et al., 2020). The anexome is anchored to the base of the primary cilium by the basal body (Brown and Zhang, 2020). The cilium basal body is located in the ciliary pocket and consists of 9 triplet groups of gamma-tubulin (Fry et al., 2014). Transition fibres connect the microtubules to the cilium membrane and help to anchor the microtubules in place (Fry et al., 2014). The primary cilium is not involved in cellular motility and therefore is instead involved in sensing chemical changes

within the local environment (Bodle et al., 2013). Within the primary cilium is a transport mechanism known as the intraflagellar transport (IFT) system, the role of the IFT is to regulate transport along the anexome (Qin et al., 2004). The IFT consists of two protein complexes: IFT-A and -B which are responsible for transporting cellular cargo in opposite directions. Both complexes are essential for IFT function (Wang, W. et al., 2021) and they help to regulate cilium length (Wang, W. et al., 2021). Fu et al. found that knocking out the IFT-A subunit *IFT121/WDR35* in mammalian cells showed that Wdr35 regulates the assembly of the cilium through the selective transport of distinct cargoes, as well as highlighting its importance in the integration of membrane proteins into primary cilium (Fu et al., 2016).

1.2.3 HH and the Primary Cilium

The primary cilium plays an essential role in the correct functioning of HH signalling (Bangs and Anderson, 2017). In the off state of the pathway, PTCH1 sits in the membrane at the base of the cilia, blocking the accumulation of SMO in the ciliary membrane (Ho and Stearns, 2021). Incorrect incorporation of PTCH1 at the ciliary membrane leads to aberrant activation of the HH pathway (Kim et al., 2015). In the absence of ligand, GLI2 and 3 are sequestered in the basal body bound to SuFu, where PKA**,** GSK3 and CK2 phosphorylate GLI2/3 proteins, leading to their proteasomal processing into repressors (He et al., 2014).

In the presence of ligand, PTCH1 bound to HH ligand gets internalised and targeted for degradation (Petrov et al., 2021). Consequently, SMO is able to translocate to the primary cilium, decreasing the activity of PKA through the coupling of SMO to Gi proteins and the removal of Gpr161 (Hwang et al., 2021).

A reduction in the activity of PKA leads to a reduced level of GLI2/3 phosphorylation, therefore reducing the proteolytic processing that GLI2 and 3 undergo, leaving full length forms of both transcription factors (Li, J. et al., 2017). Furthermore, Sufu-GLI2/3 complexes traffic to the ciliary tip, where they are phosphorylated by other kinases (ULK3 and STK36) to become fully activated transcription factors (Han et al., 2019). The presence of phosphorylated, active SMO in the cilium causes SuFu to dissociate from the GLI proteins, allowing them to translocate into the nucleus to upregulate gene transcription (Cai et al., 2022).

1.3 PTCH Proteins

1.3.1 PTCH1

1.3.1.1 PTCH1 structure

The human *Ptch1* gene comprises 23 exons that encode a large 160 kDa protein consisting of 1447 amino acids (Zhang, T. et al., 2011), alternative splicing generates three common isoforms: PTCH1-L, PTCH1-M and PTCH1-S. PTCH1-L contains a N-terminal domain sequence that is not present in either PTCH1-M or PTCH1-S, with PTCH1-S and PTCH1-M translation beginning in the first exon whereas PTCH1-S translation begins in the second exon, causing PTCH1-S to lack the PTCH1-L N terminus and the first transmembrane domain (Zhou et al., 2019). PTCH1-L is an integral membrane protein, featuring 12 transmembrane domains (12-TM), including a sterol-sensing domain (SSD) in TM4-6 (Qi, C. et al., 2019) (**Figure 1.3A**). It possesses cytosolic N- and C-termini as well as two large extracellular loops (Yu, F.Y. et al., 2014). These loops are key to the binding of HH ligands. Mutants lacking loop 2 act as dominant negative forms because they are unable to bind any HH ligands, resulting in the loss of ability to activate the HH pathway (Marigo et al., 1996; Briscoe et al., 2001). Furthermore, mutants

lacking loop 2 also exhibit increased repression on SMO, blocking its movement and subsequent activation of the GLI transcription factors (Marigo et al., 1996; Peart et al., 2002).

Evidence suggests that the structure of PTCH1 is evolutionary related to bacterial Resistance-Nodulation-Division (RND) proteins, which are involved in the transport of molecules across the cell membrane (Zhang, Y. et al., 2018). The structural similarity occurs within the transmembrane domain region of PTCH1 that contains a triad of charged residues (D499, E1018 and T1119) that play a critical role both in PTCH1 and RND proteins function. The triad facilitates conformational changes in PTCH1 upon ligand binding (Myers et al., 2017).

One similarity with RND proteins that has been hypothesised is the utilisation of an electrochemical gradient to facilitate molecular transport through PTCH1 across the membrane. To investigate the significance of each residue in the triad, Zhang et al. (2018) (Zhang, Y. et al., 2018) conducted a mutagenesis study in which each acidic residue was mutated to a neutral polar residue (D499N, D500N, E1091Q). The mutants were introduced into *Ptch1*$^{-/-}$ cells, and the canonical HH pathway activity was measured. Their results showed that these mutations hindered the function of PTCH1, showing no discernible repression on SMO. This study highlighted the importance of the triad and the associated conformational changes for the proper function of PTCH1.

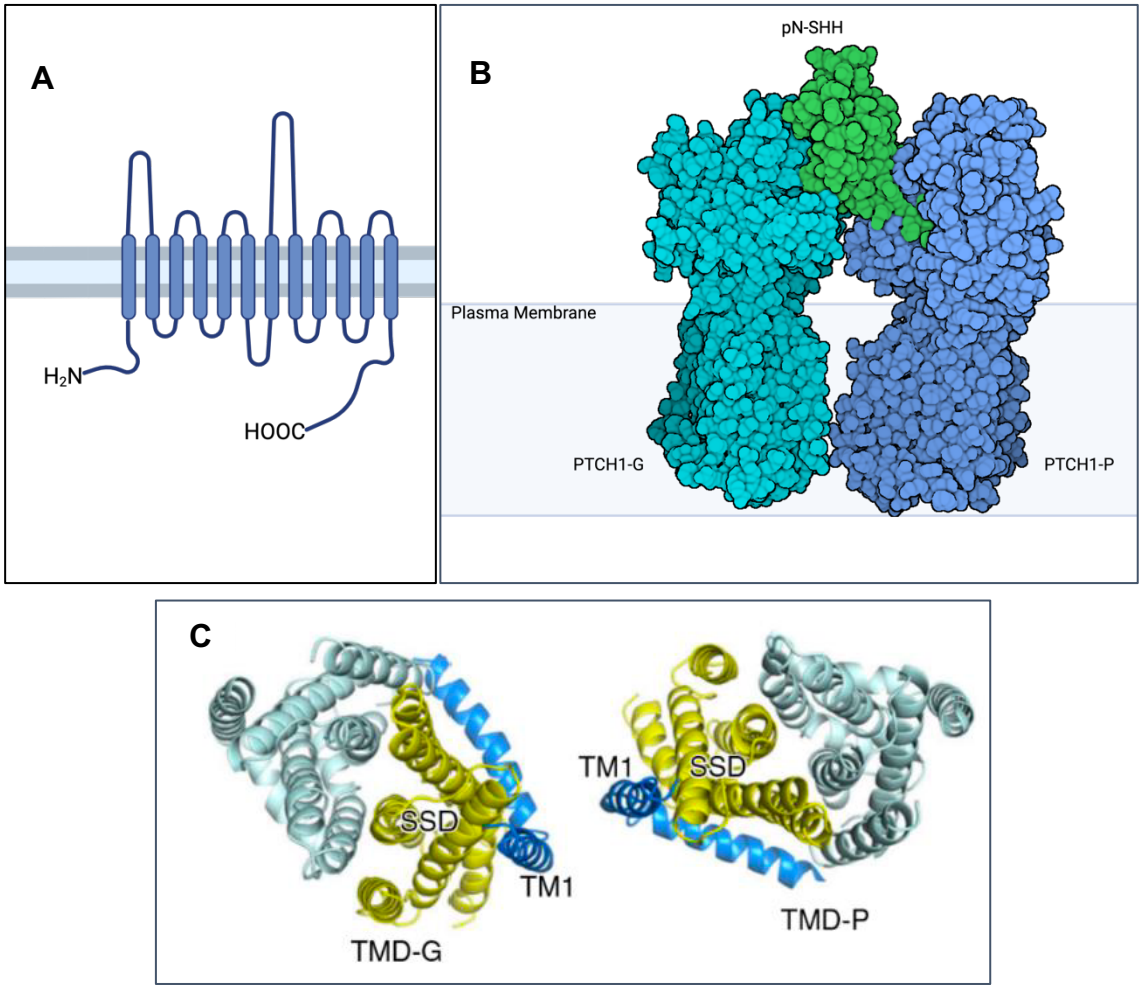

Figure 1. 3 Structure of PTCH1

(A) Simple representation of PTCH1 with its 12 transmembrane domains and its cytoplasmic domains. Figure created using BioRender.com.

(B) Cryo-EM structure of the pseudo-heterodimeric PTCH1 in complex with pN-SHH in the 2:1 ratio. PTCH1-G is the PTCH1 monomer that binds the globular domain of pN-SHH and PTCH1-P marks monomer that interacts with its palmitoyl group. Both proteins are shown without the extended cytoplasmic domains. PDB: 6E1H. Figure created using BioRender.com.

(C) Topology of the transmembrane domains of each PTCH1 protein from top down. TMD-G and TMD-P represent the transmembrane domains of PTCH1-G and PTCH1-P respectively. Figure taken from Qian et al. (2019).

Previous work has shown that the inactive conformation of PTCH1 is a heterodimer with an N-terminal-palmitoylated SHH (SHHNP) ligand in a 2:1 ratio (**Figure 1.3B**), unlike bacterial RND proteins that typically form trimers (Qian et al., 2019). Work done by Qian et al. (2019) reported the cryo-electron microscopy (cryo-EM) structure of PTCH1 and N-palmitoylated SHH in a 4:2 ratio, with PTCH1 acting as a pseudo dimer of dimers. Each PTCH1 dimer binds a single N-palmitoylated SHH molecule. The PTCH1 dimer arrangement is asymmetrical, generating a hydrophobic binding pocket for the palmitate molecule. This was work carried on from the findings of a previous study by (Qi, X. et al., 2018) who also found the structure of PTCH1 in complex with palmitoylated SHH. The study demonstrated that pN-SHH sits in between the two PTCH1 proteins and works through two different interactions with each individual PTCH1 protein. Their studies show that the palmitate-associated PTCH1 (PTCH1-P) interacts primarily with the N-terminus of SHHNP, while the globular portion of SHHNP interacts with the globular-associated PTCH1 (PTCH1-G). These are also referred to as the PTCH1-A and PTCH1-B subunits in other studies (Qi, X. et al., 2018).

In addition, PTCH1 contains a hydrophobic channel spanning the membrane and extracellular domains (Zhang, Y. and Beachy, 2023) (**Figure 1.3C**). This channel has been observed in cryo-EM structures of PTCH and has been found to contain three cholesterol-like densities. This was confirmed by Gong et al. (2018) (Gong et al., 2018), highlighting another similarity between PTCH1 and RND transporters, some of which facilitate the transport of small hydrophobic molecules. One important thing to note is that the channel in PTCH1 is hydrophobic, which is key for cholesterol transport (Gong et al., 2018). PTCH1 has been shown to reduce the levels of free cholesterol in the outer leaflet of the

plasma membrane (Kinnebrew et al., 2021). Sequence analysis between PTCH1 and bacterial RND transporters has shown significant similarity in the transmembrane domains of PTCH1 and RND transporters. The two groups of proteins share a similar protein fold.

Similarities have been drawn PTCH1 and the Neimann-Pick C1 (NPC1) protein is a membrane-bound 13-TM domain cholesterol transporter that takes cholesterol molecules that are cleaved from low-density lipoproteins (LDLs) in the lysosome (Pfeffer, 2019). The role of NPC1 is to transport the cholesterol into the cytosol for use by the cell (Li, Xiaochun et al., 2016). Mutations within NPC1 associated with Niemann-Pick Type C disease lead to the accumulation of cholesterol within lysosomes (Ribeiro et al., 2001; Liao et al., 2007). NPC1 and PTCH1 share structural similarities, in particular with their transmembrane domains (Zhang, Y. et al., 2018). Both proteins possess an SSD, and both proteins contain a hydrophobic pocket through which cholesterol moieties are pumped (Li, Xiaochun et al., 2016).

1.3.1.2 PTCH1 CTD

The CTD of the PTCH1 protein varies in length between species, between 205-272 amino acids in length (Kawamura et al., 2008) . Although the CTD does not exhibit homology to known domains in other proteins, the primary structure analysis reveals the presence of five proline-rich motifs (PRMs) (**Figure 1.4**). PRMs play an important role in protein interaction and specificity, for example, PPxP and PPxY motifs are known to bind specifically to SH3 or WW domains (Zarrinpar et al., 2003).

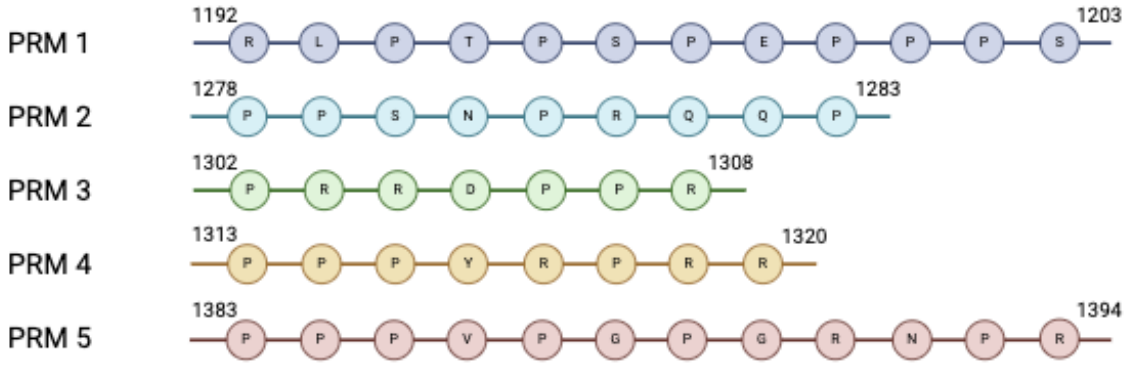

Figure 1. 4 PTCH1 CTD proline-rich motif sequences

A depiction of the sequences of the five proline-rich motifs in the CTD of human PTCH1 (isoform L; accession number: NP_000255.2). This figure highlights a TPSP motif in the first proline-rich motif and the PPPY motif in the fourth PRM necessary for interactions with ubiquitin ligases (Chen, X.L. et al., 2014). Figure created using BioRender.com

The PRMs provide structural rigidity and introduce bends or kinks into the CTD by virtue of the cyclic structure of the proline residues (Kawamura et al., 2008). The CTD is predicted to be mostly unstructured (Kowatsch et al., 2019; Qian et al., 2019), adopting a more rigid form upon protein binding, akin to an induced fit mechanism, with the adopted structure thought to be dependent on the specific interacting protein. An example of this is the intrinsically disordered region of the protein Bim, which interacts with the Bcl-xL protein, both of proteins undergo conformational changes to accommodate each protein (Bekker et al., 2023). The 4th PRM within the CTD contains a PPxY motif (PPPY) which is characteristic of interactions with WW domains. Deletion of this PPxY site in the CTD leads to a reduction in its interaction with some E3 Ubiquitin ligases (Chen, X.L. et al., 2014). Mutation of this motif, along with an additional PPPY motif in the PTCH1 middle loop to PPPA causes a loss in the interaction between PTCH1 and the ligases Itch and WWP2 (Chen, X.L. et al., 2014). Interaction of Itch with PTCH1 causes

the ubiquitylation of PTCH1 at K1413, which can induce PTCH1 internalisation and degradation.

Truncation of some portions of the CTD of PTCH1 have been associated with cancer (**Figure 1.5**), such as those caused by frameshift mutations at S1203, R1308 and Y1316, the most common PTCH1 mutations associated with endometrial, stomach and colon carcinomas respectively (Caballero-Ruiz et al., 2023) . An additional frameshift mutation at position R1422E leads to a shorter truncation of the CTD and is linked to the development of sporadic keratocystic odontogenic tumours (Qu et al., 2015). Additionally, a study identified a 32-base pair deletion resulting in CTD truncation at position 1220 (Makino et al., 2001). Mice expressing this truncated form of PTCH1 exhibit basal cell skin hyperplasia,

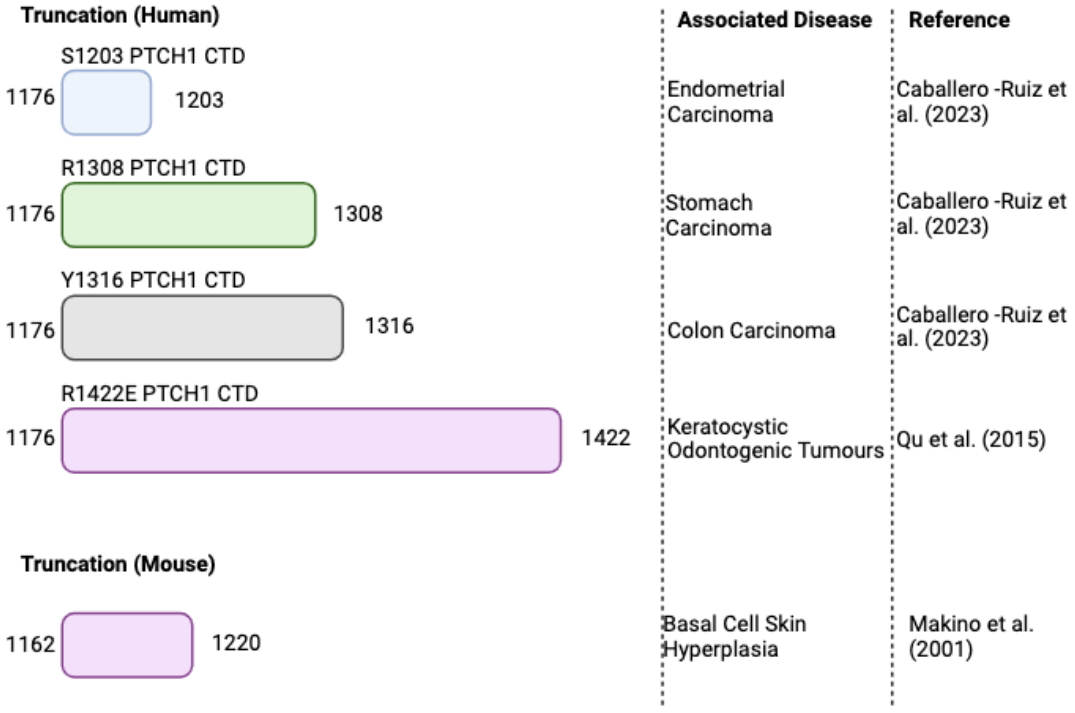

Figure 1. 5 Graphical representation of PTCH1 truncation mutants
This figure shows a selection of common PTCH1 truncation mutants in both humans and mice, with the associated disease and reference. Figure created using BioRender.com

supporting a role of the PTCH1 CTD in regulating cell growth and differentiation (Nieuwenhuis et al., 2007).

An important property of the PTCH1 protein is its localisation to the primary cilia, where it is predominantly found (Higgins et al., 2019). In a study carried out by Kim et al. (2015) (Kim et al., 2015), they demonstrated that the PTCH1 CTD is crucial for its localisation to the primary cilia. Truncation of the CTD at positions 1162, 1170 and 1180 prevented PTCH1 from localising to the primary cilia, indicating the essential role for the CTD region most proximal to the plasma membrane in this process. These results were further confirmed through the introduction of mutant PTCH1 into *Ptch1*$^{-/-}$ cells. PTCH1 localisation was confirmed through confocal microscopy and the level of PTCH1 fluorescence intensity was measured at the primary cilia. As the length of the CTD was reduced, the fluorescence intensity of PTCH1 was significantly decreased. Additionally, HH activity was shown to be higher in mutants, therefore suggesting a loss in PTCH1 function (Lu, X. et al., 2006); however, previous findings from our lab group indicate the opposite, our results have shown that PTCH1ΔCTD remains active and localises to the cilia. Immunohistochemical analysis from our lab showed that, whilst displaying lower expression levels compared to WT PTCH1, PTCH1ΔCTD was still able to localise to the cilia, and introduction of PTCH1ΔCTD into *Ptch1*$^{-/-}$ MEFs shows a level of canonical HH repression comparable to that of WT PTCH1 (Timmis, 2021).

1.3.1.3 Evidence of phosphorylation of the PTCH1 C-Terminal Domain

Several untargeted phosphoproteomic studies reported evidence of PTCH1 phosphorylation in T1195 and S1197. One of the papers that identified T1195

and S1197 as phosphorylation sites was in a study carried out by Franz-Wachtel et al. in 2012 (Franz-Wachtel et al., 2012). The goal of the study was to identify potential global phosphorylation sites of protein kinase D (PKD), a serine-threonine kinase implicated in angiogenesis, cardiac hypertrophy and bone formation (Rozengurt, 2011). The experiments were carried out in HEK293 cells – human embryonic kidney 293 cells – a commonly used cell line known for their growth reliability and their propensity for transfection. They compared phosphorylation levels in cells expressing constitutively active and kinase-dead PKD1, allowing for clear distinction and identification of PKD1 direct and indirect substrates. An advantage of this study is that they use the same cell line as this PhD, therefore direct comparisons can be made between the two. Nocodazole, a PKD activator was also used to treat the cells (Fuchs et al., 2009). Mass spectrometry was used to identify the presence of differential phosphorylation across the whole expressed proteome. Among many other proteins, phosphate groups were assigned to T1195 and S1197 of the PTCH1 CTD, with both residues calculated to have a probability of localisation of one – the highest score. This confirms them as phosphorylation sites within the CTD and suggest direct or indirect phosphorylation by PKD activation. The question remains as to what role these phosphorylation events play in the function of PTCH1, and which kinases are phosphorylating these residues. The indication is that they are functionally significant residues given their frequency of mutation in Gorlin-Goltz syndrome - a rare autosomal dominant disease, also known as with nevoid basal cell carcinoma syndrome (NBCCS) that is characterised by numerous basal cell carcinomas of the skin, medulloblastoma, jaw cysts, calcium deposits in the brain and developmental issues (Lo Muzio, 2008). Interestingly, mutations in the adjacent Pro residues between T1195 and S1197, P1194 and P1196, have also

been linked to Gorlin-Goltz syndrome in two Argentinian families (Martinez et al., 2019).

The phosphorylation of T1195 and S1197 was also detected in a study designed to identify roughly 6,000 undetected gene products due to lack of suitable antibodies or mass spec data (Shiromizu et al., 2013), part of the Chromosome-Centric Human Proteome Project (C-HPP) which aimed to track PTMs and alternative splicing of proteins. The study reported the phosphorylation of PTCH1 using a mix of samples from human colon cancer cell lines HCT116, SW480 and SW620, normal and cancer colon tissue after SILAC (stable isotope labelling by amino acids in cell culture) to enable quantitative analysis. The study also reported the phosphorylation of PTCH1 at both T1195 and S1197.

These papers and their findings clearly show that T1195 (T1181 in the mouse orthologue) is a phosphorylation site within the CTD regulated by growth factors (either PKD, insulin, or others in cancer cells). Additionally, there is a suggestion that S1197 may also be a phosphorylation site within the PTCH1 CTD, although with less confidence. These findings provide a foundation for further exploration into the role and significance of these phospho-sites in PTCH1 function and the cellular processes it regulates.

1.3.1.4 PTCH1 Mutations in Cancer

Ptch1 appears to be a hotspot gene for mutations associated with various tumours, most notably basal cell carcinoma (BCC) and medulloblastoma (Tang et al., 2010). Several papers have carried out experiments to determine which *Ptch1* mutations are the cause of BCC or Gorlin-Goltz Syndrome. The majority of

Gorlin-Goltz syndrome mutations result in early truncations or substitutions in the sterol sensing domain or other transmembrane domains, known to control canonical HH signalling (Lo Muzio, 2008), leading to PTCH1 loss of function.

Studies have shown that approximately 90% of all sporadic BCC cases (Epstein, 2008) and around 20% of medulloblastomas (Raffel et al., 1997) have an associated mutation within the PTCH1 gene which result in altered non-functional protein. It has been estimated that there are approximately 280 known germline mutations throughout the *Ptch1* gene. Many of these mutations contribute to the loss of function pathogenesis of BCC, leading to the constitutive activation of the HH pathway and subsequent tumour formation (Guo, Y.Y. et al., 2013; Yu, F.Y. et al., 2014). Though loss of the canonical function of PTCH1 has been shown to be oncogenic, some of these mutations could also alter non-canonical HH signalling, mediated through the CTD.

The study conducted by Qu et al. (2015) focused on keratocystic odontogenic tumours (KCOTs), which are benign intraosseous cystic lesions of the jaws, associated 16 out of the 19 samples analysed gave 19 PTCH1 mutations, one of which was a frameshift mutation that causes a truncation of the CTD (Qu et al., 2015). This highlights the potential importance of the CTD in the development of KCOTs. These studies provide further evidence for the involvement of PTCH1 mutations, particularly within the CTD, in the development of KCOTs and highlight the potential significance of the CTD in the pathogenesis of these tumours.

Kawamura et al. (2008) (Kawamura et al., 2008) published a paper that investigated the mutation of conserved PTCH1 CTD residues (T1195I, P1196S

and S1197F) in patients with BCC. The researchers assumed these mutations represented a loss-of-function because of their association with BCC. The mutation was hypothesised to cause an increase in the levels of canonical hedgehog signalling due to the nature of the loss of function phenotype of basal cell carcinoma. Alternatively, the mutant forms could potentially initiate non-canonical signalling of the HH pathway. Interesting to note is the P1196S mutation, as proline residues could be associated with significant structural change due to the cyclical structure of proline. Mutating this residue could alter the conformation of this region of the CTD dramatically since it is part of a short PPII motif. How this would result in functional changes, given that the CTD is predicted to be disordered, is unknown and will be part of my project.

Interestingly, there have been some studies that identified a potential mutation site within the CTD of PTCH1. One mutation of particular interest occurs at position 1195 where threonine is replaced by a serine (T1195S), one of the phosphorylation sites identified by phosphoproteomics. Mutation of this site has been implicated in the pathogenesis of basaloid squamous cell carcinoma (BSCC) (Saito et al., 2015). BSCC presents mixed features between BCC and SCC, the first driven by Hh signalling as described before, and the second driven by Erk1/2 signalling.

The study analysed 30 BSCC tissue samples and found PTCH1 mutations in 16 of cases. Of these, 13 harboured mutations in the CTD, within which, T1195S mutations were detected in 8 cases. Comparison between tumour and non-tumour tissue samples from the same patients showed that four of the eight cases with the T1195S mutation were germline mutations.

The presence of a cancer-associated mutation at a phosphorylation site, such as T1195, raises questions about its impact on protein regulation. The T1195S and T1195I mutations could potentially induce conformational changes in the PTCH1 protein, affecting its interaction with kinases or phosphatases and altering its regulatory mechanisms. However, the precise mechanisms by which the mutation affects PTCH1 function and its association with BSCC development require further investigation. A downside to this study is the small sample size, reducing the validity of these results for clinical applications; however, it does indicate a potential trend between mutation and disease, providing valuable insights for future research and clinical applications.

The identification of T1195 as a hotspot mutation site is very important for this project. Boutet et al. (2003) (Boutet et al., 2003) collected 23 familial cases and 42 sporadic cases of Gorlin-Goltz Syndrome and analysed the spectrum of mutations within tissue samples from French Gorlin-Goltz Syndrome patients. Their results identified 19 mutations, one of which was a T1195S mutation, again highlighting it as a key mutation within the PTCH1 CTD.

Another study explored the relationship between breast cancer recurrence and PTCH1 mutations (Wang, C.Y. et al., 2019). Previous studies have correlated the activation of the HH pathway in breast cancer with poor prognosis (Ramaswamy et al., 2012) and therefore the relationship needs elucidating further (Riobo-Del Galdo et al., 2019). Wang et al. sequenced *PTCH1* in breast tissue from 22 patients with recurrent breast cancer within 24 months of surgery and 22 samples from those that did not suffer tumour recurrence. *PTCH1* mutations were very

common in both groups and twice as prevalent in recurrent tumours compared to the control (68% and 34% respectively). They identified the T1195S mutation as the most prevalent mutation in the recurrence tumours. They concluded that mutations within exons 22 and 23 of PTCH1 (encoding the CTD) correlated with a much worse recurrence-free survival rate compared to mutations in other exons.

There were several limitations associated with this study, primarily the small sample size when analysing the T1195S mutation, unfortunately rendering the results not statistically significant for the point mutation, but significant for mutations in exons 22 and 23. In order to validate the association between the T1195S mutation and increased rates of breast cancer recurrence a much larger sample size is required.

The importance of the CTD phosphorylation sites and mutation hotspot sites will be explored further throughout this PhD project. Our lab hypothesised that a structural change may be induced by phosphorylation of certain residues within the CTD, perhaps affecting interaction with specific binding partners.

1.3.1.5 TPSP Forming a PPII Helix

The TPSP motif is an example of a PxPx motif, which has the propensity to form a polyproline residue II (PPII) helix (Adzhubei et al., 2013). This understanding is key as it allows for more accurate predictions of the PTCH1 CTD structure, specifically the region immediately after the final PTCH1 transmembrane domain. The CTD is thought to be predominantly unstructured, and the structure prediction tool AlphaFold predicts that the TPSP motif could adopt a helical structure with the side-chains of T1195 and S1197 occupying space in opposite

planes of the helix (**Figure 1.6**). However, the level of confidence with this structure prediction is very low (pLDDT < 50), a measure between 0-100 of structure accuracy associated with AlphaFold.

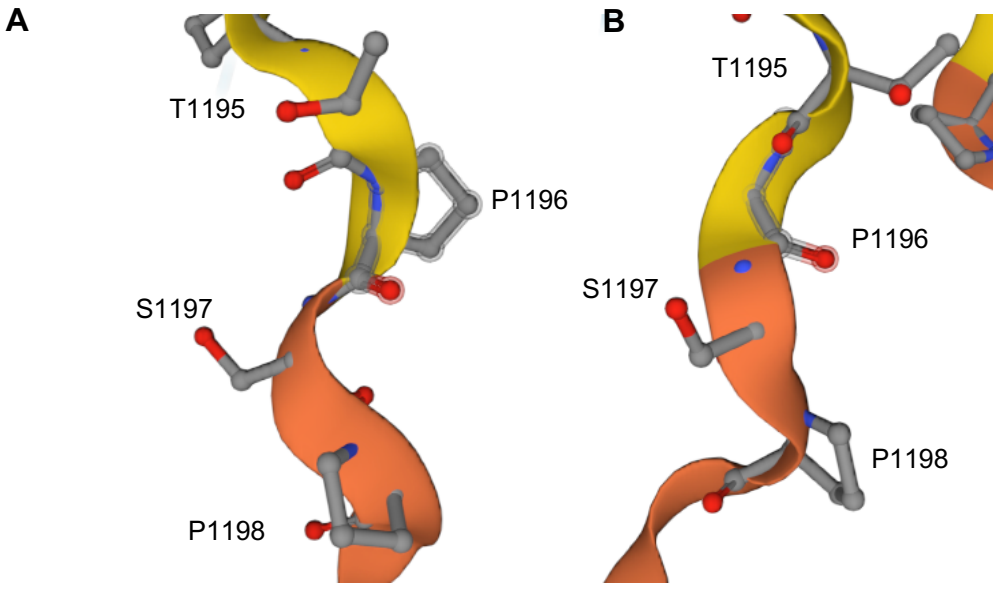

Figure 1. 6 AlphaFold prediction of the TPSP structure

Figures from AlphaFold using the sequence of PTCH1 isoform L (Uniprot: Q13635) indicating the side chains of each residue in the TPSP motif. **(B)** is **(A)** rotated slightly to show the space that the side chains occupy.

The PPII helix often exists in fibrous and globular proteins, and its conformation is such that it forms a left-handed helix with a twist of 120 degrees (Meirson et al., 2020). Unlike most protein motifs, it does not rely on van der Waal's (vdW) forces to stabilise the secondary structure, instead, the stability is driven by the stereo electric effect, and PPII helices can stabilise through the accumulation of neighbouring PPII helices (Esipova and Tumanyan, 2017). This could point to a role for the TPSP motif in PTCH1 homodimer formation, stabilising dimers.

The PPII helix is thought to be very prevalent within disordered sections of proteins, the binding of other proteins to proline-rich regions that contain a large

proportion of these PPII helices is very important for cell signalling (Esipova and Tumanyan, 2017). An example of this is the adapter protein, Cas, which is involved in cellular responses such as cell migration and integrin signalling (Yadav and Miller, 2007). Cas contains an Src-binding domain (RPLPSPP) which, when mutated disrupts the levels of Src binding and therefore decrease the levels of Cas activity as determined by autophosphorylation (Yadav and Miller, 2007).

Phosphorylation of the TPSP motif may lead to phosphorylation of cryptic neighbouring phosphorylation sites by kinases that use phospho-Ser/Thr as part of their target motif (Riobo et al., 2006). The TPSP motif might provide an environment permissive for constitutive phosphorylation. It is also thought that the formation of PPII helices might facilitate kinase binding (Esipova and Tumanyan, 2017; Narwani et al., 2017; Meirson et al., 2020).

Sequence alignment of different PTCH1 homologues across species (human, mouse and the fruit fly) revealed one key similarity between all three species with respect to this project. All three species contain a conserved TPSP sequence within the proximal region of the CTD (**Figure 1.7**).

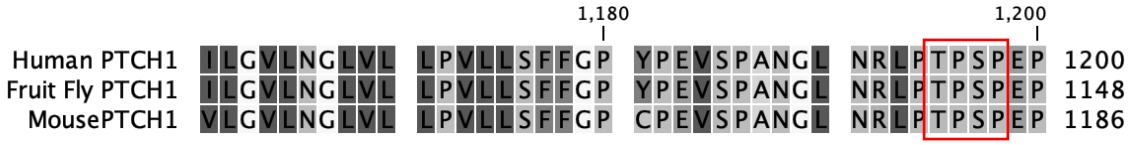

Figure 1. 7 Sequence alignment of human, mouse and fruit fly PTCH1 sequences

Sequence alignment between human, mouse and fruit fly PTCH1 sequences highlights the conservation of the TPSP motif across species. TPSP motif is indicated with a red box, residue numbers are also indicated. The figure was created using CLC Sequence Viewer 8.0.

Human: Uniprot – Q13635

Fruit fly: Uniprot – P18502

Mouse: Uniprot – Q61115

1.3.2 PTCH2

PTCH2, the other vertebrate homolog of PTCH1 has a more restricted expression pattern compared to PTCH1 with studies indicating a diminished reliance of humans on PTCH2 relative to PTCH1 (Zhulyn et al., 2015). PTCH1 is ubiquitously expressed during embryogenesis, whereas PTCH2 expression is restricted to skin and neural tube, leading to different impacts on development. As previously explained, loss of PTCH1 leads to embryonic lethality, whereas complete loss of PTCH2 results in a much less severe phenotype (Lee, Y. et al., 2006; Zhulyn et al., 2015), this is linked to the differences in embryonic expression of the two proteins. Structurally the two proteins share a sequence identity of roughly 56% which reduces significantly when comparing the two CTDs (Kawamura et al., 2008). The CTD of PTCH2, is much shorter – 89 residues for PTCH2 vs 272 residues for PTCH1 (comparison between PTCH1 and PTCH2, Uniprot codes Q13635 and Q9Y6C5 respectively). Significantly, the PTCH2 CTD lacks the key PPXY recognition site for Itch and Smurf2 that is seen in the PTCH1 CTD (Chen, X.L. et al., 2014), as previously explained, this site is necessary for the promotion

of degradation of PTCH1, the absence of this site in the PTCH2 CTD could be contributing to the improved stability for PTCH2 compared to PTCH1. Studies have shown that PTCH1 and PTCH2 both can bind all three HH ligands with comparable affinities (Carpenter et al., 1998).

The differences in importance associated with the two proteins seen in embryogenesis suggest an inability for PTCH2 to compensate for the loss in PTCH1, but not the contrary. The reduced activity of PTCH2 can be seen using *Ptch1*$^{-/-}$ MEFs, in which Gli activity can be increased slightly upon the addition of the SMO agonist SAG (Alfaro et al (2014). This result suggests that there is a marginal level of pathway repression still present in the absence of PTCH1, suggesting that PTCH2 can exert a small level of pathway repression (Alfaro et al., 2014).

1.3.2 PTCH1 and PTCH2 heterodimers

The dynamic interplay between PTCH1 and PTCH2 is slowly becoming the focus of more research (Fleet and Hamel (2018); Timmis et al. (2023), investigating their roles within PTCH protein function exposing the dominance of PTCH1 over PTCH2. However, recent work by members of this lab (Timmis et al. 2023) has uncovered a synergistic relationship between the two proteins. PTCH2 exhibits a similar sensitivity to SHH as PTCH1 (Timmis et al., 2023), with both proteins possessing a sterol-sensing domain (SSD) which can modulate downstream signalling by pumping cholesterol away from SMO (Pearse et al., 2001). Within the cholesterol channel of PTCH1 is a cluster of three residues (V111, L114 and W115), which, when mutated (V111F, L114F, W115A) disrupts the cholesterol channel and reduces canonical activity (Zhang et al. 2018). The corresponding

PTCH2 mutation (L82F, L85F, W86A) was generated by a previous student in this lab (Timmis, A. 2021), his work showed that the SSD of PTCH1 is much more critical to function than that of PTCH2, producing an inactive PTCH1 protein when mutated.

When exploring the catalytic triad within PTCH1, a D513Y mutation within the triad significantly reduced the canonical function of PTCH2 (Timmis et al. 2023). As this mutation has been identified in Gorlin Syndrome patients (Wicking et al., 1997), it highlights the importance of the catalytic triad to PTCH2 function (Kowatsch et al., 2019; Zhang et al., 2020). The corresponding PTCH1 residue – D513 – will be explored in Chapter 7 of this thesis.

An important discovery alongside this structural work was the formation of PTCH1-PTCH2 heterodimers (Timmis et al., 2023), seen through co-immunoprecipitation experiments, pulling down PTCH2 with PTCH1, as well as FRET assays which uncover the close proximity with which the PTCH1 and PTCH2 CTD are when forming heterodimers. This area of PTCH protein interaction and function will further be explored in Chapter 7.

1.4 Pin1

1.4.1 Pin1 Introduction

Proline-rich motifs such as the TPSP motif are often binding targets for modifying enzymes (Wu et al., 2018; Sanchez et al., 1996), therefore, investigations into the function of the TPSP motif that are depicted in this project also focused on possible binding partners. One of these binding partner candidates was Pin1, a

member of the peptidylprolyl isomerase (PPIase) family of proteins, specifically the parvulin subgroup (Yeh and Means, 2007; Lu, Z. and Hunter, 2014). The isomerisation of phosphorylated Ser/Thr-Pro bonds is specifically catalysed by Pin1 and is its primary function (Lu, Z. and Hunter, 2014), allowing the proline bond to rotate between the *cis* and *trans* conformation. Structurally, Pin1 is made up of two domains, functionally contrasting domains, an N-terminal WW domain and a C-terminal PPIase domain linked by a flexible loop (Nakatsu et al., 2020) (**Figure 1.6**). The WW domain interacts with the pSer/pThr-Pro, binding to the target proteins. The PPIase domain is responsible for catalysing the *cis*/*trans* isomerisation (Nakatsu et al., 2020; Yu, J.H. et al., 2020). Phosphorylation is key for the isomerisation to take place; it forms a binding site for the WW domain of Pin1 (Lu, K.P., 2003). The tryptophan residues in the WW domain are highly conserved and reside 20 amino acids apart, allowing for binding to the phosphorylated motif (Lee, Y.M. and Liou, 2018).

Pin1 is involved in several cellular processes, including the cell cycle, embryonic development and apoptosis (Yeh and Means, 2007; Sorrentino et al., 2014). Dysregulation in the involvement of these processes has been associated with numerous diseases, including cancer, neurodegenerative diseases and ageing-related diseases (Sorrentino et al., 2014).

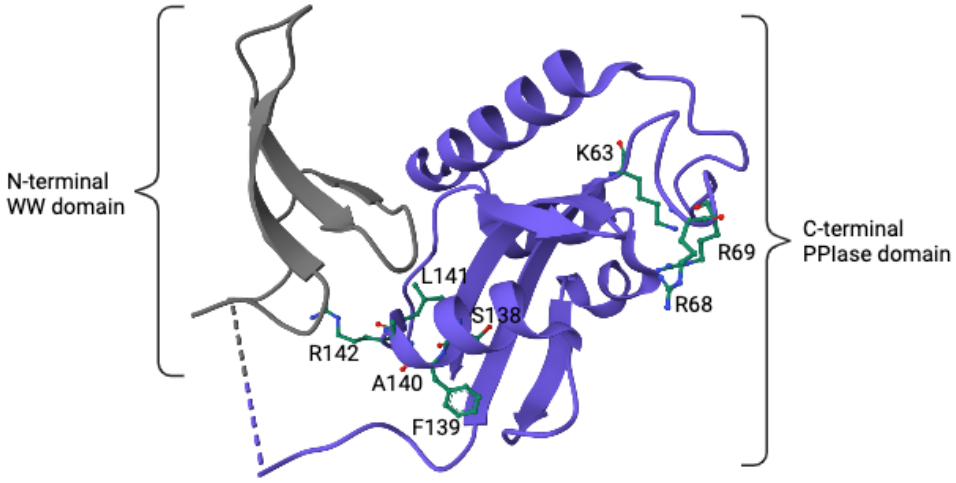

Figure 1. 8 Crystal structure of human Pin1

The structure of human Pin1 (adapted from PDB: 6VAJ) depicting the N-terminal WW domain (residues 1-39) and the C-terminal PPIase domain (residues 45-163). The structure is missing the loop linking the two domains (residues 40-45). Phosphate binding loop residues K63, R68 and R69, and the domain interface residues S138-R142 indicated. Figure created using BioRender.com.

1.4.2 Human Pin1 Structure

The human Pin1 protein is 163 amino acids in length, and both the WW domain and the PPIase domain recognise and bind to pSer/pThr-Pro motifs (Matena et al., 2018). As explained before, the WW domain is non-catalytic and functions in target recognition. The WW domain binds specifically to the target sequence in the *trans* configuration. The PPIase domain contains several important structural elements. It includes a catalytic loop (residues 64-80) involved in the isomerisation of the proline bond (Mahoney et al., 2018), residues K63, R68 and R69 create a positively charged phosphate-binding loop that is necessary for substrate recognition, facilitating binding to the pSer/pThr-Pro motif. Pin1 function has been suggested to be regulated by a domain interface (Lee, Y.M. and Liou, 2018). In the realm of Pin1's molecular interactions, a crucial domain interface

emerges between the WW domain loop and a specific region (residues S138-R142) within the PPIase domain (Lee, Y.M. and Liou, 2018). This dynamic interplay regulates the binding of Pin1 to its targets, which explains the versatility of Pin1 substrates.

1.4.3 Models of Pin1 Binding

There are four proposed mechanisms for Pin1 interactions with its substrates:

1. Sequential binding – the WW domain of Pin1 binds to one phosphorylated Ser/Thr-Pro motif in the target protein, followed by the binding of the PPIase domain to a separate pSer/pThr-Pro motif (Lu, K.P. et al., 2002; Lee, Y.M. and Liou, 2018).
2. Multimeric binding – the high affinity of the WW domain for pSer/pThr-Pro motifs binds to one member of a protein complex, allowing for the PPIase domain to interact with another target protein within the complex (Jacobs et al., 2003; Lee, Y.M. and Liou, 2018).
3. Catalysis-first binding – the PPIase domain binds to and catalyses the cis-to-trans isomerisation of the target to allow the WW domain to bind (Wintjens et al., 2001; Lee, Y.M. and Liou, 2018).
4. Simultaneous binding – the WW and PPIase domains bind to separate pSer/pThr-Pro motifs on the target protein at the same time (Lee, Y.M. and Liou, 2018).

1.4.4 Functions of Pin1

High expression and activation of Pin1 is linked to cancer formation due to its involvement in cell cycling, DNA damage response and synthesised protein folding (Yeh and Means, 2007). High expression of Pin1 correlates to a poor

prognosis in lung cancer patients (Tan et al., 2010). Pin1 overexpression induces chromosome instability and tumorigenesis (Suizu et al., 2006). It regulates the activity of many oncogenes and tumour suppressors to promote tumour growth (Yu, J.H. et al., 2020). An example of this regulation occurs firstly in human RNA polymerase II (RNAP II), the role of Pin1 is to regulate the structure and function of this protein and it does so through its interactions with its CTD (Xu et al., 2003). Xu et al. 2003 found that Pin1 is able to regulate the phosphorylation status of RNAP II through the inhibition of the phosphatase FCP1 and induction of cdc2/cyclinB causing RNAP II CTD phosphorylation. Another substrate of Pin1 is c-MYC, Pin1 regulates conformational changes in c-MYC through its isomerisation of the Ser62-Pro63 bond, regulating the stability of c-MYC and its transcriptional activity (Cohn et al., 2020). A final example is the interactions between Pin1 and Smads, a group of proteins that regulate TGFβ signalling (Matsuura et al., 2010). Matasuura et al. (2010) discovered that Pin1 interacts with Smad3 through the phosphorylation of a Thr-Pro motif (Thr179) in a TGFβ-dependant manner. They also found that knock-down of Pin1 in prostate cancer cells led to the inhibition of TGFβ-mediated migration and invasion.

1.5 Non-canonical Hedgehog Signalling

1.5.1 Brief introduction to non-canonical signalling

Non-canonical signalling refers to the roles of the HH pathway independent of regulation by GLI transcription factors. There are two types of non-canonical signalling: Type I involves the regulation of PTCH1 functions independent of SMO and Type II encompasses signalling where SMO acts as a G-inhibitory protein-coupled receptor (Riobo-Del Galdo et al., 2019). Type I signalling regulates autophagy and proliferation (Pietrobono et al., 2019), while Type II has been

shown to regulate ionic channels and small GTPases (Szczepny et al., 2017) (**Figure 1.9**).

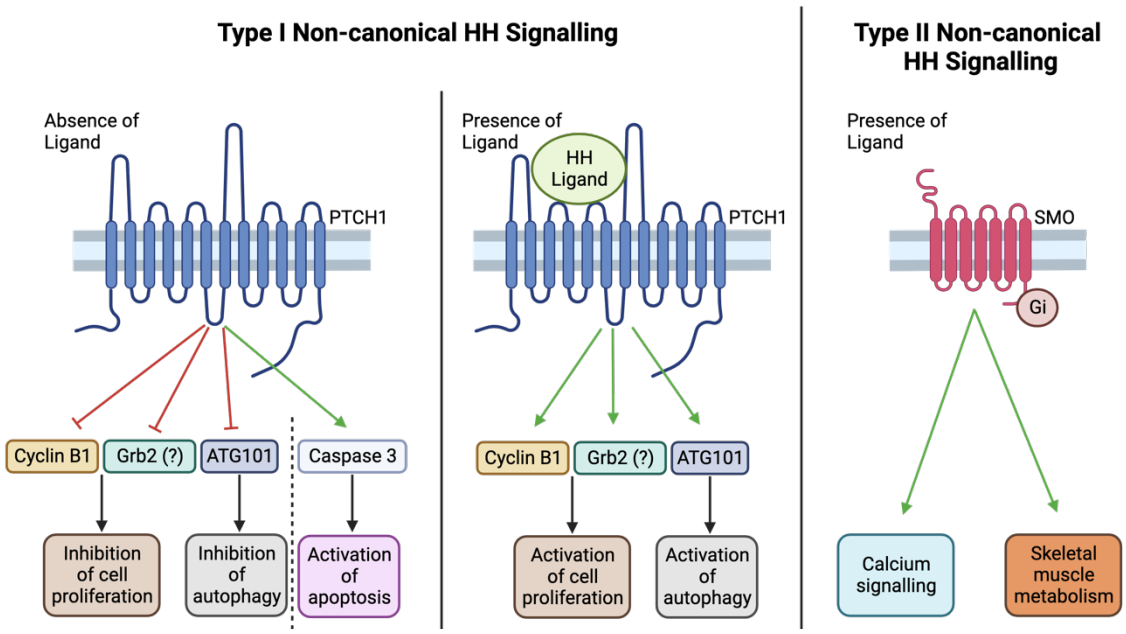

Figure 1. 9 Non-canonical HH signalling

This figure depicts examples of non-canonical HH signalling.

Type I occurs independently of SMO. In the absence of ligand, PTCH1 interacts with cyclin B1, removing it from the nucleus, blocking mitosis. It also reduces the levels of phosphorylated Erk1/2, potentially through interactions with Grb2, inhibiting cell proliferation. It interacts with the ULK complex through ATG101 to block autophagy. And finally, it activates caspase 3, activating apoptosis. In the presence of ligand, PTCH1 is internalised, and these processes are reversed.

Type II relies on SMO as a G-inhibitory protein-coupled receptor. In the presence of HH ligand, type II signalling leads to increased calcium signalling and increased skeletal muscle metabolism.

1.5.2 Autophagy

Autophagy is a highly conserved cellular process by which the cell breaks down damaged components or misfolded proteins and recycles the degradation products to promote differentiation and cellular homeostasis (Aman et al., 2021). Autophagy is often initiated in response to nutrient stress (Li, X. et al., 2020). There are three main types of autophagy, macroautophagy, microautophagy and chaperone-mediated autophagy (CMA) (Aman et al., 2021). Microautophagy is the action of the lysosome to engulf components directly from the cytoplasm (Wang, L. et al., 2023) and CMA is the process of recognition and sequestration of target components by soluble cytosolic proteins that target the substrate to the lysosome, the substrate is translocated across the lysosomal membrane for degradation (Andrade-Tomaz et al., 2020; Wang, L. et al., 2023).

Macroautophagy (hereon referred to simply as autophagy) is the bulk form of degradation, components are collected into double-membrane vesicles known as autophagosomes that deliver the contents by fusion with the lysosome (Griffey and Yamamoto, 2022). Autophagy relies on the coordination of more than thirty autophagy-related (ATG) proteins (Itakura and Mizushima, 2010). Of these proteins there are 18 main proteins involved in various stages of autophagy (Mizushima et al., 2011). These proteins are divided into different complexes:

- The Atg1/unc51-like autophagy activating kinase (ULK) complex regulates the induction of autophagosome formation through the actions of its forming subunits: ULK1/2, Atg13, FIP200 and ATG101 (Mizushima, 2010).
- The Atg9 complex aids the delivery of membrane components to the autophagosome (Reggiori and Tooze, 2012).

- The Phosphatidylinositol-3- kinase (PI3K) complex recruits binding proteins to the PAS and phosphorylates phosphatidylinositol-4,5-biphosphate (PIP2) into phosphatidylinositol-3,4,5-biphosphate (PIP3) in the phagophore membrane, allowing for the recruitment of additional autophagy-related proteins (Kma and Baruah, 2022).
- The ATG12-ATG5-ATG16L1 complex, which lipidates LC3BI to form LC3BII (Fracchiolla et al., 2020).

PTCH1-dependent non-canonical signalling is a negative regulator of autophagy (Chen, X. et al., 2018). Autophagic flux is regulated by PTCH1 through an interaction between the PTCH1 CTD and ATG101 in a region of the PTCH1 CTD truncated in some cancer types (after S1203) (Caballero-Ruiz et al., 2023). ATG101 is a subunit of the ULK complex that acts as a chaperone for ATG13. The knock-on effect of this is the incomplete process of autophagy.

Two proteins, LC3BII and p62 are used as markers for autophagy (Chen, X. et al., 2018). LC3BII is present in the membranes of autophagosomes and is thought to be important in membrane biogenesis, and p62 links some types of cargo (ubiquitylated protein aggregates) to LC3BII for incorporation into the autophagosome and degradation (Komatsu et al., 2012). Following autophagosome fusion with the lysosome, the luminal pool of p62 and LC3BII is degraded with the cargo (Islam et al., 2018). As a result, incomplete progression of autophagy leads to a build-up in both markers. When PTCH1 is over-expressed in HEK293 cells, autophagic flux is blocked and therefore the levels of these two markers increase, therefore, suggesting a role for PTCH1 sequestering ATG101 and blocking the progression of autophagy (Chen, X. et al., 2018).

The drug Bafilomycin A1 (BafA1) is used as a positive indicator for blockage in autophagic flux. BafA1 prevents the degradation of the autolysosomal cargo and it's thought that PTCH1 functions in a similar way to this (Chen, X. et al., 2018).

1.5.3 HH-regulated Erk Phosphorylation

The activation of the extracellular regulated kinase (Erk) signalling by SHH binding to PTCH1 is another example of type I non-canonical HH signalling. HH ligands can activate alternative signalling pathways such as the Erk (often referred to as the mitogen-activated protein kinase (MAPK)) pathway (Chang et al., 2010). This is a highly conserved signalling pathway, the aberrant activity of which is often implicated in physiological proliferation, cellular differentiation and, when aberrantly activated, in cancer development (Bartholomeusz et al., 2012; Samatar and Poulikakos, 2014; Bryant et al., 2019). Erk is one of several mitogen-activated protein kinases, including, Erk, JNKs and P38s(Johnson and Lapadat, 2002).

Erk signalling occurs when a growth factor binds to a specific receptor tyrosine kinase (RTK), after which, a tyrosine residue within an SH3 domain of the RTK protein becomes phosphorylated through autophosphorylation by the receptor, initiating the recruitment of adapter protein Grb2, which binds to the phosphorylated tyrosine through its SH2-binding domain (Guo, Y.J. et al., 2020). The RTK/Grb2 complex recruits another signalling molecule, SOS, a guanine nucleotide exchange factor which binds to the SH3 domain of Grb2 (Ullah et al., 2022).

SOS interacts with an inactive form of the Ras protein, which is bound to a GDP molecule. The interaction of SOS and inactive Ras promotes the exchange of GDP to a GTP molecule, activating Ras (Baltanas et al., 2020; Cook and Cook, 2021). From here, a kinase cascade is activated, the activated induces dimerization and activation of RAF isoforms (MAP kinase kinase kinase) which in turn phosphorylates MEK1/2 (a MAP kinase kinase) (Gonzalez-Hormazabal et al., 2018). The final stage is the phosphorylation of the Erk1/2 protein by phosphorylated MEK1/2 (Tanimura and Takeda, 2017). In the case of Erk1/2 activation by PTCH1, it has been proposed that Grb2 could directly interact with one of the PRMs in the PTCH1 CTD via one of its SH3 domains and activate Erk1/2 (Chang et al., 2010).

Activated Erk1/2 has two types of targets, it either targets cytoplasmic substrates, which it can phosphorylate, influencing various cellular processes, or it translocates to the nucleus to act as a transcriptional regulator by phosphorylating and modulating the activity of transcription factors (Baltanas et al., 2020; Moon and Ro, 2021). Two cytoplasmic targets of Erk1/2 are c-fos and c-Jun, causing the two to dimerise and become the transcription factor complex activator protein 1 (AP-1) (Lavoie et al., 2020). The AP-1 translocates to the nucleus and binds to the AP-1 DNA motifs to initiate the target gene transcription (Lavoie et al., 2020). Another cytoplasmic target of Erk1/2 is ribosomal-S6-kinase (RSK). Erk1/2 activates the P-90 form of RSK through phosphorylation, leading to the activation of its S6 domain of the RSK complex (Roux et al., 2007; Anjum and Blenis, 2008). Activated S6 has several regulatory functions, including the negative regulation of SOS-1, it can also translocate to the nucleus and regulate the CREB transcription factor (Li, D. et al., 2013).

Inactivation of the Erk pathway is seen through several mechanisms, firstly, through the negative feedback inactivation of the SOS-1 protein, reducing the activation of Ras (Buday and Vas, 2020). A second mode of Erk pathway inactivation is through Ras-GAPs (GTPase-activating proteins) which hydrolyse the active RAS-GTP back to the inactive, GDP-bound form of Ras (Huang et al., 2021). A final example of a negative feedback loop within this pathway comes from the activation of tyrosine phosphatase, cdc25c, by Erk1/2, causing the dephosphorylation and subsequent deactivation of the RTK EGFR (Lake et al., 2016).

There are two isoforms of Erk: Erk1 and Erk2, Erk1 is coded by the MAPK3 gene while Erk2 is coded by the MAPK1 gene (Moon and Ro, 2021). These isoforms share 84% sequence identity and share similar functionality (Li, Q. et al., 2014). Erk1 is the slightly larger isoform with a molecular weight of 44 kDa, compared to Erk2, which has a molecular weight of 42 kDa (Busca et al., 2016), making them also known as p44 and p42. Previous work from this lab has shown that transfection of MCF7 cells (a breast cancer cell line that does not express SMO) with WT PTCH1 and subsequently treated with SHH leads to a rapid increase in the levels of phosphorylated Erk1/2. This suggests a role in the repression of the MAPK/Erk pathway by PTCH1 in the absence of ligand. In addition to this, activation of Erk1/2 by SHH has been seen in cells treated with cyclopamine, which inhibits SMO activity, showing activation of Erk1/2 is an example of non-canonical HH signalling (Chang et al., 2010).

Chapter 2

Materials and Methods

Chapter 2

Materials and Methods

2.1 Cell lines and procedures

HEK293 human embryonic kidney epithelial cells and NIH3T3 murine embryonic fibroblast cells were obtained from the American Type Culture Collection (ATCC). *Ptch1*$^{-/-}$ murine embryonic fibroblasts (MEFs) were a gift from Dr Matthew Scott (Stanford University). MCF7 breast cancer epithelial cells were a gift from Dr Thomas Hughes (University of Leeds). NIH3T3 murine embryonic fibroblasts were maintained in Dulbecco's modified eagle medium (DMEM) supplemented with 10% Bovine Calf Serum (BCS), 1% Glutamax and 1% Pen/Strep. All other cell lines were maintained in DMEM, supplemented with 10% Foetal Bovine Serum (FBS), 1% Glutamax and 1% Pen/Strep. Cell lines were maintained at 37°C, 5% CO_2. For passaging prior to full confluence, the media was aspirated, and cells were washed with 2 mL PBS. Following this, the cells were incubated with 2 mL 0.25% trypsin-EDTA for 2-3 minutes. Following cell detachment, an additional 8 mL cell culture media was used to dilute the cells and deactivate the trypsin-EDTA. Cells were collected and seeded at the required density for each experiment. Refer to **Table 2.1** for information on each cell type and their maximum passage.

Cell Line	Organism	Cell Type	Tissue	Properties/ Disease	Maximum Passage
HEK293	Human	Epithelial	Embryonic kidney	Adherent	30
Ptch1 -/- HEK293	Human	Epithelial	Embryonic kidney	Adherent	30
Ptch1 -/- MEFs	Mouse	Fibroblast	Embryo	Adherent	20
SW620 SCR	Human	Epithelial	Large Intestine	Adherent/ Adenocarcinoma	20
MCF7	Human	Epithelial	Breast	Adherent/ Adenocarcinoma	20
NIH3T3	Mouse	Fibroblast	Embryo	Adherent	20

Table 2. 1 Cell lines used for experimental analysis

Table displays the origin, characteristics and maximum passages of each cell line.

2.2 Freezing cells for long term storage

This is a modified protocol from Timmis, A. J. (2021). Cells were kept in liquid nitrogen for long-term storage. Prior to freezing, cells were grown to confluence in 10 cm cell culture plates, after which they were washed with 2 mL 1X PBS, incubated with trypsin-EDTA to detach the cells, and diluted with 8 mL DMEM supplemented with 10% FBS. Cells were centrifuged at 3000 x g for 4 mins, and the resulting cell pellet was resuspended in 1 ml of freezing media (10% DMSO (Sigma #276855-100ML) in FBS) and stored in a 2 mL cryotube. The cryotubes were stored at -80°C using a Mr Frosty freezing container (Nalgene) filled with isopropanol. The cells were then placed in a liquid nitrogen Dewar for long-term storage. To recover the cells from liquid nitrogen, they were stored on dry ice for transportation and then thawed quickly at 37°C. The entire vial was placed into a flask containing 9 mL of fresh cell culture media and the cells were incubated at 37°C and 5% CO_2.

2.3 Cell counting

This protocol was adapted from thermofisher.com. Cells were counted using a haemocytometer. Briefly, cells were trypsinised and resuspended in the appropriate media, 20 μL of resuspended cells were mixed with an equal volume of trypan blue, after which 10 μL was placed into a haemocytometer chamber and the cells were counted under a microscope. For accurate counting, the following equation was used:

$$Number\ of\ cells\ per\ mL = \left(\frac{total\ number\ of\ cells\ in\ 4\ quadrants}{4}\right) \times\ 10{,}000$$

Cells were then diluted with media and seeded at the correct densities for each experiment.

2.4 Transient cell transfection using Transporter 5

For cell culture experiments that required the overexpression of proteins but were insensitive to serum concentrations, transfection was carried out using Transporter 5, a polyethylenimine (PEI)-based transfection reagent (Polysciences #26008), the experiment was carried out according to the manufacturer's protocol. Cells were seeded into the appropriate cell culture dish in fresh growth medium with 10% FBS and incubated overnight. Once the cells had reached 70-80% confluence, the media was aspirated and replaced with DMEM supplemented with 2% FBS for 1-2 hrs. During the incubation, the transfection master mix was prepared using the appropriate volumes of DNA (shown in **Table 2.2**). The DNA/NaCl master mix was vortexed briefly before adding the appropriate amount of the Transporter 5 transfection reagent. The mix was vortexed again and incubated at room temperature for 30 mins before being

added to the appropriate cells and mixed well. The cells were incubated at 37°C, and 5% CO_2 for 6 hours, after which the media was replaced with 10 mL of fresh growth medium (DMEM supplemented with 10% FBS). The cells were incubated at 37°C and 5% CO_2 overnight before being lysed for immunoprecipitation.

Plate	Culture Volume (mL)	Plasmid DNA (μg)	NaCl (μL)	Transporter™5 (μL)
6-well plate	2	2	200	8
60 mm dish	5	6	500	24
100 mm dish	10	10	1000	40
T75 flask	15	18	1500	72

Table 2. 2 Volumes of Transporter™5 components

2.5 Transient cell transfection using Lipofectamine™ 2000

For cell culture experiments that were sensitive to serum concentrations, transfection was carried out using Lipofectamine 2000™ (Thermo Fisher Scientific #11668019), the experiment was carried out according to the manufacturer's protocol. HEK293 cells were seeded at a density of 6 x 10^5 cells/ml in an antibiotic-free growth medium. The cells were allowed to reach 90% confluence before transfection (roughly 20-24 hrs post-seeding). For 6-well plates, 250 μL of OptiMEM (Gibco #31985062) was mixed with 4 μg DNA and incubated at room temperature for 5 min. In a separate Eppendorf, 250 μL of OptiMEM was mixed with 5 μL of Lipofectamine 2000 and incubated for 5 minutes at room temperature. The Opti-MEM + Lipofectamine 2000™ tube was added to the Opti-MEM + DNA tube, mixed thoroughly, and incubated at room temperature for 30 mins before being added dropwise to the cells.

2.6 Bacterial Transformation

Protocol for this experiment was adapted from Timmis, A. J. (2021). A 50 μL aliquot of bacterial cells (DH5-α for plasmid amplification, BL21 (DE3) for protein expression) was thawed on ice for 30 mins. Up to 1 μg of plasmid DNA was added and mixed gently by flicking. The cells were incubated on ice for 30 mins, with gentle swirling every 10 mins to incorporate. The cells were heat shocked at 42°C for 45 s before being placed back on ice for an additional 3 mins. 500 μL of pre-heated SOC media was added to the cells before being incubated at 37°C for 1 hr and rotated at 220 rpm. 100 μL of cells were plated onto LB-agar plates with the correct antibiotic to match the plasmid resistance. The plates were incubated at 37°C overnight.

2.7 Pin1-GST Protein Production and Purification

This protocol is adapted from Ren, X.D. (2000). Separate aliquots of BL21 (DE3) cells were transformed with the Pin1-GST (Addgene #19027, Uniprot #Q13526), and GST (Pin1 sequence removed from Addgene #19027, Uniprot #Q13526) plasmids and plated onto LB agar plates containing Ampicillin antibiotic. After overnight incubation, a colony was picked and placed into a 250 mL flask containing 50 mL of LB supplemented with ampicillin. The flask was placed in a shaker overnight at 37 °C and 220 rpm. 20 mL of the overnight culture was added to 500 mL LB supplemented with ampicillin in a 2 L flask, incubated at 37°C with shaking at 220 rpm until the OD600 measured 0.8. At this point, 250 μL of 1M IPTG was added to each flask (final concentration: 0.5 μM) to induce expression of the gene of interest. The cultures containing IPTG were incubated for 2 hrs at 37°C and 220 rpm. The bacteria were then centrifuged at 4,500 x g for 20 mins,

after which the supernatant was removed, and the pellet was transferred to a 50 mL falcon tube and stored at -80°C until use.

On the day of protein purification, the bacterial pellet was thawed on ice. Once thawed, the pellet was resuspended completely in 10 mL lysis buffer (50 mM Tris pH 7.5, 1% Triton X-100, 150 mM NaCl, 5 mM $MgCl_2$). DTT, aprotinin, leupeptin and PMSF were added immediately before use (final concentrations of 1 mM, 10 mg/mL, 10 mg/mL and 1 mM respectively). The lysate was sonicated on ice (70% amplitude, 30 s on, 40 s off repeated eight times). After sonication, the lysates were cleared by centrifugation at 23,000 x g for 45 minutes at 4°C. The supernatant was transferred to a fresh, pre-chilled 50 mL falcon tube. The supernatant was rotated gently with 0.6 mL (wet volume) Glutathione Sepharose 4G beads (GE 17-0756-01) at 4°C for one hour. The beads were spun down at 1,000 x g and the supernatant was removed, being careful not to carry over any beads. The beads were washed 6 times in 10 mL washing buffer (50 mM Tris pH 7.5, 0.5% Triton X-100, 150 mM NaCl, 5 mM $MgCl_2$). DTT, aprotinin, leupeptin and PMSF were added immediately before use (final concentrations of 1 mM, 1 mg/mL, 1 mg/mL and 1 mM respectively). Finally, the beads were resuspended in 8 mL washing buffer plus 10% glycerol. Resuspension was done with a Pasteur pipette to ensure a homogenous suspension without damaging the protein or the beads. 0.4 mL aliquots were made, and flash-frozen in liquid nitrogen before being stored at -80°C.

2.8 Quantification of protein concentration

This protocol is adapted from Ren, X.D., (2000). To measure the concentration and purity of the bead-bound purified Pin1-GST and GST proteins, 10 μL of beads

were denatured in Laemmli buffer, and the proteins were separated by SDS-PAGE on a 12% gel with BSA standards as controls (500, 250, 125, 62.5 and 31.25 μg/mL concentrations). The gel was stained using Coomassie-blue overnight. The gel was de-stained using H_2O in 3 x 30 mins washes. The gel was imaged, and the bands were analysed using ImageJ. The concentration of the aliquots was determined using the BSA standards.

2.9 Pin1 Binding Assay Protocol

This protocol is a modified version of the co-immunoprecipitation protocol frm Chen et al., (2018). HEK293 cells were plated into 10 cm dishes and transfected 24 hrs later at a confluence of 80% using the Transporter 5 transfection method. 24 hrs post-transfection, the plates were lysed in 400 μL co-immunoprecipitation buffer (50 mM Tris, pH 7.5, 150 mM NaCl, 1% NP-40, 1 mM EDTA, 1 mM EGTA, 2.5 mM $MgCl_2$, 0.5% sodium deoxycholate, supplemented with 1X protease (abcam # ab27005) and phosphatase (Sigma #P0044-5ML) inhibitors, and 100 uM PMSF). All three compounds were added immediately before buffer use. The cells were scraped, and the lysates were transferred to pre-chilled 1.5 mL Eppendorf tubes. The lysates were rotated at 4°C for 30 mins, followed by centrifugation at 13,000 x g for 15 mins at 4°C to pellet any cell debris. During the centrifugation step, 500 μL (wet volume) of Glutathione Sepharose 4B agarose beads were equilibrated with co-immunoprecipitation buffer by spinning down the beads at 1,000 x g, removing the supernatant and resuspending in 400 μL of buffer, this was repeated three more times before a final resuspension in 400 μL buffer to make a homogeneous suspension.

Following centrifugation, 20 μL of the lysate was transferred to a fresh, pre-chilled Eppendorf containing 4 μL 6X Laemmli buffer and mixed to serve as “whole cell lysate” control in western blots. These samples were heated at 42°C for 30 mins before being stored at -20°C until analysis. The remaining supernatant from the clarified lysate was transferred to a fresh pre-chilled 1.5 mL Eppendorf. Non-specific binding to Sepharose was eliminated by treatment of the clariid lysates with 30 μL of equilibrated Sepharose beads and incubation at 4°C with rotation for 1.5 hrs. The beads were centrifuged at 1,000 x g for a few seconds, the supernatant was collected and split evenly (~200 μL each) between two fresh, pre-chilled 1.5 mL Eppendorf tubes. 5 μg of Pin1-GST beads was added to one of the Eppendorfs whilst 2.5 μg of GST beads was added to the other (due to differences in protein purification yield). The tubes were incubated with rotation at 4°C for 2 hrs.

The samples were centrifuged at 1,000 x g for a few seconds, the supernatant was discarded, and the beads were washed by gentle resuspension in 200 μL co-immunoprecipitation buffer supplemented with PMSF and protease and phosphatase inhibitors. This wash step was repeated three times. After the final wash step, almost all of the supernatant was removed, leaving ~10 μL of buffer covering the beads. 4 μL of 6X Laemmli buffer was added to the beads followed by gentle flicking to resuspend the beads. The samples were then heated at 42°C for 30 mins before being stored at -20°C until analysis. When running a gel, the entire sample, including the beads, was loaded in the gel.

2.10 GLI-Luciferase reporter assay

This protocol is a modified version from Timmis et al., (2023). All GLI-Luciferase reporter assays were carried out in *Ptch1*$^{-/-}$ MEFs. Briefly, a 90% confluent 10 cm plate was trypsinised and resuspended in 50 mL DMEM supplemented with 10% FBS. 500 μL of the cell suspension was added to each well of a 24-well plate and incubated overnight at 37ºC and 5% CO_2. Roughly 24 hrs post-seeding the cells were transfected with the appropriate plasmid DNA using Transit-X2 (Mirus #MIR 6000) transfection reagent, following the manufacturer's protocol. For each 24-well plate 1.2 mL Opti-MEM was added to a 1.5 mL Eppendorf tube. To this, 19.4 μL 8XGBS-luc (250 ng/μL) and 10.8 μL pRL-SV40 (10 ng/μL) were added. The Eppendorf tube was vortexed before the Opti-MEM-DNA solution was split into 200 μL aliquots in separate fresh 1.5 mL Eppendorf tubes. To each 200 μL aliquot, 6 μL of the appropriate plasmid (250 ng/μL) was added, and the tube was vortexed. After this, 6μL of Transit-X2 reagent was added to each tube, the tubes were vortexed and incubated in the tissue culture hood for ~30 mins at room temperature before 50 μL of the transfection mix was added dropwise to each well. 24-hours after transfection, the media was aspirated a replaced with DMEM supplemented with 0.5% FBS, 500 μL per well. The cells were incubated for 48 hrs at 37ºC and 5% CO_2. After the 48 hrs, the media was aspirated, and each well was washed with 500 μL ice-cold PBS. The PBS was aspirated and 100 μL of 1X passive lysis buffer (PLB) (Promega) was added to each well. The plate was incubated at room temperature with gentle rocking for 30 mins. Analysis was carried out using the Promega dual-luciferase reporter kit, using a Promega Glomax 20/20 luminometer.

2.11 Co-Immunoprecipitation Assay

This protocol is a modified version from Chen et al., (2018) HEK293 cells were seeded into 10 cm dishes at a density of 2 x 10^5 cells/mL. 24 hours post-seeding, cells were transfected at a confluence of >70% using the Transporter 5 protocol and incubated overnight at 37°C, 5% CO_2. 24 hrs post-transfection, the plates were placed on ice, the media was aspirated, and the cells were washed with 2 mL ice-cold PBS, followed by addition of 700 μL of Co-immunoprecipitation buffer supplemented with the appropriate protease and phosphatase inhibitors, and 0.2 mM PMSF. The cells were scraped on ice and transferred to a pre-chilled 1.5 mL Eppendorf tube before being rotated at 4°C for 30 mins. The cells were spun down for 15 mins at 17,000 x g and 4 °C. 20 μL of the supernatant was transferred to a fresh, pre-chilled 1.5 mL Eppendorf tube containing 4 μL 6X Laemmli buffer and heated at 45°C for 30 mins. The remaining supernatant was transferred to a fresh, pre-chilled 1.5 mL Eppendorf and the pellet was discarded. The supernatant was incubated with the appropriate antibody at the recommended concentration (**Table 2.5**) for 2 hrs at 4°C with constant rotation, followed by incubation with 15 μL Protein-G Dynabeads (Invitrogen) for 1 hr at 4°C and constant rotation. After three, 1 mL washes in the lysis buffer, the beads were resuspended in 25 μL 2X Laemmli buffer and heated at 45°C for 30 mins. Laemmli buffer was collected from the beads and placed in a fresh, pre-chilled 1.5 mL Eppendorf tube and stored at -80°C until being run on a gel.

2.12 Western Blotting

This protocol has been modified from Chen et al., (2018). To analyse protein samples, samples were subjected to analysis by SDS-PAGE, using polyacrylamide resolving gels with varying percentages (6-12%) topped with a

4% stacking gel, or run on pre-cast gels (ThermoFisher). Gels were placed in a tank with 1X running buffer (Alfa Aesar J61006.K7) (10X running buffer diluted in H_2O), the samples were loaded into the stacking gel alongside Plu Protein™ Dual Colour Standard Marker (Bio-RAD) before being run at 80 V for ~30 mins until they reached the resolving gel. After this, the voltage was increased to 120 V and the samples were run until they reached the bottom of the gel. Pre-cast gels were run at 200 V for ~40 mins until the proteins reached the bottom of the gel. Following this, the proteins were transferred from the gels onto PVDF membrane (Bio-RAD) which has been pre-soaked in methanol. The gels were loaded into buffer tanks topped up with 1X transfer buffer (10X transfer buffer Alfa Aesar diluted in H_2O and supplemented with 20% Methanol). The gels were transferred at 50 V for 2 hrs. After the transfer, the membranes were washed in 10 mL 1X tris-buffered saline, 1% Tween-20 (TBST) before being incubated in 10 mL TBST supplemented with either 5% BSA or 5% milk at room temperature for one hour at room temperature with gentle rocking. After this stage, the membranes were washed three times in 10 mL TBST before being incubated overnight at 4ºC with gentle rocking in the appropriate primary antibody diluted in TBST supplemented with either 5% BSA or 5% milk according to the manufacturer's directions (**Table 2.5**).

Following overnight incubation, the membranes were washed three times for five mins using 10 mL TBST before being incubated in 10 mL of the appropriate HRP-conjugated secondary antibody (**Table 2.6**) according to the manufacturer's direction for 1 hr at room temperature with gentle rocking. The membranes were washed again using three 10 mL TBST washes, 5 mins each wash. Imaging was carried out using an ECL substrate and imaged using the ChemiDoc (BIO-RAD).

2.13 WST-1 Cell Viability Assay

This protocol was performed to the manufacturer's instructions (Roche # 11644807001) *Ptch1*$^{-/-}$ HEK293, and MCF7 cells were seeded into 4 96-well plates for determination of viability at 0, 24, 48 and 72 hrs), 100 μL cells per well at a density of 1 x 10^5 cells/mL. 100 μL media was added to a two-well border surrounding the test wells to eliminate evaporation from the test wells. The cells were incubated overnight at 37°C and 5% CO_2. 24 hrs post-seeding the cells were transfected with the Transporter5 transfection protocol. At the same time, the WST-1 reagent was thawed in the dark at room temperature and 10 μL was added to each well of the t=0 plate. The WST-1 reagent is light sensitive and therefore it was added to the cells with the lights off the plate was immediately wrapped in foil, gently swirled to mix the reagent, and placed in the incubator at 37°C and 5% CO_2 for 1 hr. After incubation, the plate was gently shaken for one minute before the absorbance (OD Difference, 450 nm – 650 nm) was recorded. The WST-1 reagent protocol was repeated for the t=24 hrs, t = 48 hrs, and t = 72 hrs plates.

2.14 Colony Formation Assay (CFA)

This protocol was adapted from Caballero et al., (2023). SW620 and NIH 3T3 cells were plated into 6-well plates at a density of 6 x 10^6 per well into 2 mL of DMEM supplemented with 10% FBS (for SW620 cells) or 10% BCS (for NIH 3T3 cells). 24 hrs post-seeding the cells were transfected with the appropriate plasmid using the Lipofectamine 2000 transfection protocol. 24 hrs post-transfection the media was aspirated, the cells were washed with 1 mL PBS and trypsinised with 0.5 mL trypsin-EDTA (0.25%) per well. The cells were resuspended in 4.5 mL

DMEM (FBS or BCS) and collected into a 15 mL falcon tube. 1 mL of the cell suspension was transferred to a 1.5 mL Eppendorf and the cells were pipetted up and down using a 200 μL pipette to ensure a single-cell suspension. Cells were counted using a haemocytometer and re-seeded into a fresh 6-well plate at a density of 1,000 cells per well. The plates were agitated gently to ensure even distribution across the well before being incubated at 37°C and 5% CO_2 until significant colony formation for observed by the naked eye (~10 days). During this time, culture media was refreshed every 3 days. Once significant colony formation had occurred, the media was aspirated, the cells were washed with PBS and the cells were fixed using 1 mL Methanol per well and left in the tissue culture hood for 15 minutes. The methanol was then aspirated off and 1 mL 0.05% crystal violet solution (Sigma) in H_2O was added to each well and left to stain for 15 mins. The crystal violet solution was aspirated off and the cells were washed with PBS to remove excess crystal violet before the cells were left to dry in the tissue culture hood. Once dry, the plates were analysed on a white light box, a picture was taken to count the colonies accurately, and the plates were wrapped in parafilm and stored at room temperature for further analysis.

2.15 Autophagic Flux Assay

This protocol was adapted from Chen et al., (2018). HEK293 cells were plated into 6-well plates at a density of 6 x 10^6 cells per well. 24 hrs post-seeding the cells were transfected using the Lipofectamine 2000 transfection protocol, transfecting 2 wells for each plasmid. 24 hrs post-transfection the media was aspirated, the cells were washed with PBS and pair of samples were treated with either 100 μM Bafilomycin A1 (Tocris Bioscience ™ 13-341-0U) or the equivalent volume of DMSO. Both treatments were done in 10% FBS DMEM, 2 mL per well,

and the cells were incubated at 37°C and 5% CO_2 for 4 hrs. Following incubation, the plates were transferred to ice, the media was aspirated, and the cells were washed with ice-cold PBS. The PBS was aspirated, 200 μL 1X Laemmli buffer was added to each well, and the cells were scraped into fresh, pre-chilled 1.5 mL Eppendorf tubes. Following this, the cells were sonicated on ice at 20% amplitude for 15 seconds before being heated at 95°C for 10 mins. The samples were frozen at -20°C for up to a month before analysis using Western Blot.

2.16 Erk1/2 Phosphorylation Assay

This protocol was adapted from Chang et al., (2010). *Ptch1*$^{-/-}$ HEK293 cells were plated into 6-well plates at a density of 6 x 10^6 cells per well. 24 hrs post-seeding, the cells were transfected using the Transporter 5 protocol, transfecting two wells for each plasmid. 6 hrs post-transfection, the media was aspirated, the cells were washed with PBS, and the media was changed to 0% FBS DMEM media. The cells were incubated overnight at 37°C and 5% CO_2. ~20 hrs post-transfection, the media was aspirated, the cells were washed with PBS and half of the samples were treated with 100 ng/ml rSHH (Bio-Techne #8908-SH-005/CF) in serum-free DMEM. The cells were incubated at 37°C and 5% CO_2 for 15 mins before the media was aspirated, the cells were washed with ice-cold PBS, and 200 μL of 1X Laemmli buffer was added to each well. The cells were scraped and sonicated on ice before being heated at 45°C for 10 mins. The samples were stored at -20°C for up to a month before analysis on a Western Blot.

2.17 Site-directed mutagenesis

Site-directed mutagenesis was carried out using 2 different cloning kits and used according to the manufacturer's protocols:

QuikChange II XL Site-Directed Mutagenesis Kit (Agilent Technologies)

1X Reaction Buffer, 20 ng DNA template, 125 ng forward primer, 125 ng reverse primer 1 μL dNTP mix, 3-5 μL QuikSolution and double distilled H_2O up to a volume of 50 μL were combined in a PCR tube. 1 μL (2.5 units) of PfuUltra HF DNA Polymerase was added to the tube and mixed gently by flicking. Amplification via PCR was carried out in a PCR thermocycler (**Table 2.3**). Following PCR amplification, 1 μL of DpnI was added to the tube, mixed gently, and incubated at 37 °C for 1 hr. During this incubation, an aliquot of XL10-Gold ultracompetent cells was thawed on ice and 45 μL was transferred to a pre-chilled 14 mL BD Falcon polypropylene round-bottom tube. To the cells, 2 μL beta-mercaptoethanol was added and incubated on ice for 10 mins, with gentle swirling every 2 mins. After, 2-5 μL of the DpnI-treated PCR product was added to the cells and the cells were incubated on ice for 30 mins before being heat-shocked at 42°C for 30 s and placed back on ice for an additional 3 mins. Pre-warmed SOC media (0.5 mL) was added to the cell mixture and the mixture was incubated at 37°C for 1 hr, shaking at 225 rpm.

Q5 Site-Directed Mutagenesis Kit (NEB)

1X Q5 Hot Start High Fidelity 2X Master Mix, 0.5 μM forward primer, 0.5 μM reverse primer, 1-20 ng template DNA and nuclease-free H_2O were combined into a PCR tube. Amplification via PCR was carried out in a PCR thermocycler (**Table 2.3**). Following PCR amplification, 1 μL of the PCR product was combined with 5 μL 2X KLD Reaction Buffer, 1 μL 10X KLD Enzyme Mix and 3 μL Nuclease-free Water. The mixture was pipetted up and down gently before being incubated at room temperature for 5 minutes. During this incubation, an aliquot of NEB 5-

alpha Competent *E. coli* cells was thawed on ice. Once thawed, 5 μL of the KLD mix was added to the cells and flicked to mix well. The mixture was placed on ice for 30 mins before being heat shocked at 42°C for 30 s. Immediately following the heat shock, the cells were placed back on ice and incubated for 5 mins. 950 μL of room temperature SOC media was pipetted into the mixture, and it was incubated at 37°C for 60 mins with shaking (250 rpm). Finally, the cells were mixed thoroughly by flicking the tube, and then 100 μL of cells were spread onto an LB agar plate supplemented with the appropriate antibiotic before being incubated overnight at 37°C. The following day, colonies were picked for expansion and sequencing analysis.

Q5 Site-directed mutagenesis kit was used to generate the ΔTPSP plasmid, QuikChange XL II was used to generate all other single substitution mutations. All primers were obtained from Integrated DNA Technologies as HPLC-purified oligos (**Table 2.7**).

Polymerase Used	Cycling Steps						
	Initial Denaturation	No. Cycles	Number of cycle repeats			Final Extension	Hold
			Denaturation	Annealing	Extension		
Q5® High-Fidelity DNA Polymerase (NEB)	98, 30 s	30	98, 10 s	60-72, 25 s	72, 30 s per kb	72, 7 m	4
QuikChange XL II Site-Directed Mutagenesis PfuTurbo DNA polymerase (Agilent)	95, 1 m	18	95, 50 s	60-68, 50 s	68, 1-2.5 m per kb	68, 10 m	4

Table 2. 3 PCR Conditions for site-directed mutagenesis

Specific conditions for each polymerase associated with the different polymerases.

2.18 Cloning

PCR cloning was carried out using the Phusion® High-Fidelity Kit (NEB) according to the manufacturers protocol. All primers were obtained from Integrated DNA Technologies as HPLC-purified oligos (**Table 2.6**). Briefly, PCR amplification was carried out by combining 10 μL 5X Phusion HF Buffer, 1 μL 10 mM dNTPs, 2.5 μL each of the forward and reverse primers (10 μM), 2 uL of 5 ng/μL template DNA and 34 μL nuclease-free water into a PCR tube before adding 0.5 uL Phusion DNA Polymerase to the reaction mix and mixing gently. The PCR tube was placed into a PCR thermocycler, and PCR amplification (**Table 2.4**). Following PCR amplification, the PCR products were used for further cloning.

Polymerase Used	Cycling Steps						
	Initial Denaturation	No. Cycles	Number of cycle repeats			Final Extension	Hold
			Denaturation	Annealing	Extension		
Phusion® High-Fidelity DNA Polymerase (NEB)	98, 30 s	30	98, 10 s	60-72, 25 s	72, 30 s per kb	72, 7 m	4

Table 2. 4 PCR conditions for Phusion® sub-cloning

2.19 Protein labelling for NMR studies

This protocol was adapted from Oberoi et al. (2010). A GB1-PTCH1(1176-1240) (Uniprot # Q13635, pETM6T1 backbone) construct, generated previously by Dr Mark Richards (University of Leeds), was transformed into BL21 (DE3) cells using the bacterial transformation protocol. The following day, a colony was picked from the plate and placed into a 250 mL flask containing 50 mL LB with kanamycin and

incubated overnight at 37°C with shaking at 220 rpm. After 16 hrs, the 50 mL culture was transferred to a fresh, autoclaved 2 L flask containing 1 L LB supplemented with kanamycin. The flask was incubated at 37°C with shaking at 220 rpm until the OD600 reached 0.7. The culture was centrifuged at 4500g for 20 mins, the supernatant was discarded, and the pellet was resuspended and washed in 500 mL PBS. The pellet was centrifuged at 4500g for 20 mins, the PBS discarded, and the pellet resuspended in 250 mL filtered minimal media (0.49 g $^{15}NH_4Cl$, 2.5 g D-glucose, 2.5 mL βME vitamin solution, 250 μL micronutrient solution, 250 μL 2 M $MgSO_4$, 50 μL 1 M $CaCl_2$, 250 μL 0.01 M $FeSO_4.7H_20$). The bacterial suspension was placed into a 2 L flask and incubated at 20°C with rotation at 220 rpm for 2 hrs. 250 μL IPTG (final concentration 1 mM) was added to the flask and then incubation continued for 16 hours at 20°C. The IPTG-induced culture was centrifuged at 4500g for 20 minutes at 4°C and the pellet was stored at -80°C in a 50 mL falcon tube until purification.

2.20 Purification of GB1-PTCH1(1176-1240) for NMR studies

This protocol has been adapted from McIntyre et al., (2017). The bacterial pellet was resuspended in 35 mL loading/washing buffer (20 mM Tris, 150 mM NaCl, pH 8) containing one protease inhibitor complete (EDTA-free) tablet and mixed for 10 mins. The suspension was sonicated on ice for 5X 20 s ON: OFF pulses. The sonicated lysate was transferred to a 50 mL centrifuge tube, balanced, and centrifuged at 20,000 rpm for 45 mins at 4°C. The supernatant was filtered through a 0.45 um filter twice to clarify. The Äkta pump was prepared by washing pumps A and B with buffer A (20 mM tris, 150 mM NaCl, pH 8) and buffer B (20 mM tris, 150 mM NaCl, 500 mM imidazole, pH 8) respectively. Buffer A was then

run through the Äkta at a rate of 2 mL/minute until a baseline was established (~5 minutes). Meanwhile, a 5 mL His-Trap column was charged with 20 mL $NiCl_2$, 20 mL H_2O was flushed through the column, followed by 20 mL of buffer A, and finally the lysate was passed through the column. The 5 mL His-Trap column was attached to the Äkta and a buffer mix (A + B) was run through the column at a rate of 3 mL/min with 1.8 mL fractions being collected in a 96-well collection plate. The buffer mix was initially run at 0% buffer B for ~10 mins, then 1% buffer B for ~1 min, and then up to 100% buffer B over 15 mins. Samples corresponding to the correct peak on the graph were heated at 95°C for 10 minutes before being subjected to SDS-PAGE using a pre-cast 4-20% gel and run using 1X running buffer at 200 V for ~40 mins. The gel was then incubated in Coomassie stain for ~30 mins. The gels were analysed using a white light box. The samples corresponding to the correct molecular weight of the purified protein were pooled together into 3500 MWCO dialysis tubing before adding 900 μL 1 mg/mL TEV to cleave the NusA(His_6) tag from the GB1-$PTCH1_{(1176-1240)}$. The ends of the dialysis tubing were clasped together, leaving space at the top for air to allow the tubing to float, and was placed in a large beaker containing 3 L of TEV cleavage buffer (50 mM Tris, 50 mM NaCl, 2 mM beta-mercaptoethanol, pH 8). Following this, the His-Trap column was stripped (50 mM EDTA) and recharged (0.1 mM $NiSO_4$). Additionally, SEC buffer (20 mM $(K)PO_4$, 150 mM NaCl, 0.5 mM TCEP, pH 6.5) was filtered and de-gassed before being pumped through the Äkta and the SEC column using 180 mL at a rate of 1 mL/min.

Following this, the TEV-cleaved, dialysed solution was transferred to a 50 mL Falcon tube. The 5 mL His-Trap column was washed with 20 mL buffer A and then the dialysed protein solution was passed through the His-Trap before being

loaded onto the Äkta. A collection plate was added to collect 1.8 mL fractions. Initially, 100% buffer A was passed through the column (~20 mL), followed by the addition of buffer B (10% of total buffer) and allowed to flow through the column (~15 mL) before the level of buffer B in the mix was increased to 100% over the course of 15 minutes. Samples from selected fractions were analysed through Western Blot and Coomassie staining. The fractions showing bands consistent with the molecular weight of the protein at ~17 kDa were pooled and concentrated down to ~ 2.5 mL in 2 x 3000 MWCO concentrators (4,000 x g at 4 °C). The samples were taken from the concentrator and stored in fresh, pre-chilled 1.5 mL Eppendorf tubes overnight. The His-Trap column was stripped and recharged. The following day, 20 mL (K)PO_4 buffer was injected into the 5 mL loop of the Äkta, followed by 2.5 mL of the protein solution. The Äkta was run at a rate of 1 mL/min and 1.8 mL fractions were collected in a fraction collection plate. Selected fractions were run on SDS page and stained using Coomassie Blue before being analysed. The samples that produced a band of ~ 14 kDa were concentrated using a 3000 MWCO concentrator by centrifugation down to a volume of ~1 mL total and a rough concentration of 600 μM.

2.21 NMR Experimentation and analysis

This protocol has been adapted from Batchelor et al. (2022). ^{1}H-^{15}N HSQC spectra were collected using 100 μM isotopically-labelled GB1-$PTCH1_{(1176-1240)}$ protein. The protein sample was made up to a total volume of 500 μL, supplementing with Buffer A. The samples were then sent to the NMR facility for analysis. Each spectrum was collected on a Brucker 600 MHz Oxford NMR magnet. Spectra were recorded at 5, 10, 15, 20, 25 and 30°C, with each data set

being processed using NMRpipe (Delaglio et al., 1995) and further analysis was performed using CCPNMR Analysis Version 2.5.2 (Vranken et al., 2005).

For triple resonance spectra, the same processed was used but using ^{1}H-^{13}C-^{15}N-labelled GB1-PTCH1$_{(1176\text{-}1240)}$. The spectra recorded were: HNCO, HNcaCO, HNcoCA, HNCA, HNcocaCB and HNcaCB. These spectra were recorded on a Brucker 600 MHz NMR magnet. HNcaCO, HNcocaCB and HNcaCB sprctra were recorded using non-uniform sampling (NUS). Where required, experiments recorded using NUS were reconstructed using SMILE (Ying et al., 2017). An aliphatic 1H-13C HSQC spectrum and a HBHAcoNH experiment (using 20% NUS) were recorded at 10°C to facilitate assignment and provide additional ^{1}H resonance measurements. Again, the spectra were processed using NMRpipe (Delaglio et al., 1995) and analysis was performed using CCPNMR Analysis Version 2.5.2 (Vranken et al., 2005). Assignments were transferred from triple resonance experiments to all ^{1}H-^{15}N HSQC spectra.

Following the assignment of the ^{1}H-^{15}N HSQC peaks, the secondary shifts were calculated using theoretical and experimental shift data (Sahu et al., 2014). To calculate the secondary shifts, the difference between the theoretical shifts (calculated using the Expasy ProtParam tool) and the experimental shifts (extracted from the CCPNMR Analysis data) was calculated and plotted using GraphPad Prism version 9.

For phosphorylation analysis, a ^{1}H-^{15}N HSQC of an isotopically labelled 15N GB1-PTCH1$_{(1176\text{-}1240)}$ was generated, and the spectrum was obtained at 20°C. Following this, the sample was removed and ERK1 was added (50 mM Tris-HCl

pH 7.5, 50% glycerol, 150 mM NaCl, 0.1 mM EGTA, 0.1% 2-mercaptoethanol, 0.02% Brjj-35, 0.2 mM PMSF, 1 mM Benzamidine) to the sample to a final concentration of 1μM, along with ATP (final concentration of 1 mM). Several ^{1}H-^{15}N HSQC spectra were recorded over the course of 1.5hrs and any changes in peak shift were noted. Each spectrum was collected on a Brucker 600 MHz Oxford NMR magnet, with each data set being processed using NMRpipe (Delaglio et al., 1995) and further analysis was performed using CCPNMR Analysis Version 2.5.2 (Vranken et al., 2005).

2.22 Mass spectrometry sample generation and analysis

This protocol has been adapted and optimised from Chen et al., (2018). For each sample, 3 x 10-cm dishes of HEK293 cells were transfected using the Transporter 5 protocol. 24 hrs post-transfection, the media was aspirated, the cells were washed in 2 mL PBS, the PBS was aspirated, and the cells were lysed in 700 μL co-immunoprecipitation buffer supplemented with protease inhibitors, phosphatase inhibitors and PMSF. The lysates were rotated at 4°C for 30 mins before being centrifuged at 17,000 x g and 4°C for 15 mins. The supernatants were collected and placed in Eppendorf tubes on ice. 4 μL of Myc-tag antibody (16286-1-AP) was added to each lysate and then rotated at 4°C for 1.5 hrs. 40 μL of protein-G Dynabeads were added to each lysate, then rotated at 4°C for an additional 1 hr. The lysates were then washed using 500 μL of co-immunoprecipitation buffer (supplemented with phosphatase and protease inhibitors, and PMSF), using a magnetic rack to separate the Dynabeads from the supernatant. The samples were only washed once before being pooled together into an Eppendorf. The beads were resuspended in 100 μL 2X Laemmli buffer and heated at 45°C for 30 mins. The beads were separated from the

Laemmli using the magnetic rack and the Laemmli sample was stored at -80°C before analysis. The samples were flash-frozen in 100 μL aliquots using liquid nitrogen and stored at -80°C for long-term storage.

The presence of PTCH1 within the immunoprecipitate was confirmed by Western blotting using a small aliquot of the immunoprecipitate, the remainder of the sample was submitted to the on-site mass spectrometry facility where the sample was processed. Briefly, the sample was digested using trypsin, the eluted peptides were concentrated, and the LC-MS/MS analysis was carried out using a Vanquish Neo UHPLC system connected to an Orbitrap Eclipse Tribrid mass spectrometer (Thermo Fisher software Scientific). The raw data files were analysed using the proteome discovery (Thermo Fisher Scientific Version 3.0.0757).

2.22 Multiple Sequence Alignment

This protocol has been adapted from Pearson, W.R. (2014). This database search aimed to determine the conservation of the TPSP motif in PTCH related proteins across species, and whether the presence of the motif can infer function. All database searches were done with comparisons to the longest human PTCH1 splice variant: PTCH1 Isoform L (accession number: NP_000255.2), and the searches were carried out using an unbiased approach, encompassing all species types. The proteins collected were PTCH1 proteins from a wide range of species and potential homologues of PTCH1 – the uncharacterised nature or mislabelling of certain proteins made it harder to confirm homology. To collect the proteins, database searches were carried out using the Basic Local Alignment Search Tool (BLAST) provided by NCBI. Protein sequences selected for

comparison with NP_000255.2 were required to be full-length sequences. The main organism groups were identified: mammals, fish, reptiles, insects and nematodes. The search was extended to each subset within these groups to identify differences within the TPSP sequence. Multiple sequence alignments (MSAs) were carried out using BLASTp searches. BLASTp alignments were carried out using the NCBI databases (specifically the non-redundant protein sequences database). Briefly, alignments were done using the Human PTCH1 isoform L sequence (accession number: NP_000255.2) as the query sequence. Alignments were carried out across all species, going up in taxonomy from order to class, division and kingdom to find the limit of conservation across all eukaryotes. Searches were performed across animals, plants and fungi.

When analysing animals, sequences were collected for mammals, fish, birds, reptiles, and amphibians. Sequences were taken from all secondary subgroups from each order of animals. For mammals, analysis covered >75% of mammalian sequences (*Rodentia, Chiroptera, Soricomorpha*). Fish (*Ostiecthyes, Chondrichthyes, Agnatha*), Reptiles (*Testudines, Squamata, Crocodilia, Chordata*), Amphibians (*Anura, Caudata, Gymnophiona*), Birds (*Aves*), Nematodes and Insects. Where no confirmed sequences were available, expected protein sequences were used.

Sequence alignments were continued, looking at all orders of eukaryote (mammals, fish, birds, reptiles, and amphibians). Analysis of fungi sequences produced only expected or hypothetical proteins which shared significant coverage of the query sequence (<48%). None of the fungi sequences collected exhibited the TPSP motif. When analysing plant sequences, alignment searches

produced only hypothetical and expected protein sequences, None of the sequences collected exhibited the TPSP motif.

A minimum of five species were analysed for conservation in each sub-group of organisms and a single sequence was displayed per sub-group in the figures.

2.23 Statistical Analysis

Statistical analysis was carried out using GraphPad Prism software versions 9 and 10. This was also used to generate graphs. One-tailed and 2-tailed t-tests, and one-way ANOVA analysis was done where appropriate.

Primary Antibody	Species	Diluent	Concentration	Company	Product Code
DYKDDDDK Tag (mAb)	Mouse	5% BSA	1:5000 (WB)	Proteintech	66008-4-Ig
GFP-tag (mAb)	Rabbit	5% milk	1:5000 (WB)	Proteintech	66002-1-Ig
HA-tag (PolyAb)	Rabbit	5% milk	1:5000 (WB)	Proteintech	51054-2-AP
HA-tag (mAb)	Mouse	5% BSA	1:1000 (WB)	Cell Signalling	66006-2-Ig
HRP-conjugated GAPDH	Mouse	5% milk	1:5000(WB)	Proteintech	HRP-60004
LC3B	Rabbit	5% BSA	1:1000 (WB)	Cell Signalling	2775S
MYC-tag (pAb)	Rabbit	5% milk	1:5000 (WB) 1:200 (IP) 1:200 (MS)	Proteintech	16286-1-AP
MYC-tag (mAb)	Mouse	5% BSA	1:1000 (WB) 1:200 (IP)	Cell Signalling	2276
p44/p42 MAPK (Erk1/2)	Rabbit	5% BSA	1:1000 (WB)	Cell Signalling	4695S
P-p44/p42 MAPK	Rabbit	5% BSA	1:1000 (WB)	Cell Signalling	4376S
p62	Rabbit	5% BSA	1:1000 (WB)	Cell Signalling	39749S

Table 2. 5 Primary antibody conditions

Information regarding each primary antibody, including the relevant concentrations and diluent for each experiment type.

WB = Western Blot.

IP = Immunoprecipitation.

MS = Mass spectrometry.

Secondary Antibody	Concentration	Company	Product Code
Goat anti-mouse IgG (H+L)-HRP	1:5000	Bio-RAD	1706515
Goat anti-rabbit IgG (H+L)-HRP	1:5000	Bio-RAD	1706515

Table 2. 6 Secondary antibody conditions

Information regarding each secondary antibody, including the relevant concentrations for western blot analysis.

Mutation/Insert	Direction	Primer Sequence (5'-3')
T1195A	Fwd	GAACCGCCTGCCCGCACCCTCCCCTGAGC
	Rev	GCTCAGGGGAGGGTGCGGGCAGGCGGTTC
S1197A	Fwd	CTGCCCACACCCGCCCCTGAGCCAC
	Rev	GTGGCTCAGGGGCGGGTGTGGGCAG
T1195A/S1197A	Fwd	GGGGTGGCTCAGGGGCGGGTGCGGGCAGGCG
	Rev	CCGCTGCCCGCACCCGCCCCTGAGCCACCCC
T1195D	Fwd	GAACCGCCTGCCCGACCCCTCCCCTGAGC
	Rev	GCTCAGGGGAGGGGTCGGGCAGGCGGTTC
T1195S	Fwd	GAACCGCCTGCCCTCACCCTCCCCTGAGC
	Rev	GCTCAGGGGAGGGTGAGGGCAGGCGGTTC
P1196L	Fwd	GAACCGCCTGCCCACACTCTCCCCTGAGC
	Rev	GCTCAGGGGAGAGTGTGGGCAGGCGGTTC
ΔTPSP	Fwd	GAGCCACCCCCCAGCGTG
	Rev	GGGCAGGCGGTTCAAGCC
CTD 1176--1240	Fwd	GACGACCGAACTAGTAGCTTCTTTGGACCATAT
	Rev	TTGCTAGTAGAATTCTCAGTGCCGAAGCTCCTC
PTCH2ΔC-FLAG	Fwd	GACTACAAAGACGATGACGAC
	Rev	CAGGATGGACAGCAGCAC
PTCH1 CTD	Fwd	TTCTTTGGACCATATCCTG
	Rev	GTTGGAGCTGCTTCC

Table 2. 7 Primer sequences

Names and sequences of all primers used for mutagenesis and cloning experiments.

Chapter 3

Phosphorylation of the proximal PTCH1 C-terminal domain in wildtype and cancer-associated mutants

Chapter 3

Phosphorylation of the proximal PTCH1 C-terminal domain in wild-type and cancer-associated mutants

3.1 Introduction

All current structural studies of PTCH1 present the protein mainly as a structurally ordered protein within its transmembrane and extracellular domains, but lack information on the cytoplasmic domains, which are believed to be intrinsically disordered (Kowatsch et al., 2019; Qian et al., 2019). Information regarding the structure of one of these cytoplasmic domains, the CTD, is restricted to prediction tools such as AlphaFold, therefore opening these structural predictions to interpretation. Studies have previously investigated the structure of PTCH1 with a truncated CTD to achieve a suitable protein expression level for structural studies (Kowatsch et al., 2019). Intrinsically disordered proteins (IDPs) or ID domains, such as the PTCH1 CTD (Kowatsch et al., 2019; Qian et al., 2019)lack a defined 3D structure, existing as unfolded, exposed sections of protein which adopt structure upon changing environments or PTMs (Kulkarni et al., 2017). One of these PTMs is phosphorylation which occurs relatively frequently in IDPs (Newcombe et al., 2022), with some examples of single phosphorylation events able to induce complex functional and structural changes for these proteins (Kulkarni et al., 2017; Lenton et al., 2017). Therefore, a large body of research is focused on understanding the significance of these phosphorylation events within IDPs.

The sequence identity between the two vertebrate PTCH proteins, PTCH1 and PTCH2 is roughly 56% but drops to ~20% when comparing just the two CTDs.

Therefore, similarities and differences between the two CTDs can point towards differing functional roles of the two proteins.

Of particular interest in this project is the first PRM of the PTCH1 CTD and, in particular, the phosphorylation states of T1195 and S1197 which have been reported in untargeted whole-cell phosphoproteomic studies (Franz-Wachtel et al., 2012; Ochoa et al., 2020). The PRM in which these two residues sit are predicted by AlphaFold to adopt a PPII helix, as explained in this thesis introduction. Mutation of T1195 and the interspacing P1196 residue has been reported in breast cancer recurrence and in Gorlin syndrome patients (prone to cancer development), respectively, suggesting a potential oncogenic role of each mutation. These mutations could be associated with a PTCH1 loss-of-function phenotype in patients or a *de novo* gain-of-function, indicative of aberrant HH signalling. As phosphorylation is a key regulatory PTM in signalling pathways (Newcombe, E., 2020), phospho-site mutations are of particular interest when investigating protein function and disease progression. Investigating the conservation of the TPSP motif across PTCH1 homologues and across species could provide information regarding the role of the motif in PTCH1 function.

3.2 Aims & Hypothesis

The connection between mutations within the TPSP motif, HH signalling, and cancer development is poorly understood and needs significant investigation. Given the report of phosphorylation in this motif, I hypothesised that mutations of the TPSP motif would perturb the phosphorylation status and structure of the protein region, which consequently affect the tumour suppressor function of PTCH1.

Therefore, the aims of this chapter are:

1. To investigate the conservation of the TPSP motif across species, identifying any links between homologous protein function, as well as links between species-specific PTCH1 function and HH pathway activity.
2. Generate non-phosphorylatable and phosphomimetic mutants in the TPSP motif of PTCH1.
3. Compare the phosphorylation profiles of wild-type and mutant PTCH1 proteins through mass spectrometry analysis.

3.3 Results

3.3.1 Evolutionary conservation of the TPSP motif of PTCH1 and PTCH1-like proteins

The first step was to confirm the presence of the TPSP motif in all available isoforms of *Homo sapiens* PTCH1 and then to determine whether this motif appears in both *Homo sapiens* PTCH2 isoforms 1 and 2. Protein sequence analysis can be a powerful tool to identify homologous proteins, pinpoint unknown protein functions, and guide research of potential structural changes that could occur because of protein mutations (Chung, S.Y. and Subbiah, S., 1996). The strength of the sequence homology is determined by the sequence similarity one protein shares with another. Therefore, sequence identity can be used to infer homology.

Sequence similarity looks for common ancestry, this may suggest regions with important functions, or it may be sheer coincidence. Sequence identity is measured in percentage, sequence alignments with greater than 40% allow to distinguish between similar and non-similar protein pairs; however, this distinction becomes harder and harder as the sequence similarity (or sequence identity) reaches 25-30% (Chung, S.Y. and Subbiah, S., 1996). This range of sequence identity is known as the 'Twilight Zone', where it is difficult to distinguish true protein matches between homologues and false positives, meaning that sequence similarity may be caused by a genuine homologous link, or the sequences may have aligned purely by chance (Rost, 1999). Therein lies the difficulty of aligning sequences.

For the protein sequence searches, several protein databases can be searched, each with positives and negatives associated with them, for example, the non-redundant (nr) protein sequences database is a much larger selection of proteins; however, many of the sequences are unverified and may contain labelling errors, making sifting through the database very difficult (Schnoes et al., 2009; Kahn, 2011). Conversely, the UniProt and SwissProt databases contain protein sequences that are verified, which are updated very infrequently so a search on UniProt will produce far fewer results than the nr database, but the reliability of that data is far greater (Schnoes et al., 2009; Kahn, 2011).

This database search aimed to determine the conservation of the TPSP motif in PTCH related proteins across species, and whether the presence of the motif can infer function. All database searches were done with comparisons to the longest human PTCH1 splice variant: PTCH1 Isoform L (accession number: NP_000255.2), and the searches were carried out using an unbiased approach, encompassing all species types. The proteins collected were PTCH1 proteins from a wide range of species and potential homologues of PTCH1 – the uncharacterised nature or mislabelling of certain proteins made it harder to confirm homology. To collect the proteins, database searches were carried out using the Basic Local Alignment Search Tool (BLAST) provided by NCBI.

Preliminary searches of protein databases – looking at the PTCH sequences of specific homologues from specific species – identified the TPSP motif as being present within *Homo sapiens*, *Mus musculus* and *Drosophila melanogaster* patched proteins. This suggested that the TPSP motif may be prevalent across many species types and the thought was that protein database searches may

uncover potential functional roles or a much larger motif within the PTCH1 CTD. To investigate this, an unbiased approach was used, first searching the whole nr protein database before searching for PTCH proteins within a specific genus/order of species to steadily narrow the search area. There was a specific criterion for selecting each protein, the twilight zone of the searches was defined by those proteins that had a minimum of 30% query coverage – including the CTD – and a sequence identity within that query coverage of at least 30%.

Sequence alignment of human PTCH2 against PTCH1 Isoform L in **Figure 3.1A** shows that the full TPSP motif is not seen in PTCH2, with PTCH2 harbouring a shorter SP motif. As the canonical activity of PTCH2 is significantly reduced in comparison to PTCH1, any sequence differences between the two protein sequences could point to the evidence behind the differences in activity of the proteins. Therefore, the fact that PTCH2 is missing an equivalent of T1195 suggests that T1195 may be integral to PTCH1 activity, and a mutated T1195 could disrupt the sequence and reduce PTCH1 activity.

Additionally, comparisons were made against NPC sterol transporter proteins, which share homology with PTCH1. The TPSP motif is not present in these proteins (data not shown), suggesting it may not play a role in cholesterol transport. This finding agrees with published cryo-EM structures of PTCH1, which show a hydrophobic tunnel involved in cholesterol transport in different regions of PTCH1, unrelated to the CTD. However, the TPSP motif must be required for another critical function of PTCH1 (or must regulate turnover or localisation), since mutations within it are associated with Gorlin Syndrome and cancer.

Sequence alignments were continued, looking at all orders of eukaryote (mammals, fish, birds, reptiles, and amphibians). Analysis of fungi sequences produced only expected or hypothetical proteins which shared significant coverage of the query sequence (<48%). None of the fungi sequences collected exhibited the TPSP motif. When analysing plant sequences, alignment searches produced only hypothetical and expected protein sequences, None of the sequences collected exhibited the TPSP motif.

Analysis of mammalian sequences (*Rodentia, Chiroptera, Soricomorpha* and *Primates*) (**Figure 3.1B**), all shared a high sequence identity with human PTCH1, importantly, exhibiting the TPSP motif. Additionally, when analysing fish (**Figure 3.1 E,** *Osteichthyes* and *Agnatha*) and bird (**Figure 3.1F,** *Aves*) protein sequences shows the conservation of the TPSP motif.

Interestingly, when aligning reptile and amphibian PTCH1 sequences against human PTCH1 (**Figure 3.1C**), there appears to be a change in the sequence to motif TPSS. This sequence change removes a proline residue which may introduce a slight structural change in the CTD and prevent phosphorylation of the serine by (S/T)P-directed kinases. It is important to note that reptiles have a functioning HH signalling pathway, similar to that of humans, with differences occurring in the expression patterns of the HH ligands (Xia et al., 2019). This trend is also seen amongst certain orders of amphibians (**Figure 3.**1**D**) and fish (**Figure 3.1E**), which are also species harbour a functioning HH pathway for limb development (Singh et al., 2015). Figure **3.1G** shows a sequence alignment between human PTCH1 and PTCH-related proteins found in nematodes. The sequence alignment shows that nematode PTCH orthologues do not contain the

TPSP motif, and instead, the sequence contains a polyproline region. An interesting thing to note is that nematodes have functional PTCH proteins that is used for transport (Kuwabara et al., 2000) however, they do not have a complete functional HH pathway. This again suggests that the TPSP motif might not be involved in molecular transport and instead plays a different role in the activation or regulation of the HH pathway.

A limitation associated with this study is that many of the reptile and amphibian and fish sequence alignments, only theoretical or expected protein sequences were available. Consequently, sequence differences may not be an accurate reflection of the true peptide sequence. For example, that the TPSS motif in certain reptilian PTCH1 proteins (**Figure 3.1C**) may not be the true PTCH1 peptide sequence.

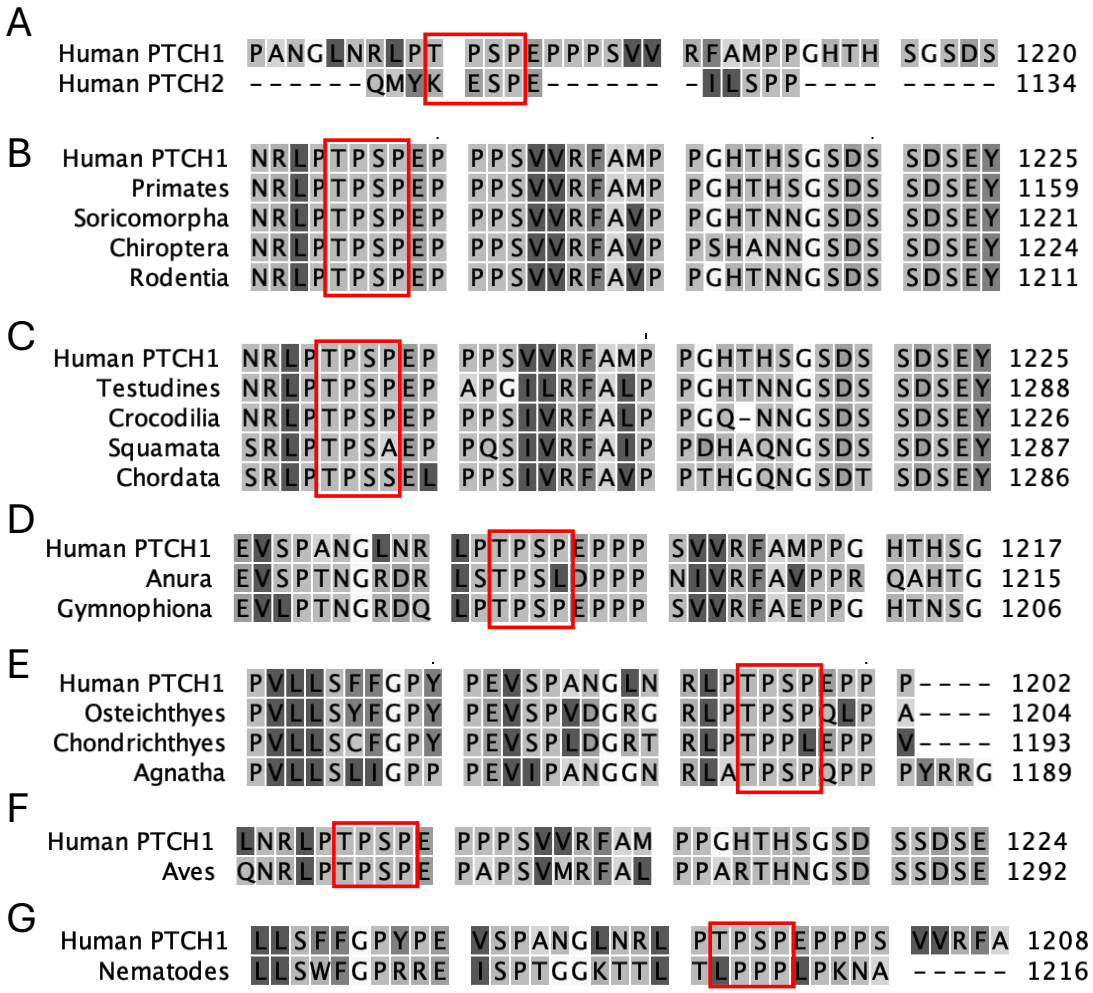

Figure 3. 1 Multiple sequence alignments highlight conservation of the TPSP motif

Sequence alignment between PTCH1 Isoform L (NP_000255.2) and (**A**) Human PTCH2 (Q9Y6C5); (**B**) examples of sequences from orders of mammals that account for >75% of all mammalian species (Primates: NP_001077071.1; Soricomorpha: XP_037349889.1; Chiroptera: XP_054444066.1; and Rodentia: NP_032983.1); (**C**) examples of sequences from all orders of reptiles (Testudines: XP_039401523.1; Squamata: XP_061482451.1; Chordata: XP_026530262.1; and Crocodilia: XP_019410507.1); (**D**) examples of sequences from orders of amphibians where sequence data was available (Anura: MEE6459609.1; Gymnophiona: XP_030049507.1); (**E**) examples of sequences from all orders of fish (Osteichthyes: XP_028661175.2;

Chondrichthyes: XP_060694417.1; Agnatha: BBF90244.1); (**F**) example bird sequence (XP_030368772.1); (**G**) example nematode sequence (NP_001360447.1). Each figure shows a single sequence selected from a minimum of 5 per order of species. All sequences were collected from the non-redundant protein sequences database through NCBI BLAST (Camacho et al., 2009). Sequence alignments were carried out using CLC Sequence Viewer Version 8.

In conclusion, the TPSP motif is conserved in all PTCH1 splicing variants of vertebrates, with the exception of certain reptiles and amphibians where the motif may be found as TPSS, TPSL or TPPL. It is also found in the single Patched isoform of insects, suggesting an important structural/functional role of the TPSP motif, while also suggesting an element of redundancy of P1198 in the function of the TPSP motif. More interestingly, the TPSP motif is replaced by a PPPP or LPPP motif in nematodes which do not possess an HH signalling pathway equivalent, again, potentially uncovering TPSP motif function.

3.3.2 Basal phosphorylation of T1195 and S1197 is detectable in wild-type PTCH1 by mass spectrometry

To confirm the phosphorylation of T1195 and S1197 in the TPSP motif of PTCH1, previously reported in global phosphoproteomic studies, I first set up a reproducible experimental protocol to specifically investigate that region of PTCH1 by mass spectrometry. To do this, a myc-tagged PTCH1 protein (isoform L, of 1447 amino acids) (**Figure 3.2**) was expressed in HEK 293 cells, followed by isolation of myc-PTCH1 from the whole cell lysate by immunoprecipitation with a myc-tag antibody (Proteintech). The presence of PTCH1 within the immunoprecipitate was confirmed by Western blotting using a small aliquot of the immunoprecipitate, the remainder of the sample was submitted to the on-site

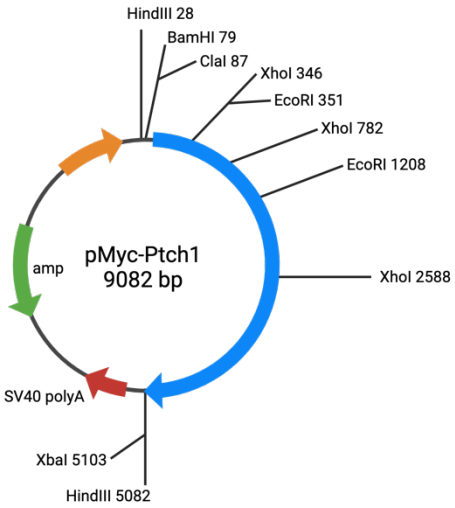

Figure 3. 2 myc-PTCH1 plasmid map

Schematic of the myc-PTCH1 plasmid that was used as the parental plasmid for all TPSP mutations. Cut sites and antibiotic resistance are noted on the plasmid map.

Figure created using BioRender.com

mass spectrometry facility where the sample was processed. analysed using the proteome discovery software (Thermo Fisher Scientific Version 3.0.0757).

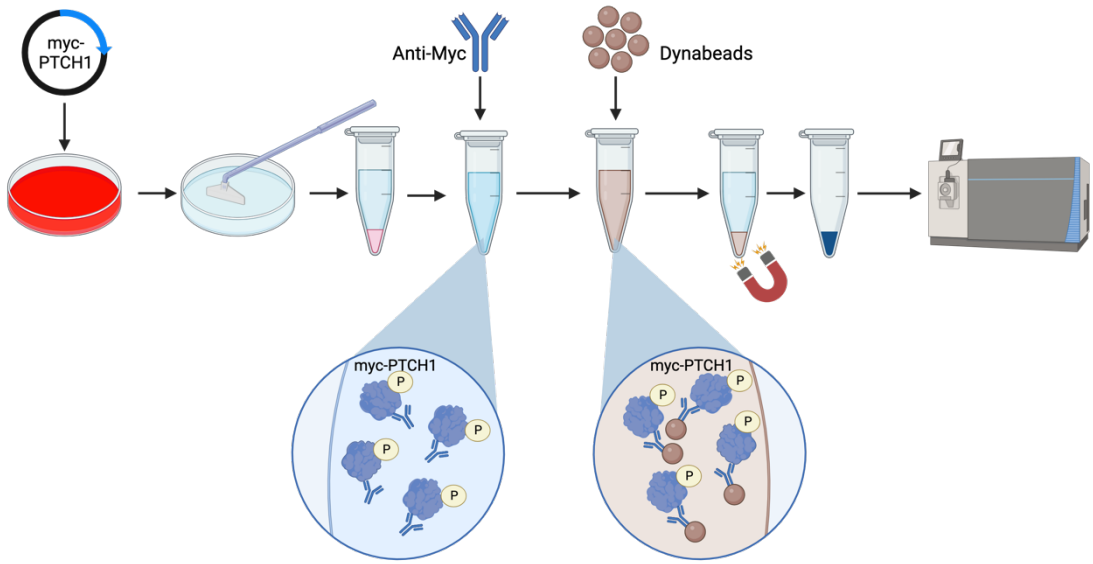

Figure 3. 3 Mass spectrometry experimental workflow

Myc-PTCH1 was over-expressed in HEK293 cells. 24 hours post-transfection, the cells were scraped, lysed and spun down, and the supernatant was collected. Lysates were incubated with an anti-myc antibody followed incubation with protein-G Dynabeads. A magnet was used to isolate the Dynabeads and the supernatant was removed. Laemmli buffer was added to the Dynabeads, which were then heated. The Dynabeads were removed from the Laemmli buffer using a magnet and discarded, the sample was sent for mass spectrometry analysis. Figure created using Biorender.com

This protocol underwent several steps of optimisation to obtain a phosphorylated protein. Initially, only a single plate of HEK293 cells were used to generate a protein sample. This was shown to be an insufficient number of cells to generate a level of protein to be detected by the on-site mass spectrometry machine. Therefore, this was increased to three plates per protein sample which was able to produce enough protein to be detected by the mass spectrometry machine. Next, the optimisation focused on generating a phosphopeptide using a phosphatase inhibitor. Initial tests were unable to detect a phospho-peptide using

the phosphatase inhibitor to the manufacturer's instructions **(**Sigma #P0044). Further experiments used increasing concentrations of phosphatase inhibitor until it was shown to produce a detectable phosphopeptide through mass spectrometry.

Figure 3.4 shows the phosphorylation profile of the proximal CTD of wild-type PTCH1 (residues 1176-1225), the software used (Proteome discovery software ThermoFisher Scientific Version 3.0.0757) detected the presence of a phosphate residue in the first PRM of the PTCH1 CTD which is indicated by the letter 'P' above the sequence. The sequence is monophosphorylated as is indicated in **Table 3.1,** indicating a difference in mass between the phosphorylated an unphosphorylated peptides of 79.97 Da, indicating the presence of a phosphate group (Jagannadham, M.V. and Nagaraj, R., 2008). The presence of two 'Ps' above the sequence is due to the software being unable to distinguish which residue the phosphate group is bound to. Analysis of the data suggests the presence of one phosphate within that peptide; however, it is not possible to determine which residue, T1195 and S1197, is phosphorylated. These results seem contradictory to those from previous phosphoproteome studies which indicate phosphorylation of both T1195 and S1197 (Ochoa et al., 2020); however, the results from the previous studies did not distinguish whether both residues were phosphorylated at the same time. Thus, my PTCH1 targeted data are likely to be a more faithful representation of the phosphorylation state of the TPSP motif. Therefore, following a significant amount of optimising, the decision was taken to progress with further experiments using the results in **Figure 3.4** and **Table 3.1** as the basis.

Given the low confidence in precise assignments of the phosphorylation sites from the mass spectrometry results, I generated site-specific, non-phosphorylatable PTCH1 mutants to establish which of the residues is phosphorylated in growing cells. To generate phospho-dead mutants, alanine substitutions were done to render the mutants incapable of phosphorylation. This involved mutating both residues T1195 and S1197 to alanine. This was done both individually and simultaneously in the same plasmid. From this point onwards, these phospho-dead mutants will be denoted as T1195A, S1197A and T1195A/S1197A.

Additionally, a ΔTPSP mutant was generated in the myc-PTCH1 plasmid which involved removing the TPSP motif. Many difficulties were encountered during the cloning process, the most significant of which was the fact that the region being cloned is a very GC-rich region. These regions have a much higher resistance to denaturation, making it more difficult for the primers to anneal and increased the annealing temperature of the mutagenesis PCR. Additionally, the primers used to amplify GC-rich regions have a much higher propensity to form primer dimers, therefore, reducing the efficiency of primer binding. As a result, a significant portion of time was spent optimising all mutagenesis reactions to successfully overcome these problems.

Plasmid	Sequence	Peptide Mass			
		Unphosphorylated	Phosphorylated	Difference	Phosphorylation State
WT PTCH1	LPTPSPEPPPSVVR	1471.8035	1551.7735	79.97	Mono

Table 3. 1 Proof of mono-phosphorylation of the TPSP motif

The difference in peptide mass between the phosphorylated and unphosphorylated forms of the LPTPSPEPPPSVVR peptide. The software used (Proteome discovery software ThermoFisher Scientific Version 3.0.0757) predicts with high confidence the presence of a phosphate residue on either T1195 or S1197. The data shows a difference in peptide mass of 79.97 which corresponds to the molecular weight of a phosphate group (Jagannadham, M.V. and Nagaraj, R., 2008) This data set is from a single experiment.

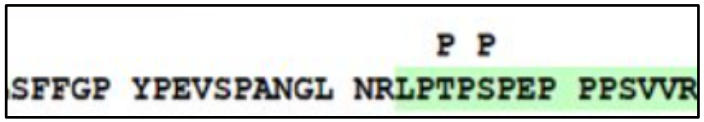

Figure 3. 4 Mass spectrometry analysis of myc-PTCH1 immunoprecipitates

Amino acid sequence of a region of PTCH1 CTD (residues 1176-1225) with identified post-translational modifications. The green highlight represents the sequence coverage from the protein digest. Digest was done with trypsin. The software used (Proteome discovery software ThermoFisher Scientific Version 3.0.0757)predicts with high confidence the presence of a phosphate residue on either T1195 or S1197. The peptide is monophosphorylated, however, the software cannot determine which residue – T1195 or S1197 – is phosphorylated.

3.3.3 T1195 and S1197 mutations do not affect PTCH1 expression level

A comparison of mutant protein expression by western blot showed that the mutations do not have any impact on the protein expression levels, which was further quantified by densitometry analysis of the blots (**Figure 3.5**). This result was expected as previous work demonstrated that, although the CTD is necessary for ensuring PTCH1 stability, only the initial 11 amino acids of the CTD are required for this (Zhang, Y. et al., 2018). Complete deletion of the CTD has been shown to lead to a reduction in protein stability but smaller deletions of the CTD have the contrary effect, increasing PTCH1 stability. As a result, it would not be anticipated that the TPSP point mutants or the microdeletion would influence PTCH1 stability and turnover, a hypothesis which is confirmed by these findings. Phospho-dead (**Figure 3.5**) and microdeletion mutants (**Figure 3.6**) display comparable expression to WT PTCH1.

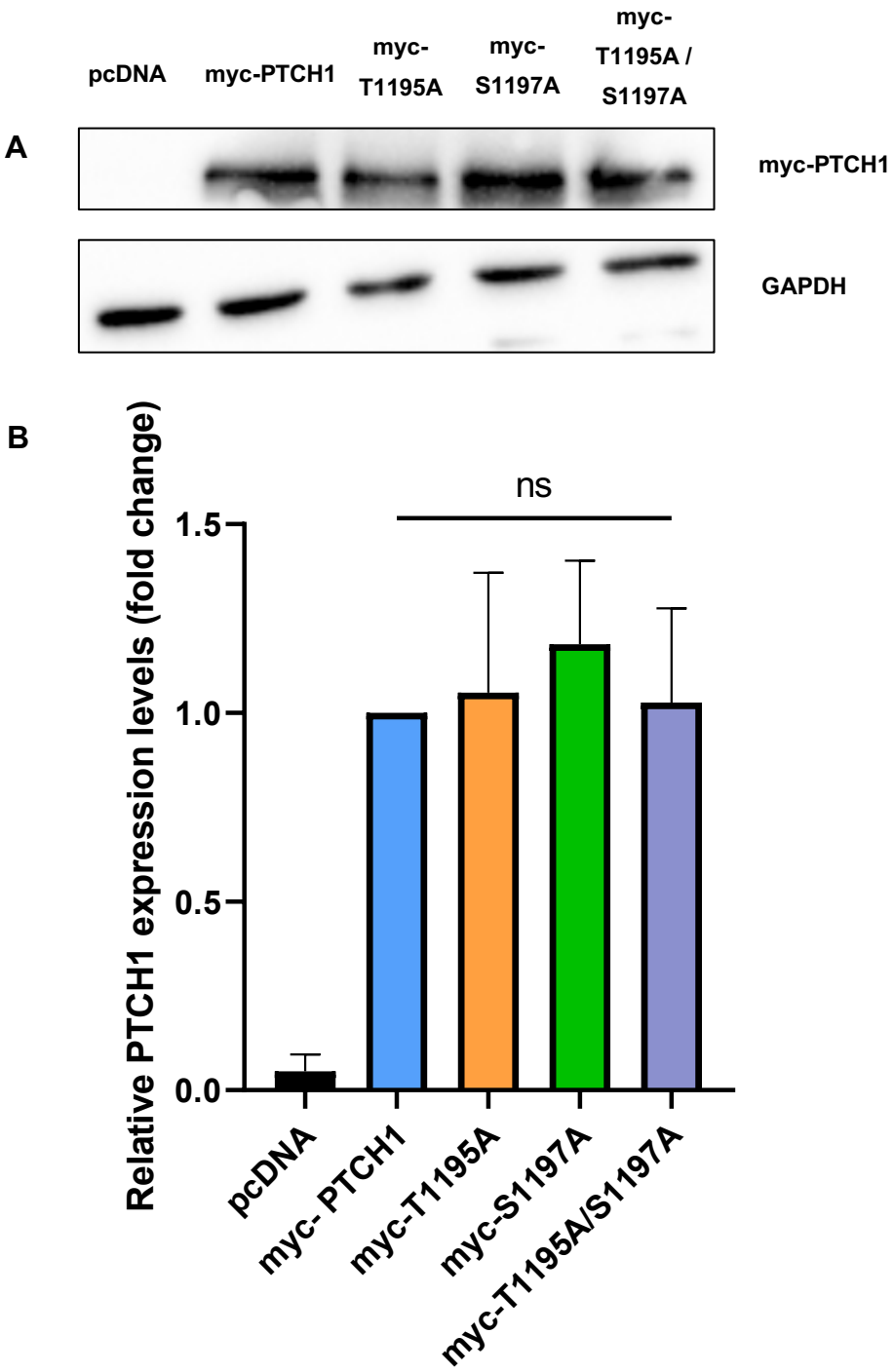

Figure 3. 5 Phospho-dead mutants do not affect PTCH1 protein levels

(A) Western blot confirming the expression of WT PTCH1, T1195A, S1197A and T1195A/S1197A in HEK 293 cells, using anti-myc antibody. Protein loading control GAPDH confirmed total protein per lane. **(B)** Densitometry analysis of western blot of the phospho-dead mutants shown in **(A)** and normalised to GAPDH and expressed as fold change.

N = 3, ns = not significant.

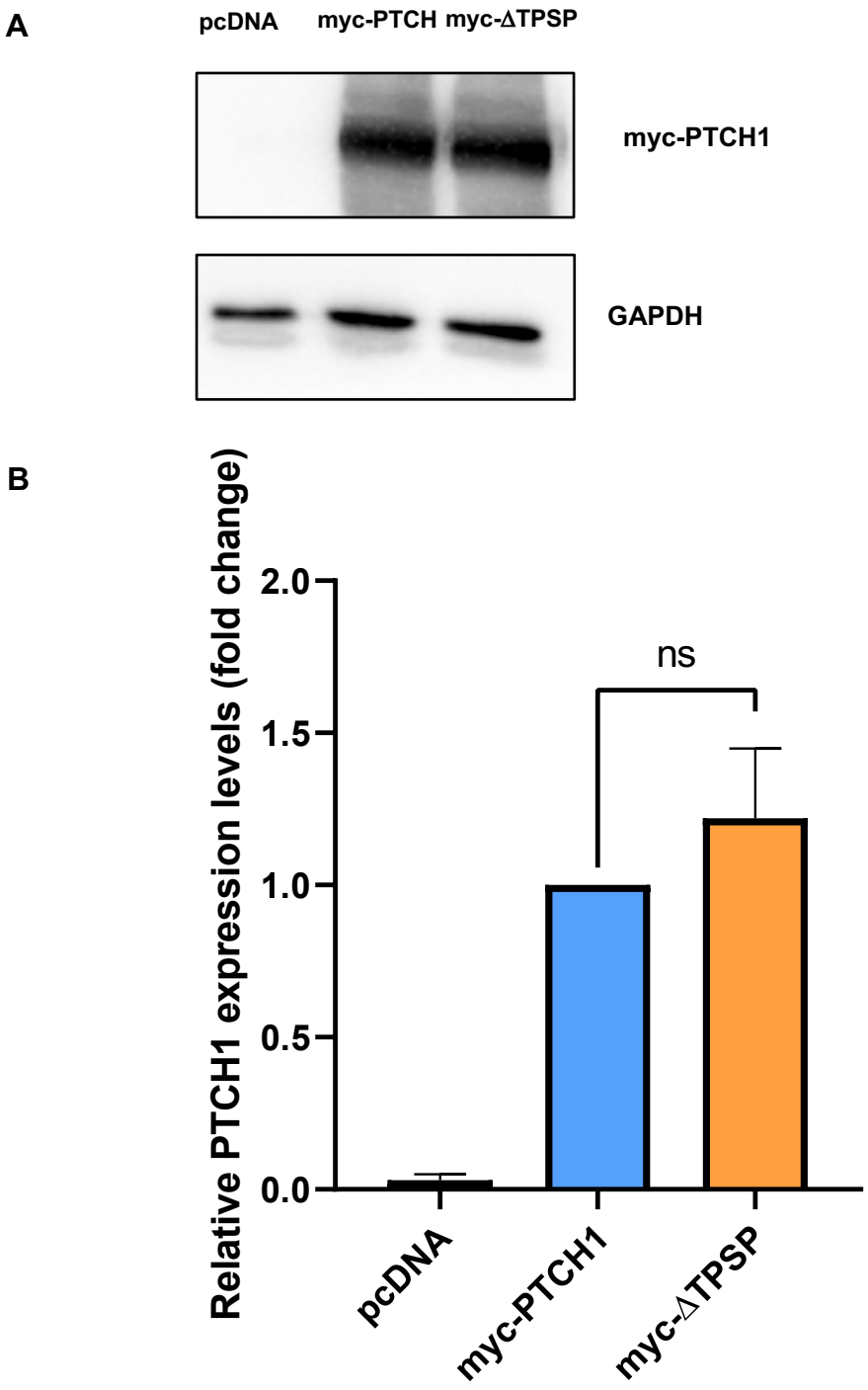

Figure 3. 6 TPSP Deletion mutant does not affect PTCH1 protein levels

(A) Western blot confirming the expression of WT PTCH1 and DTPSP in HEK 293 cells, using anti-myc antibody. Protein loading control GAPDH confirmed total protein per lane. **(B)** Densitometry analysis of western blot of the phospho-dead mutants shown in **(A)** and normalised to GAPDH and expressed as fold change.

N = 3, ns = not significant.

3.3.4 Mass spectrometry analysis of single or double non-phosphorylatable mutants indicate that either residue can be phosphorylated, but both cannot be phosphorylated at the same time

After determining that phospho-dead TPSP mutants do not impact PTCH1 expression or stability, the next step was to analyse the phosphorylation profiles of the two, singularly mutated, phospho-dead proteins, using mass spectrometry. This was to determine whether both T1195 and S1197 are capable of being phosphorylated in cells in growth medium. As previously reported, my results from a single experiment showed that both residues can be phosphorylated (**Figure 3.7** and **Table 3.2)**.

The peptide mass data in **Table 3.2** shows a difference in the peptide mass of 79.96634 Da for all three peptides which corresponds to the addition of a single phosphate group, indicating the possibility that all three peptides exist in a monophosphorylated state under these conditions. Further repeats are required to truly confirm the phosphorylation state of the TPSP motif. The data in **Figure 3.7** highlights the predicted sites of phosphorylation, again indicated by 'P' above each residue. The software used (Proteome discovery software ThermoFisher Scientific Version 3.0.0757) was unable to determine which residue – T1195 or S1197 – is phosphorylated, this is evidenced by the addition of a 'P' above both residues in the sequence. The overall abundance of phosphorylation (in the 4-12% range) is significant in comparison with the abundance of proteins using a phosphorylation-dependent switch such as ERK1/2, which induces proliferation when only 4-5% of the total ERK is phosphorylated.

Remarkably, phosphorylation occurs in only one residue at a time, since the peptide containing the TPSP motif is never detected with two phosphate groups. Perhaps a dually phosphorylated peptide is entropically unfavourable and therefore the phosphorylation states of this motif alternate between one residue and the other. Mutation of S1197 to alanine reduced the phosphorylation abundance, suggesting two possibilities: either S1197 is the preferred phosphorylation site, or it reduces binding of a kinase that phosphorylates T1195.

A limitation of this technique is the inability to precisely locate the phosphate residue, as seen in **Figure 3.7** which is restricted to software prediction. As a result, further investigation through NMR is necessary which is addressed in Chapter 4 of this thesis. Additionally, another limitation with this study is the low-level abundance of phosphorylation for both peptides. In fact, if only 10% of the WT sequence is phosphorylated – as is seen in table 3.2 – then the probability of detecting a doubly phosphorylated peptide would be <1% which may fall below the detection threshold of the mass spectrometry machines. Therefore, the only firm conclusion that can be drawn from this data is that both T1195 and S1197 are capable of being phosphorylated, whilst indicating again that the WT sequence may only exist in a monophosphorylated state.

Plasmid	Sequence	Peptide Mass				Abundance		
		Unphosphorylated	Phosphorylated	Difference	Phosphorylation State	Unphosphorylated	Phosphorylated	% Abundance
WT PTCH1	LPTPSPEPPPSVVR	1472.81075	1552.77709	79.96634	Mono	619119424	65206432	10.53
T1195A	LPAPSPEPPPSVVR	1456.81584	1536.78217	79.96633	Mono	395709120	17393246	4.40
S1197A	LPTPAPEPPPSVVR	1442.80019	1522.76652	79.96633	Mono	395839104	47245592	11.94

Table 3. 2 Relative abundance of phosphorylated peptides in phospho-dead mutants

The ratio of relative abundances of each phosphorylated peptide against its unphosphorylated counterpart for WT PTCH1, T1195A and S1197A. The data shows that the WT sequence appears to exist in a monophosphorylated state (difference of 79.97), with T1195A and S1197A indicating that both residues can be phosphorylated. This data is representative of a single experiment.

T1195A

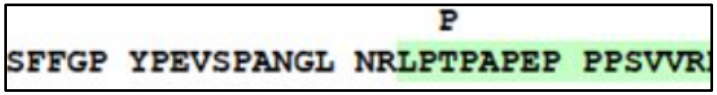

S1197A

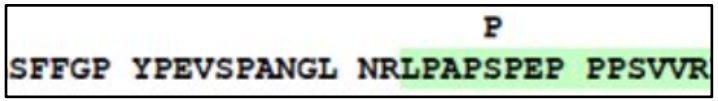

Figure 3. 7 Mass spectrometry analysis of T1195A and S1197A immunoprecipitates

The amino acid sequence of a region of PTCH1 T1195A CTD (residues 1176-1206) and PTCH1 S1197A CTD (residues 1176-1206) with identified post-translational modifications, with their locations predicted with high confidence by (Proteome discovery software ThermoFisher Scientific Version 3.0.0757). The green highlight represents the sequence coverage from the protein digest.

3.3.5 Disease-associated and phosphomimetic mutations do not impact PTCH1 expression or turnover

To assess the functional implications of disease-associated mutations within the TPSP motif (T1195S and P1196L), mutants were generated as described before by site-directed mutagenesis. several mutations were introduced through site-directed, PCR-based mutagenesis. Confirmation of the mutations was done through Sanger sequencing, after which, each plasmid was maxi prepped for future experimentation.

To explore the functional significance of the disease-associated mutants, T1195S and P1196L mutants were generated, as well as a phosphomimetic mutant, T1195D, which mimics the negative charge of a phosphate group, but structurally resembles more closely a phosphorylated serine. This mutant was generated for investigation into the potential effect of constitutive phosphorylation because there is no mutation that faithfully mimics phospho-threonine. This allowed me to determine whether the significance of cancer development linked to the T1195S mutant could be due to changes in the basal phosphorylation state at position 1195 or whether these are because of other, more niche effects of the residue alteration. Expression of the three plasmids was confirmed to be comparable to the parental myc-PTCH1 expression (**Figure 3.8**).

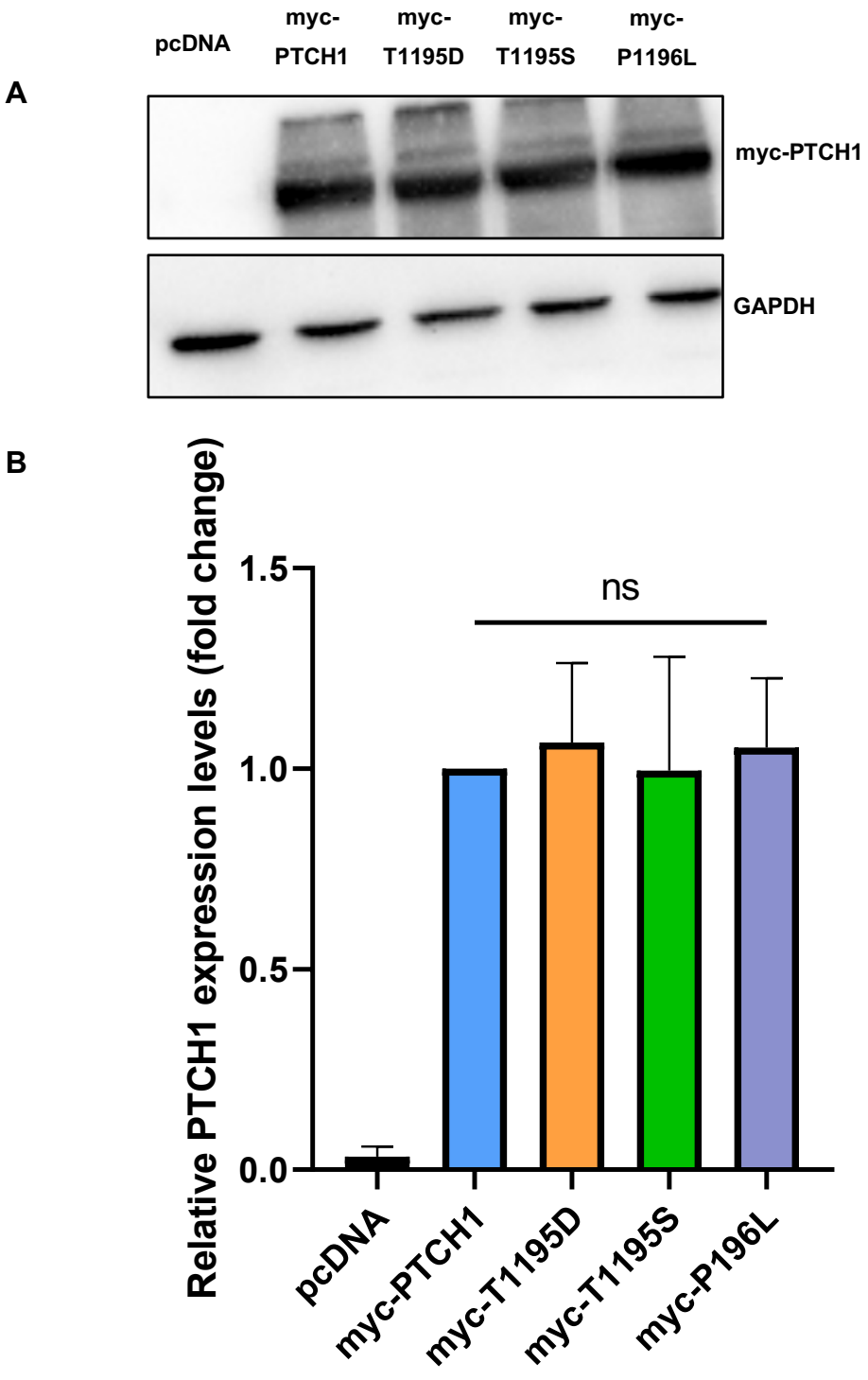

Figure 3. 8 Disease-associated mutants do not affect PTCH1 protein level
(A) Western blot confirming the expression of WT PTCH1, T1195D, T1195S and P1196L in HEK 293 cells, using anti-myc antibody. Protein loading control GAPDH confirmed total protein per lane. **(B)** Densitometry analysis of western blot of the phospho-dead mutants shown in **(A)** and normalised to GAPDH and expressed as fold change.
N = 3, ns = not significant.

3.3.6 Disease-associated mutations change the phosphorylation profile of the TPSP motif of PTCH1

The phosphorylation of serine and threonine residues are incredibly important events in cellular signalling, changes in a protein phosphorylation profile can have drastic impacts on protein function. As a result, it is important to investigate any potential phosphorylation changes that occur because of mutations in or surrounding a phosphorylation site. As shown above, both T1195 and S1197 are capable of being alternatively phosphorylated (**Table 3.2**). To analyse the phosphorylation profile of all mutants, the mutant PTCH1 proteins were overexpressed in HEK293 cells, followed by immunoprecipitation 24 hours after transfection. Immunoprecipitates of mutant PTCH1 proteins were sent for proteomic analysis by mass spectrometry, and immunoprecipitates of WT PTCH1 were sent as a side-by-side control.

Figure 3.9 and **Table 3.3** show the phosphorylation profiles of the first PRM of the PTCH1 CTD in the T1195S and P1196L mutants. The data shows that in the T1195S mutant, the SPSP motif, is monophosphorylated - as evidenced by the difference in peptide mass between the phosphorylated and unphosphorylated peptides (**Table 3.3**) – suggesting the overall phosphorylation profile of the 'TPSP' motif is similar to WT PTCH1**;** however, the location of the single phosphorylation is undetermined, hence the presence of a phosphate group above both residues in **Figure 3.9**.

However, the analysis software used (Proteome discovery software ThermoFisher Scientific Version 3.0.0757) predicted with high confidence that the phosphate sits on either residue 1195 or 1197, although it cannot be said for

certain hich residue of the peptide the phosphate group sits on. Interestingly, the abundance of phosphorylated SPSP peptides is significantly higher than WT PTCH1 in a side-by-side run (**Table 3.3**), suggesting that T1195S could increase the ratio of phosphorylated PTCH1 or reduce the action of a phosphatase. Further repeats are required to confirm this.

In contrast, the P1196L mutant abolished phosphorylation in the TLSP motif (**Table 3.2**). Interestingly, the software predicted with high confidence that this mutant resulted in the detection of phosphorylation at S1203, a residue more C-terminal of the TLSP motif, which is not phosphorylated in WT PTCH1. Additionally, this phosphorylation site was not detected by other phosphoproteome analysis studies (Franz-Wachtel et al., 2012; Ochoa et al., 2020), suggesting that this phosphorylation event is new and specific to the P1196L mutant.

The data becomes especially interesting when analysing it in conjunction with the AlphaFold structure prediction of the PTCH1 CTD. From the AlphaFold rendering, it is suggested that the TPSP motif is positioned in such a way that the threonine and serine residues sit in opposite planes (in a cis-trans configuration), facilitating the potential phosphorylation of both residues. In the case of the P1196L mutant, this configuration could be disrupted by the loss of structural rigidity and stability that comes from the proline residue that sits between the two phosphorylatable amino acids. This could be shifting both the serine and the threonine into the same plane, which could restrict the phosphorylation of either residue. Alternatively, the P1196L mutant may indicate that the interspacing proline is

essential for kinase recognition of the motif, and its mutation impedes phosphorylation.

Notably, the new phosphorylation in S1203 that is detected in the P1196L mutant corresponds to the site of a partial truncation of the CTD seen in several types of cancer that are unable to interact with the autophagy-related protein ATG101 and have an enhanced autophagy phenotype (Caballero-Ruiz et al., 2023).

However, a limitation with this work is that all of this data is derived from a single experiment which limits the robustness and significance of the findings, indeed the observed disparity between the abundances of the WT phosphopeptide (10.5% and 4.9%) shows the need for further repeats of this experiment are needed in order to validate the findings and provide better insights into the TPSP phosphorylation profiles.

Plasmid	Sequence	Peptide Mass				Abundance		
		Unphosphorylated	Phosphorylated	Difference	Phosphorylation State	Unphosphorylated	Phosphorylated	% Abundance
WT PTCH1	LPTPSPEPPPSVVR	1472.81075	1552.77709	79.96634	Mono	135984128	6672453	4.91
T1195S	LPSPSPEPPPSVVR	1458.7951	1538.76144	79.96634	Mono	93574926	1637764	17.50
P1196L	LPTLSPEPPPSVVR	1488.84206	1568.80839	79.96633	Mono	141257418	4169575	2.95

Table 3. 3 Relative abundance of phosphorylated peptides in mutant constructs

The ratio of relative abundances of each phosphorylated residue against its unphosphorylated counterpart for WT PTCH1, T1195S and P1196L. The data shows that both T1195S and P1196L exist in a monophosphorylated state given the difference in the peptide mass between phosphorylated and unphosphorylated peptides This data is representative of a single experiment.

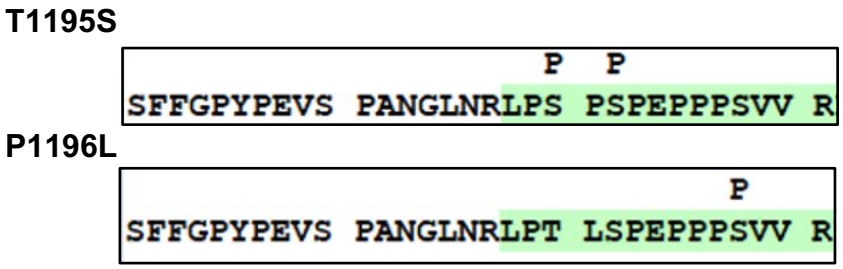

Figure 3. 9 Analysis of TPSP phosphorylation of PTCH1 by mass spectrometry.

The amino acid sequence of a region of PTCH1 T1195S CTD (residues 1176-1225) and PTCH1 P1196L CTD (residues 1176-1206) with identified post-translational modifications, with their locations predicted with high confidence by (Proteome discovery software ThermoFisher Scientific Version 3.0.0757).

3.4 Discussion

Growing evidence demonstrates that the PTCH1 CTD is involved in various non-canonical HH functions (Chen et al., 2018; Chang et al., 2010). Specifically, the PRMs within the CTD have been implicated in several non-canonical functions, with mutation or loss of these PRMs associated with disease development (Chang et al., 2010). Despite this, an area with very little research focus on it is the TPSP motif that sits in the first PRM, surprisingly thid region has been linked to the development of cancers in several different studies (Kawamura et al., 2008; Saito et al., 2015; Wang et al., 2019) necessitating further investigation.

This chapter expands on the previous sequence analysis of the first PRM of the PTCH1 CTD, advancing the understanding of the conservation of the TPSP motif shown by other groups (Chang et al., 2010). Notably, this work highlights the high conservation of the TPSP motif that display a functional, canonical HH signalling pathway, whilst also uncovering its absence in species that do not possess a functional pathway, such as nematodes. Most interesting of all was the discovery that certain reptile and amphibian species harbour a modified sequence (*Chordata*), pointing to the lack of importance of the 'SP' of the TPSP motif for certain reptiles.

Here, I present data that provides significant insights into the phosphorylation profile of the first PRM of the PTCH1 CTD in wild-type and cancer-associated TPSP motif mutants. The phosphorylation profile of wild-type PTCH1, combined with those of the phospho-dead mutants T1195A and S1197A, indicate that both T1195 and S1197 can be phosphorylated but it does not appear to be simultaneous. Therefore, the conclusion of this chapter is that the motif exists in

a monophosphorylated state in growing cells, either phospho-T1195 or phospho-S1197. This data suggests that the designation of both T1195 and S1197 as phosphorylated residues in the basal state by Franz-Wachtel et al (2012) and Ochoa et al. (2020) is likely to be because of an inability of the studies to determine the precise phosphosite location and does not reflect dual phosphorylation.

With T1195S being the predominant mutation in disease progression, and the lack of S1197 mutations in cancer, my initial hypothesis was that T1195 would be most likely the only phosphorylated. This combined with the altered TPSS motif seen in certain reptiles suggesting that the 'TP' is the more important residue pair. When analysing the phosphorylation profile of the disease-associated mutations, it is interesting to note that while their presence in cancer patients would suggest that both mutations result in loss-of-function of the PTCH1 phenotype, they show vastly different and opposing phosphorylation profiles in the first PRM of their respective CTDs.

The heightened phosphorylation of the mutant residue in T1195S could suggest a perturbed negative regulation of motif phosphorylation or an enhanced sensitivity to phosphorylation either from the same kinase or from a different kinase. Mutation of the threonine to a serine could alter the kinase or phosphatase affinity, increasing the abundance of phosphorylated protein. The absence of phosphorylation within resides 1195-1198 seen in the P1196L mutant suggests that phosphorylation of this motif may not be the driver of a loss-of-function phenotype, instead, suggesting that it could lead to a gain-of-function or different mechanisms of action in T1195S and P1196L mutants, perhaps through

disruptions to potential binding partners interactions. Alternatively, whilst the absence of phosphorylation between residues 1195-1196 may not confer the loss-of-function phenotype, the additional phosphorylation of S1203 might. This additional phosphorylation could be a result of steric changes that are caused by the loss of minor structural rigidity that would normally be provided by the interspacing proline residue. These possibilities are explored in future chapters.

Mass spectrometry is a useful tool to use when analysing changes in protein phosphorylation profiles (McLachlin, D.T. and Chait, B.T., 2001; Garcia et al., 2005). The mass spectrometry data builds on previous work by Ochoa et al. (2020) and Franz-Wachtel et al (2012), utilising a similar methodology and the same cell type to further understand the phosphorylation dynamics of the TPSP motif. The mass spectrometry data provides an essential starting point into the understanding of the TPSP motif and how single changes in its peptide sequence can cause significant disease development.

However, limitations in the repeatability of this data prevent the formation of conclusive insights from this chapter. Further repeats are required to fully understand any changes in the phosphorylation profile. The data do however offer an insight into the dynamics of PTCH1 phosphorylation, contributing to a better understanding of the PTCH1 CTD, whilst raising questions about the relative significance of each phosphorylation event. It points to a potentially very intricate but dynamic phosphorylation homeostasis that, when disturbed, can result in disease development.

Chapter 4

Investigation into the structure of the proximal region of the PTCH1 CTD by nuclear magnetic resonance and the structural significance of TPSP phosphorylation

Chapter 4

Investigation into the structure of the proximal region of the PTCH1 CTD by nuclear magnetic resonance and the structural significance of TPSP phosphorylation

4.1 Introduction to protein NMR

4.1.1 Brief introduction to protein NMR

Protein nuclear magnetic resonance (NMR) is an extremely useful technique that can be used to elucidate protein structure, composition, and modifications (Bax and Clore, 2019). Briefly, NMR spectroscopy utilises a magnetic field to manipulate the magnetic properties of isotopic nuclei to aid structural analysis. Spinning atomic nuclei generate magnetic fields which are normally oriented randomly, however, when placed in a strong magnetic field, they align either with or against the magnetic field (Marion, D., 2013). Oscillation between these two states is known as the Larmor procession (van Geuns et al., 1999). ^{1}H, ^{15}N and ^{13}C each have a spin state of ½ (Marion, D., 2013). These magnetic moments do not remain stationary and instead, rotate around the Z axis. The frequency of this procession, known as the Larmor frequency, is dependent on the strength of the magnetic field and is specific to each nucleus type (van Geuns et al., 1999). The application of a minimal, oscillating magnetic field perpendicular to the Z axis, known as radiofrequency, disrupts this alignment, causing the nuclei to emit electromagnetic radiation which can be detected and produce a peak specific to each isotopic nucleus (Marion, 2013).

The typical types of NMR spectra that can be produced are either 2D or 3D (Howard, M.J., 1998). To analyse protein structure, 3D NMR-spectroscopy

experiments are required. With regards to protein NMR and this specific chapter, the three isotopes that are used are ^{1}H, ^{13}C and ^{15}N. When exposed to a magnetic field, ½-spin nuclei such as ^{13}C and ^{15}N adopt an orientation that can occur in one of two states: either a low-energy state (α-state) or a high-energy state (β-state) (Roldós, V. et al. 2011). The α-state is aligned in the same direction as the applied magnetic field, the β-state is aligned in the opposite direction. Each nucleus then absorbs a certain amount of energy, causing the atom to reach an excited state, the atoms fluctuate between the a- and β-states. The greater the magnetic field (measured in MHz), the greater the energy difference between the α- and β-states, and the greater the sensitivity of the NMR spectra (Bax and Clore, 2019). Spectra for this chapter were collected using 600 MHz and 750 MHz machines. The peak that is produced from each residue can be impacted by several factors, including, the neighbouring residues and the level of shielding which is given to them by their associated electrons and the electrons from neighbouring atoms, meaning that each nucleus has a unique fingerprint that conforms to certain similarities that are shared with the same nuclei type, but that that differ depending on the surrounding atoms (Hu et al., 2021).

Protein structure analysis begins with generating a ^{1}H-^{15}N HSQC spectrum, using isotopically labelled hydrogen (^{1}H) and nitrogen (^{15}N). To generate these spectra, magnetisation is transferred from hydrogen to the attached ^{15}N via what is known as J-coupling (Barnwal et al., 2007). The signal is detected when the magnetisation is transferred back from the ^{15}N to the ^{1}H. From this, each amino acid produces its own individual peak that is displayed on a spectrum (O'Connell et al., 2009).

To be able to assign a residue to each peak, ^{13}C labelled proteins must be used (O'Connell et al., 2009). The use of isotopically labelled carbon allows for the introduction of a third axis onto the spectrum, making it a 3D spectrum. Each axis displays the resonance from each atom type: the x-axis displays the ^{1}H resonance, the y-axis displays the ^{15}N resonance and the z-axis displays the ^{13}C resonance. Each type of 3D spectrum associated with protein NMR provides peaks for the Cα, Cβ and CO atoms, which can be collated together to assign each peak in the ^{1}H-^{15}N HSQC (O'Connell et al., 2009).

Each amino acid has a range of values that can be applied to its Cα and Cβ atoms. For example, the chemical shift of the Cα of threonine often displays a range of 68-72 ppm with its most common occurrence at 69 ppm. The Cβ occupies a frequency range of 59-66 ppm, most commonly appearing at 61 ppm. This information can be used to predict assignments (**Figure 4.1**).

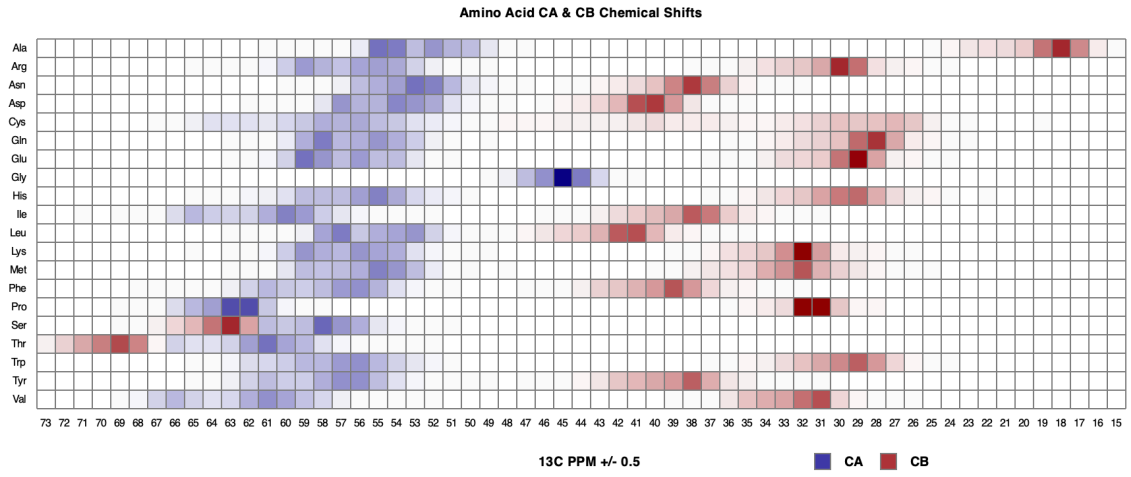

Figure 4. 1 Amino acid chemical shifts

Chart showing the range of chemical shifts for the Cα (blue) and Cβ (red) peaks associated with each amino acid. Figure taken from CcpNmr Analysis (2.5.2) (Vranken et al., 2005).

4.1.2 Challenges of studying IDP structure

The CTD of PTCH1 is predicted to be intrinsically disordered (Kowatsch et al., 2019). IDPs lack a stable tertiary structure and therefore are difficult to crystalise and analyse through x-ray crystallography and cryo-EM, techniques which rely on the formation of a stable structure or few conformers for analysis. Structures of IDPs using these methods require a binding partner which, unfortunately, only presents the structure of the IDP in one of many possible conformations. Therefore, NMR is the more appropriate technique used to study IDPs. NMR spectra can be used to provide a timescale of the dynamics of a protein, whilst also providing exact details of the overall structure it may adopt, and information on any changes to specific shifts of residues in response to the introduction of binding partners or being subject to PTMs, providing a general picture of structural trends and moieties. Studying the structure of IDPs comes with challenges, for example, the flexibility of an IDP can cause the peaks on NMR spectra to overlap as their chemical shifts are similar as a result of their similarly disordered environment, making spectra difficult to interpret, and peak alignment more challenging (Sahu et al., 2014). The unstructured nature of IDPs proteins causes the peaks to overlap instead of conforming to specific areas of the spectrum as is expected with a more structured protein. Therefore, analysis of IDPs and IDRs tends to be restricted to shorts segments of protein <100 amino acids. IDPs are also more exposed in their nature, due to restricted shielding from neighbouring residues that α-helix and β-sheet residues may be afforded, therefore, IDPs are much more susceptible to attacks from proteases (Rezaei-Ghaleh et al., 2012).

4.1.3 Structural analysis of the PTCH1 CTD

So far, structural studies of PTCH1 have been limited to its transmembrane and extracellular domains, such as the cryo-EM structure of PTCH1 produced by Zhang et al. (2018). Information regarding the structure of the CTD is largely limited to the use of structure prediction tools such as AlphaFold, which uses sequence data to predict the most likely structure adopted by the proteins in the absence of binding partners. The CTD is known to be intrinsically disordered (Kowatsch et al., 2019; Qian et al., 2019); however, it is unknown the extent of minor structural motifs that are present. These could likely adopt a more rigid structure when environmental conditions or binding partners are present. Therefore, this chapter presents a more in-depth structural analysis of the proximal region of the PTCH1 CTD with a particular focus on the TPSP motif within the first PRM and the possible kinases responsible for phosphorylating that motif.

4.2 Aims & Hypothesis

The aims

1. To produce recombinant PTCH1 CTD – residues 1176-1240 – tagged with a GB1 solubility tag, followed by isotope labelling, isolation and purification for NMR spectroscopy.
2. To confirm the disordered nature of the PTCH1 CTD through NMR spectroscopy. Analyse chemical shifts to identify regions of the CTD that have partial order or secondary structure.
3. To test the ability of one or more candidate kinases to phosphorylate the TPSP motif.

4.3 Results

4.3.1 Construction of pETM6T1 GB1-PTCH1$_{(1176-1240)}$ plasmid vector

To first investigate the structure of the PTCH1 CTD, a bacterial expression plasmid had to be generated. A significant portion of time was needed to optimise the cloning conditions for this construct, using a plasmid encoding the entire PTCH1 CTD (pETM6T1 GB1-PTCH1 CTD), previously generated by Fraser Exley under supervision of Dr Mark Richards (University of Leeds) as the backbone. Briefly, I excised the PTCH1 CTD out of the pETM6T1 construct before amplifying my region of interest (residues 1176-1240) and ligating that into the plasmid backbone. I chose to use this method instead of amplifying the desired section of the vector through PCR amplification to reduce the chances of erroneous DNA replication by the polymerase. The plasmid backbone contains a His tag to aid purification, a TEV cleavage site, a GB1 tag which aids solubility and the PTCH1 sequence. The construct contains a TEV protease recognition site: ENLYFQ*(S/G/A/M/C/H) where the asterisk indicates the TEV cut site. The neighbouring amino acid can be any of the residues listed in the parentheses, however, the most efficient cut site is generated when the residue is a serine, which is the case for this construct. The TEV protease is a highly specific cysteine protease that recognises the site and is used for the removal of affinity tags such as the NusA(His_6) affinity tag that will be used in these experiments. The NusA(His_6) tag is a bulky affinity tag that is used in purification because of its interaction with Ni^+ columns. The strong affinity of the tag to the Ni^+ ions allows for improved purification of the target protein, which can be eluted out using increasing concentrations of imidazole ($C_3N_2H_4$), a cyclic organic compound that outcompetes the NusA(His_6) tag, with the Ni^+ ions to release the tagged protein from the column. The function of the GB1 protein fused to the protein of interest

is to increase its solubility, allowing recombinant proteins to remain in solution during experimentation, which is essential for NMR experimentation.

The aim was to express the PTCH1 CTD region including residues 1176-1240 (**Figure 4.2**). The sequence chosen encompassed the $TPSP_{1195-1198}$ motif as well as only additional SP motif in the CTD, $SP_{1185-1186,}$ to analyse potential influences on the surrounding residues caused by modifications to the TPSP motif or to S1185. Successful cloning of the construct fused in frame N-terminally to NusA(His_6) and GB1 was confirmed by Sanger Sequencing.

4.3.2 Purification of GB1-PTCH1$_{(1176-1240)}$

Production of the GB1-$PTCH1_{(1176-1240)}$ protein was done by transforming BL21 (DE3) cells, followed by induction of protein expression using 0.5M IPTG. The protein was isolated by affinity chromatography using a HisTrap column using an Äkta system and the NusA tag was cleaved overnight through incubation with TEV protease. The samples were run through the Äkta again to remove the His-NusA tag. **Figure 4.3A** shows the lysate pre- and post-TEV cleavage, showing two distinct bands in the cleaved samples representing the GB1-$PTCH1_{(1176-1240)}$ at 14 kDa and a band at 55 kDa representing the NusA tag. The figure also shows the flow-through which shows a band consistent with the 14 kDa protein as well as some residual NusA. **Figure 4.3A** also shows a selection of fractions that were collected from the Äkta that represent the acquisition of isolated GB1-$PTCH1_{(1176-1240)}$. The flow-through was pooled with the necessary collected fractions and run on a size exclusion chromatography (SEC) column to further purify the GB1-$PTCH1_{(1176-1240)}$ protein, fractions were collected from the Äkta and analysed through SDS-PAGE. **Figure 4.3B** shows the sample pre-SEC, indicating the two

distinct proteins, followed by aliquots from a selection of the collected fractions, indicating successful purification of the GB1-PTCH1$_{(1176-1240)}$ protein. These fractions were collected and concentrated down to 650 μM for NMR analysis.

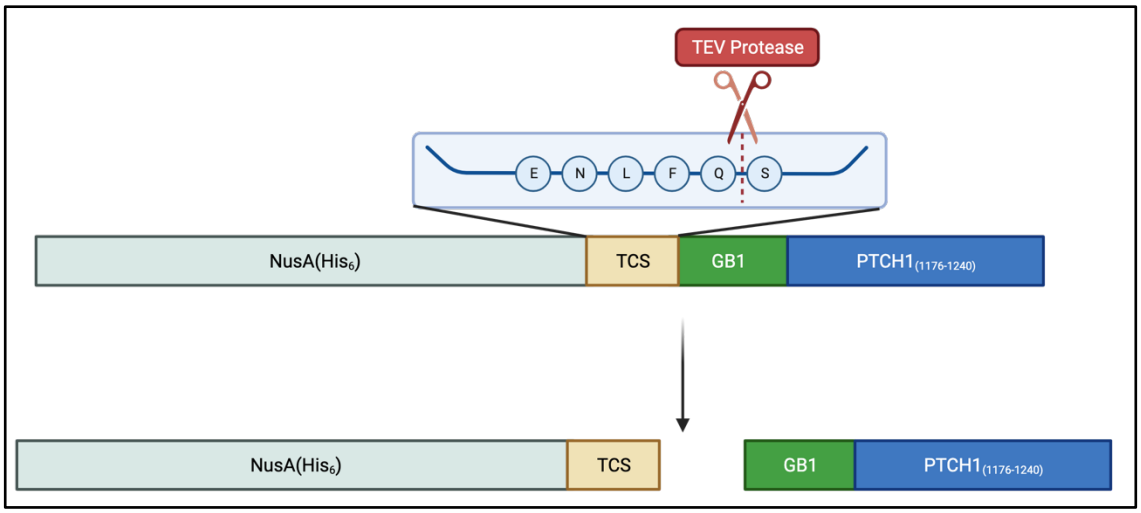

Figure 4. 2 Schematic representing cleavage by TEV protease

The original NusA(His$_6$)-GB1-PTCH1$_{(1176-1240)}$ construct was cleaved using TEV protease, after which the target protein was eluted and collected for analysis. Figure generated using BioRender.com.

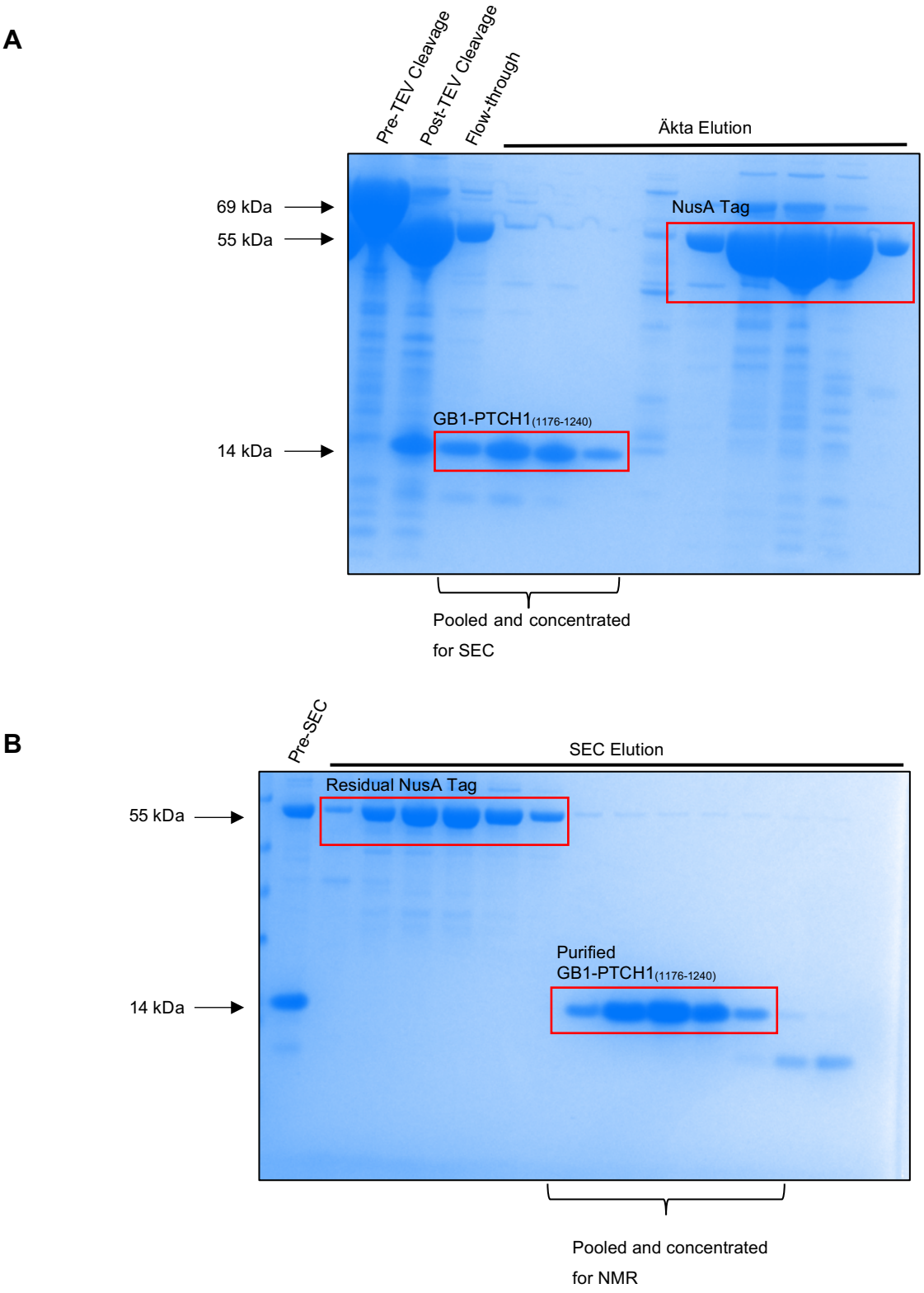

Figure 4. 3 Figure Coomassie staining of purification blots

Coomassie stains indicating **(A)** post-TEV cleavage, clear cleavage of the NusA tag from the GB1-PTCH1$_{(1176-1240)}$ protein and **(B)** post-size exclusion, indicating the isolation of purified GB1-PTCH1$_{(1176-1240)}$ following the removal of impurities and excess NusA tag.

4.3.2 PTCH1$_{(1176-1240)}$ ^{1}H-^{15}N-HSQC shows high levels of disorder within the proximal region of the PTCH1 CTD

To begin with, a ^{1}H-^{15}N-HSQC was generated using a ^{15}N-^{13}C-labelled GB1-PTCH1$_{(1176-1240)}$ construct (**Figure 4.4**). The spectrum from shown in **Figure 4.4** was obtained at 10°C and represents an unassigned GB1-PTCH1$_{(1176-1240)}$ protein – peaks in red – and a previously obtained spectrum of the GB1 tag alone – peaks in black. The spectrum in **Figure 4.4** shows a low dispersion of peaks indicated by a dashed box. Most of the surrounding peaks overlap well with a known GB1 fingerprint spectrum seen in black. The doublet peaks detected from the peaks of the side chain -NH_2 groups of glutamine and asparagine appear in the top right corner of the spectrum. The peaks associated with the GB1 solubility tag are more dispersed across the ^{1}H dimension, and the majority of the peaks associated with PTCH1$_{(1176-1240)}$ are clustered together in the centre of the spectrum. As mentioned before, this clustering is indicative of an IDP (Dyson, H.J. and Wright, P.E., 2021), confirming, as expected, that the proximal region of the CTD is highly disordered. Three additional ^{1}H-^{15}N HSQCs were recorded at 15°C and 20°C to easily transfer assignments across from 10°C to 20°C for later experiments such as the phosphorylation of the CTD which may require temperature variation.

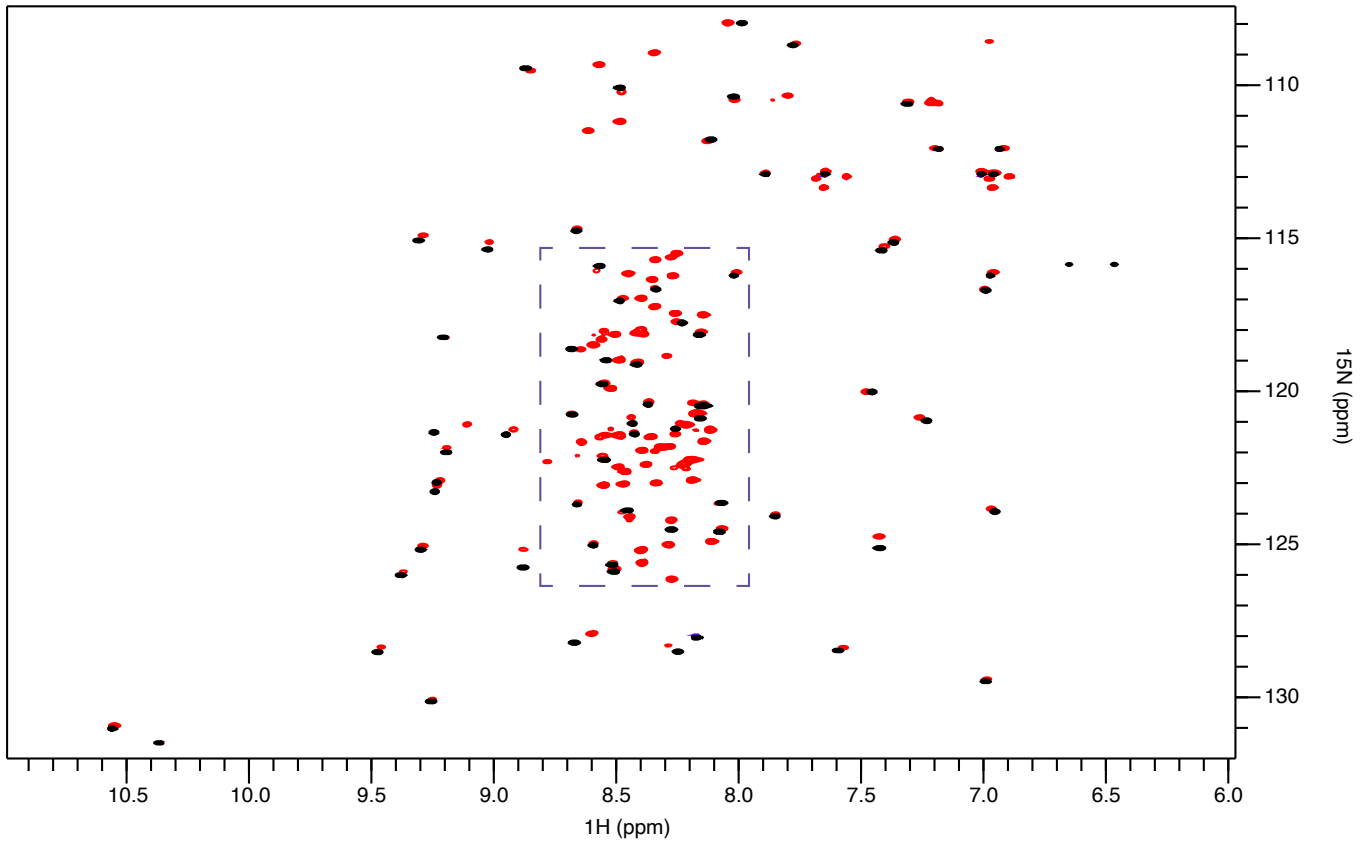

Figure 4. 4 Unassigned ^{1}H-^{15}N HSQC spectrum for GB1-PTCH1$_{(1176-1240)}$

Spectrum ^{1}H-^{15}N HSQC spectrum of the GB1-PTCH1$_{(1176-1240)}$ protein (red) with a previously obtained ^{1}H-^{15}N HSQC spectrum of the GB1 fusion tag (black). The disordered region of the protein is indicates with a dashed box in the centre of the spectrum. The experiment was run on a 600Hz actively shielded Oxford Instruments NMR magnet, the spectrum was recorded as 10°C.

4.3.3 Peak assignment of the proximal region of the PTCH1 CTD

The next stage was to assign each residue to a peak using a selection of 3D, ^{1}H-detected experiments using a dually isotopically labelled (^{15}N and ^{13}C) GB1-PTCH1$_{(1176\text{-}1240)}$. The spectra recorded were HNCA, HNCO, HNCACB, HNCACO, and HNCOCA at 10°C and pH 6.5. These spectra provided the necessary data for ^{13}C atoms in each residue, they were combined for the accurate assignment of a peak to each residue except the proline residues which have no free amide group to produce a signal for a peak. The images in **Figure 4.5** show how sequential assignments can be done by aligning peaks in the same shift region and correlating them to their expected shift pattern as seen in **Figure 4.5**. Triple resonance experiments link each peak in my HSQC to a carbon nucleus, by matching the carbon shift between different picks I made sequential links between adjacent residues within the sequence, characteristic shifts for certain residue types provide fixed points to match onto the specific sequence (**Figure 4.5)**. Only when all three pairs match is it likely to be a good link. I chose for the assignment of this protein to begin at residue 1240 at the CTD of the protein as it is known that the C-terminal residue produces a very clean, distinct peak on the ^{1}H-^{15}N HSQC (as indicated in **Figure 4.4**). As a result, the assignment was done working back from this point until a proline residue was reached. Once this occurred, the assignment was started at a different residue with a characteristic shift (**Figure 4.**1). **Figure 4.6A** shows the completed assignment for the ^{1}H-^{15}N HSQC for the GB1-PTCH1$_{(1176\text{-}1240)}$ protein, focusing on the disordered area of the protein (**Figure 4.6B**) and the assignment of the TPSP motif. Within the IDP fingerprint region, there is some peak overlap and peak broadening caused by the flexibility of the IDP, making the assignment of some residues particularly difficult (**Tables 4.1 and 4.2**).

Residue Number	Residue	H	N	C	CA	CB
1	Gly	-	-	-	-	-
2	Ala	8.66	123.63	177.33	52.29	19.66
3	Met	8.4	119.02	175.47	55.43	33.79
4	Ala	8.49	125.77	174.57	50.81	21.84
5	Gln	8.14	118.08	175.35	55.54	30.73
6	Tyr	9.36	125.84	175.08	57.13	42.99
7	Lys	9.19	121.87	173.15	55.41	36.19
8	Leu	8.51	125.68	174.14	52.68	42.4
9	Ala	9.25	130.07	175.15	50.66	19.73
10	Leu	8.55	122.15	175.41	54.43	42.56
11	Asn	8.87	125.19	174.87	51.68	38.56
12	Gly	8.01	110.45	173.38	44.73	-
13	Lys	9.1	121.1	178.53	59.05	32.69
14	Thr	8.84	109.53	173.94	62.14	69.65
15	Leu	7.42	124.73	173.76	55.08	43.69
16	Lys	8.26	124.18	176.08	54.31	34.87
17	Gly	8.46	110.18	171.73	45.04	-
18	Glu	8.53	119.73	175.43	54.79	33.77
19	Thr	8.58	116.06	172.26	60.42	69.76
20	Thr	8.12	111.91	174.06	59.99	73.32
21	Thr	9.02	115.14	171.18	62.38	69.84
22	Glu	8.06	124.49	176.07	54.87	31.26
23	Ala	9.28	125	177.57	51.4	23.88
24	Val	8.65	114.73	175	62.96	32.14
25	Asp	7.36	115.06	174.45	52.81	41.82
26	Ala	8.42	121.37	179.16	54.6	17.48
27	Ala	8.13	120.45	180.98	54.73	17.86
28	Thr	8.34	116.62	176.19	66.93	67.94
29	Ala	6.98	123.83	177.12	54.94	17.47
30	Glu	8.46	116.96	177.22	59.65	29.18
31	Lys	7	116.7	180.06	59.72	32.32
32	Val	7.27	120.85	179.83	66.03	31.79
33	Phe	8.44	120.84	178.34	56.68	37.45
34	Lys	9.23	123.09	179.56	59.68	31.61
35	Gln	7.48	120.01	177.06	58.67	28.18
36	Tyr	8.24	121.05	178.97	61.84	38.49
37	Ala	9.21	122.91	179.3	56.23	17.86
38	Asn	8.26	117.74	179.25	56.9	38.87
39	Asp	8.91	121.28	177.06	56.9	40.03
40	Asn	7.41	115.28	173.97	53.7	40.06
41	Gly	7.77	108.64	174.23	47.05	-
42	Val	8.16	120.7	173.89	61.99	33.16

43	Asp	8.58	127.85	174.5	52.47	43.33
44	Gly	8.04	107.94	171.79	45.56	-
45	Glu	8.19	120.45	177	55.45	31.47
46	Trp	9.44	128.32	177.05	57.88	30.28
47	Thr	9.28	114.92	172.68	60.52	72.35
48	Tyr	8.67	120.81	173.27	56.93	41.58
49	Asp	7.57	128.39	173.26	51.83	43.04
50	Asp	8.58	124.98	178.21	56.39	41.8
51	Ala	8.35	120.33	179.71	55.09	18.35
52	Thr	6.99	103.42	175.13	60.35	70.33
53	Lys	7.85	123.98	174.76	57.53	30.59
54	Thr	7.31	110.63	174.76	62.09	71.98
55	Phe	10.35	131.41	174.22	57.31	42.32
56	Thr	9.19	118.25	172.79	61.54	70.85
57	Val	8.09	123.7	173.81	58.45	32.74
58	Thr	8.47	123.93	173.85	60.96	70.12
59	Glu	8.27	128.25	175.99	56.45	31.48
60	Thr	8.62	118.56	174.48	61.98	69.86
61	Ser	8.54	118.27	174.49	58.53	-

Table 4. 2 GB1-tag chemical shifts

This is a table of chemical shifts of all peaks assigned to the GB1-tag, unambiguously from multiple 3D spectra of ^{1}H-^{15}N-^{13}C GB1-PTCH1$_{(1176\text{-}1240)}$. Missing shifts are due to peak overlap and peak broadening making it difficult to assign unambiguously.

Residue Number	Residue	H	N	C	CA	CB
1176	Ser	-	-	173.77	58.25	63.77
1177	Phe	8.21	122.35	175.09	57.99	-
1178	Phe	8.23	122.41	175.38	57.35	39.86
1179	Gly	7.79	110.32	171.34	44.5	-
1180	Pro	-	-	176.53	62.97	-
1181	Tyr	8.25	121.37	174.01	55.76	38.01
1182	Pro	-	-	176.69	63.08	-
1183	Glu	8.62	121.68	176.5	56.54	30.19
1184	Val	8.27	121.76	175.92	62	32.92
1185	Ser	8.54	121.38	172.8	56.27	63.34
1186	Pro	-	-	176.98	63.3	-
1187	Ala	8.43	124.08	177.79	52.85	18.92
1188	Asn	8.33	117.22	175.82	53.22	38.83
1189	Gly	8.34	108.93	174.23	45.56	-
1190	Leu	8.11	121.28	177.21	55.33	42.22
1191	Asn	8.47	118.97	174.79	53.26	38.68
1192	Arg	8.2	121.08	175.98	55.8	30.85
1193	Leu	8.38	125.15	175.18	53.05	41.49
1194	Pro	-	-	176.74	62.84	-
1195	Thr	8.4	118.02	172.86	59.92	69.83
1196	Pro	-	-	176.71	63.05	-
1197	Ser	8.58	118.43	172.64	56.48	63.24
1198	Pro	-	-	176.65	62.99	-
1199	Glu	8.46	122.98	174.04	54.23	29.66
1200	Pro	-	-	-	-	-
1201	Pro	-	-	-	-	-
1202	Pro	-	-	176.96	-	-
1203	Ser	8.43	116.09	174.58	58.42	63.68
1204	Val	8.17	122.12	175.88	62.17	32.91
1205	Val	8.29	125.02	175.77	62.37	32.89
1206	Arg	8.38	125.52	175.6	55.75	31.06
1207	Phe	8.3	121.75	174.99	57.39	39.81
1208	Ala	8.26	126.09	176.88	51.97	19.39
1209	Met	8.34	121.43	173.86	53.04	32.27
1210	Pro	-	-	-	-	-
1211	Pro	-	-	177.64	63.26	-
1212	Gly	8.56	109.3	174.01	45.13	-
1213	His	8.29	118.84	175.1	55.83	30.07
1214	Thr	8.26	115.59	174.2	61.84	69.92
1215	His	8.63	121.57	174.81	55.76	29.69
1216	Ser	8.54	117.97	174.96	58.44	63.92
1217	Gly	8.6	111.47	174.25	45.36	-

1218	Ser	8.33	115.7	174.28	58.37	63.91
1219	Asp	8.48	122.47	176.38	54.35	41.18
1220	Ser	8.34	116.32	174.89	58.5	63.73
1221	Ser	8.5	118.13	174.49	58.77	63.76
1222	Asp	8.37	122.39	176.57	54.57	41.06
1223	Ser	8.26	116.21	174.85	58.86	63.77
1224	Glu	8.45	122.62	176.42	56.93	29.97
1225	Tyr	8.17	120.71	176.09	58.25	38.67
1226	Ser	8.14	117.47	174.5	58.25	63.85
1227	Ser	8.37	118.08	174.66	58.47	-
1228	Gln	8.39	121.93	176.23	55.98	29.45
1229	Thr	8.25	115.47	174.71	61.99	69.84
1230	Thr	8.24	117.4	174.54	61.94	69.92
1231	Val	8.33	122.94	176.32	62.39	32.69
1232	Ser	8.51	119.88	175.09	58.57	63.84
1233	Gly	8.47	111.18	174.09	45.34	-
1234	Leu	8.14	121.63	177.62	55.08	42.47
1235	Ser	8.38	116.94	174.86	58.52	63.61
1236	Glu	8.54	123.06	176.64	57.01	30.16
1237	Glu	8.47	121.41	176.46	56.82	30.04
1238	Leu	8.17	122.86	177.06	55.02	42.15
1239	Arg	8.19	122.21	175.32	56.01	30.72
1240	His	8.1	124.9	178.96	56.8	30.05

Table 4. 2 PTCH1$_{(1176\text{-}1240)}$ shift list

This is a table of chemical shifts of all peaks assigned to PTCH1$_{(1176\text{-}1240}$, unambiguously from multiple 3D spectra of ^{1}H-^{15}N-^{13}C GB1-PTCH1$_{(1176\text{-}1240)}$. Prolines remain unassigned due to the absence of peaks in all 3D spectra. Other missing shifts are due to peak overlap and peak broadening making it difficult to assign unambiguously.

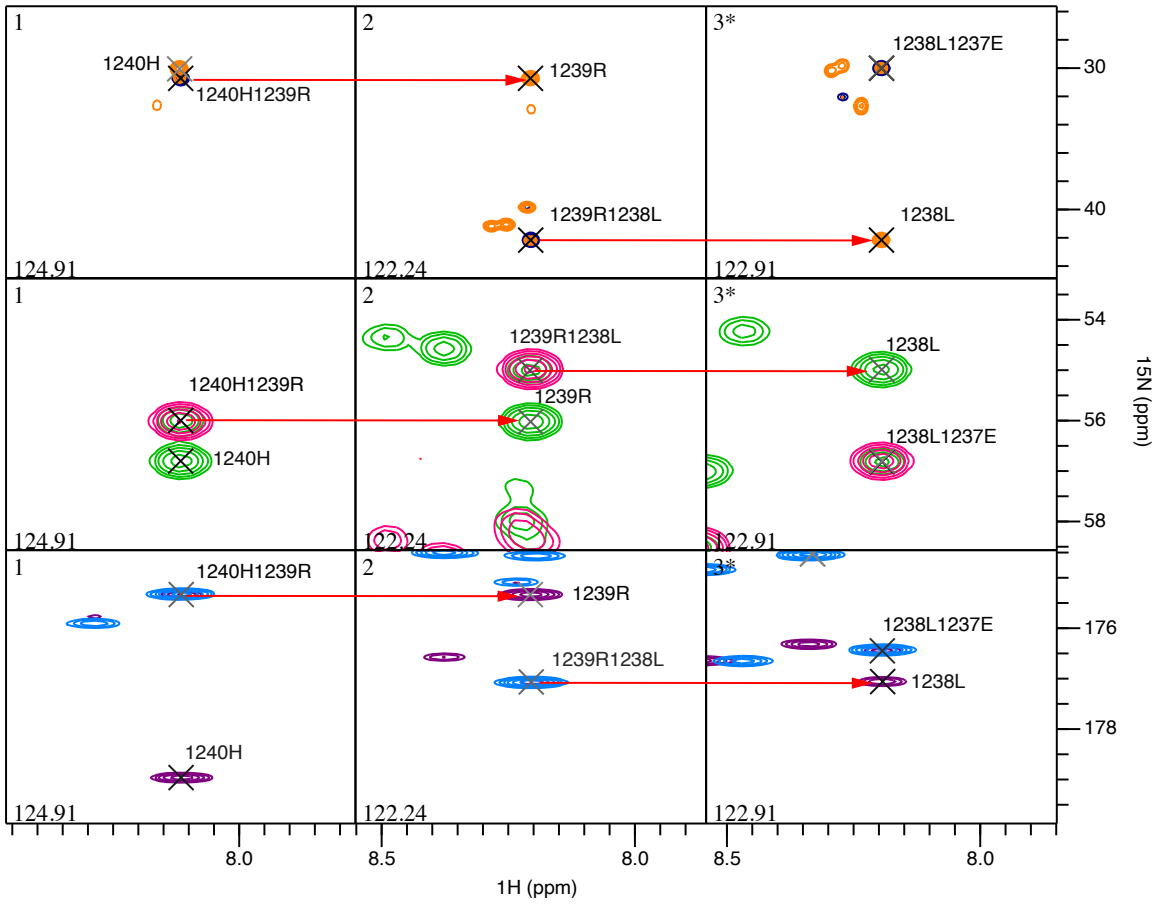

Figure 4. 5 Sequential assignment of the GB1-PTCH1$_{(1176\text{-}1240)}$ peaks

These figures show the combination of the HNCA (green), HNCO (light blue), HNCACB (orange), HNCACO (purple), HNCOCACB (dark blue) and HNCOCA (pink) spectra, showing the assignment of residues 1240, 1239 and 1238, with a marker to show the patching peaks.

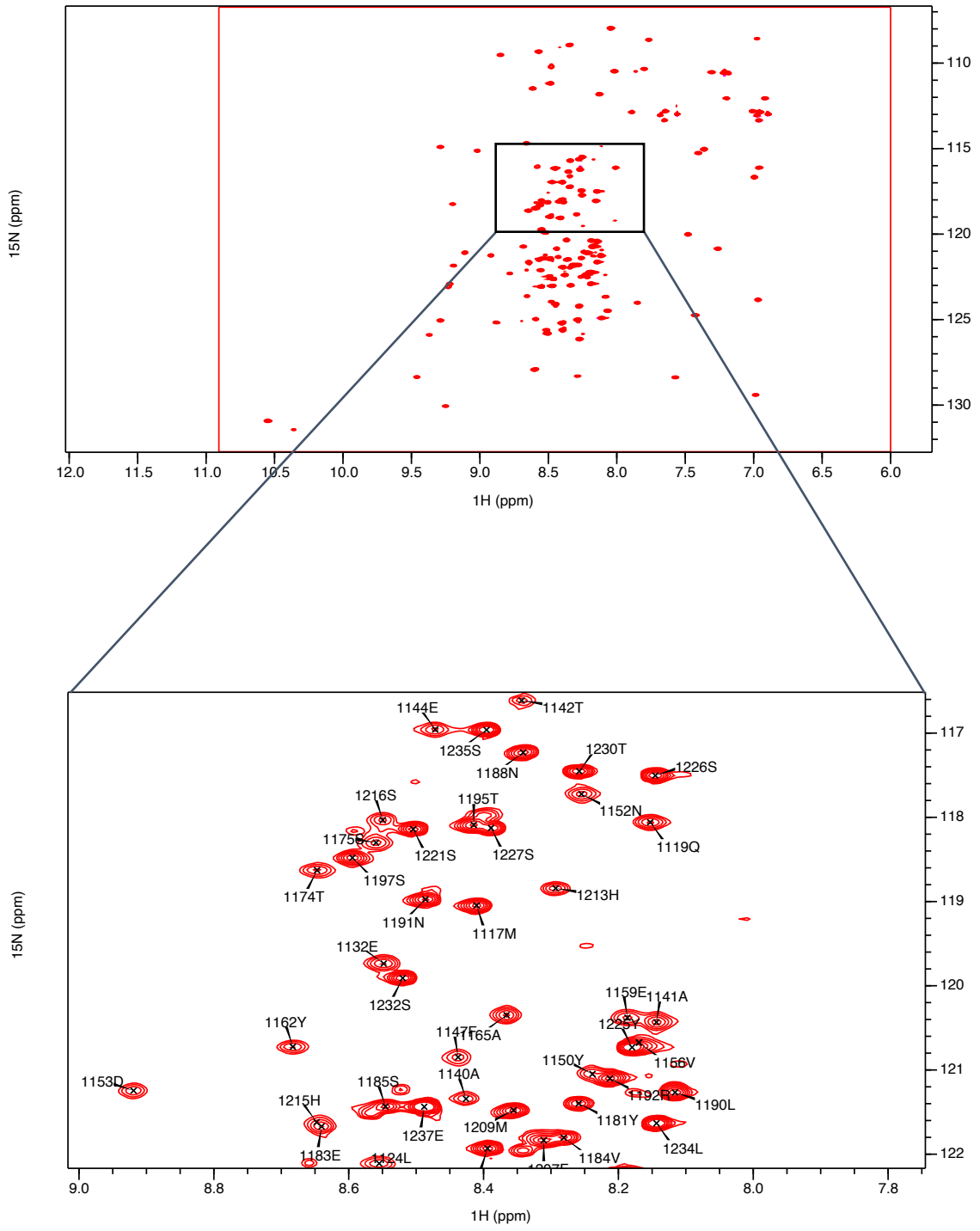

Figure 4. 6 Fully assigned ^{1}H-^{15}N HSQC for GB1-PTCH1$_{(1176-1240)}$

The spectrum for GB1-PTCH1$_{(1176-1240)}$. A focused image on an area of the central IDP fingerprint with complete assignment. Residues T1195 and S1197 are present. This spectrum was recorded a Brucker 600 MHz NMR magnet at 20ºC.

4.3.4 The proximal region of the PTCH1 CTD shows very little structure or propensity to adopt structure upon environmental pressure

Secondary shifts of atoms can be used to infer significant information regarding the secondary structure of a protein. The secondary shift of atoms is defined as the difference between the observed chemical shifts and the random coil chemical shifts which are the predicted shifts of a protein devoid of any secondary structure (Wishart and Sykes, 1993). Cα and CO atoms that form an α-helix will display a positive chemical shift whereas those adopting a β-sheet conformation will display negative chemical shifts (Mielke, S.P. and Krishnan, V.V., 2009). This information can be used to predict the structural propensities of a protein, whether they are likely to adopt a certain structure depending on its environment.

The resonances of each peak from the GB1-PTCH1$_{(1176\text{-}1240)}$ spectrum were used to calculate the secondary shifts for each residue, which are displayed in **Figure 4.7**. **Figure 4.7A** shows the secondary shifts of the Cα atoms and **Figure 4.7B** shows the secondary shifts for the CO atoms. As expected, the ordered structure of the GB1 tag is highlighted in both charts, showing a series of negative N-terminal chemical shifts – indicative of a β-sheet formation – followed by a series of positive chemical shifts – indicative of an α-helix formation – and finally showing a β-sheet CTD with negative secondary shifts, agreeing with the structure of the GB1 tag (Andreas et al., 2016). When analysing the secondary shift information of the PTCH1$_{(1176\text{-}1240)}$ fragment, there does not appear to be any secondary structure points, with the protein adopting a largely disordered conformation, a result which is expected when compared to previous structure prediction studies (Kowatsch et al., 2019; Qian et al., 2019). When focusing on the TPSP motif of the CTD, the suggestion is that this motif does not adopt an

ordered structure, such as a PPII helix which has been predicted by AlphaFold, and instead is a totally disordered region of the protein. Whilst this data contradicts the predicted structure of the proximal region of the CTD, it is important to note that this does not confirm that the entire, full-length CTD will be disordered. These results provide a possible orientation that the CTD may adopt, enhancing the idea that the CTD may be intrinsically disordered. The low confidence associated with the predicted structures highlights the importance of performing experimental analysis.

A

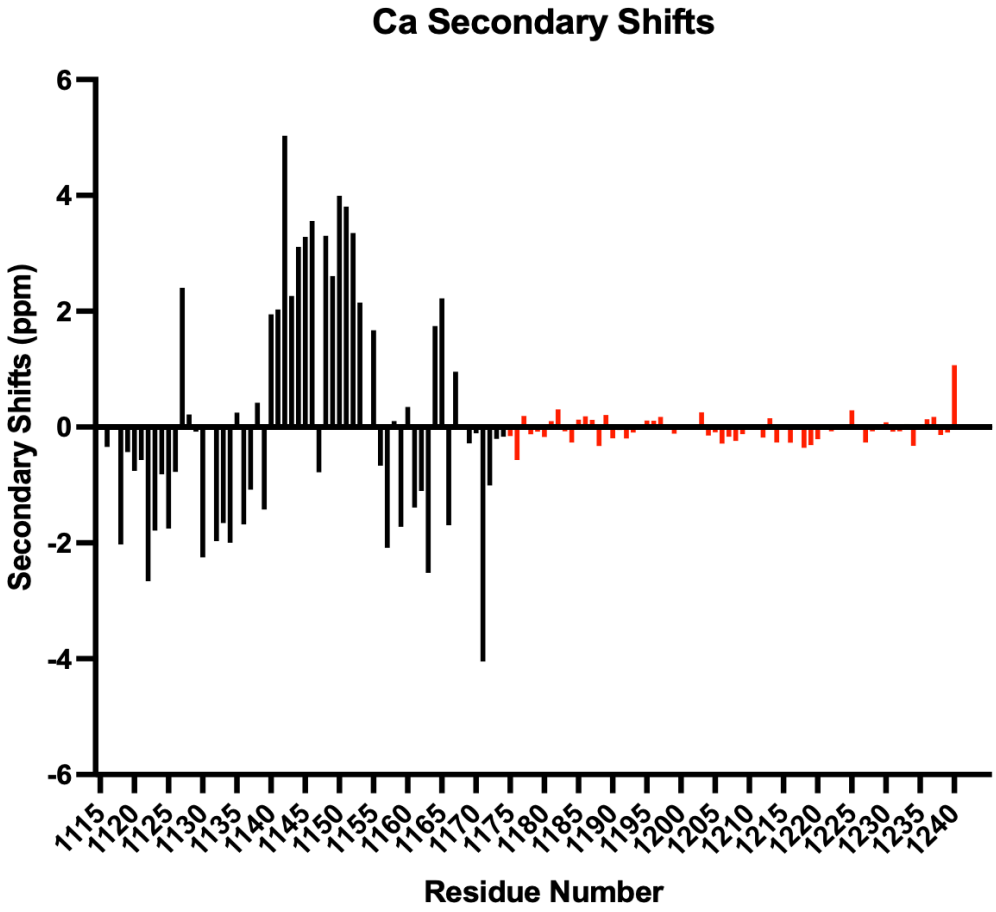
Ca Secondary Shifts
Secondary Shifts (ppm)
6
4
2
0
-2
-4
-6
1115
1120
1125
1130
1135
1140
1145
1150
1155
1160
1165
1170
1175
1180
1185
1190
1195
1200
1205
1210
1215
1220
1225
1230
1235
1240
Residue Number

B

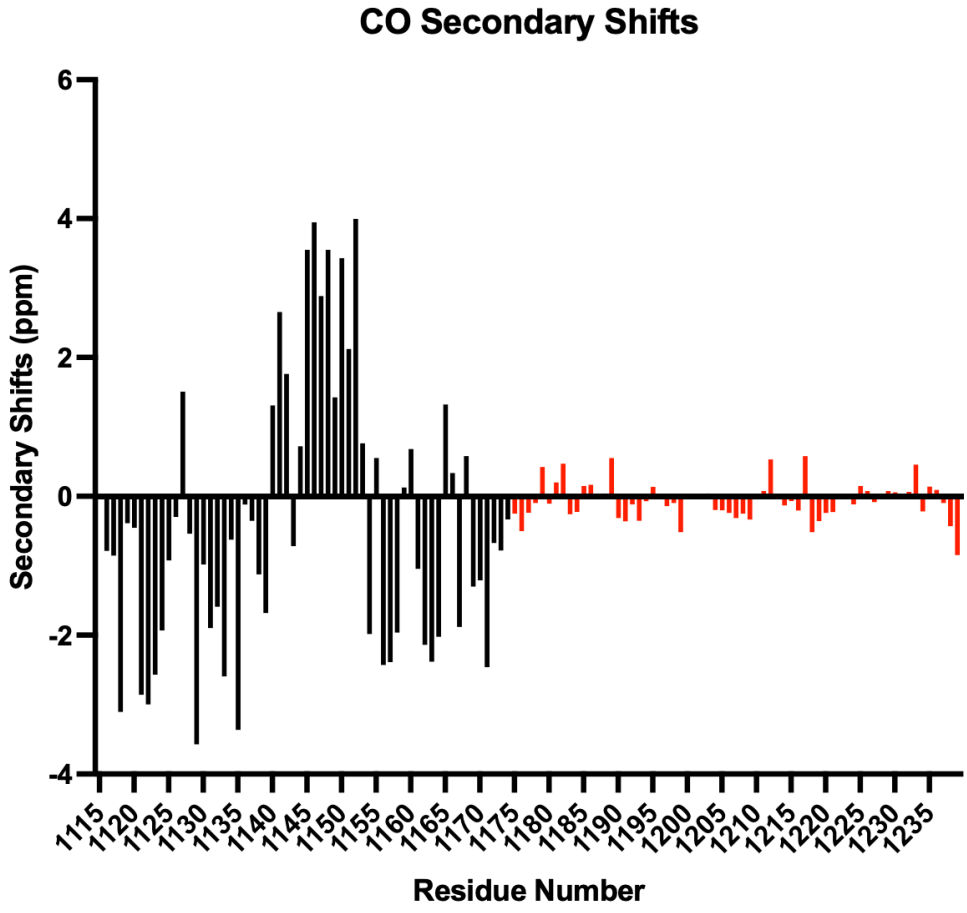
CO Secondary Shifts
Secondary Shifts (ppm)
6
4
2
0
-2
-4
1115
1120
1125
1130
1135
1140
1145
1150
1155
1160
1165
1170
1175
1180
1185
1190
1195
1200
1205
1210
1215
1220
1225
1230
1235
Residue Number

Figure 4. 7 Secondary shifts of GB1-PTCH1$_{(1176-1240)}$

Charts showing the secondary shifts associated with **(A)** the Cα atoms and **(B)** the carbonyl carbon atoms. Calculated from the differences between the observed chemical shifts and the random coil chemical shifts. Negative secondary shifts indicate β-strand formation, positive secondary shifts indicate α-helix formation. GB1 tag indicated in black, PTCH1$_{(1176-1240)}$ indicated in red. The GB1 chemical shifts match the structure of the GB1 tag (strand-helix-strand).

4.3.5 The kinase ERK1 can phosphorylate the proximal region of the PTCH1 CTD *in vitro*

The next aim of this study was to identify a kinase responsible for the phosphorylation of the TPSP motif and to investigate which residue is most likely to be phosphorylated *in vitro*, as previous work has shown that the TPSP motif is monophosphorylated, but it is unclear which residue is most likely to be phosphorylated. Kinase prediction tools and phosphorylation motif analysis uncovered ERK1 and ERK2 amongst others (**Table 4.1**) as a candidate kinase for the TPSP motif.

Kinase	Site	% likelihood
GSK3b	T1195	99.33%
	S1197	79.30%
CDK14	T1195	96.98%
	S1197	90.91%
JNK2	T1195	95.26%
	S1197	84.29%
CDK2	T1195	69.65
	S1197	70.97

ERK1	T1195	88.13%
	S1197	76.36%
ERK2	T1195	91.31%
	S1197	73.75%

Table 4. 3 Candidate kinases for T1195 and S1197

A list of candidate kinases for the phosphorylation of T1195 and S1197, with the % likelihood of phosphorylation. Kinases were predicted using (phosphosite.org)

phosphorylation of either T1195 or S1197. Whilst Erk was not predicted to be the most likely candidate kinase to phosphorylate this motif, there were several reasons why it was chosen to test its ability to phosphorylate the TPSP motif: firstly, the apparent involvement of the TPSP motif in PTCH1 regulation of ERK phosphorylation as explored in Chapter 3, maybe investigating a feedback loop between mutation of the TPSP motif and phosphorylation by Erk, therefore, it would be important to understand whether ERK is capable of phosphorylating the TPSP motif. Another reason for investigating ERK as a candidate kinase stems from the known increase in phospho-ERK levels present in breast cancer cells, a cancer type in which mutation of the TPSP motif (T1195S) is associated with recurrence (Wang, C.Y. et al., 2019). Therefore, the suggestion could be that the TPSP motif and Erk interact to regulate the levels of phosphorylated Erk, maintaining low basal levels of phospho-Erk, and mutation of the TPSP motif removes the specificity for Erk binding or it disrupts it, therefore leading to the hyper-phosphorylation of Erk, making it available for the upregulation of the transcription of target genes to promote cellular proliferation. Additionally, recombinant ERK1 was already available in the lab, prompting me to consider it before other candidate kinases. To investigate phosphorylation of the CTD by

ERK1, a ^{1}H-^{15}N HSQC of an isotopically labelled ^{15}N GB1-PTCH1$_{(1176\text{-}1240)}$ was generated (**Figure 4.8**), the spectrum was obtained at 20°C. Following this, the sample was removed and ERK1 was added (50 mM Tris-HCl pH 7.5, 50% glycerol, 150 mM NaCl, 0.1 mM EGTA, 0.1% 2-mercaptoethanol, 0.02% Brjj-35, 0.2 mM PMSF, 1 mM Benzamidine) to the sample to a final concentration of 1μM, along with ATP (final concentration of 1 mM), and another ^{1}H-^{15}N HSQC was recorded and any changes in peak shift were noted. **Figure 4.8** shows the emergence of a strong peak, noted in blue, that appears on the left-hand side of the spectrum. This shift pattern is indicative of threonine phosphorylation. There were noticeable emergences of additional peaks in the central portion of the spectrum, these peaks could be associated with neighbouring residues which are impacted on by the phosphorylation of a neighbouring residue. Whilst the new large peak development was indicative of threonine phosphorylation, it needed to be properly confirmed as the phosphorylation site. To do this, the first step was to track the changes in peak intensity over time in response to the introduction of ERK1. To do this, the two spectra – unphosphorylated and phosphorylated – were generated, the assignments were copied across from the spectra of **Figure 4.6** and the peak intensities for each residue at each of the two time points (0hr and 1.5hrs) were collected. To display changes in peak intensities, a ratio of peak intensities was calculated, using the 0hr spectrum as a reference point.

To identify the region of phosphorylation, peak intensities in ^{1}H–^{15}N HSQC spectra were tracked over a period of 1.5 h. Changes in assigned peak intensities were analysed because the kinase experiment was performed using ^{15}N-labelled GB1-PTCH1$_{(1176\text{-}1240)}$ protein; it was therefore not possible to assign the new peaks emerging for phosphorylated protein using standard (H/N/C) triple

resonance experiments. Instead, reduction in peak intensity for unphosphorylated species in $^{1}H–^{15}N$ HSQC spectra was used to identify the region in which the phosphorylation took place. Using further experiments such as a TOCSY HSQC, I could determine the specific site of phosphorylation.

The % peak intensity at 1.5 h compared to 0 h for each residue is displayed in **Figure 4.9.** The data clearly shows two troughs in the peak intensity ratio for the PTCH1 CTD section of the protein: between 1181 and 1199. This is also the region where phosphorylation was observed in the mass spectrometry data (**Figure 3.4**). From the fractional loss in intensities, the NMR data suggest a much higher abundance of phosphorylated protein (~40%) compared to the mass spectrometry data (~10%). This difference could be due to the use of different sized constructs which could affect the abundance of phosphorylation. Additionally, it is unclear which experiment – mass spec or NMR – has a kinase concentration that is similar to physiological conditions. There are many factors at play when considering kinase concentrations in a *in vivo* experiment including pH, cell cycle stages, cell type and epigenetic regulation. Therefore, it is very difficult to determine the exact concentration of cellular kinases, making it difficult to compare the abundance of phosphorylation between NMR and mass spectrometry experiments. The data in **Figure 4.9** only confirm that phosphorylation has taken place, but it does not indicate the number of phosphorylation events or the location of the phosphorylation events. Most of the changes in peak intensity observed in **Figure 4.9** will be due to the proximity of those residues to the phosphorylation site(s), shifting peaks caused by changes in the local environment.

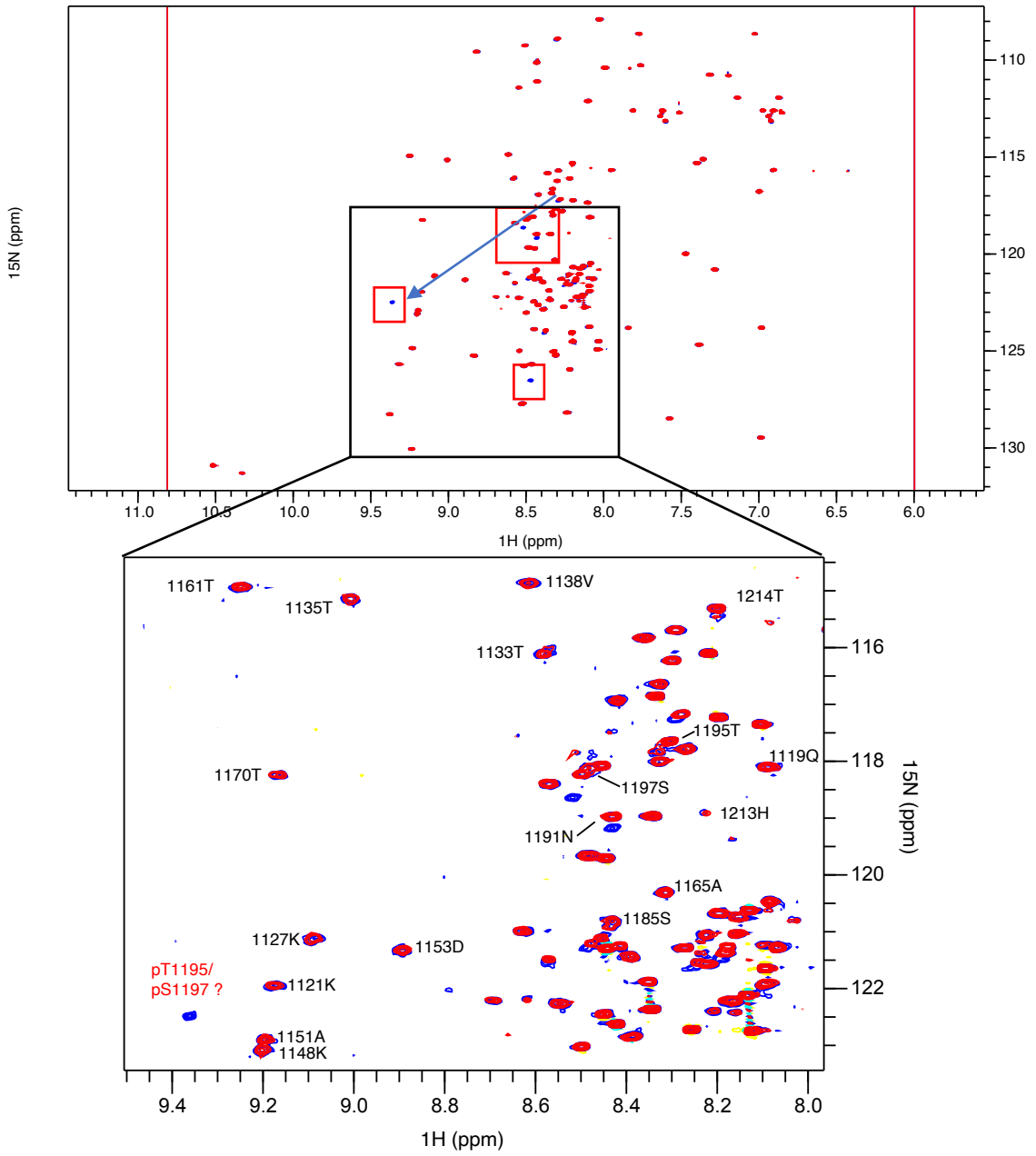

Figure 4. 8 Spectrum of GB1-PTCH1$_{(1176\text{-}1240)}$ phosphorylated by ERK1

(A) Spectra of unphosphorylated (RED) and phosphorylated (BLUE) GB1-PTCH1$_{(1176\text{-}1240)}$ overlayed, with red boxes indicating the more significant new peaks, and a blue arrow indicating the predicted shift of the phosphorylated T1195 residue. **(B)** The same spectrum zoomed in on the new shifts, highlighting the overlap of many peaks from the assigned, unphosphorylated spectrum with the unassigned, phosphorylated spectrum. One of the new blue peaks in the bottom left of the spectrum, which is predicted to be the pSer/pThr peak has been labelled as such. Both spectra were recorded on a Brucker 600 MHz NMR magnet at 20ºC.

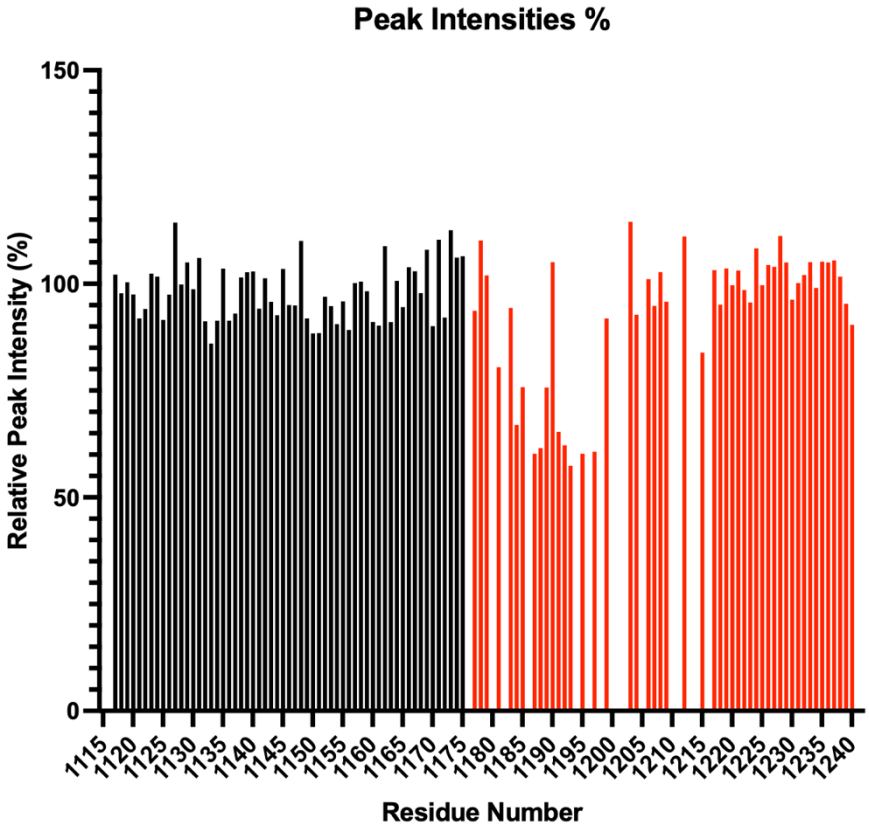

Figure 4. 9 Changes in peak intensities of GB1-PTCH1$_{(1176\text{-}1240)}$ upon Erk phosphorylation

The % change in peak intensities of the GB1-PTCH1$_{(1176\text{-}1240)}$ protein, 1.5 hrs after phosphorylation with Erk. GB1 residues indicated in black, PTCH1$_{(1176\text{-}1240)}$ residues indicated in red. Gaps in the peaks are due to proline residues which do not have an associated peak. The chart shows changes in peak intensities most notably within the region of residues 1180-1205 which encompasses the TPSP motif.

4.3.6 Threonine 1195 is an ERK1 phosphorylation substrate *in vitro*

As there was no triple resonance chemical shift data for the phosphorylated GB1-PTCH1$_{(1176\text{-}1240)}$ protein, further experimental analysis was needed to determine the exact site of phosphorylation. To elucidate which residues were phosphorylated by ERK1, attention first turned to T1195, it is the only threonine that sits within the regions of diminished peak intensities and therefore can be distinguished from the other phosphorylatable residues in those regions, both of which are serine residues. Threonine residues differ from serine residues by having an additional methyl group in the side chain. This structural difference can be used to confirm the type of residue being phosphorylated by ERK1 by using a ^{15}N-TOCSY HSQC experiment which specifically correlates peaks in the ^{1}H–^{15}N HSQC spectrum with shifts for protons in the side chain of the associated residue (Marion et al. 1989). **Figure 4.10** is a ^{1}H–^{15}N HSQC obtained after phosphorylation with ERK1. The spectrum highlights two peaks marked with an X with very similar ^{1}H chemical shifts, the higher one indicates one of the new peaks that has appeared after treatment with ERK1 (downfield shifted, typical for a phosphorylated residue, Salenko et al., 2008), and the lower peak corresponds to W1160 of the GB1 tag. The low protein concentration limits the sensitivity of the experiment, so the TOCSY HSQC was recorded as a 2D plane (^{1}H–^{1}H). Without the ^{15}N correlation to distinguish them, cross peaks from side chain protons for these two residues produce peaks at the same HN position in the TOCSY HSQC, which will need to be distinguished. The TOCSY HSQC was obtained after phosphorylation at 20 °C (**Figure 4.11**). The spectrum produced 6 cross-peaks that fall on a line in the spectrum. The Hα and Hβs of GB1-Trp can be distinguished from known assignments. The remaining cross peaks come from the new phospho-peak in the HSQC spectrum and include one at X ppm, which

is only consistent with a threonine γ-methyl proton and incompatible with serine. The remaining peaks at X/Y ppm are consistent with the Hα and Hβ of phosphorylated threonine. (A phosphoserine would produce Hβ cross peaks at ~4 ppm (Conibear et al. 2019) This data confirms that the shifted peak indicated in **Figure 4.8** belongs to a threonine, when combined with the peak intensity data in **Figure 4.9**, confirms the emergence of phosphorylated T1195. These data do not rule out whether other residues are phosphorylated as well, therefore, it is of paramount importance to investigate whether S1185 is phosphorylated by ERK1/2 and any additional kinases.

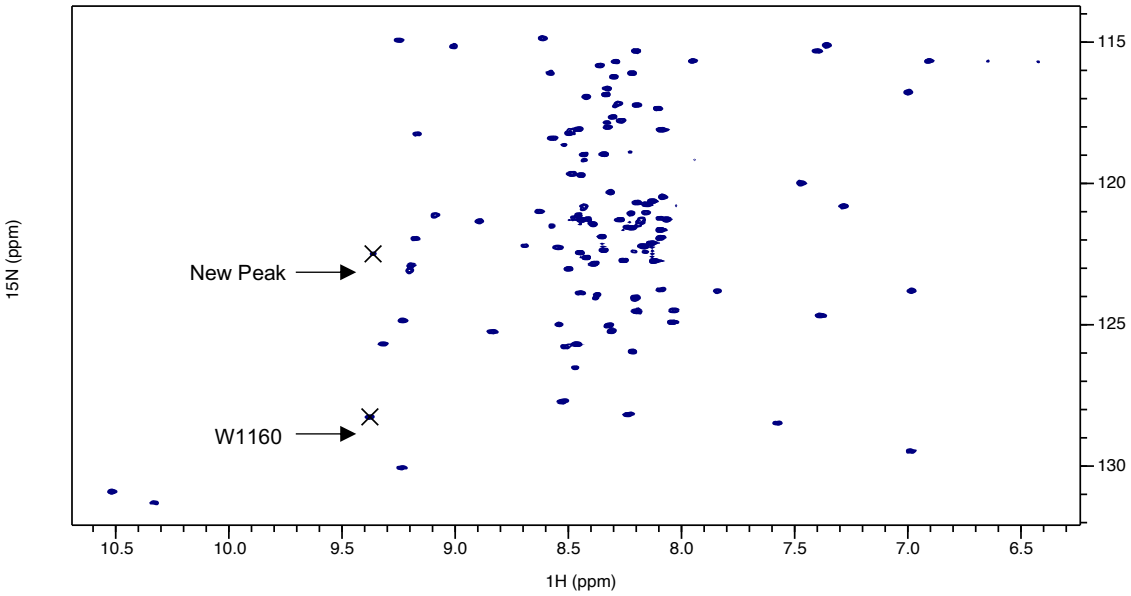

Figure 4. 10 A ^{1}H-^{15}N HSQC of phosphorylated GB1-PTCH1$_{(1176\text{-}1240)}$
Figure showing a 2D ^{1}H-^{15}N HSQC of phosphorylated GB1-PTCH1$_{(1176\text{-}1240)}$ with W1160 and the new peak marked on the spectrum. The spectrum was obtained at 20°C and the assignments were copied across from an unphosphorylated spectrum. The spectrum shows the emergence of a new peak which is indicated on the spectrum. The new peak sits in very similar planes and both residues have hydrocarbon side chains which will produce peaks in the TOCSY HSQC which will need to be distinguished.

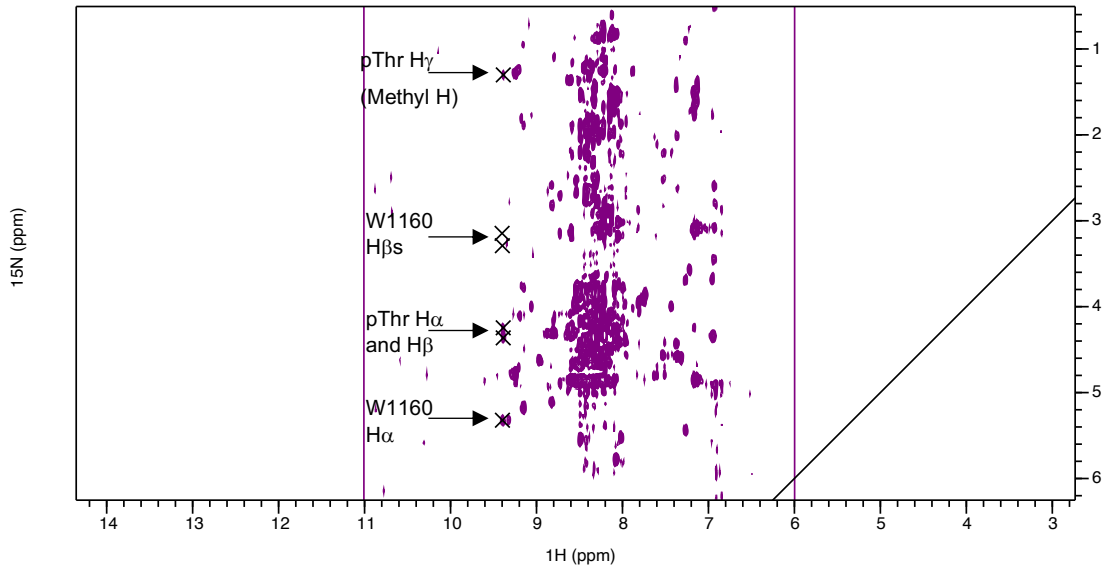

Figure 4. 11 TOCSY HSQC of phosphorylated GB1-PTCH1$_{(1176\text{-}1240)}$

TOCSY HSQC of phosphorylated GB1-PTCH1$_{(1176\text{-}1240)}$ with the Hα, Hβ and Hγ peaks marked, indicating the presence of a shifted methyl group associated to a phosphorylated threonine residue. This spectrum proves that the new peak corresponds to a phospho-threonine because of the presence of a peak representing a methyl H atom at ~1.2 ppm ^{15}N. This peak would not be present if the phosphorylated residue was a serine as the serine side chain does not contain a methyl group. Additionally, the Hβ peaks for a serine would be present at ~4 ppm (^{15}N) (Conibear et al. 2019), compared to the peaks at ~3.1 ppm (^{15}N) as is seen on this spectrum.

4.4 Discussion

Here, I present an approach to the investigation of TPSP motif phosphorylation using NMR, beginning with the successful cloning of the proximal region of the PTCH1 CTD into a suitable vector for NMR. Residue assignment provided several difficulties consistent with assigning IDPs, one significant challenge being the clustering of peaks in the centre of a spectrum, causing peaks to merge. The consistent observation from all this data is the confirmation of the disordered nature of the proximal CTD region.

This chapter presents further evidence that the PTCH1 CTD is disordered, complementing the data from Qian et al. (2019) and Zhang et al., 2018, which both predicted a disordered protein in their structural studies. The data further solidified the idea that the TPSP exists in a monophosphorylated state, further expanding on the data from other mass spectrometry analysis studies of the PTCH1 CTD (Franz-Wachtel et al., 2012; Ochoa et al. 2020). However, it is important to acknowledge the limitation of this study in using a truncated section of the CTD to analyse the structure and phosphorylation status, which may not fully represent the native state of the PTCH1 CTD

NMR was chosen as the approach for this chapter as it's a useful tool to analyse disordered proteins (Kosol et al., 2013) as well as a tool to analyse phosphorylation and structural changes in IDPs (Gibbs et al., 2017).

Comparisons between the NMR and mass spec data from Chapter 3, it reveals a consistent pattern of monophosphorylation of the TPSP motif, albeit with varying phosphorylation levels (approximately 60% in the NMR data vs. 5-10% in

mass spec data). This discrepancy raises questions regarding the most accurate representation of the phosphorylation state of the TPSP motif, with more clarity needed on which method better reflects the native context more accurately.

Another limitation of this study is the analysis and focus on only one kinase, particularly when considering other papers such as Wang et al. (2019) postulated that the T1195S mutation disrupts the activity of protein kinase C as well as disrupting the structure of PTCH1. It would be interesting to expand on this prediction by analysing longer, mutant forms of the CTD – in particular T1195S – to explore changes in the structure. It's important to analyse the additional kinases which are predicted to be more likely responsible for the phosphorylation of the TPSP motif (**Table 4.2**).

Future research could shift towards the two potential β-strand motifs through the use of circular dichroism (CD), which is another method that studies the secondary structure of a protein, which may provide more information on whether those β-strands exist in different conditions, and the likelihood of them occurring. Because this region interacts with β-arrestin1 (Hattie Ollerton – work unpublished), it would be interesting to repeat this structural study adding recombinant unlabelled β-arrestin1 to investigate if the β-strand(s) in this region adopt a more rigid conformation.

Research could extend to focusing on the distal region of the CTD (1240-1447) to investigate the level of disorder associated with this region, and whether it mirrors the disorder associated with the proximal region. The analysis would also allow for investigations into the effect of other well-characterised binding partners

such as ATG101 and ITCH, both of which are known to bind in the distal region of the CTD, on the CTD conformation. These investigations would determine whether the CTD structure undergoes changes upon interactions with these proteins, it would uncover how transient or permanent these interactions are, providing more information on the non-canonical functions of PTCH1.

This data also uncovers the possibility of a previously undetectable phosphorylation site in S1185. Previous attempts were made to investigate the phosphorylation of S1185 through mass spec, but this was unsuccessful due to lack of sequence coverage in that region. The discovery of S1185 as a phosphorylation site by ERK1 would be an important one as it would uncover another site which could have significance in signalling events. Indeed, it is the only other SP or TP motif within the CTD, making it a candidate for the binding of Pin1 or a related prolyl isomerase. This idea is postulated in Chapter 6 but unsuccessful attempts to mutate this residue to an alanine meant I was unable to investigate its role in the binding of Pin1 as well as investigating its role in other PTCH1 roles exhibited in Chapter 5.

Altogether, this chapter contributes significantly to the understanding of the structure of the proximal region of the PTCH1 CTD. It furthers the idea that the PTCH1 CTD is unstructured and identifies ERK1 as a kinase that targets T1195 in the TPSP motif. It hints at slightly structural elements, which require further investigation, as well as it uncovers an additional phosphorylation site at S1185 which could have a significant role in the function of PTCH1.

Chapter 5

Functional significance of the TPSP motif and associated mutations

Chapter 5

Functional significance of the TPSP motif and associated mutations

5.1 Introduction

As demonstrated in Chapter 3, the TPSP motif is highly conserved across species that exhibit a functional HH pathway. Notably, this motif can be phosphorylated, and mutations within that motif can perturb the phosphorylation status of the first PRM. Consequently, it warrants a comprehensive investigation into the functional significance of the TPSP motif, and the subsequent effects that disease-associated mutations have on any observable function.

PTCH1 has a wide range of signalling functions that can be categorised into two groups: canonical and non-canonical (Chen et al., 2018). The loss-of-function phenotype linked with the cancer-associated TPSP motif mutations points towards an involvement of the motif in canonical HH signalling (Kawamura et al., 2008). However, the number of non-canonical HH processes associated with the CTD highlights the importance of investigating both canonical and non-canonical functions. The phosphorylation states of the TPSP motif and the known importance of phosphorylation on signalling cascades suggest a key role for the TPSP motif but the exact role is unknown and requires further investigation.

The different phosphorylation profiles exposed in Chapter 3 show the influence of mutations on the phosphorylation state of the first PRM, however, the difference between the phosphorylation states of the two disease-associate mutants raises a fundamental query – whether the apparent loss of function is a consequence of a change in phosphorylation, the emergence of a novel

phosphosite at S1203 (for the P1196L mutant), or a key structural change. Therefore, my main objective was to further understand the functional role that the TPSP motif plays in PTCH1 function, and analyse any alterations brought about through mutation.

5.2 Aim and Hypothesis

The predominant aim of this experiment was to investigate the consequence of phosphorylation of the TPSP motif on PTCH1 function, by comparing the activity of wild-type and mutated variants (T1195A, S1197A, T1195A/S1197A, T1195D, T1195S, P1196L and ΔTPSP). This will be achieved by using a range of cell-based assays to investigate known functions of PTCH1 (canonical and non-canonical).

5.3 Results

5.3.1 Phosphorylation of the TPSP motif is not required for canonical HH signalling

The GLI-luciferase assay (**Figure 5.1**) was employed to assess the ability of the TPSP mutants to inhibit GLI-dependent transcription and their ability to respond to N-SHH. *Ptch1*$^{-/-}$ MEFs were used as the model for the GLI-Luciferase reporter assays as they lack active endogenous PTCH1. Consequently, the basal canonical HH activity is high in these cells, allowing for analysis of the activity of each PTCH1 CTD mutant in comparison with WT PTCH1. Transfection using this method is known to greatly overexpress proteins when comparing endogenous expression levels (Chong et al., 2021). Unfortunately, there is no known study which directly quantifies endogenous PTCH1 levels in PTCH1$^{+/+}$ MEF cells, however, analysis of luciferase activity in PTCH1$^{+/+}$ MEF cells compared to cells transfected with PTCH1 shows that transfection causes significant overexpression (Timmis, 2021) When transfected with wild type PTCH1, the activity is dramatically reduced (**Figure 5.2**), caused by the blockage of SMO activation and therefore reducing the activation of the GLI proteins which cannot bind to the 8X GLI repeated binding sites of the plasmid.

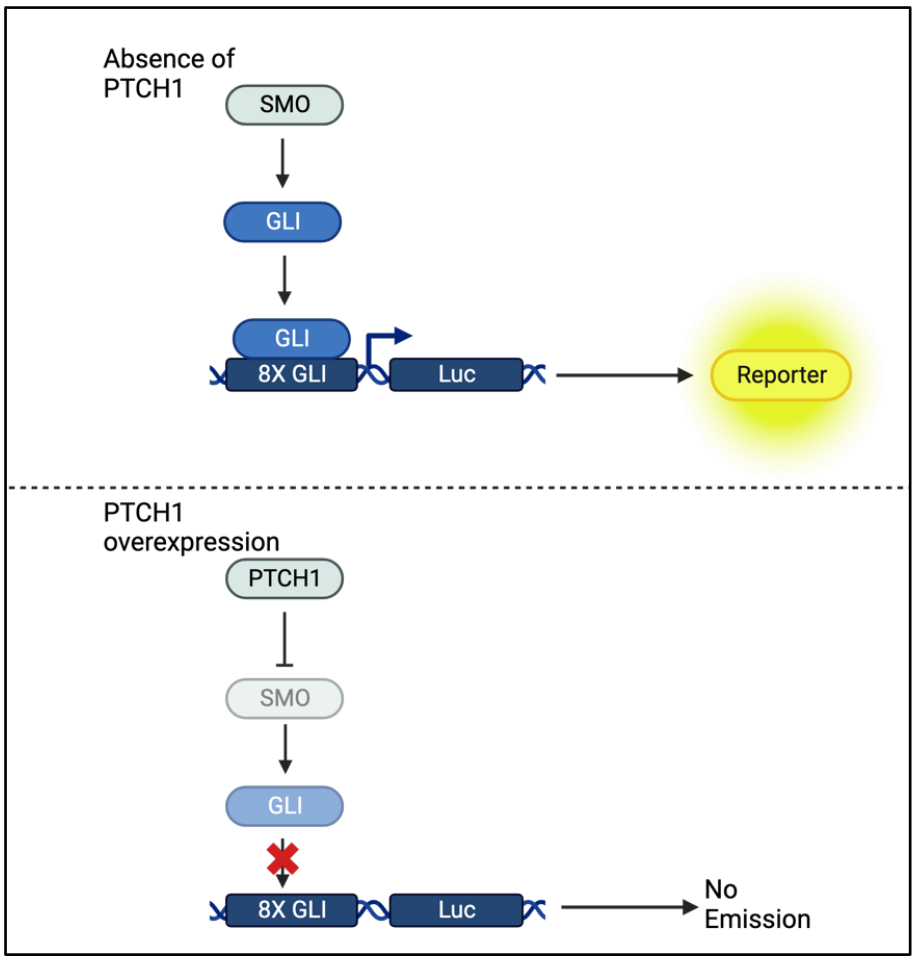

Figure 5. 1 GLI-Luciferase reporter assay

Schematic showing that, (A) in the absence of PTCH1 – *Ptch1*$^{-/-}$ MEFs – there is no repression on SMO, meaning it can activate GLI transcription factors which can bind to the eight repeats of GLI binding sites. Binding of GLI proteins leads to the expression of the Firefly luciferase enzyme, which emits bioluminescence which can be detected and measure. (B) Overexpression of PTCH1 blocks the activation of the GLI proteins, therefore, downregulating the expression of the luciferase enzyme and thus there is no bioluminescent emission. Figure created using BioRender.

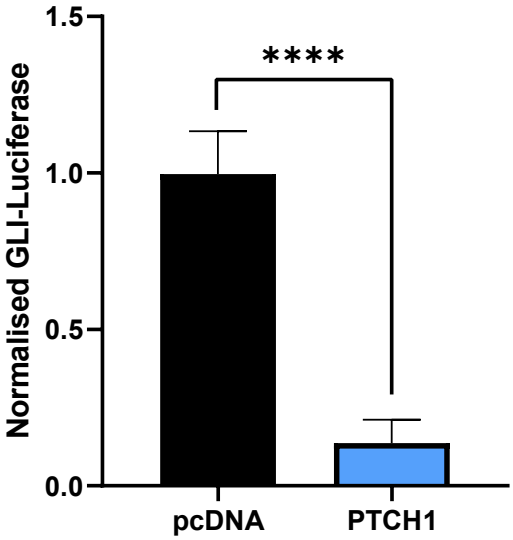

Figure 5. 2 GLI-Luciferase activity in the presence of PTCH1

GLI-Luciferase reporter assay of *Ptch1*$^{-/-}$ MEFs transfected with pcDNA empty vector and PTCH1 highlighting the reduced canonical HH eactivity in the presence of PTCH1.

N = 3, **** = p<0.0001

Comparison of the activity of WT and the TPSP phosphorylation mutants T1195A, S1197A, T1195A/S1197A and T1195D in this assay revealed that, like wild type PTCH1, all mutants significantly reduced the transcriptional activity of the endogenous GLI transcription factors to a similar level compared to the negative control, empty vector pcDNA 3.1+ (**Figure 5.3**). This data, therefore, strongly indicate that the phosphorylation status of the PTCH1 TPSP motif do not affect canonical signalling.

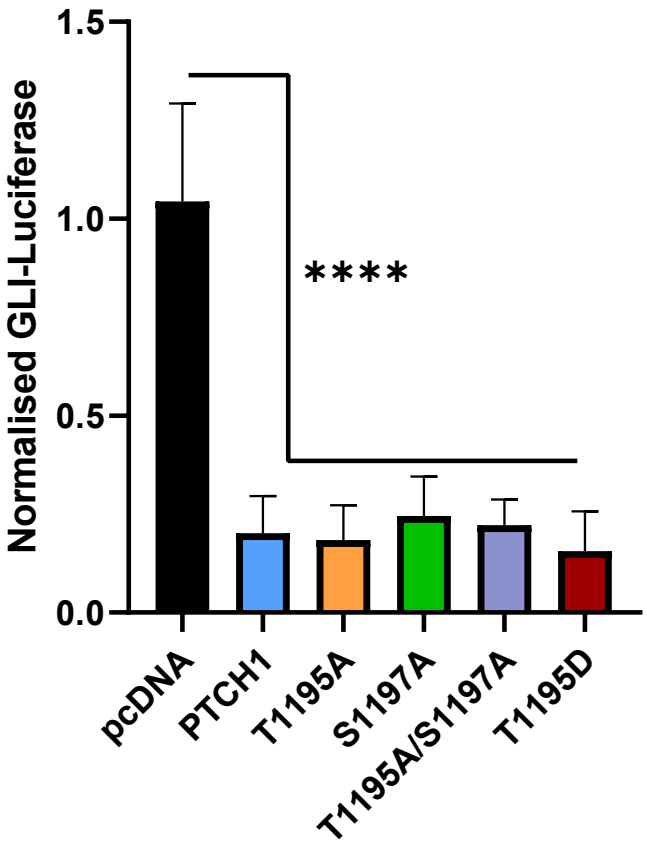

Figure 5. 3 Phosphorylation mutants of the TPSP motif does not result in impaired GLI transcription

(A) GLI-Luciferase reporter assay of *Ptch*$^{-/-}$ MEFs transfected with the phospho-dead mutants also caused a significant reduction in GLI transcription.

N = 3, **** = p<0.0001

5.3.2. Cancer-associated mutations in the TSPS motif do not affect the canonical function of PTCH1

Comparison of the activity of WT and disease-associated TPSP mutants, T1195S and P1196L (Wang, C.Y. et al., 2019), revealed that the two mutant PTCH1 proteins are able to reduce the transcriptional activity of the endogenous GLI transcription factors to a similar level compared again to the negative control, empty vector pcDNA 3.1+ (**Figure 5.4A**). To ensure that WT PTCH1 expression levels were not excessively high, potentially masking any subtle changes in activity in the mutants, an additional GLI-luciferase experiment was carried out using decreasing amounts of plasmid encoding WT and PTCH1 mutants, with pcDNA 3.1+ empty vector being used to keep constant the total transfected DNA mass. The amounts of mutant plasmid chosen were 100%, 75%, 50% and 25%, with the total DNA mass being supplemented with pcDNA to ensure consistent DNA levels. The data in **Figure 5.4B** demonstrates a steady increase in GLI-luciferase activity that is inversely correlated with the concentration of all plasmids.

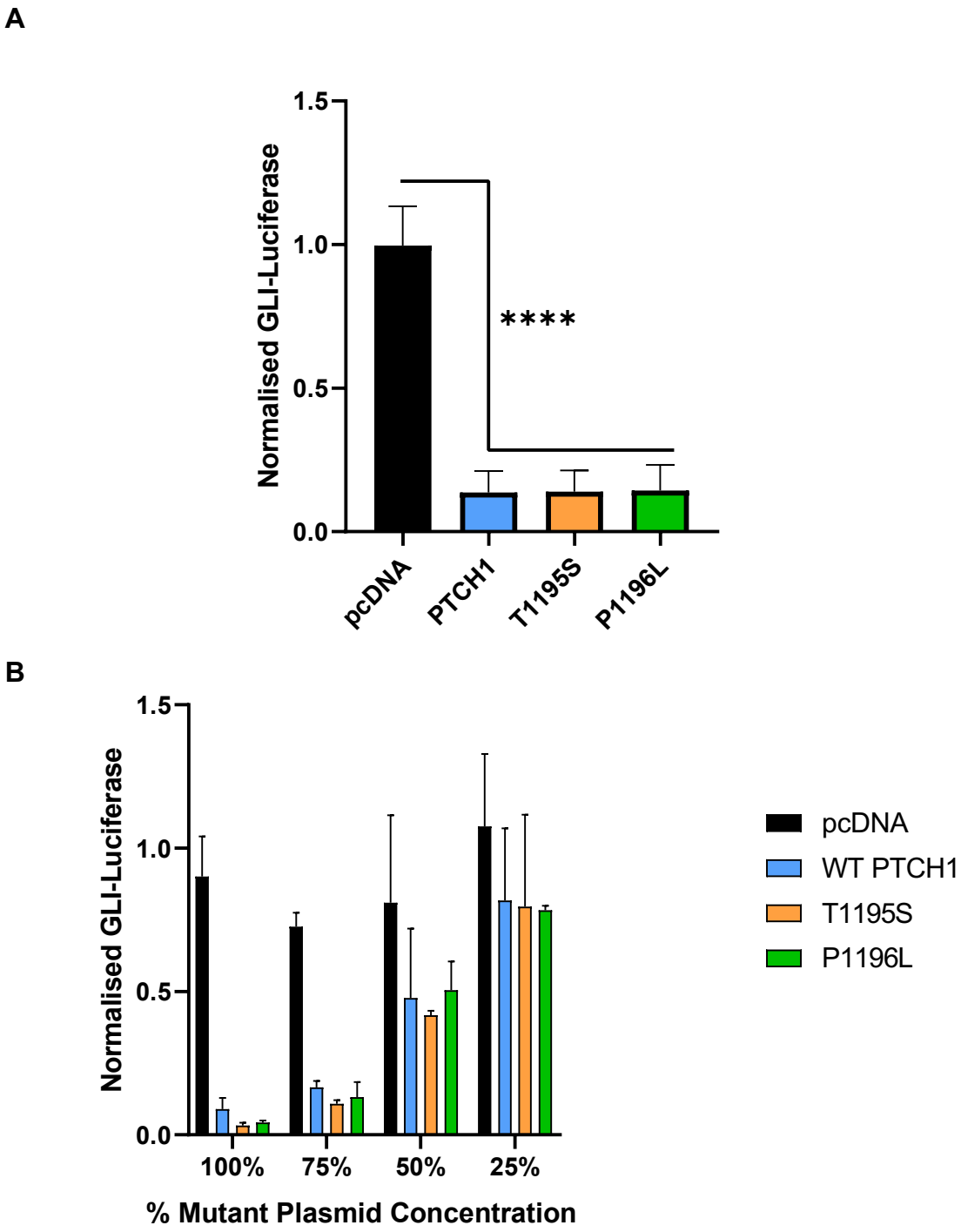

Figure 5. 4 Disease-associated mutants of the TPSP motif does not result in impaired GLI transcription

GLI-luciferase reporter assays of *Ptch1*$^{-/-}$ MEFs, transfected with reporter constructs and specific plasmid combinations. **(A)** Transfection with the disease-associated mutants also caused a significant reduction in GLI transcription. **(B)** Transfection with reducing levels of disease-associated mutant plasmid caused an associated increase in GLI transcription. X-axis indicates the percentage of total plasmid that is a mutant plasmid, total plasmid levels were made up to 100% by supplementing with pcDNA.

Given that none of the mutants in the TPSP motif have an obvious impact on canonical PTCH1 function, we tested if the motif altogether was involved by testing a deletion mutant. As seen in **Figure 5.5**, the presence or absence of the TPSP motif does not affect GLI-luciferase inhibition by PTCH1.

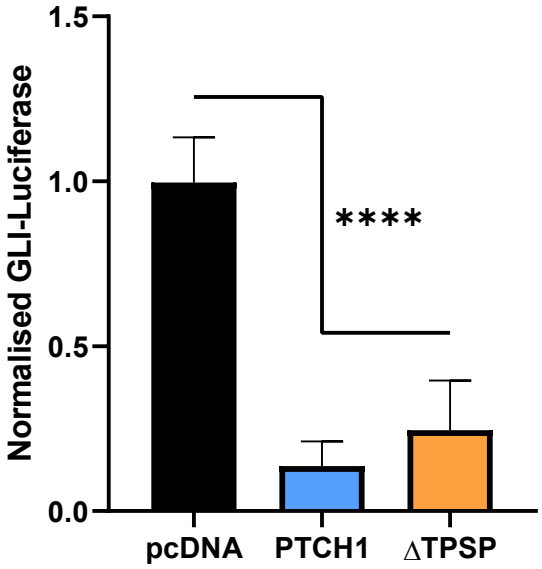

Figure 5. 5 Deletion of the TPSP motif does not result in impaired GLI transcription

GLI-luciferase reporter assay of *Ptch1*$^{-/-}$ MEFs, transfected with reporter constructs and specific plasmid combinations. Transfection with the ΔTPSP mutant caused a significant reduction in GLI transcription., similar to that of WT PTCH1.

N = 3, **** = p<0.0001

In summary, this data confirms that the TPSP motif is not involved in canonical HH signalling. This outcome is expected and aligns with previous research from this lab, which has established that the CTD is dispensable for the canonical function of PTCH1 (Timmis, 2021).

5.3.3 The TPSP motif is not necessary for PTCH1 inhibition in response to SHH binding

The next goal was to explore whether the TPSP motif could somehow affect the response of PTCH1 to HH ligand binding, with a particular focus on the most predominant and widely-expressed HH ligand, SHH, explore whether TPSP mutations alter the responsiveness of PTCH1 to SHH. A series of additional GLI-Luciferase reporter assays were carried out. For this experiment, *Ptch1*$^{-/-}$ MEFs were co-transfected with each phosphorylation TPSP mutant and a plasmid encoding SHH, together with the reporter plasmids. As illustrated in **Figure 5.6A**, the GLI-luciferase activity levels of the mutants reached the same level of pcDNA alone when co-transfected with N-SHH, showing that SHH inhibits PTCH1 activity. The magnitude of the luciferase increase was similar to what was seen with WT PTCH1, the positive control, indicating that the phosphorylation state of the TPSP motif does not play a role in PTCH1's response to N-SHH, nor they seem to impact the sensitivity of PTCH1 to N-SHH and subsequent release of the blockage in canonical HH signalling. In a similar way, the cancer-associated PTCH1 mutants displayed a normal response to N-SHH (**Figure 5.6B**), suggesting that the disease-associated mutants do not impact the sensitivity of PTCH1 to N-SHH.

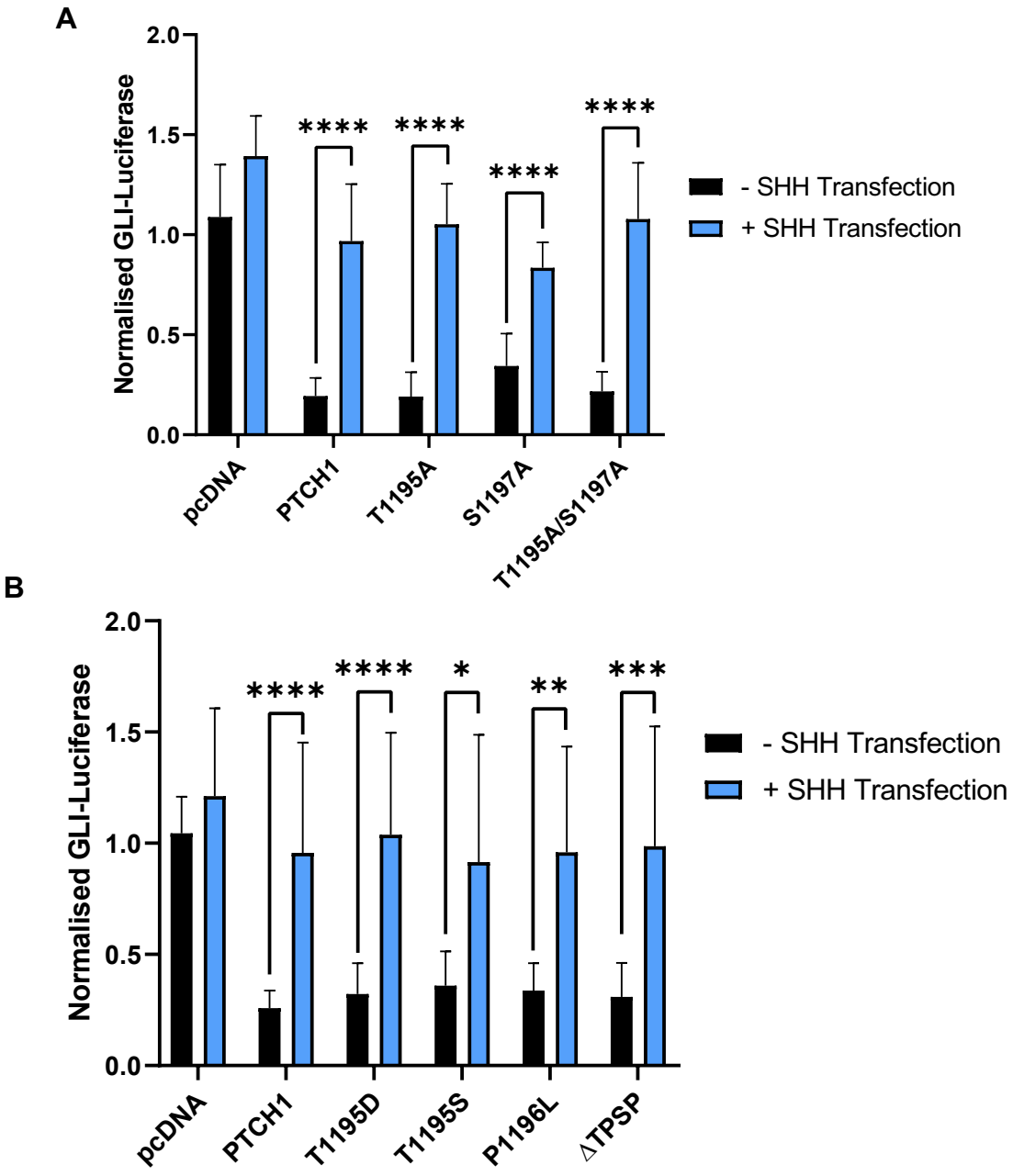

Figure 5. 6 Phospho-dead and disease-associated mutants of the TPSP motif do not alter the sensitivity of PTCH1 to N-SHH

GLI-luciferase reporter assays of *Ptch1*$^{-/-}$ MEFs, transfected with reporter constructs and specific plasmid combinations. Co-transfection of *Ptch1*$^{-/-}$ MEFs with reporter constructs, mutant plasmids and N-SHH plasmid completely removed the repression of GLI transcription by **(A)** phospho-dead mutants and **(B)** disease-associated mutants in response to N-SHH.

N = 3

* = p<0.05, ** = p<0.01, *** = p<0.001, **** = p<0.0001

5.3.4 The TPSP motif is not involved in regulation of autophagy by PTCH1

Autophagy is the process by which the cell recycles damaged or misfolded cellular components in response to stress, to make essential nutrients available to the cell. The process of autophagy begins with the collection of damaged cargo into double-membraned vesicles known as autophagosomes, which upon by fusion with lysosomes results in full degradation of the cargo.

Previous work from this lab group has shown that the PTCH1 CTD interacts with the autophagy-related protein ATG101, causing a blockage in autophagy and a build-up of undegraded autophagosomal cargo (Chen, X. et al., 2018). The research shows that deletion of residues 1308-1447 causes a loss in the binding of ATG101, therefore suggesting that the more distal region of the CTD is required for ATG101 binding. This would therefore suggest that the TPSP motif is not involved in the binding of ATG101; however, there could be a scenario whereby ATG101 requires two binding motifs within the CTD. Deletion or mutation of one of these motifs could be enough to lose binding (as indicated with the 1308 truncation mutant), but a secondary binding site, perhaps the TPSP motif, is also required.

Blockage in autophagy leads to the build-up of two proteins: LC3BII and p62 which can be used as markers for autophagic flux. LC3BII is involved in autophagosome membrane biogenesis, and p62 links ubiquitylated cargo to LCB3II for incorporation into the growing autophagosome before formation of a closed vesicle. Complete autophagy leads to the luminal pool of p62 and LC3BII being degraded along with the cargo. Blockages in autophagy caused by PTCH1

prevent this degradation from happening, causing an increase in the levels of these two markers (Chen, X. et al., 2018).

When investigating autophagy, the drug bafilomycin A1 (Baf A1) is used to artificially block autophagosome-lysosome fusion, leading to a build-up of p62 and LC3BII over time as autophagosomes accumulate. However, if the autophagic flux is already blocked, addition of Baf A1 does not lead to further accumulation of those markers. This positive control can be used to compare levels in the blockage of autophagy. While the expectation is that mutations in the TPSP motif do not have an impact on the ability of PTCH1 to block autophagy, given that ATG101 binding requires the most C-terminal region of the CTD, I hypothesized that the TPSP motif could exert a modulatory effect.

To investigate the role of the TPSP motif in the blockage of autophagy by PTCH1, I used HEK 293 cells, a model that was previously used to describe this function (Chen, X. et al., 2018). HEK 293 cells were transfected with wild type PTCH1 and the phosphorylation site mutants in duplicate wells. The cells were treated with either Baf A1 or a DMSO control for 4 hrs ~20 hrs post-transfection before the samples were collected and analysed by western blot for p62 and LC3BII. Densitometry analysis was used to measure the intensity of the bands, and the ratio of each protein in the Baf A1-treated and DMSO-treated samples was calculated.

Figure 5.7 shows that expression of wild type PTCH1 increases the levels of p62 and LC3BII, resulting in a reduced ratio of the markers when normalised to Baf A1. As expected, the presence or absence of phosphorylatable residues within

the TPSP motif plays no role in the ability of PTCH1 to inhibit autophagy, as evidenced by the similar increase in p62 and LC3BII. The results imply that phosphorylation of the TPSP motif does not interfere with PTCH1's autophagy-blocking function. As shown in **Figure 5.8**, neither of the cancer mutants impaired or enhanced autophagic flux blockade by PTCH1. Furthermore, the deletion of the TPSP motif did not affect autophagy, confirming that the TPSP motif is not involved in the regulation of autophagy by PTCH1.

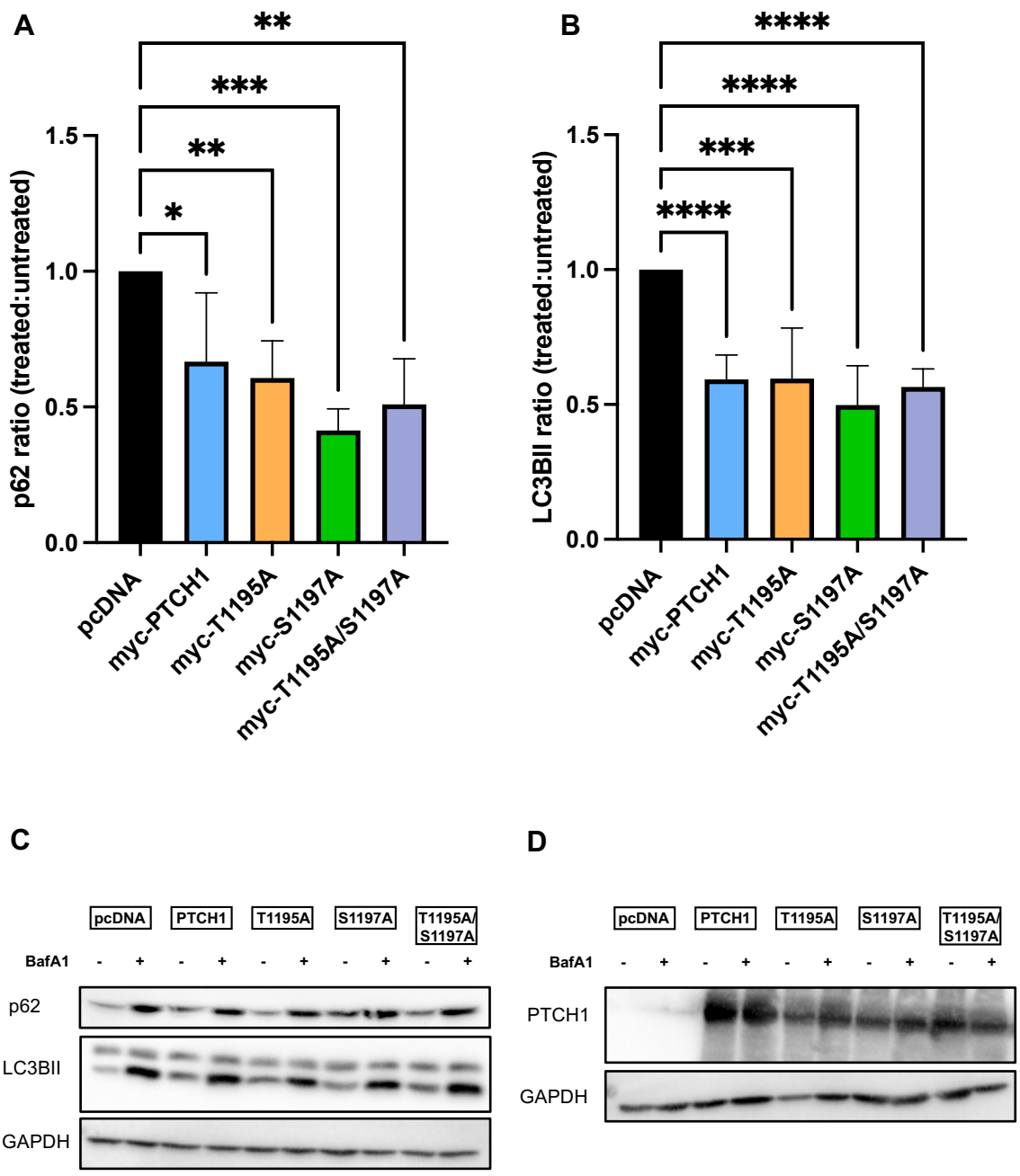

Figure 5. 7 Phospho-dead mutation of the TPSP motif does not affect blockage of autophagy by PTCH1

HEK293 cells transfected with pcDNA, PTCH1 and phospho-dead TPSP mutants, treated with BafA1 or the equivalent volume of DMSO. Quantification of densitometry analysis, showing the ratio of BafA1-treated:DMSO-treated of **(A)** p62 and **(B)** LC3BII. Western blot images of **(C)** p62, LC3BII and GAPDH **(D)** PTCH1 and GAPDH.

N = 3

* = p<0.05, ** = p<0.01, *** = p<0.001, **** = p<0.0001

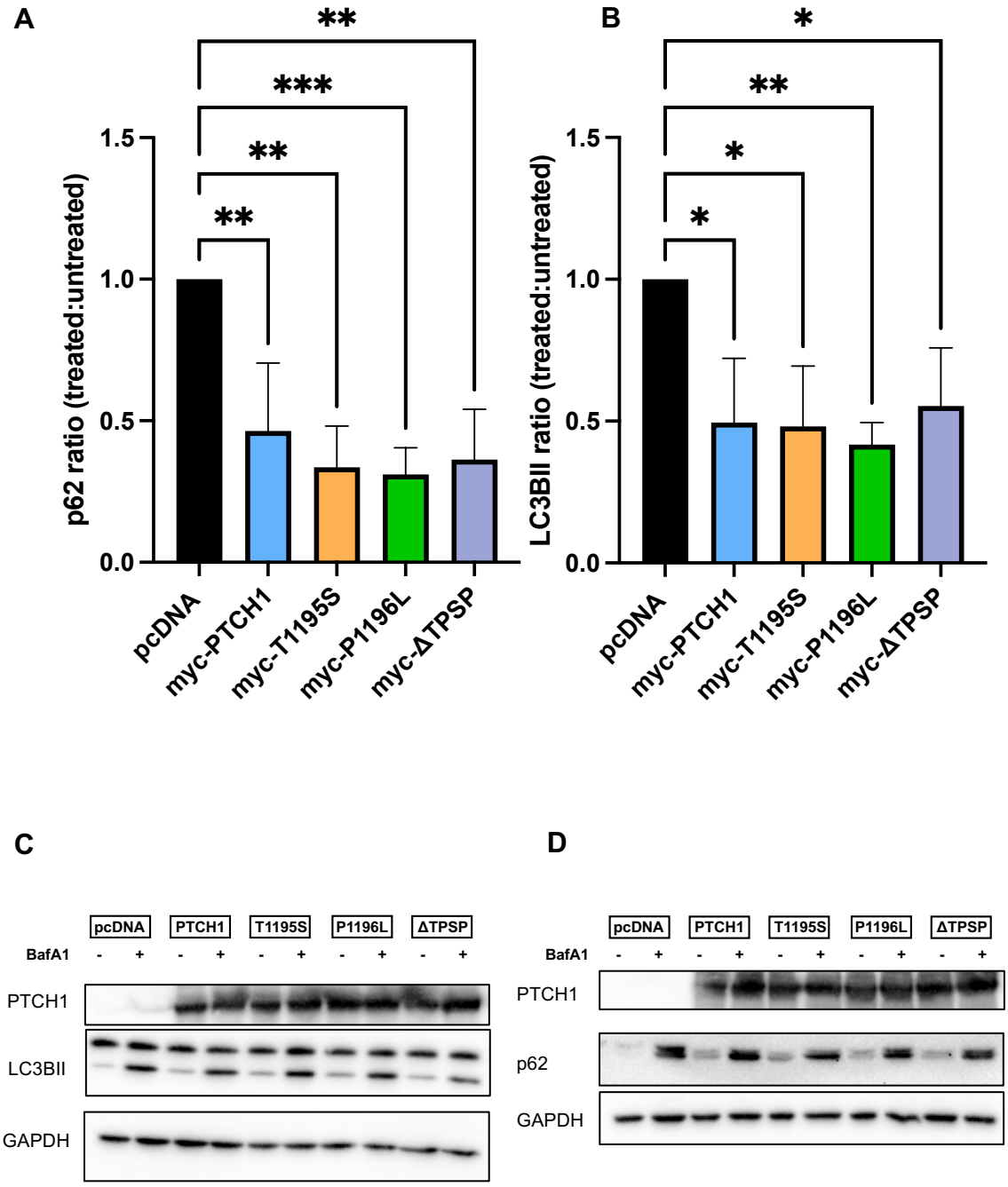

Figure 5. 8 Disease-associated TPSP motif mutations do not affect blockage of autophagy by PTCH1

HEK293 cells transfected with pcDNA, PTCH1 and phospho-dead TPSP mutants, treated with BafA1 or the equivalent volume of DMSO. Quantification of densitometry analysis, showing the ratio of BafA1-treated:DMSO-treated of **(A)** p62 and **(B)** LC3BII. Western blot images of **(C)** p62, LC3B II and GAPDH **(D)** PTCH1 and GAPDH.

N = 3

* = p<0.05, ** = p<0.01, *** = p<0.001

5.3.5 Disease-associated TPSP mutations display higher Erk1/2 phosphorylation upon ligand binding

The next stage was to investigate the role of the TPSP motif in the regulation of Erk1/2 phosphorylation by PTCH1. Previous unpublished work from this lab has shown that treatment of MCF7 cells with SHH leads to an increase in the levels of phosphorylated Erk1/2. MCF7 cells are a breast cancer cell line that does not express SMO, therefore it can be inferred from this previous finding that the increase in phosphorylated Erk1/2 is a function of PTCH1 that is independent of SMO activity, and instead could be influenced through the CTD of PTCH1. Within the CTD are several Class I and Class II SH3-binding sites which are candidates for Grb2 binding and therefore could be influencing Erk1/2 signalling by binding to Grb2.

In fact, previous work has shown that one of the SH3 domains of Grb2 was able to interact with the CTD of PTCH1 (Chang et al., 2010), but the binding site is unknown. One of the candidate SH3-binding sites encompasses the TPSP motif, therefore, the decision was taken to investigate any relationship between the TPSP motif and Erk1/2 phosphorylation. To investigate this, *Ptch1*$^{-/-}$ HEK cells were transfected with disease-associated TPSP mutants and the ΔTPSP mutant alongside WT PTCH1 and pcDNA These cells were used because their absence of endogenous PTCH1, allowing me to over-express PTCH1 constructs and allowing for clear analysis of any changes in ERK1/2 phosphorylation levels between each construct. These cells were used instead of the MCF7 cells as they are much easier to maintain and transfect. The data in **Figure 5.10** shows that expression of WT PTCH1 significantly reduces the basal levels of ERK1/2 phosphorylation compared to pcDNA only. Interestingly, the two cancer-associated mutants had a lesser effect on ERK1/2 phosphorylation, and upon acute treatment with 100 ng/mL rSHH, they led to a significant increase in phospho-ERK1/2. Unexpectedly, treatment of WT PTCH1 with rSHH did not cause phospho-Erk1/2 levels to increase, suggesting a higher concentration of rSHH is required to elicit a response. The data indicates that the disease-associated mutations are more sensitive to rSHH levels than WT PTCH1 and that they promote a heightened level of ERK1/2 signalling in the absence and presence of SHH ligand. This augmented sensitivity could lead to an increase in the transcription of growth-promoting genes and thus would explain the malignant phenotype associated with these mutations. Of note, the phosphomimetic T1195D mutant and the ΔTPSP mutant showed intermediate phenotypes between wild type PTCH1 and the cancer-associated mutants, both in basal ERK1/2 phosphorylation and in response to rSHH.

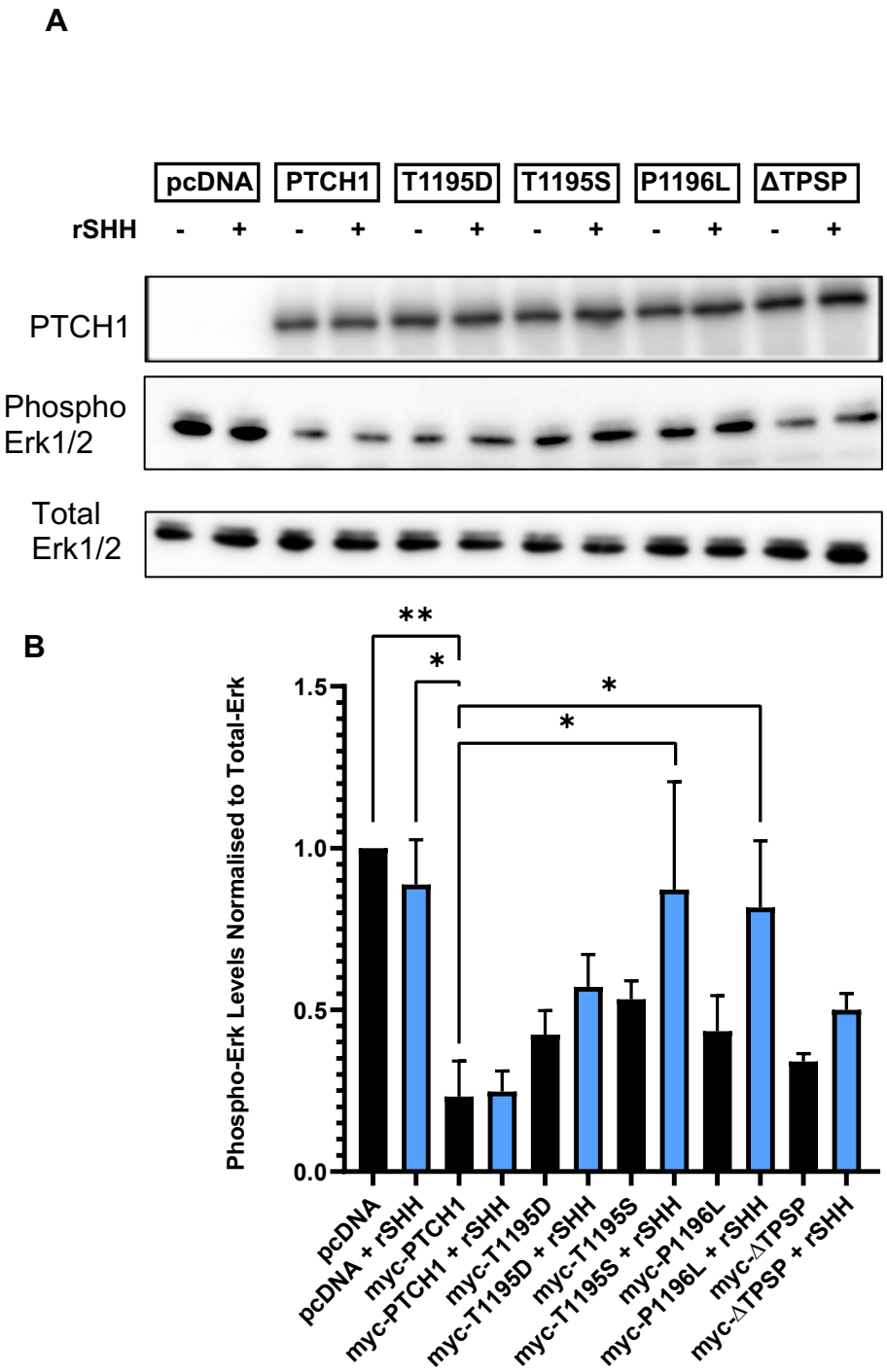

Figure 5. 9 Disease-associated TPSP mutations display higher Erk1/2 phosphorylation upon ligand binding

Ptch1$^{-/-}$ HEK cells were transfected with various TPSP mutants before being serum-starved overnight, followed by treatment with 100 ng/mL rSHH for 15 minutes. **(A)** Western blot images of myc-PTCH1, Erk1/2 and phospho-Erk1/2. **(B)** Densitometry analysis.

N = 3,

* = p<0.05, ** = p<0.01.

5.3.6 Disease-associated TPSP mutants exhibit a higher level of cell proliferation

The WST-1 assay (Roche # 05015944001) was used to analyse the difference in anti-proliferative activity between the disease-associated PTCH1 mutants T1195S and P1196L and wild type PTCH1, the association between mutants and cancer progression suggests a loss of PTCH1 tumour suppressor function. The WST-1 assay works in a way where the greater the levels of cell proliferation, the greater the level of formazan produced by viable cells which can be detected and quantified. Previous work in this chapter showed that the TPSP motif is not involved in canonical signalling, but that the cancer-associated mutants have a reduced ability to suppress the phosphorylation of Erk1/2 in response to stimulation by rSHH compared to wild-type PTCH1, as seen by the increased basal levels of pErk1/2. This could be an indication of increased Erk signalling and therefore suggesting that the mutants might promote cell survival and proliferation. The WST-1 assay was carried out by transfecting the different PTCH1 variants in *Ptch1*$^{-/-}$ HEK293 cells and analysing viable cell numbers over the course of 72 hrs. Although not significant, the results in **Figure 5.11** indicate cells expressing T1195S, P1196L and ΔTPSP mutants may exhibit greater levels of proliferation compared to cells expressing wild type PTCH1. As this data is only a single experiment, further repeats are necessary to be able to draw firm conclusions on the impact of TPSP mutants on cell proliferation. However, this result suggests that the TPSP motif, or specific mutations within could play a crucial role in regulating cell proliferation. The fact that TPSP mutants could potentially lead to an increase in cell proliferation implies that this motif could have a suppressive or inhibitory role in controlling cell growth. This trend is also

significant as it points towards a contribution of the TPSP towards a hallmark of cancer. This indicates that a normal function of the TPSP motif is to oppose ERK1/2 signalling and cell proliferation and that mutations in this motif can drive dysregulated cell division and growth regulation that is fundamental for tumour development.

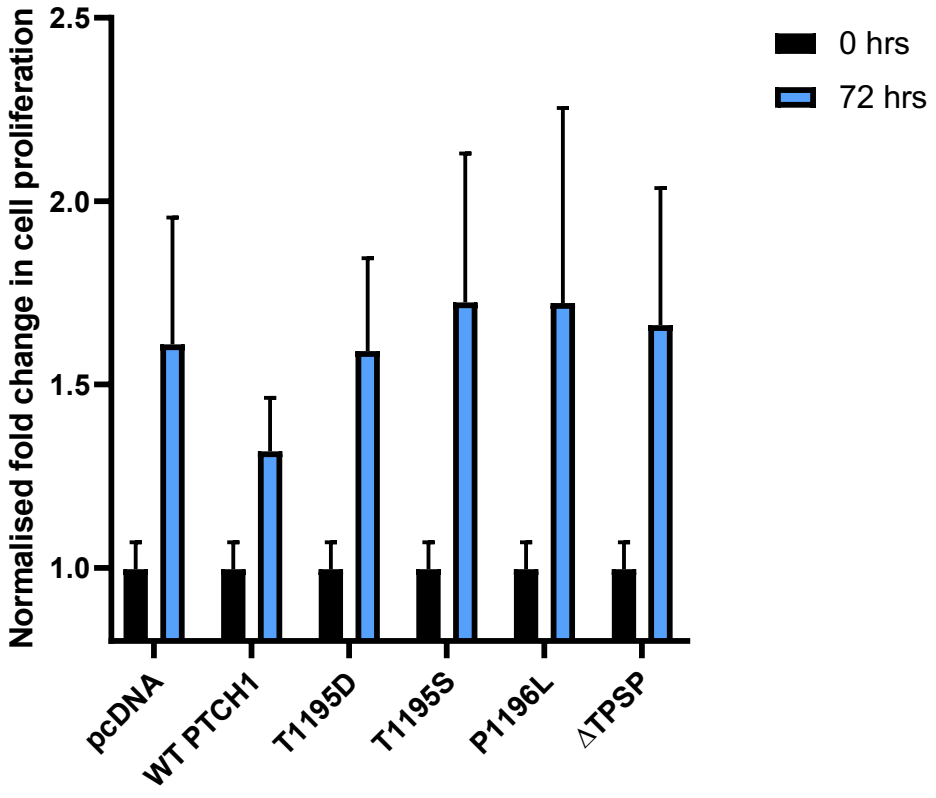

Figure 5. 10 Disease-associated mutants could exhibit higher levels of cell proliferation

WST-1 assay was performed in *Ptch1*$^{-/-}$ HEK293 cells, transiently transfected with each mutant and left to grow for 72 hrs. This graph is representative of a single experiment. Each well was treated with the WST-1 reached for 1 hr at 37°C and 5% CO_2. The OD450-650 difference was measured and the fold-change in absorbance was plotted.

5.4 Discussion

Here, I have presented a systematic approach to uncovering the functional role and significance of the TPSP motif. As confirmed in Chapter 3, the TPSP motif is not involved in the stability or turnover of PTCH1, therefore leaving several canonical and non-canonical functions of PTCH1 in which it could be involved.

There were several significant findings from this chapter: firstly, the finding that the TPSP is not involved in the activation of the non-canonical pathway. This finding directly contradicts the predictions put forward by both Kawamura et al. (2008) and Wang et al. (2019), this chapter provides experimental evidence where previously the work was purely hypothetical. The luciferase data comes from a solid experimental plan used in other studies (Morales, C. 2021; Timmis et al., 2023) showing that all luciferase data produced in this chapter is reliable and reflects motif function.

Where these experiments falter is the use of excessive protein levels achieved through plasmid overexpression, which does not reflect cellular protein levels. As a result, it cannot be definitively concluded that the effect of each TPSP mutant on pathway activity is truly representative of cellular activity. It does, however, provide a solid foundation further research. It supports the notion that the SSD is likely to have a greater involvement in canonical HH activity of PTCH1.

The autophagy findings confirm, using a trusted experimental procedure (Chen et al. 2014; Caballero et al., 2023), the hypothesis that the TPSP would not be involved in the regulation of autophagic flux, agreeing with the findings from

Caballero et al. (2023) that show this regulation from the distal portion of the PTCH1 CTD.

The discovery that the TPSP motif is involved in the regulation of Erk is significant. It builds on previous work from Riobo et al. (2006) and Chang et al. (2010) who first discovered a non-canonical link between PTCH1 and Erk phosphorylation. The negative regulation of Erk phosphorylation had already been reported by these groups; however, the exact mechanism by which this occurred was unknown. Here, I demonstrate that the TPSP motif plays a fundamental role in the regulation of Erk phosphorylation. This finding does not uncover the molecular mechanism of how ERK1/2 phosphorylation is regulated by the TPSP motif, only that it has a functional connection. As mutations to the TPSP motif increase the levels of phospho-Erk1/2 in response to SHH, they could potentially stimulate many downstream effectors of ERK1/2 signalling that regulate proliferation and survival, such as ribosomal S6 kinase- cAMP response element-binding protein (CREB) interaction (Bonni et al., 1999). The observed connection between a mutated TPSP motif and enhanced phospho-Erk levels is consistent with the links seen between PTCH1 mutations and BCC cases (Hahn et al., 1996; Johnson et al., 1996).

The immediate next step for this research is to repeat the WST-1 assay data, analysing cell viability. While the WST-1 assay is widely regarded as a method to analyse metabolic activity (Wahab et al., 2017), any small changes in experimental conditions may have a big impact on the results. Therefore, repeats are necessary to ensure the validity of this data. Additionally, different cell lines could be used to help verify the generalisability of the observed effects. Indeed,

stable transfection of cells to establish a long-term transfection would be another model for looking at colony formation.

Using these methods would further the understanding of the role of the TPSP motif and the impact of mutations on PTCH1 functions. Altogether, this chapter presents a comprehensive investigation into the functional role of the TPSP motif, through the analysis of canonical and non-canonical roles of PTCH1. The findings suggest a role of this motif in regulation of ERK1/2 signalling by non-canonical type I HH signalling and a consequent impact on cell proliferation that agrees with the association of TPSP mutations with cancer.

Chapter 6

Investigation into the interactions between Pin1 and PTCH1

Chapter 6

Investigation into the interactions between Pin1 and PTCH1

6.1 Introduction

In Chapter 3 of this thesis, work was focused on examining the phosphorylation profile of WT PTCH1 under basal conditions, whilst also exploring alterations in the phosphorylation patterns associated with TPSP mutants. The most significant observation was the loss of phosphorylation at both T1195 and S1197 in the P1196L mutant. This finding is significant as changes in the phosphorylation profile of a protein can lead to significant changes in protein-protein interactions and downstream signalling events.

Chapter 5 of this thesis built upon these findings by investigating the impact of these mutations and their role in both canonical and non-canonical functions of PTCH1. The data from this chapter highlighted a potential role in the ability of PTCH1 to block ERK1/2 phosphorylation and the enhanced cell viability associated with the T1195S and P1196L mutations. The precise mechanisms governing the influence of PTCH1 on ERK1/2 phosphorylation is unclear as it is also whether the increased proliferation is associated with the increased basal phospho-ERK1/2 levels, a link difficult to confirm since blocking ERK activation will strongly impact cell proliferation in the presence or absence of PTCH1. Therefore, the final period of my project focused on investigating potential binding partners of the phosphorylated TPSP motif to further understand the link between the TPSP motif and downstream changes in ERK1/2 phosphorylation.

Interest in this project therefore shifted to researching potential binding partners for this motif. Through this research, the protein prolyl isomerase (PPIase) Pin1 which binds phospho-(S/T)P motifs appeared as a strong candidate for a binding partner. The role of Pin1 is to interconvert the proline peptide bonds between the cis and trans conformations and its hyperactivity and overexpression has been linked with a poor prognosis in several cancer types including breast cancer (Wulf et al. 2001). This is of importance because, as previously explained, the T1195S mutation has been linked to an increase in breast cancer recurrence (Wang et al. 2019). Pin1 is a very well-understood and well-studied isomerase; however, due to its multitude of targets and the complexity of the interplay between its targets, there is still much we do not know about how Pin1 promotes tumorigenesis.

There have previously been no studies investigating the link between Pin1 and PTCH1, therefore this chapter presents an extremely novel, but well-founded area of research. The basis for this research stems from the knowledge that a mutated TPSP motif is strongly associated with disease progression and that I showed that this motif is important in the ability of PTCH1 to reduce ERK1/2. However, it is unknown whether PTCH1 effect on ERK1/2 activation is direct or indirect and through what mechanism. Pin1 is a known tumour activator, and, in the context of the RAS/MAPK/ERK signalling pathway, it has been shown that the Pin1 inhibitor Juglone can block the activation of this pathway as well as the Wnt signalling pathway (Wu et al. 2022).

6.2 Aims and Hypothesis

The sequence and phosphorylation pattern of the TPSP motif of PTCH1 suggests that it could be a recruiting motif for Pin1. There are no previous studies linking Pin1 and PTCH1. It was decided in this project to investigate this potential relationship, with a particular focus on the role of the TPSP motif. This direction stemmed from the previous data in this project analysing the functional implication of the TPSP motif on the canonical and non-canonical functions of PTCH1, which support a role for the TPSP motif in regulating cell proliferation and ERK1/2 phosphorylation.

The rationale behind this investigation stems from the knowledge that Pin1 interacts with its target proteins through phospho-(S/T)P motifs, the knowledge that the TPSP motif is phosphorylated in normal physiological states on T1195 or S1197, and the knowledge that cancer-associated mutations in the TPSP motif alter its phosphorylation profile, thus provide a solid foundation for investigating the potential of Pin1 binding to PTCH1 and if it has any functional consequences.

The specific aims of this chapter were:

- To investigate the potential binding capacity of Pin1 to PTCH1 using a pulldown binding assay.
- Using this knowledge, to identify the exact binding location and the involvement of the TPSP motif using several PTCH1 mutant proteins.

6.3 Results

6.3.1 Pin1 interacts with PTCH1

To investigate the interaction between Pin1 and PTCH1, I first expressed a Pin1-gluthathione-S-transferase (GST) fusion and GST alone in *E. coli*, to use as pulldown bait. These proteins were produced using BL21 (DE3) cells transformed with either a Pin1-GST plasmid or a GST plasmid. Protein production was induced using 1 mM IPTG after which the cells were harvested, and the proteins were purified as explained in the Methods. The isolated proteins were purified by means of the high affinity of GST to glutathione (GSH) using GSH-Sepharose beads. Given the difference in molecular weight between Pin1-GST and GST (48 kDa vs 25 kDa), the following experiments testing the binding of PTCH1 were performed with double the amount of Pin1-GST compared to GST to keep an equimolar ratio.

Purified Pin1-GST and GST were loaded onto SDS-PAGE gels alongside known decreasing concentrations of BSA protein standards before being stained with Coomassie blue to estimate protein concentration. From the data shown in **Figure 6.1**, the expected molecular weight of each protein was confirmed, the relative concentration of each preparation, and the correct volume of protein and beads to be loaded in the pulldown assays was calculated. From the previous reading, I chose to use 5 ug of GST and 10 ug of Pin1-GST bait proteins to be incubated with each cell lysate and analyse PTCH1 binding.

The next step involved incubating the GSH beads with fresh lysates of HEK293 cells transiently expressing the desired protein, with the lysate being split into two

even aliquots to incubate with Pin1-GST and with GST alone to establish the degree of nonspecific binding **(Figure 6.2)**.

The first set of experiments were designed to confirm whether Pin1 binds to PTCH1 performing a Pin1-GST pulldown assay followed by western blot of myc-tagged PTCH1. **Figure 6.2** depicts cell lysates expressing WT myc-PTCH1 incubated with Pin1-GST and GST separately, alongside the control lysates expressing empty vector *pcDNA 3.1+* and Pin1-GST and GST beads. The inclusion of pcDNA samples and beads serve as a reference to evaluate the specificity of any interaction seen. Comparison of the samples containing PTCH1 shows a much stronger pulldown of myc-PTCH1 with Pin1-GST beads than with GST beads **(Figure 6.3A)**, indicating that Pin1 interacts with PTCH1. The absence of an immunoreactive band in the lanes of the control samples and the beads highlight the specificity of the assay. The enrichment of PTCH1 in the lanes incubated with Pin1-GST compared to GST alone was further confirmed by densitometry analysis **(Figure 6.3B)**. It is worth noting that there are some non-specific interactions between myc-PTCH1 and GST alone or to the beads themselves, highlighting the importance of the controls that were chosen to subtract non-specific binding.

The data from this experiment successfully confirm an interaction between Pin1 and wild-type PTCH1, as we predicted. This initial finding is a crucial step to understanding the functional roles of Pin1 in the context of PTCH1 and HH signalling.

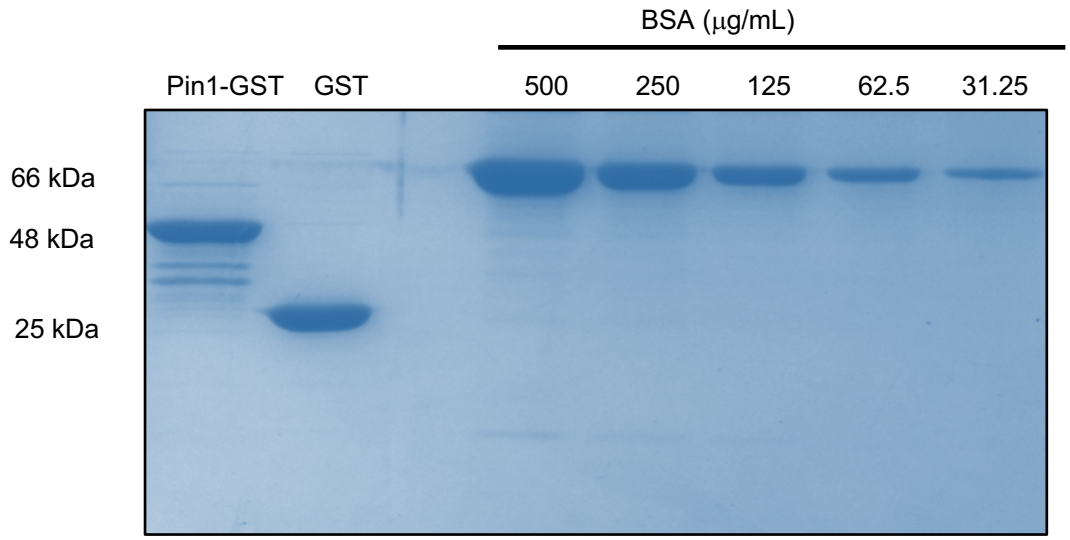

Figure 6. 1 Purification of Pin1-GST and GST proteins and estimation of yield using BSA standards

SDS-PAGE gel stained with Coomassie blue stain showing the protein concentration 5 μL of Pin1-GST and GST proteins bound to Glutathione Sepharose ™ 4B beads, alongside the indicated amounts of a BSA protein standard, loading 5 μL of each standard.

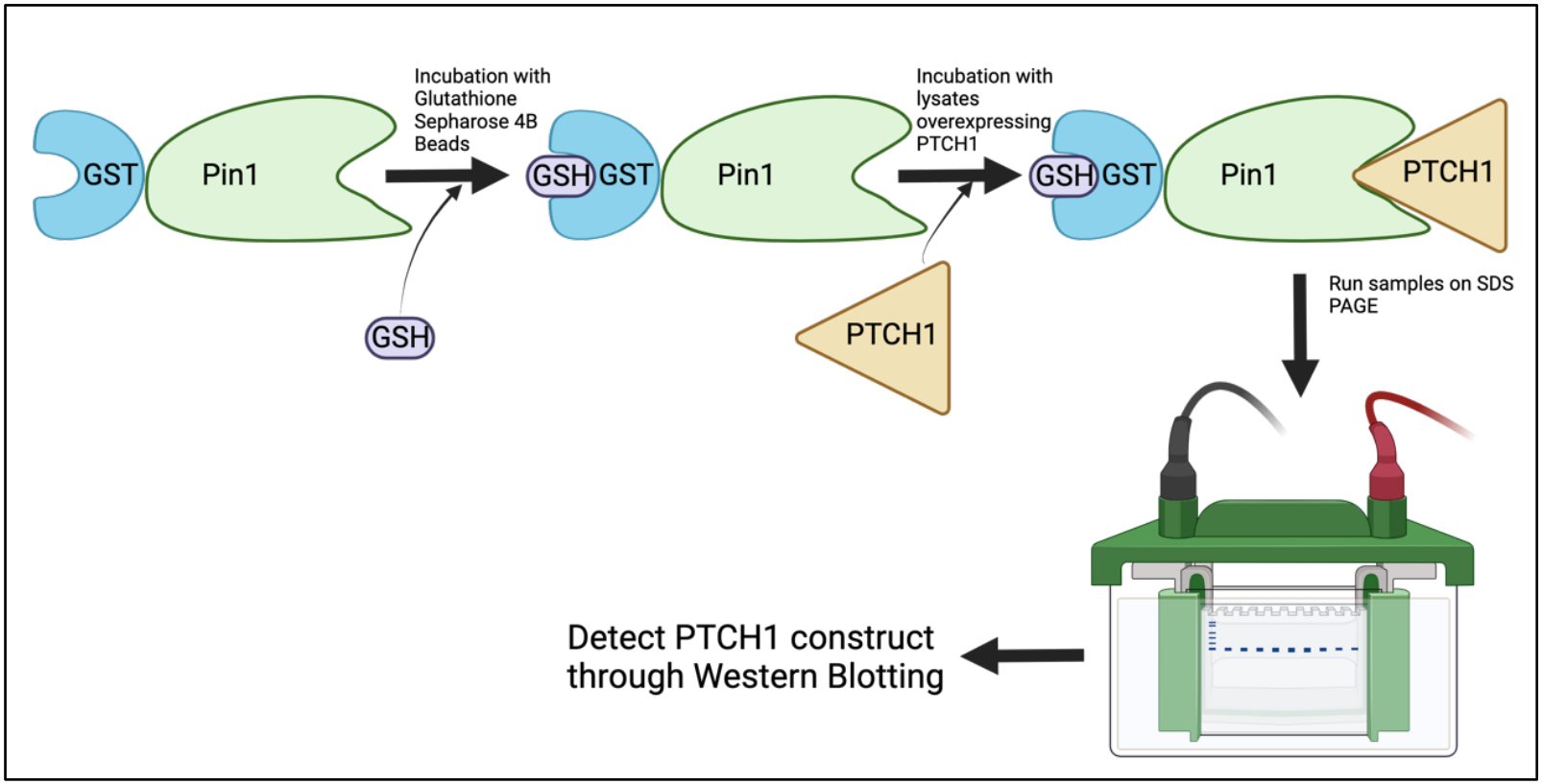

Figure 6. 2 Experimental design of the Pin1 binding assay

Pin1-GST and GST proteins were produced in BL21 DE3 cells before being incubated with Glutathione (GSH) Sepharose 4B beads. The beads were then incubated with lysates overexpressing PTCH1 proteins before they were subjected to SDS-PAGE and PTCH1 proteins were detected using western blot analysis. Image generated using Biorender.com.

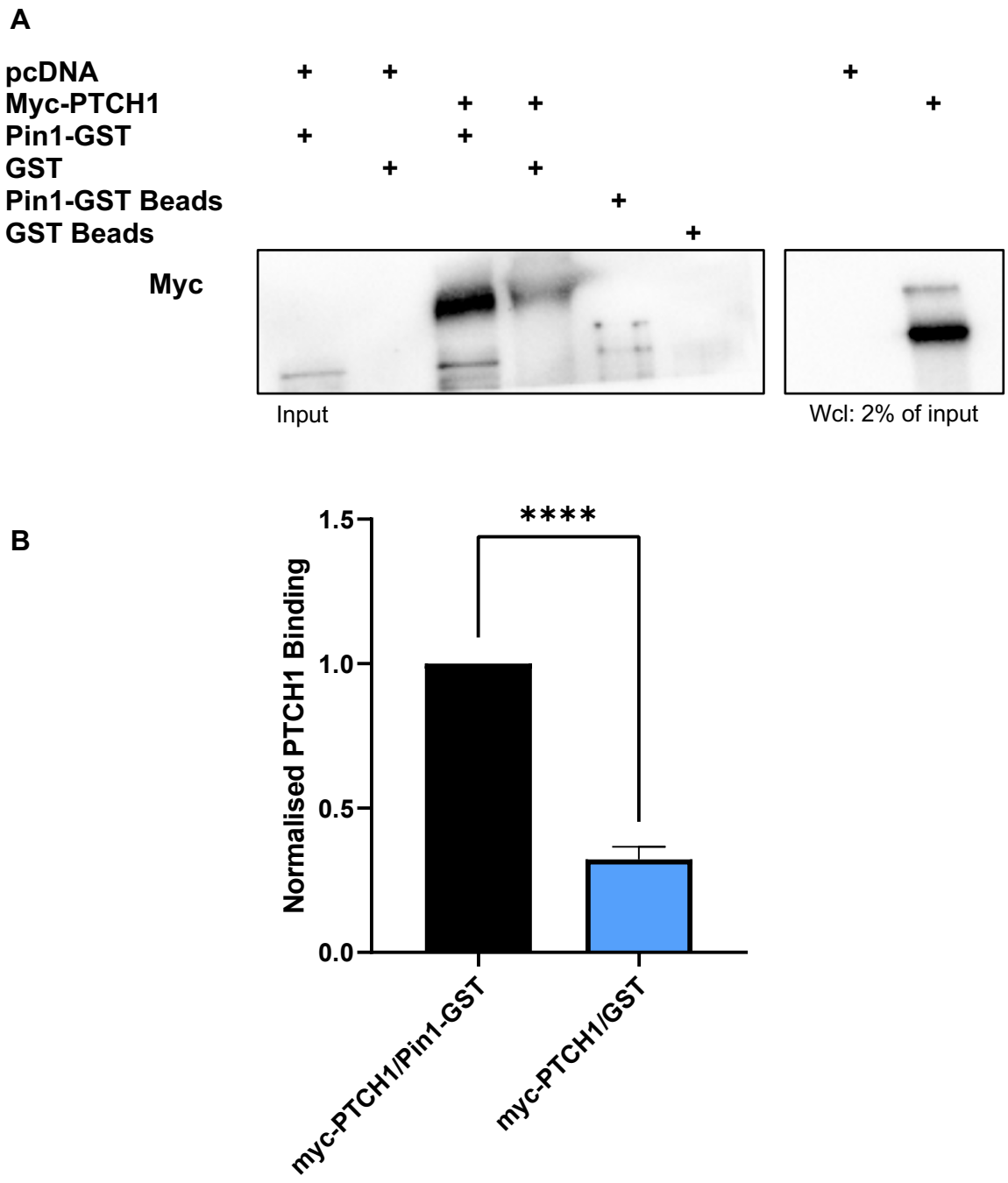

Figure 6. 3 Pin1 interacts with PTCH1

(A) HEK293 lysates overexpressing pcDNA and myc-PTCH1 were split into two and incubated with Pin1-GST and GST beads. The samples were analysed through western blotting, using anti-myc antibody to detect the myc-PTCH1 protein. Protein beads were run alongside the samples, and whole cell lysates (wcl) were run to check protein expression. **(B)** Quantification of Pin1 binding using densitometry

N = 3, **** = p<0.0001

6.3.2 Pin1 interacts with the PTCH1 CTD

To investigate the precise location of the Pin1 binding site(s) within PTCH1, and to determine the involvement of the TPSP motif, it was first decided to confirm whether the isolated CTD of PTCH1 can interact with Pin1. HEK293 lysates overexpressing full length PTCH1-HA, or the CTD-HA fragment were incubated with Pin1-GST and GST proteins before being analysed by western blotting.

The results clearly demonstrate that Pin1 does interact with the PTCH1 CTD **(Figure 6.4)**. The detection of PTCH1 CTD-HA in the lane where CTD-HA was incubated with Pin1-GST provides evidence of a specific interaction between Pin1 and the PTCH1 CTD.

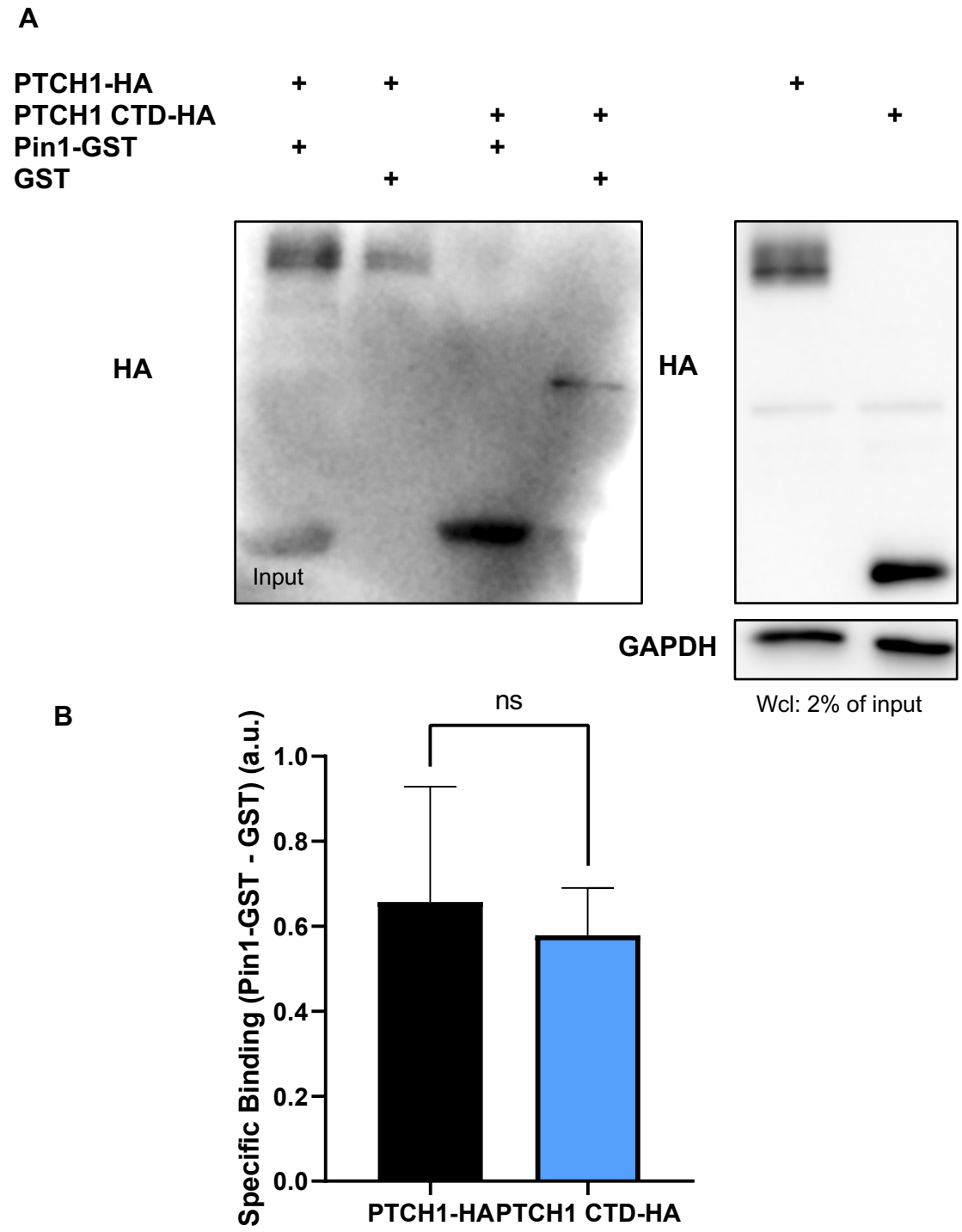

Figure 6. 4 Pin1 interacts with the PTCH1 CTD

(A) HEK293 lysates overexpressing PTCH1-HA and PTCH1 CTD-HA were split into two aliquots and incubated with Pin1-GST and GST beads. The samples were analysed through western blotting, using anti-HA antibody to detect each protein, and whole cell lysates were run to check protein expression and to ensure even loading. **(B)** Quantification of Pin1 binding using densitometry.

N = 3, * = $p<0.05$

6.3.3 The TPSP motif is not essential for Pin1 binding to PTCH1

The interaction between Pin1 and the PTCH1 CTD is of particular interest. The TPSP motif has been identified as a potential target for Pin1 because of the associated proline-directed phosphorylation of the serine and threonine residues. The next part of the experimental plan was to determine whether Pin1 interaction requires the TPSP motif. To do this, the Pin1 binding assay was carried out using the variety of TPSP mutants that were described in the previous chapter. Firstly, the aim was to determine whether Pin1 binds at TPSP. This was investigated using the ΔTPSP and double alanine (T1195A/S1197A) mutant that cannot be phosphorylated. Western blot and subsequent densitometry analysis show that removal of the TPSP motif and removal of the capacity for phosphorylation does not reduce the binding capacity of Pin1 to PTCH1 **(Figure 6.6)**.

Research then shifted to understanding whether the disease-associated mutant T1195S impacted the binding of Pin1 to PTCH1, in particular the P1196L mutant that promoted phosphorylation of S1203. The hypothesis behind this experimental decision was to understand whether disease-associated mutations improve the binding of Pin1 to PTCH1, impacting the tumour suppressor function of PTCH1. Pin1 upregulation has been observed in breast cancer, with elevated Pin1 associated with poorer prognosis. This is interesting as there has been an observed connection between the T1195S mutant and an increased incidence of breast cancer recurrence. The working hypothesis was that the increased abundance of phosphorylation detected by mass spectrometry in the T1195S mutant might facilitate Pin1 binding and enhance its oncogenic functions, as a first step towards understanding the mechanism linking the PTCH1 mutation to increased incidence of breast cancer recurrence.

Analysis in **Figure 6.7** yielded the surprising result that the disease-associated mutant T1195S does not appear to influence the ability of Pin1 to bind to PTCH1. This result suggests that while the TPSP motif may still play a secondary role in Pin1 binding, it is not essential for the interaction. A plausible explanation for this could be that PTCH1 possesses multiple Pin1 binding sites within the CTD or in the CTD and other intracellular domains, with Pin1 interacting in a sequential binding mechanism, as previously discussed in the introduction. In addition, whilst the TPSP may not be required for Pin1 binding, it could still mediate a role of Pin1 on PTCH1 regulation, for example, if the TPSP motif is isomerised by Pin1 bound to another region.

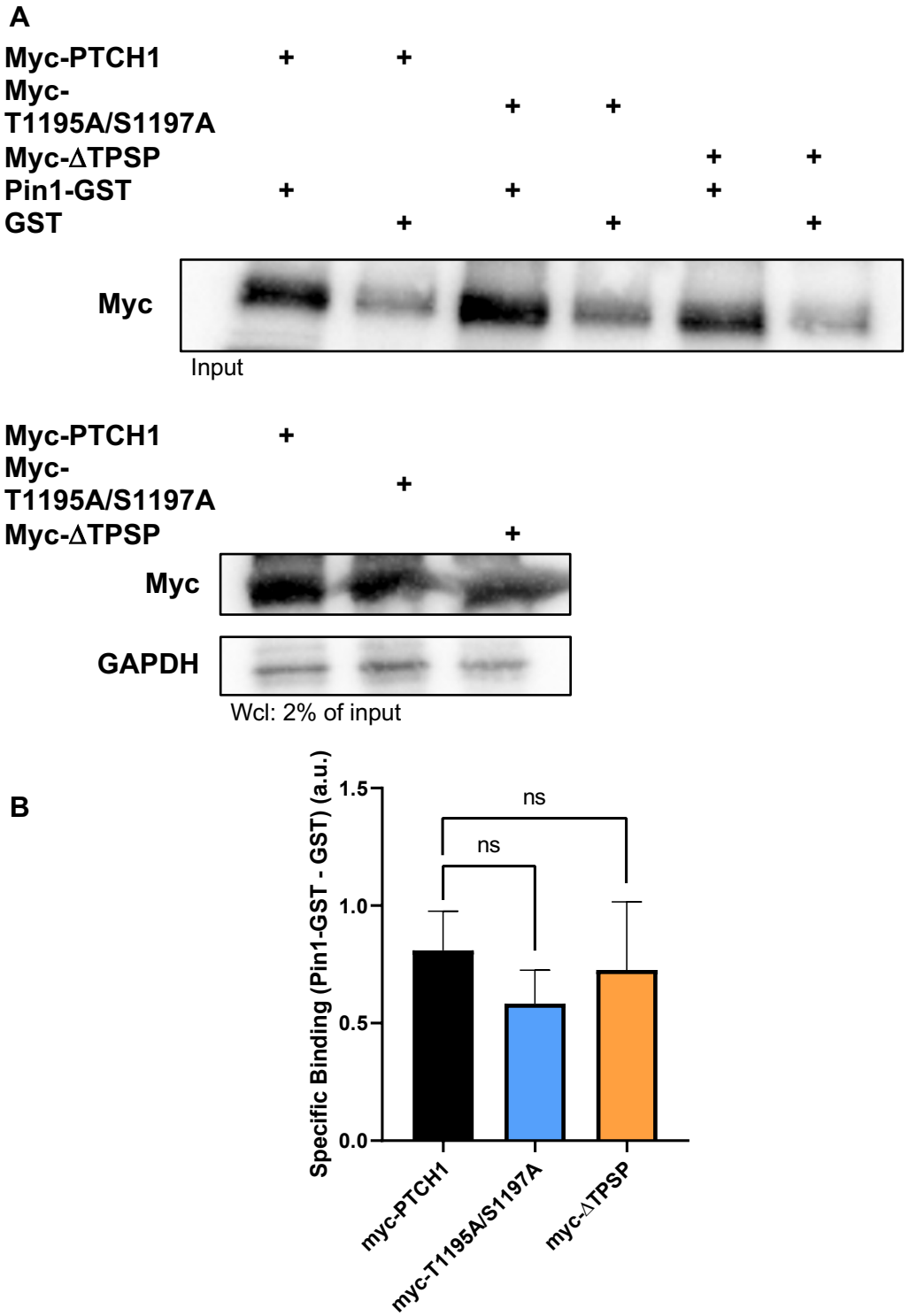

Figure 6. 6 TPSP motif is not involved in the binding of Pin1 in basal conditions

(A) HEK293 lysates overexpressing myc-PYCH1, T1195A/S1197A and ΔTPSP were split into two aliquots and incubated with Pin1-GST and GST beads. The samples were analysed through western blotting, using anti-myc antibody to detect the proteins, and whole cell lysates were run to check protein expression and to ensure even loading. **(B)** Quantification of Pin1 binding using densitometry.

N = 3, ns = not significant.

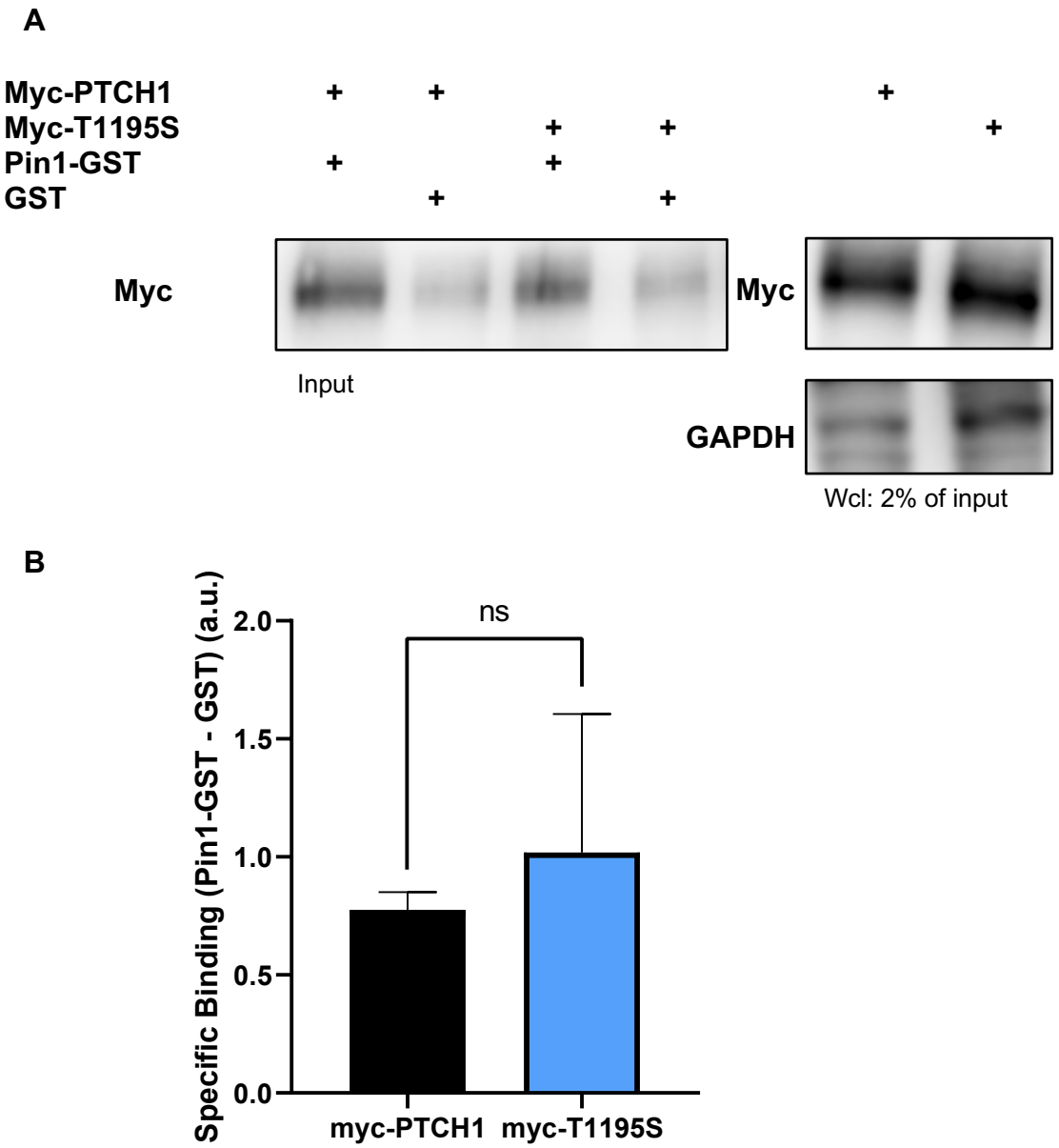

Figure 6. 7 T1195S mutation does not alter Pin1 binding in basal conditions **(A** HEK293 lysates overexpressing myc-PTCH1 and PTCH1 myc-T1195S were split into two aliquots and incubated with Pin1-GST and GST beads. The samples were analysed through western blotting, using anti-myc antibody to detect each protein, and whole cell lysates were run to check protein expression and to ensure even loading. **(B)** Quantification of Pin1 binding using densitometry. N = 3, ns = not significant.

6.3.4 Pin1 interacts with PTCH2

Given that Pin1 interaction with PTCH1 is independent of the TPSP motif, I investigated whether this binding was exclusive to PTCH1 or if Pin1 could similarly interact with PTCH2. Sequence alignments between the two proteins show a sequence identity of ~56%, with the sequence identity primarily appearing in their transmembrane domains. Regarding this project, as has previously explained, PTCH1 shares minimal homology with the CTD of PTCH1, however, there are TP and SP sequences within PTCH1 that are shared with PTCH2, these can be used to identify potential Pin1 binding sites (**Table 6.1**). To investigate the potential for binding of Pin1 to PTCH2, the Pin1 binding assay was used to compare binding to cell lysates expressing PTCH1-HA or PTCH2-HA. The samples were subjected to SDS-PAGE and subsequently analysed using a western blot with the anti-HA antibody (Proteintech). Importantly, PTCH1-HA was run alongside PTCH2-HA to allow comparisons in the levels of binding to Pin1 using the same antibody. The western blot and densitometry analysis in **Figure 6.8** shows that Pin1 interacts with PTCH2 at a level equivalent to that observed with PTCH1. The significance of this result is notable. The absence of the TPSP motif in PTCH2 highlights the versatility of Pin1 as a binding partner, and explains the lack of effect of the PTCH1 TPSP mutants on their ability to interact. The data also suggest that the potential functional role of Pin1-PTCH1 interaction may extend to PTCH2. Understanding the extent to which Pin1 influences PTCH2 and PTCH1 in the context of canonical and noncanonical HH signalling could have implications for therapeutic interventions.

PTCH1 Residue Numbers	PTCH2 Residue Number	TP/SP
-	4, 5	SP
162, 163	-	TP
230, 231	187, 188	TP
369, 370	324, 325	TP PTCH1 SP PTCH2
618, 619	570, 571	SP
640, 641	-	SP
701, 702	-	SP
-	705, 706	SP
-	1018, 1019	SP
1185, 1186	-	SP
1195, 1196	-	TP
1197, 1198	1127, 1128	SP
--	1132, 1133	SP
	1184, 1185	SP

Table 6. 1 TP and SP motifs in PTCH1 and PTCH2

A table highlighting TPS and SP motifs within PTCH1 and PTCH2 with corresponding residue numbers. All of these sites are potential Pin1 binding sites.

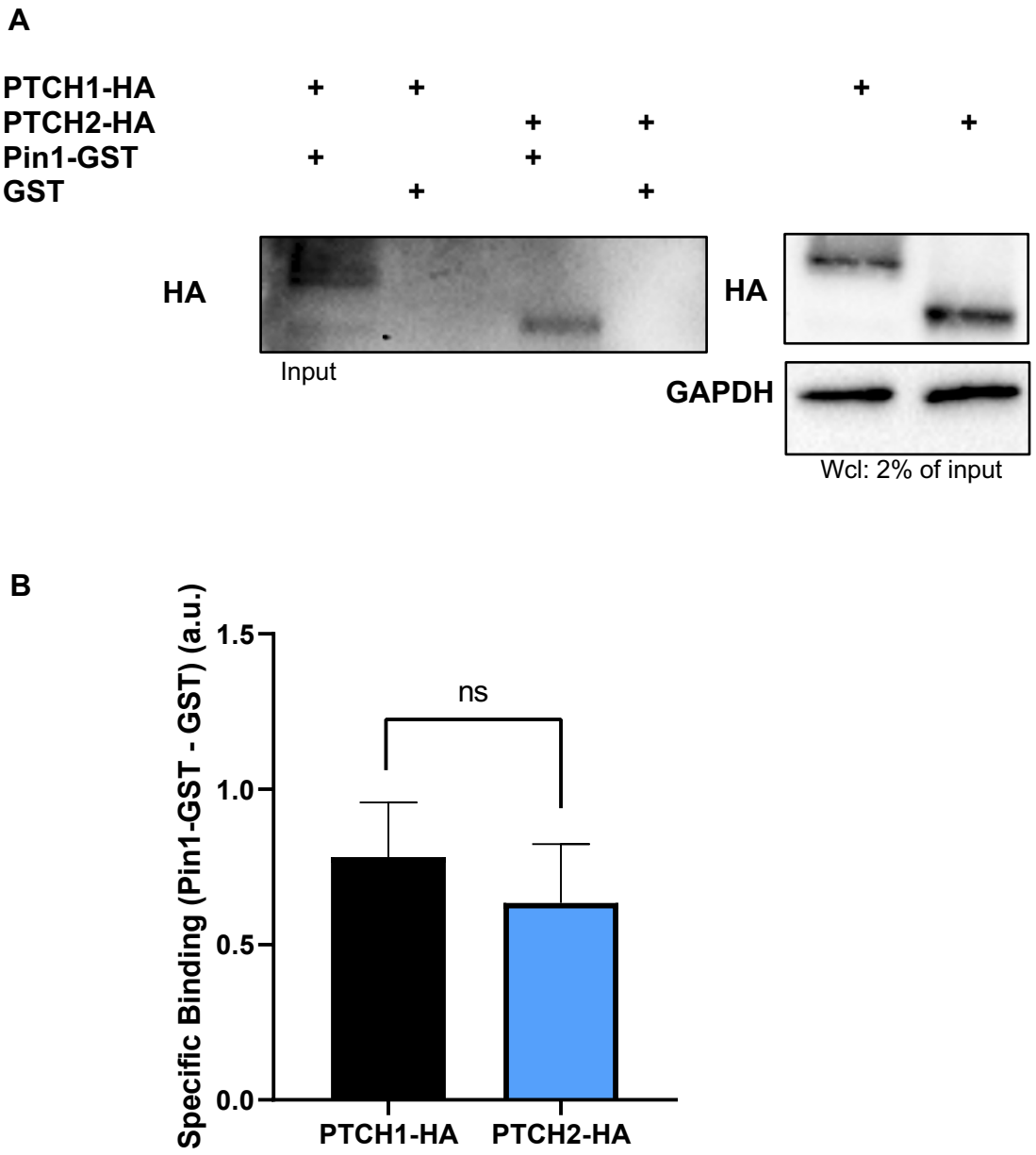

Figure 6. 8 Pin1 interacts with PTCH2

(A) HEK293 lysates overexpressing PTCH1-HA and PTCH2-HA were split into two aliquots and incubated with Pin1-GST and GST beads. The samples were analysed through western blotting, using anti-HA antibody to detect the proteins, and whole cell lysates were run to check protein expression. **(B)** Quantification of Pin1 binding using densitometry.

N = 3, ns = not significant

6.3.5 Overexpression of Pin1 does not appear to alter canonical HH signalling

A preliminary investigation into the functional significance of the Pin1-PTCH1 interaction was limited to investigating the effect of Pin1 overexpression on repression of canonical HH signalling by PTCH1 in *Ptch1*$^{-/-}$ MEFs. The experiment aimed to determine whether elevated levels of Pin1 would have a noticeable effect on HH signalling. To investigate this, the GLI-luciferase reporter assay was used and carried out in *Ptch1*$^{-/-}$ MEFs, a cell line which are able to form cilia much more readily than HEK293 cells, allowing for the analysis of canonical HH signalling in the cilia through the use of the GLI-luciferase reporter assay. The cells were co-transfected with myc-PTCH1 and Pin1-HA plasmids, together with 8xGBS-luciferase and pTK-Renilla reporters, before being serum starved for 48 hrs and the relative GLI-luciferase levels being measured. The choice to use 50% PTCH1 was to mirror the 50% PTCH1 used in the Pin1:PTCH1 co-transfection, this ensures that any changes in canonical pathway activity between the samples is not caused by differing levels of PTCH1 and therefore can allow for a clear analysis of the impact of Pin1 on canonical HH signalling. The levels of DNA were kept consistent by supplementing with pcDNA 3.1+. The data in **Figure 6.9** shows that Pin1 overexpression does not impact inhibition of canonical HH signalling by PTCH1.

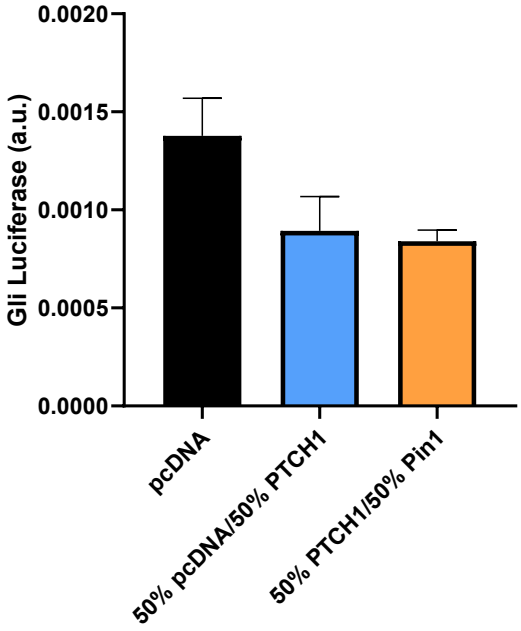

Figure 6. 9 Pin1 overexpression does not affect PTCH1 canonical activity

Ptch1$^{-/-}$ MEFs were transfected with myc-PTCH1 and Pin1-HA and the relative GLI activity was measured using the GLI-luciferase reporter assay. 50% pcDNA/50% PTCH1 experimental condition indicates that 50% of the total DNA was pcDNA and 50% was myc-PTCH1. This was to ensure that any changes in activity levels seen in the 50% PTCH1/50% Pin1 was due to Pin1 and not PTCH1. Representative of a single experiment with four wells for each condition combined and the mean displayed.

6.4 Discussion

The results presented in this chapter highlight a novel interaction between the PPIase, Pin1, and the human PTCH proteins, PTCH1 and PTCH2. Unexpectedly, the binding does not involve the TPSP domain that we hypothesised. This data highlights the complexity of Pin1 binding by demonstrating the binding of Pin1 to a domain of PTCH1 – the CTD – that shares little sequence homology with PTCH2. This immediately points to multiple Pin1 binding sites within both PTCH1 and PTCH2, the downstream effects of which are yet unknown. The binding of Pin1 to PTCH1 may result in a similar or totally different cellular response to then it binds to PTCH2, this remains to be investigated.

Contrary to initial expectations, the mutation of the TPSP motif does not diminish Pin1 binding to PTCH1. Removal of the capacity for phosphorylation and the removal of the entire motif did not alter the levels of PTCH1 binding. This result suggests that, while Pin1 may interact with the TPSP motif, it is not fully reliant on it for binding. This raises the question of what other mechanisms or motifs within PTCH1 may mediate the Pin1-PTCH1 and Pin1-PTCH2 interactions. An explanation for this could be that the concentrations of Pin1-GST employed in the binding assay exceed the levels necessary for PTCH1 and Pin1 to reach their maximum binding capacity. Consequently, this could lead to an oversaturation of Pin1, producing inconsistent data that indicates binding is only occurring because protein concentrations are so high and not reflective of true, physiological binding. Changes in Pin1 binding between mutants and homologues may be more evident at a more physiological concentration of Pin1 and PTCH1, which could be explored by co-immunoprecipitation. This may yield clearer insights into Pin1-PTCH1 interactions.

The CTD of PTCH1 contains three plausible TP and SP motifs for Pin1 binding, two of which were investigated in this chapter using the TPSP mutant constructs. The mass spectrometry data presented earlier in this thesis was unable to confirm the phosphorylation of the other SP motif within the PTCH1 CTD (S1185-P1186), so it is unknown whether S1185 represents a feasible binding site for Pin1. Interestingly, PTCH2 contains two SP motifs in its C-tail, one analogous to the TPSP location of PTCH1 and a second one further downstream, which should also be investigated as potential binding sites. Attempts were made to generate a phospho-dead mutant of the S1185 residue of PTCH1 to investigate this, but this was unfortunately unsuccessful.

Analysing both this and the Pin1-PTCH2 data provides an interesting insight into how Pin1 interacts with the PTCH proteins. Notably, the low level of sequence homology between the CTDs of both proteins, Pin1 is still able to interact with both domains. This data suggests that the interaction between the Pin1 and the PTCH proteins is not solely dictated by sequence homology or the presence of a TPSP motif. Instead, Pin1 appears to employ several modes of interaction with these proteins.

Future investigation of this subject is vitally important, the apparent complex nature of PTCH1-Pin1 interactions points towards a novel non-canonical function of PTCH1. Additionally, the immense range of proteins that Pin1 regulates, and its many links to cancer development and a poor prognosis mean that a relationship between Pin1 and PTCH1 could uncover a previously unknown

avenue for cancer treatment research. Modulation of PTCH1 by Pin1 must be better understood as it could open a new target for cancer therapeutics.

Future experimental analysis could involve carrying out the GLI-luciferase assay when co-transfecting *Ptch1*$^{-/-}$ MEFs with Pin1-HA and TPSP mutant plasmids. This approach would shed light on whether a mutated TPSP motif influences canonical HH signalling in the presence of higher levels of Pin1. The complex nature of Pin1-PTCH1 interactions not only opens our eyes to further understanding the molecular mechanisms at play within the HH signalling pathway but also holds significant promise for broader research implications. The interplay between Pin1 and PTCH1 is intriguing and continued exploration into this is vital.

Chapter 7

Investigating the heteromeric interactions between PTCH1 and PTCH2

Chapter 7 Investigating the heteromeric interactions between PTCH1 and PTCH2

7.1 Introduction

The understanding of the relationship between PTCH1 and PTCH2 remains limited, with a need to develop the understanding further. Sequence analysis of the two proteins reveals a sequence identity of 56%, with the greatest similarity occurring in the transmembrane domains (Kawamura et al., 2008; Qian et al., 2019). Despite both proteins possessing extracellular domains, their sequence homology in these regions is notably lower (**Figure 7.1B**).

Prior studies conducted by other groups have demonstrated that the SSD of PTCH2, which has high homology with the SSD of PTCH1, can effectively repress SMO (Fleet and Hamel 2019).

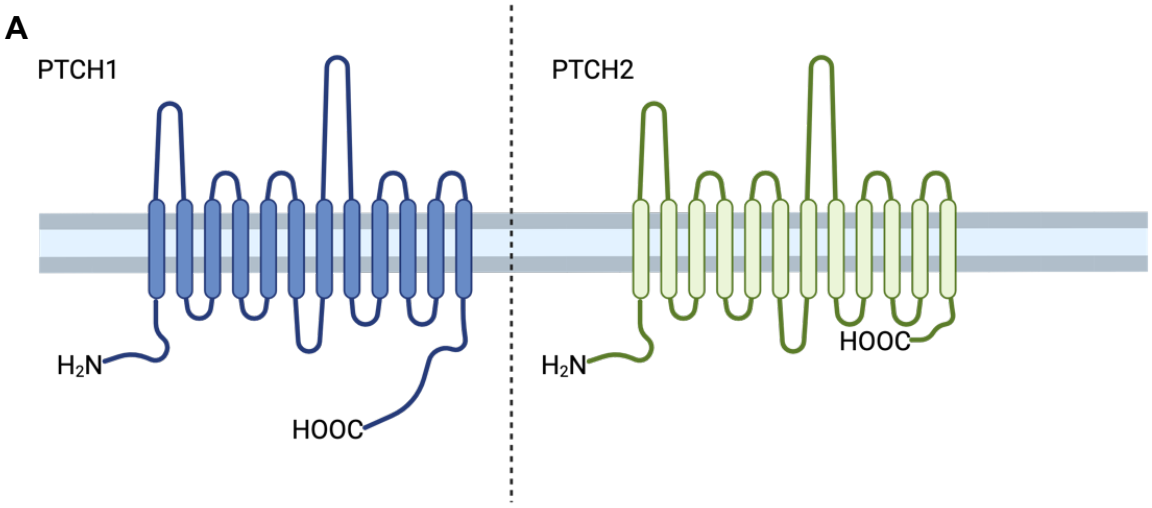

B


Human PTCH1 MASAGNAAEP QDRGGGGSGC IGAPGRPAGG GRRRRTGGLR RAAAPDRDYL 50
Human PTCH2 MT--------- ---------- ---------- ----RSPPLR ELP------- 11
Human PTCH1 HRPSYCDAA- FALEQISKGK ATGRKAPLWL RAKFQRLLFK LGCYIQKNCG 99
Human PTCH2 --PSYTPPAR TAAPQILAGS L---KAPLWL RAYFQGLLFS LGCGIQRHCG 56
Human PTCH1 KFLVVGLLIF GAFAVGLKAA NLETNVEELW VEVGGRVSRE LNYTRQKIGE 149
Human PTCH2 KVLFLGLLAF GALALGLRMA IIETNLEQLW VEVGSRVSQE LHYTKEKLGE 106
Human PTCH1 EAMFNPQLMI QTPKEEGANV LTTEALLQHL DSALQASRVH VYMYNRQWKL 199
Human PTCH2 EAAYTSQMLI QTARQEGENI LTPEALGLHL QAALTASKVQ VSLYGKSWDL 156
Human PTCH1 EHLCYKSGEL ITTETGYMDQI IEYLYPCLII TPLDCFWEGA KLQSGTAYLL 249
Human PTCH2 NKICYKSGVP LIENGMIERM IEKLFPCVIL TPLDCFWEGA KLQGGSAYLP 206
Human PTCH1 GKPPLRWTNF DPLEFLEELK KINYQVDSWE EMLNKAEVGH GYMDRPCLNP 299
Human PTCH2 GRPDIQWTNL DPEQLLEELG PFA-SLEGFR ELLDKAQVGQ AYVGRPCLHP 255
Human PTCH1 ADPDCPATAP NKNSTKPLDM ALVLNGGCHG LSRKYMHWQE ELIVGGTVKN 349
Human PTCH2 DDLHCPPSAP NHHSRQAPNV AHELSGGCHG FSHKFMHWQE ELLLGGMARD 305
Human PTCH1 STGKLVSAHA LQTMFQLMTP KQMYEHFKGY EYVSH-INWN EDKAAAILEA 398
Human PTCH2 PQGELLRAEA LQSTFLLMSP RQLYEHFRG- DYQTHDIGWS EEQASTVLQA 354
Human PTCH1 WQRTYVEVVH QSVAQNSTQK VLSFTTTTLD DILKSFSDVS VIRVASGYLL 448
Human PTCH2 WQRRFVQLAQ EALPENASQQ IHAFSSTTLD DILHAFSEVS AARVVGGYLL 404
Human PTCH1 MLAYACLTML RWDCSKSQGA VGLAGVLLVA LSVAAGLGLC SLIGISFNAA 498
Human PTCH2 MLAYACVTML RWDCAQSQGS VGLAGVLLVA LAVASGLGLC ALLGITFNAA 454
Human PTCH1 TTQVLPFLAL GVGVDDVFLL AHAFSETGQN KRIPFEDRTG ECLKRTGASV 548
Human PTCH2 TTQVLPFLAL GIGVDDVFLL AHAFTEALPG T--PLQERMG ECLQRTGTSV 502
Human PTCH1 ALTSISNVTA FFMAALIPIP ALRAFSLQAA VVVVFNFAMV LLIFPAILSM 598
Human PTCH2 VLTSINNMAA FLMAALVPIP ALRAFSLQAA IVVGCTFVAV MLVFPAILSL 552
Human PTCH1 DLYRREDRRL DIFCCFTSPC VSRVIQVEPQ AYTDTHDNTR YSPPPPYSSH 648
Human PTCH2 DLRRRHCQRL DVLCCFSSPC SAQVIQILPQ ---ELGDGT- ----VPVG-- 592
Human PTCH1 SFAHETQITM QSTVQLRTEY DPHTHVYYTT AEPRSEISVQ PVTVTQDTLS 698
Human PTCH2 -IAHLT---- -ATVQAFTHC EASSQHVVTI LPPQAHLVPP P----SDPLG 632
Human PTCH1 CQSPESTSST RDLLSQFSDS --SLHCLEPP CTKWTLSSFA EKHYAPFLLK 746
Human PTCH2 SELFSPGGST RDLLGQEEET RQKAACKSLP CARWNLAHFA RYQFAPLLLQ 682
Human PTCH1 PKAKVVVIFL FLGLLGVSLY GTTRVRDGLD LTDIVPRETR EYDFFIAAQFK 796
Human PTCH2 SHAKAIVLVL FGALLGLSLY GATLVQDGLA LTDVVPRGTK EHAFLSAQLR 732
Human PTCH1 YFSFYNMYIV TQKA-DYPNI QHLLYDLHRS FSNVKYVMLE ENKQLPKMWL 845
Human PTCH2 YFSLYEVALV TQGGFDYAHS QRALFDLHQR FSSLKAVLPP PATQAPRTWL 782
Human PTCH1 HYFRDWLQGL QDAFDSDWET GKTMPNNYKN GSDDGVLAYK LLVQTGSRDK 895
Human PTCH2 HYYRNWLQGI QAAFDQDWAS GRITRHSYRN GSEDGALAYK LLIQTGDAQE 832
Human PTCH1 PIDISQLTKQ RLVDADGIIN PSAFYIYLTA WVSNDPVAYA ASQANIRPHR 945
Human PTCH2 PLDFSQLTTR KLVDREGLIP PELFYMGLTV WVSSDPLGLA ASQANFYPPP 882
Human PTCH1 PEWVHDKADY MPETRLRIPA AEPIEYAQFP FYLNGLRDTS DFVEAIEKVR 995
Human PTCH2 PEWLHDKYDT TGEN-LRIPP AQPLEFAQFP FLLRGLQKTA DFVEAIEGAR 931
Human PTCH1 TICSNYTSLG LSSYPNGYPF LFWEQYIGLR HWLLLFISVV LACTFLVCAV 1045
Human PTCH2 AACAEAGQAG VHAYPSGSPF LFWEQYLGLR RCFLLAVCIL LVCTFLVCAL 981
Human PTCH1 FLLNPWTAGI IVMVLALMTV ELFGMMGLIG IKLSAVPVVI LIASVGIGVE 1095
Human PTCH2 LLLNPWTAGL IVLVLAMMTV ELFGIMGFLG IKLSAIPVVI LVASVGIGVE 1031
Human PTCH1 FTVHVALAFL TAIGDKNRRA VLALEHMFAP VLDGAVSTLL GVLMLAGSEF 1145
Human PTCH2 FTVHVALGFL TTQGSRNLRA AHALEHTFAP VTDGAISTLL GLLMLAGSHF 1081
Human PTCH1 DFIVRYFFAV LAILTILGVL NGLVLLPVLL SFFGPYPEVS PANGLNRLPT 1195
Human PTCH2 DFIVRYFFAA LTVLTLLGLL HGLVLLPVLL SILGPPPEVI ------QMYK 1125
Human PTCH1 PSPEPPPSVV RFAMPPGHTH SGSDSSDSEY SSQTTVSGLS EELRHYEAQQ 1245
Human PTCH2 ESPE------- -ILSPP---- ---------- ---------- -------APQ 1137
Human PTCH1 GAGGPAHQVI VEATENPVFA HSTVVHPESR HHPPSNPRQQ PHLDSGSLPP 1295
Human PTCH2 GGG------- ---------- ---------- ---------- ---------- 1140
Human PTCH1 GRQGQQPRRD PPREGLWPPP YRPRRDAFEI STEGHSGPSN RARWGPRGAR 1345
Human PTCH2 ---------- ---------- ---------- ---------- -LRWGA---- 1145
Human PTCH1 SHNPRNPAST AMGSSVPGYC QPITTVTASA SVTVAVHPPP VPGPGRNPRG 1395
Human PTCH2 ---------- --SSSLPQSF ARVTT----- SMTVAIHPPP LPGAYIHPA- 1177
Human PTCH1 GLCPGYPETD HGLFEDPHVP FHVRCERRDS KVEVIELQDV ECEERPRGSS 1445
Human PTCH2 ------PD-- ----EPPWSP AATSSGNLSS ---------- ----RGPGPA 1201
Human PTCH1 SN 1447
Human PTCH2 TG 1203

Figure 7. 1 The structures and alignments of PTCH1 and PTCH2
(A) A visual depiction of PTCH1 and PTCH2 highlighting the similarities in their transmembrane domains and the differences in lengths of their CTDs. Figure generated using Biorender.com **(B)** Sequence alignments between human PTCH1 (Q13635) and PTCH2 (Q9Y6C5), showing the sequence homology between the two proteins. The greatest level of sequence similarity appears within the transmembrane domains (PTCH1: residue 101-1176; PTCH2 residue 58-1115). Generated using CLC Sequence Viewer 8.0.

Mutations associated with *Ptch2*, akin to those seen in *Ptch1*, lead to phenotypes associated with Gorlin syndrome; however, these phenotypes are comparatively less severe in *PTCH2* mutants and very rare. This finding suggests that the role of PTCH2 is much less significant than PTCH1. Indeed, complete knockout of *PTCH1* leads to embryonic lethality whereas complete knockout of *PTCH2*, while leading to some defects in progeny – including skeletal abnormalities, jaw cysts and basal cell tumours – is not lethal.

Regarding PTCH2 activity as a repressor of canonical HH signalling, analysis through GLI-luciferase reporter assays in *Ptch1*$^{-/-}$ MEFs indicates that PTCH2 reduces GLI transcriptional activity by about 20% compared to the maximal inhibition achieved by PTCH1. This difference in activity suggests that the reduced lethality of PTCH2-deficient mice compared to PTCH1 knockouts could be due to the loss of a small fraction of the sum of the activity of PTCH1 and PTCH2. Previous work has also shown that PTCH2 exhibits a similar binding affinity for N-SHH as PTCH1 (Timmis, 2021). Co-transfection of *Ptch1*$^{-/-}$ MEFs with PTCH2 with increasing concentration of SHH-encoding plasmids – allowing us to measure the effect of the paracrine and autocrine SHH produced by the cells, exhibited a dose-dependent reduction in PTCH2 activity, almost entirely

relieving repression of SMO. Given that PTCH2 appears to have a small but important role, a previous PhD student in the lab investigated the possibility that PTCH1 and PTCH2 could form a complex (Timmis, 2021). That research revealed that both PTCH1 and PTCH2 can form homodimers, confirmed through Co-IPs and FRET-recovery after photobleaching (FRAP) assays that indicated a physical interaction between monomers. Subsequently, the propensity of PTCH proteins to form heterodimers was confirmed through FRAP assays. Functional assays showed that the heterodimers exhibit greater activity that comparable amounts of PTCH1 and PTCH2 alone, suggesting a synergistic activity. A competition-based FRAP assay was utilised to investigate whether there was any competition between the PTCH1 and PTCH2 monomers, indicating a preference for the formation of homo- or hetero-interactions. The data from this work indicated that excessive overexpression of PTCH2 only partially impaired the interactions between PTCH1 monomers, suggesting that PTCH1 homodimers appear to be the more favourable interaction (Timmis et al., 2023).

As explained previously, both PTCH1 and PTCH2 share similarities in their sterol sensing domains (SSDs) which initiate protein responses when sterol moieties are detected (Wu et al., 2022). A triple mutation in PTCH1, PTCH1-V111F, L114F, W115A (PTCH1-VLW) has been shown to disrupt a cholesterol channel, potentially blocking cholesterol from being pumped by PTCH1 and affecting the activity of PTCH1 (**Figure 7.2A**)(Zhang, Y. et al., 2018). The residues of PTCH2 predicted to occupy the same position, obtained by threading the PTCH2 sequence onto the published cryo-EM structure of PTCH1 (**Figure 7.2**) , were mutated by a previous member of the lab. PTCH2-L82F, L85F, W86A (PTCH2-LLW) activity was tested alongside PTCH1-VLW in GLI-luciferase assays. The

results confirmed that the PTCH1-VLW mutant exhibits impaired canonical activity (as reported by Zhang, 2018), but that the PTCH2-LLW mutant behaves very similarly to wild-type PTCH2. Both the LLW and VLW mutants do not appear to impair their respective protein expression, localisation, and interaction. These data combined indicate the SSD of PTCH1 is vital to canonical PTCH1 signalling but less important to the canonical signalling activity of PTCH2.

When assessing the effect of inclusion of one of the mutant PTCH proteins in heterodimers with a wild-type protein, we found that PTCH1 activity is essential for heterodimer activity, which is not affected when the SSD of PTCH2 is mutated. Conversely, when co-transfecting wild type PTCH2 with PTCH1 VLW mutant, the resulting heterodimers are inactive.

The final preliminary piece of research associated with this chapter investigates the catalytic triad within PTCH1 and PTCH2. Recent research indicates an interaction between D513 and E1095 in TM 10 of PTCH1 forming a salt bridge that, by extension, allows for the formation of a hydrophobic cavity (**Figure 7.3**) (Kowatsch et al. 2019; Zhang et al., 2020). The corresponding residue in PTCH2 (D469) was mutated previously in this lab (D469A) and its activity was assessed using the GLI-luciferase reporter assay in *Ptch1*$^{-/-}$ MEFs. The results indicate minimal canonical activity but when co-transfected with PTCH1 the activity is restored.

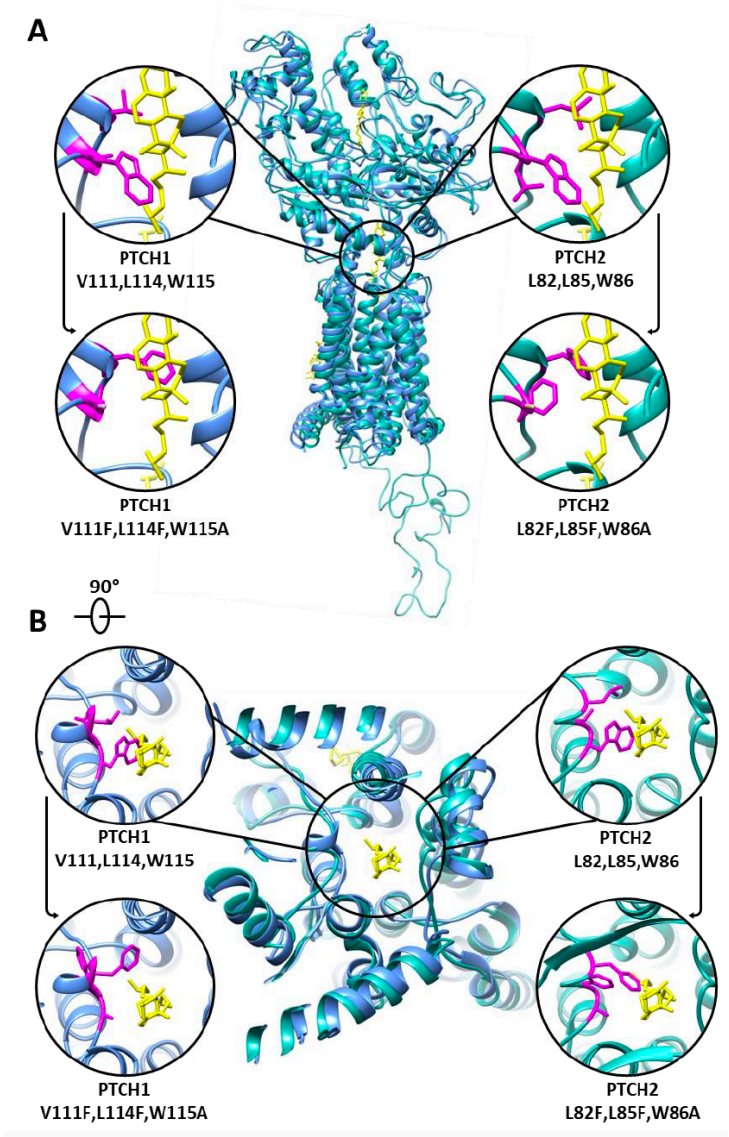

Figure 7. 2 Predicted location of PTCH1 VLW and PTCH2 LLW residues

(**A**) Side-on and (**B**) ariel views of PTCH2 (Blue, Uniprot Q9Y6C5) overlayed onto mouse PTCH1 (Purple, PDB: 6MG8) highlighting the PTCH1 VLW and corresponding PTCH2 LLW residues and their side chains (purple). The figures show where they sit within the hydrophobic channel of each protein alongside cholesterol molecules (yellow), as well as the corresponding mutations displayed at the bottom of **A** and **B.** Structural analysis was done using Chimera. Figures taken from Timmis, A. (2021).

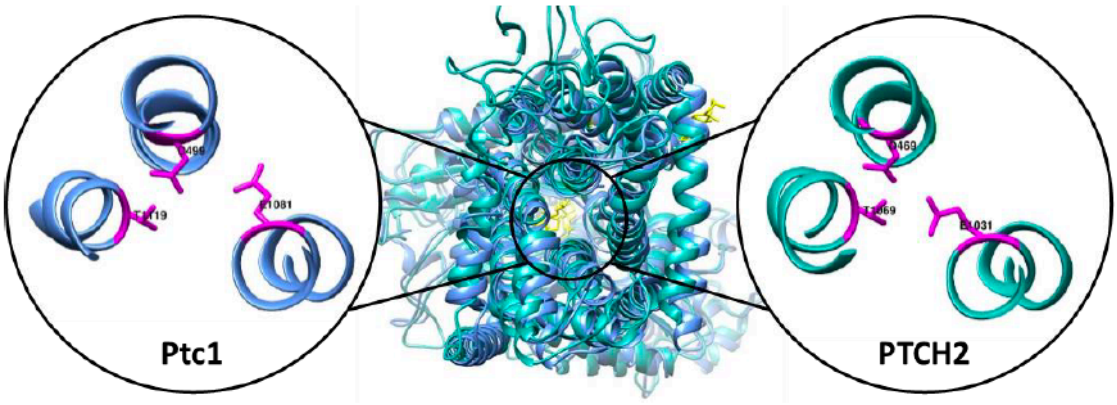

Figure 7. 3 Depiction of the PTCH1-D499 and PTCH2-D469 residues

A bottom view of human PTCH2 (Blue, Uniprot: Q9Y6C5) overlayed onto mouse PTCH1 (Purple, PDB: 6MG8) indicating the positions of PTCH1-D499 (D513 in human PTCH1) and PTCH2-D469 with their interacting partners. The side chains of these residues are shown in magenta. Sequence analysis was carried out using Chimera. Figure taken from Timmis, A. (2021).

7.2 Aims and Hypothesis

The data presented in this chapter represents my contribution to a forthcoming paper currently being under review and published as a preprint in BioRvix (Timmis et al., 2023). The primary objective of this chapter was to build on the foundational research outlined in the introduction.

The specific aims of this chapter were as follows:

1. To investigate the responsiveness of PTCH1/PTCH2 heterodimers to N-SHH.
2. To investigate the contribution of the ionic transport conserved triad to PTCH1 canonical function.

7.3 Results

7.3.1 PTCH1/PTCH2 heterodimers exhibit a similar sensitivity to N-SHH as their monomeric counterparts

The initial phase of these experiments was to determine the sensitivity of PTCH1/PTCH2 heterodimers to the physiological, dually lipidated, Shh ligand (N-SHH). Previous research using unlipidated Shh indicated that it has a similar binding affinity for both PTCH1 and PTCH2. However, the interaction of the unlipidated ligand is thought to occur solely through the binding of its globular domain to a PTCH monomer. In the models proposed for heterodimer formation, we hypothesised that SHH may have a differential affinity for heterodimers if only the PTCH1 subunit is able to engage the lipidated SHH. Therefore, it is very important to evaluate the potency of lipidated SHH in the presence of heterodimers.

To test this hypothesis, *Ptch1*$^{-/-}$ MEFs were transiently transfected with pcDNA, PTCH1, PTCH2 or 50% PTCH1 and 50% PTCH2. Following 48 hrs of serum starvation, the cells were treated with increasing concentrations of dually-lipidated SHH at previously established EC_{50} (30 ng/mL) and saturating concentrations (100 ng/mL) through GLI-luciferase assays conducted in NIH 3T3 cells (Hattie Ollerton, data not shown). The data reveals that increasing concentrations of SHH revert the inhibition of GLI-luciferase activity by PTCH1/PTCH2 heterodimers with a similar pattern that in cells expressing PTCH1 or PTCH2 individually **(Figure 7.4)**. Previous work by Timmis (2021) has shown that, when PTCH1 and PTCH are co-transfected, they form a mixture PTCH1/PTCH2 heterodimers and the individual homodimers, meaning that, in part, the responsiveness of PTCH1/PTCH2 to rSHH is being driven by these

three protein combinations, including PTCH1/PTCH2 heterodimers. Therefore, my conclusion is that homo and heterodimers share a similar level of responsiveness to N-SHH. One caveat to mention regarding this data is co-transfection of PTCH1 and PTCH2 does not guarantee 100% formation of PTCH1/PTCH2 heterodimers, instead, PTCH1 monomers may still be forming at a maximum 50% of the total, providing the dose-dependent response to dually lipidated N-SHH.

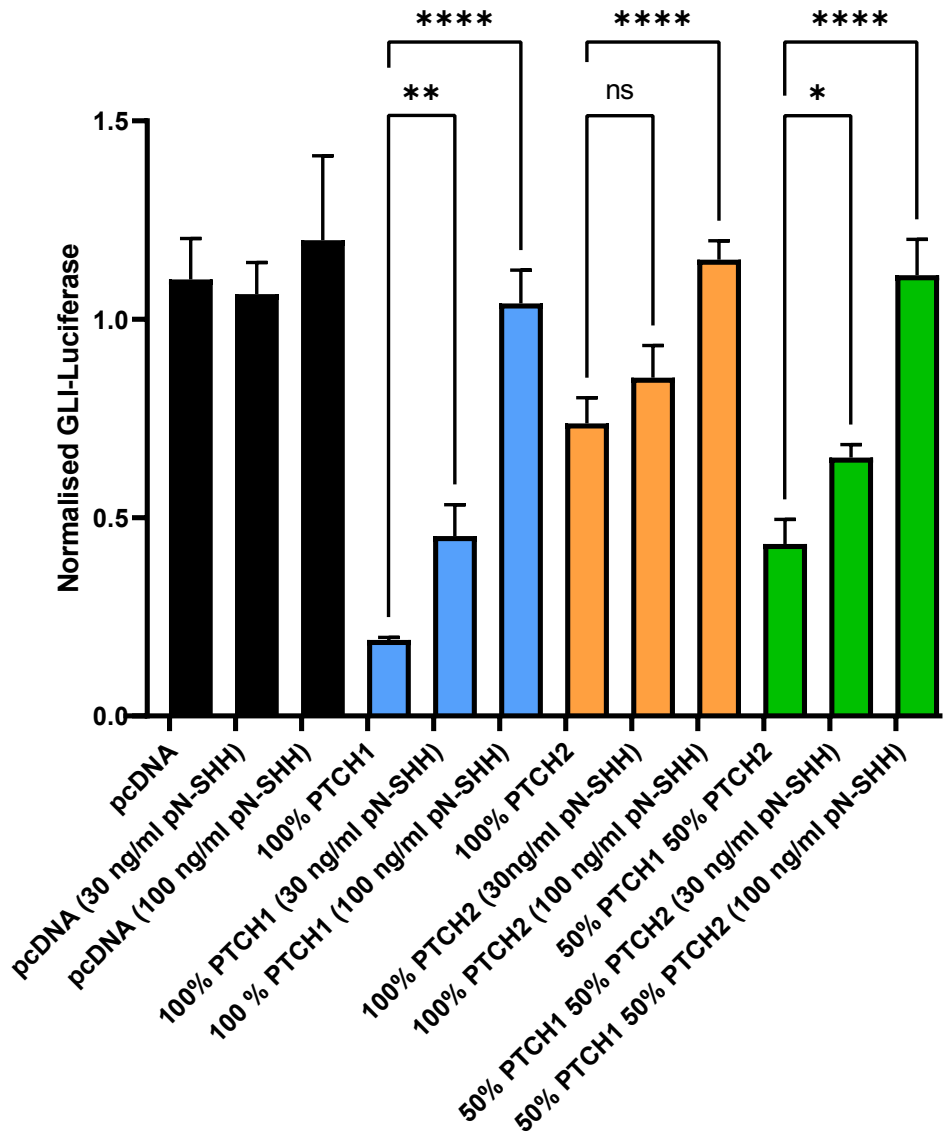

Figure 7. 4 PTCH1/PTCH2 heterodimers are responsive to SHH

Activation of GLI transcription factors at mid and high concentrations of pN-SHHC in *Ptch1*$^{-/-}$ MEFs transiently transfected with 100% pcDNA, 100% PTCH1, 100% PTCH2 or 50% PTCH1 and 50% PTCH2. All plasmid combinations were treated with 30 ng/ml and 100 ng/ml pN-SHH. Results indicate a dose-dependent response to pN-SHHC. PTCH1/PTCH2 heterodimers exhibit a similar responsiveness to pN-SHHC as PTCH1 and PTCH2.

N = 3, * = $p<0.05$, ** = $p<0.01$, **** = $p<0.0001$, ns = not significant

7.3.2 PTCH1 cation mutant can compensate for PTCH2 LLW loss-of-function in heterodimers

The second contribution to this project was an experiment aimed to determine whether a mutation in one of the key residues in the catalytic triad of PTCH1 (D513Y) – previously identified as a germline mutation in Gorlin syndrome – could impair the activity of PTCH1/PTCH2 heterodimers through disrupting the interaction between the N-terminal palmitate molecule of HH ligands and the hydrophobic pocket (Tukachinsky et al., 2016) . To investigate this, the first step to confirm if the PTCH1 D513Y has an impaired activity. To this end, PTCH1 D513Y was transfected into *Ptch1*$^{-/-}$ MEFs and the canonical activity was assessed using the GLI-Luciferase reporter assay, in comparison to wild type PTCH1 and the PTCH2 D469A mutant. The results in **Figure 7.3** indicate a reduction in canonical activity in the PTCH1 D513Y mutant; however, the mutant showed reduced but not full loss of activity, unlike the effect seen with the corresponding PTCH2 mutant, D469A. This difference could be attributed to a reduced but not fully inhibited ionic transport in PTCH1 D513Y, or to formation of a small amounts of heterodimers with endogenous Ptch2.

Next, we wanted to test if the cation transport activity in the heterodimers could be provided by PTCH2. To test this hypothesis, co-expression of PTCH1 D513Y and PTCH2 LLW – individually displaying very low levels of activity – into *Ptch1*$^{-/-}$ MEFs was performed to determine if the impaired mutants could reconstitute the inhibitory canonical activity in the GLI-Luciferase reporter assay. The data in **Figure 7.3** show that the co-transfection of the two mutants restores the high canonical activity of the heterodimer and the PTCH1 homodimer. This data suggests that PTCH1/PTCH2 heterodimers exist where each monomer can

serve a distinct function, with cholesterol transport being mainly provided by the PTCH1 subunit and PTCH1 or PTCH2 providing the energy for that transport through ionic transfer.

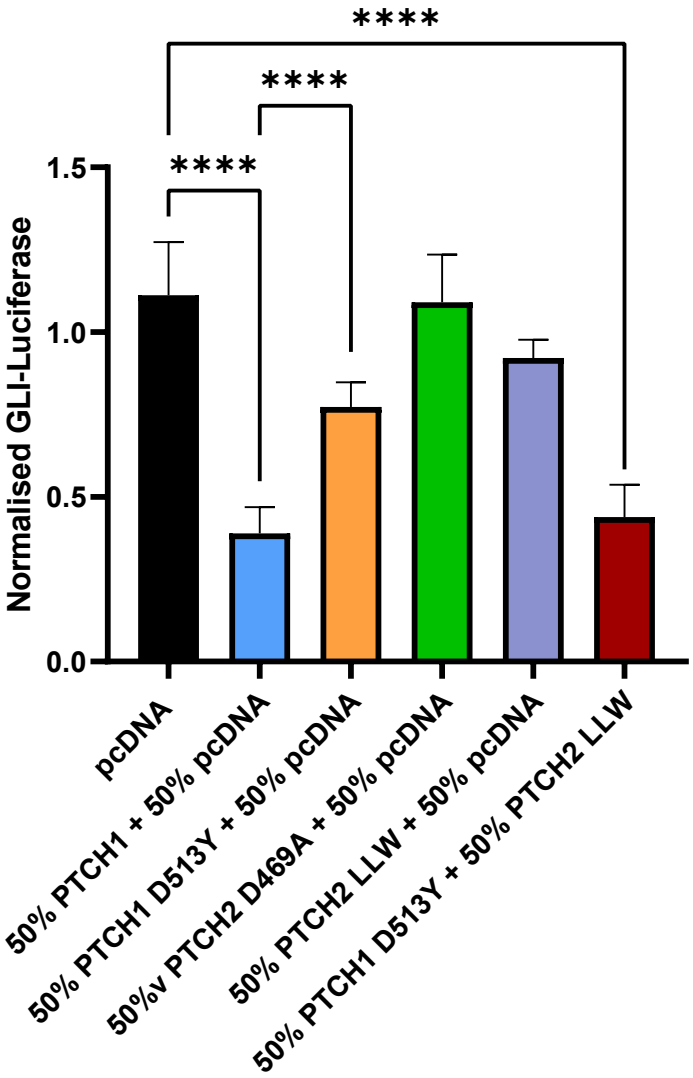

Figure 7. 2 PTCH1 D513Y and PTCH2 LLW form active heterodimers

Investigation of GLI transcription factor activity in *Ptch1*$^{-/-}$ MEFs transiently transfected with pcDNA, PTCH1, PTCH2, PTCH1 D513Y and PTCH2 LLW, or combinations of these plasmids. The high activity phenotype of PTCH1 that is lost by PTCH1 D513Y is recovered by the addition of PTCH2 LLW.

N = 3, **** = p <0.0001

7.3.2 The activity of PTCH2 is not driven by the CTD

Previous work from the lab has attempted to investigate the role of the CTD of each PTCH protein and its contribution to canonical HH signalling (Timmis, 2021). Deletion of the PTCH1 CTD appears to enhance PTCH1 activity, seen through comparable canonical activity levels comparable to that of PTCH1 despite a much-reduced expression of PTCH1-ΔC. This was also seen with PTCH2 and PTCH2-ΔC. As there is a distinct lack of sequence similarity between the two CTDs, it could explain the reduced function of PTCH2 compared to PTCH1. Therefore, it was decided to generate a construct of PTCH1 with the CTD of PTCH2, PTCH1-CTD2, which expressed to similar levels of PTCH1 and localised to the cilia in the same location as PTCH1. The PTCH1CTD2-FLAG construct was shown to be completely inactive, and the PTCH1:PTCH1CTD2 pseudo homodimers in a 50:50 ratio did not reproduce the activity seen from 100% PTCH1. This data combined with the PTCH1ΔC data provides an interesting question about the influence of the PTCH1 CTD on activity, with deletion improving PTCH1 activity, yet a domain swap with its homologue significantly reduces its activity. Another research group has previously attempted to investigate the activity of PTCH2 when fused to the CTD of PTCH1 through the co-expression of two halves of PTCH2 as separate polypeptides, P2-N+P2-CTD1 following transfection (Fleet and Hamel, 2018). The combination of construct was reported to be inactive, in comparison to activity of the two halves encoding the wild-type sequence; however, the reliance on the two domains to interact non-covalently is not the most accurate way to test the true activity of a PTCH2CTD1 protein. It was previously hypothesised that a PTCH2CTD1 protein would have increased activity compared to PTCH2CTD1 as the CTD is much longer and can therefore interact with the middle loop of PTCH2.

The aim of this work was to determine the functional differences between the CTDs of the two PTCH proteins. To investigate this, a construct of PTCH2-FLAG with the PTCH2 CTD replaced with the PTCH1 CTD was generated by amplifying the PTCH1 CTD of the *myc-PTCH1* plasmid as well as amplifying *PTCH2-FLAG* plasmid without the CTD using the Phusion High-Fidelity DNA Polymerase (NEB) before ligating the two PCR products through blunt-end ligation using the T4 Ligase (NEB). Successful cloning was confirmed through Sanger sequencing. Expression was checked through Western blot. **Figure 7.6A** shows a comparable level of expression of PTCH2CTD1-FLAG and its parental plasmid, PTCH2-FLAG, quantified through densitometry (**Figure 7.6B**). Localisation of PTCH2CTD1-FLAG was tested and shown to localise to the cilia (Timmis et al., 2023). Finally, the activity of PTCH2CTD1-FLAG was tested using the GLI-Luciferase reporter assay in *Ptch1*$^{-/-}$ MEFs (**Figure 7.7**). The fusion protein does not show increased activity compared to wild-type PTCH2, which is unlikely to be caused by ciliary localisation or expression levels. These results in combination with previous findings show that swapping both CTDs results in inactive proteins. In the case of PTCH1, swapping the CTD leads to a decrease in activity, highlighting that the CTD of PTCH1 may contribute to PTCH1 activity, and that when swapped with the CTD of PTCH2, this activity is lost. This also points to the idea that the CTD of PTCH2 could be contributing to the lower activity of PTCH2. This is a significant finding, however, the expectation then would be that swapping the CTD of PTCH1 onto PTCH2 would be able to increase the activity of PTCH2, mimicking the activity of PTCH1. This is not what occurs, suggesting that the CTD of PTCH1 is not able to influence the activity of the PTCH2CTD1 chimera. These results pose an interesting question: is the inactivity of the two

chimeras linked to the CTDs, or is the experimental procedure used to switch the CTDs disrupting PTCH function, rendering both proteins inactive.

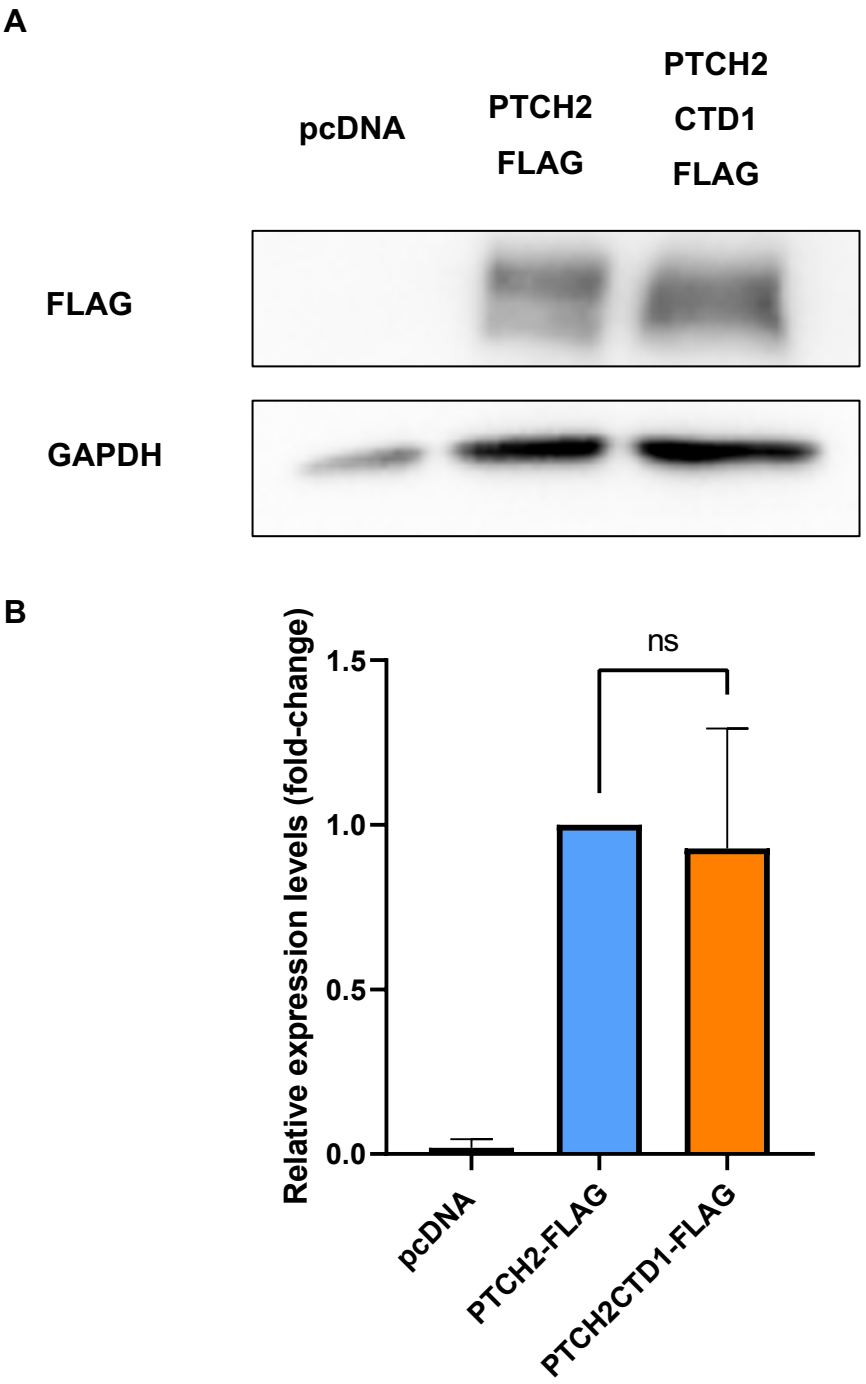

Figure 7. 3 Expression levels of PTCH2-CTD1-FLAG

Western blot analysis of HEK293 cells overexpressing pcDNA, PTCH2-FLAG and PTCH2-CTD1-FLAG. **(A)** shows comparable expression between the two proteins. **(B)** Densitometry analysis of blots normalised to GAPDH levels. N=3, ns = not significant

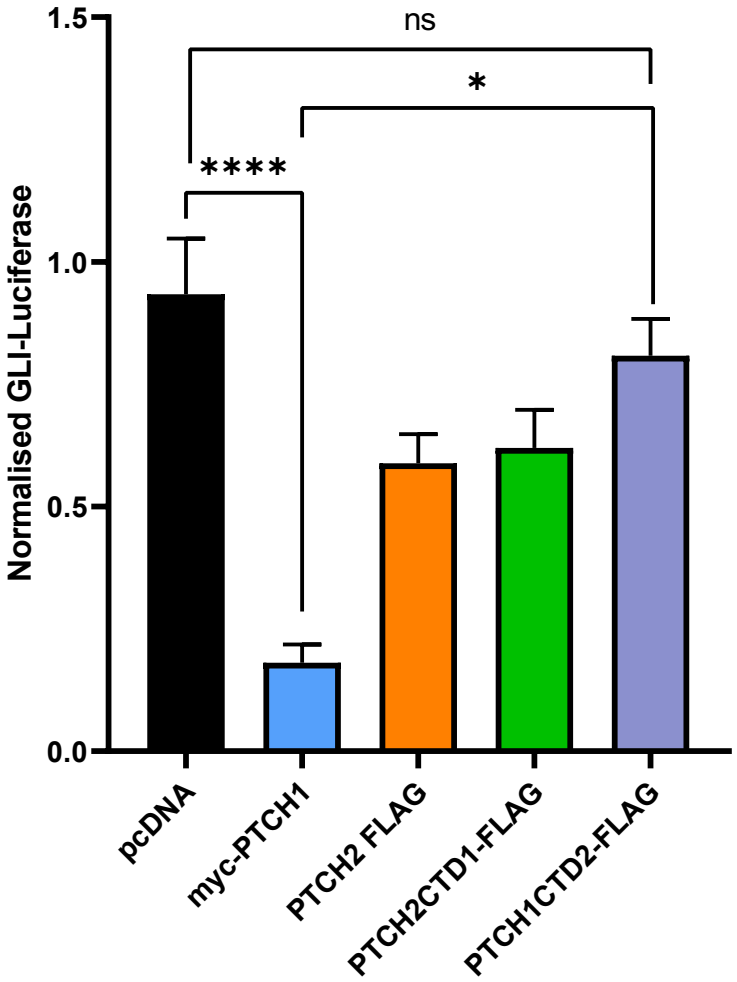

Figure 7. 4 Activity levels of PTCH2-CTD1-FLAG

GLI-Luciferase assay of *Ptch1*$^{-/-}$ MEFs transfected with pcDNA, PTCH1, PTCH2, PTCH1-CTD2-FLAG and PTCH2-CTD2-FLAG. The data was collected after 48 hrs serum starvation of the cells. The data shows no significant differences in the activities of both CTD swap constructs.

N=3, * = p<0.05, **** = p<0.0001

7.4 Discussion

The understanding of the relationship between PTCH1 and PTCH2 is slowly improving. Previous data that is built on in this chapter first highlighted the capability of PTCH1 to form homo- and heteromeric-interactions that allow for the binding of HH ligands, with data indicating that PTCH1 homodimers are the more favourable formation of dimer. Previous data from this lab (Timmis et al., 2023) also shows that both individual multimers of PTCH1 and PTCH2 and heteromers have a similar sensitivity to co-transfected N-SHH despite the lower basal activity of PTCH2 in isolation compared to PTCH1. When SHH is co-transfected, the continuous production of ligand results in internalisation and degradation of PTCH1 (and possibly PTCH2), making difficult to interpret their initial response. New data presented here indicates that PTCH1-PTCH2 heterodimers have a similar responsiveness to addition of recombinant, dually-lipidated N-SHH to that of PTCH1 and PTCH2 homodimers. Differences between latter and initial experiments show a lower activity for the heterodimers compared to WT PTCH1 in the absence of ligand; however, PTCH1-PTCH2 heterodimers display much higher activity than PTCH2 homodimers. This data points towards the formation of heterodimers compensating for loss-of-function mutations, maintaining a fully active PTCH protein complex.

Analysis of cryo-EM data suggests the possibility of unbound monomeric PTCH1 that may remain functionally active based on evidence of sterol moieties in the structure that suggest active transport (Qian et al., 2019; Rudolf et al., 2019). However, it is important to note that cryo-EM data of purified PTCH1 containing deletions in cytosolic domains might not reflect the *in-situ* arrangement of native active PTCH1.

The data presented in **Figure 7.3** indicates that a mutation in the ionic transport triad within the transmembrane domains of PTCH1 reported in a patient with Gorlin syndrome (Tukachinsky et al., 2016) significantly reduces PTCH1 activity. In comparison, the PTCH2 cation gate mutant D469A lacks any observable activity, whereas the PTCH1 D513Y mutant, whilst much less active, still displays minimal activity. When PTCH1 D513Y is co-expressed with PTCH2 LLW to allow formation of a heterodimer, the data suggests a strong recovery of PTCH canonical activity, implying a synergistic i*n trans* relationship between the monomers. Each subunit could play distinct roles in the heterodimer function, with PTCH2 LLW potentially providing cation transport that compensates for the D513Y mutation in PTCH1. It can be inferred that heterodimers are being formed and not homodimers because both homodimers are inactive (**Figure 7.3**), therefore, any changes in activity must be driven by the formation of heterodimers. Here, this data provides valuable insight into the functional roles played by each monomer, indicating that PTCH1 is primarily responsible for the efflux of cholesterol from the cell, the efflux can be driven by the protonmotive force produced from either PTCH1 or PTCH2. Because cholesterol transport is so important to PTCH1 function, we propose that the palmitate modification of SHH interacts with the PTCH1 monomer in a heterodimeric setting, with SHH's globular domain interacting preferably with PTCH2.

There has been growing evidence to support the idea that the CTD of PTCH1 is involved in canonical activity, including a link between the CTDs of each protein and their relative activities. Swapping the CTD of PTCH1 with the CTD of PTCH2 renders an inactive chimeric protein, as was suggested by complementation

studies co-expressing two halves of PTCH in an earlier report (Fleet and Hamel, 2018), who generated a pseudo PTCH2CTD1 chimera. This result demonstrates that the divergent CTDs of PTCH1 and PTCH2 have exquisitely evolved to maximise each isoform function and that the lower activity of PTCH2 is not the result of a shorter and non-homologous CTD.

Chapter 8

General Discussion

Chapter 8

General Discussion

The data in Chapter 3 provided two key insights: i) the TPSP motif is highly conserved across many species, with an indication that the SP motif is less important to PTCH1 function due to reduced conservation, and ii) the TPSP appears to exist as a monophosphorylated motif in normal physiological conditions. This finding underpins the loss-of-function phenotype associated with the disease-associated TPSP mutants (Kawamura et al., 2008; Wang et al., 2019). This suggests that the change of threonine to serine could change kinase specificity or enhance kinase interaction or activity (Roskoski Jr, R., 2010). Perhaps changes in phosphorylation status could cause disruptions within the motif and surrounding residues that alter downstream signalling events. Future work could look at further optimising the mass spectrometry experimental method to return a higher abundance of phosphorylated peptides, which would allow for verification of the TPSP motif's phosphorylation state. Additionally, mass spectrometry could be used to expand on PTCH1 CTD binding partners through BioID proximity labelling, a method whereby biotin ligase is fused to PTCH1 and would promiscuously biotinylate interacting proteins (Roux et al. 2018). These proteins would then be detectable through mass spectrometry (Cheerathodi, M.R. and Meckes, D.G., 2020). This method would uncover CTD binding partners, and, through the use of TPSP mutants, we could uncover TPSP-specific binding partners.

The data in Chapter 4 provided three key insights: i) further evidence the proximal region of the PTCH1 CTD is disordered, ii) further evidence that the TPSP motif

preferentially exists in a monophosphorylated state, and iii) providing a candidate kinase for the phosphorylation of the TPSP motif. The NMR data took this a step further and unequivocally demonstrated that phosphorylation by ERK1 occurs at T1195, suggesting that whichever kinase phosphorylates TPSP physiologically may preferentially phosphorylate T1195. This finding appears to contradict the higher abundance of phosphorylation detected in the T1195A mutant compared to the S1197A mutant by mass spectrometry, suggesting other kinases may be important *in vivo*. It would be interesting to investigate the other candidate kinases that were proposed in Chapter 4 have the same preference for T1195 as ERK1. These kinases include GSK3β a known HH signalling antagonist (Jia et al. 2002), perhaps GSK3β negatively regulates PTCH1 through its interactins with the TPSP motif, and when mutation occurs, this regulation is disturbed.

The data in Chapter 5 provides three key insights: i) further evidence that the TPSP motif is not involved in the canonical function of PTCH1, ii) the TPSP motif is involved in the regulation of Erk phosphorylation by PTCH1, and iii) TPSP mutants may cause cells to have increased viability. Somewhat surprisingly, the GLI-luciferase data showed that neither the TPSP motif nor its phosphorylation state are involved in the regulation of canonical HH signalling, contradicting the original hypothesis that the loss-of-function phenotype associated with disease-associated mutations in the TPSP motif is caused by an aberrantly active HH pathway (Kawamura et al., 2008; Wang, C.Y. et al., 2019). Identification of disrupted phospho-Erk levels indicates a role of the TPSP motif in a relatively poorly understood non-canonical function of PTCH1. The relationship between PTCH1 and Erk1/2 was proposed to be mediated through interactions with one of the SH3 domains of Grb2 to one of the PRMs within the PTCH1 CTD (Chang

et al., 2010). Further experimentation is required to identify a link between the TPSP motif and Erk phosphorylation. For example, it would be good to conduct co-immunoprecipitation assays on PTCH1 TPSP mutants and investigate changes to Grb2 binding – similar to the method employed by Chang et al. (2010). Secondly, there is a need to investigate whether changes in phospho-Erk levels correspond to increased Erk signalling and cell growth in a PTCH1-dependent setting. This could be done by transfecting cells with mutant TPSP motif plasmids and quantifying Erk kinase activity, using a library of biosensors to quantify active Erk in cell lysates (Zamora-Olivares, D. 2020). This method could uncover a link between TPSP mutants and increased cell viability. Also of importance is the need to analyse the distal region of the CTD, absent in our shorter NMR peptide, looking for patterns in structure, and investigating the binding of proteins such as ATG101 which a previous member of the lab has been able to show can be pulled down with PTCH1, this method has been used very effectively previously by (Chen et al. 2018; Caballero-Ruiz et al. 2023). These binding events may induce conformational changes in the CTD which would be detectable in NMR, and it would also allow identification of the binding site of ATG101, which is only known to be downstream of R1308.

The data in Chapter 6 provides one key insight: Pin1 interacts with PTCH1. this discovery adds to the complexity of PTCH1 and PTCH2 signalling. This opens a series of avenues for research, including investigating the role of Pin1 in non-canonical PTCH1 signalling, especially on ERK1/2 phosphorylation and cell proliferation, an aspect that I could not follow up due to lack of time. It would be interesting to investigate the regulation of Pin1 activity by PTCH1. For example, could PTCH1 sequester Pin1? Do PTCH1 CTD mutations lead to reduced

sequestration of Pin1, leading to an increase in the levels of Pin1 available to regulate and activate transcription factors to increase cell proliferation? Mutation of S1185 to a non-phosphorylatable residue such as alanine, in combination with the unphosphorylated T1195A/S1197A mutant, is vitally important as it is the only remaining S/T-P motif in the CTD (accession number NP_000255.2). The prediction is that mutation of all three phosphorylation sites should abolish Pin1 binding to PTCH1 and that mutation of the equivalent S1197 in PTCH2 should do the same, this is because of the absence of any additional TP or SP sites within the PTCH1 CTD, therefore there are no more potential Pin1 binding sites. Investigations into the promiscuity of Pin1 binding to PTCH proteins are of paramount importance, helping to better understand Pin1's role in HH signalling. Does Pin1 play the same role in HH function regardless of which PTCH protein it interacts with? Are there multiple Pin1 binding sites within each PTCH protein, that can overcome the mutation/deletion of other sites? I hypothesise that the binding of Pin1 to PTCH proteins requires multiple binding sites, displaying a sequential binding mechanism whereby the WW domain binds to one site, bringing the Pin1 PPIase domain close to another binding site. The GST-pulldown assays support this hypothesis. Alternatively, Pin1 might bridge more than one molecule of PTCH1 – since it exists in oligomeric form – or involve binding to the PTCH1/PTCH2 heteromers. Notwithstanding the binding region, the discovery that Pin1 interacts with PTCH1 and PTCH2 might provide a novel insight in cancer, as Pin1 overexpression is linked to poor prognosis in most cancer types. Therefore, it would be important to investigate the consequences of disrupting this interaction in cancer progression. Numerous studies have shown that Juglone is an effective inhibitor of Pin1 (Costantin et al. 2016; Zhao et al. 2019; Yu et al. 2020), it would be interesting to see whether there are impacts on

canonical and non-canonical functions of PTCH1 through the inhibition of Pin1 with Juglone, this would provide a greater understanding of the relationship between Pin1 and PTCH1. Alternatively, screening for small molecule modulators of these interactions could lead to the development of targeted therapies for HH pathway-related disorders, including cancers driven by HH pathway dysregulation (Wei et al 2017).

Finally, the data in Chapter 7 provides key insights: i) PTCH1-PTCH2 heterodimers are equally sensitive to SHH as PTCH1 and PTCH2 homodimers, ii) the catalytic triad of PTCH1 is important to canonical function, and iii) the reduced activity of PTCH2 is not the result of a shorter CTD. This finding was contrary to the expectation given that the reverse chimera, PTCH1 fused to the CTD of PTCH2 is completely inactive despite normal ciliary localisation. Data from another PGR suggests a functional interaction of the CTD with the middle loop, which could be isoform-specific. The data from this chapter is significant because it would be worth generating chimeric constructs with replacements of both the CTD and the middle loop and identifying whether there is a physical interaction between the two domains through co-IP or other methods. Work could be done to further characterise PTCH1/PTCH2 heteromers and their differential activities in HH pathway regulation. This could involve detailed biochemical and structural studies to understand how heterodimerisation influences ligand binding and downstream signalling.

Final conclusions

Altogether, this study:

- Provides a better understanding of the functional significance of phosphorylation of the first PRM of the PTCH1 CTD.
- Uncovers a novel interaction between both PTCH isoforms and Pin1.
- Sheds light on the structural composition of the proximal region of the CTD, something that has merely been speculated on in the past.

This thesis contributes to the growing picture of PTCH1 structure and function, encompassing both canonical and non-canonical signalling.

Chapter 9 - Bibliography

AC Wahab, N.F., Kannan, T.P., Mahmood, Z., Rahman, I.A. and Ismail, H., 2017. Methods in cytotoxicity testing: A review. *Recent Patents on Materials Science*, *10*(1), pp.50-59

Adzhubei, A.A., Sternberg, M.J. and Makarov, A.A. 2013. Polyproline-II helix in proteins: structure and function. *J Mol Biol.* **425**(12), pp.2100-2132.

Alfaro, A.C., Roberts, B., Kwong, L., Bijlsma, M.F. and Roelink, H. 2014. Ptch2 mediates the Shh response in Ptch1-/- cells. *Development.* **141**(17), pp.3331-3339.

Alman, B.A. 2015. The role of hedgehog signalling in skeletal health and disease. *Nat Rev Rheumatol.* **11**(9), pp.552-560.

Alvarez, J.I., Dodelet-Devillers, A., Kebir, H., Ifergan, I., Fabre, P.J., Terouz, S., Sabbagh, M., Wosik, K., Bourbonniere, L., Bernard, M., van Horssen, J., de Vries, H.E., Charron, F. and Prat, A. 2011. The Hedgehog Pathway Promotes Blood-Brain Barrier Integrity and CNS Immune Quiescence. *Science.* **334**.

Aman, Y., Schmauck-Medina, T., Hansen, M., Morimoto, R.I., Simon, A.K., Bjedov, I., Palikaras, K., Simonsen, A., Johansen, T., Tavernarakis, N., Rubinsztein, D.C., Partridge, L., Kroemer, G., Labbadia, J. and Fang, E.F. 2021. Autophagy in healthy aging and disease. *Nat Aging.* **1**(8), pp.634-650.

Andrade-Tomaz, M., de Souza, I., Rocha, C.R.R. and Gomes, L.R. 2020. The Role of Chaperone-Mediated Autophagy in Cell Cycle Control and Its Implications in Cancer. *Cells.* **9**(9).

Andreas, L.B., Jaudzems, K., Stanek, J., Lalli, D., Bertarello, A., Le Marchand, T., Cala-De Paepe, D., Kotelovica, S., Akopjana, I., Knott, B., Wegner, S., Engelke, F., Lesage, A., Emsley, L., Tars, K., Herrmann, T. and Pintacuda, G. 2016. Structure of fully protonated proteins by proton-detected magic-angle spinning NMR. *Proc Natl Acad Sci U S A.* **113**(33), pp.9187-9192.

Anjum, R. and Blenis, J. 2008. The RSK family of kinases: emerging roles in cellular signalling. *Nat Rev Mol Cell Biol.* **9**(10), pp.747-758.

Arveseth, C.D., Happ, J.T., Hedeen, D.S., Zhu, J.F., Capener, J.L., Klatt Shaw, D., Deshpande, I., Liang, J., Xu, J., Stubben, S.L., Nelson, I.B., Walker, M.F., Kawakami, K., Inoue, A., Krogan, N.J., Grunwald, D.J., Huttenhain, R., Manglik, A. and Myers, B.R. 2021. Smoothened transduces Hedgehog signals via activity-dependent sequestration of PKA catalytic subunits. *PLoS Biol.* **19**(4), pe3001191.

Baltanas, F.C., Zarich, N., Rojas-Cabaneros, J.M. and Santos, E. 2020. SOS GEFs in health and disease. *Biochim Biophys Acta Rev Cancer.* **1874**(2), p188445.

Bangs, F. and Anderson, K.V. 2017. Primary Cilia and Mammalian Hedgehog Signaling. *Cold Spring Harb Perspect Biol.* **9**(5).

Barnwal, R.P., Rout, A.K., Chary, K.V. and Atreya, H.S. 2007. Rapid measurement of 3J(H N-H alpha) and 3J(N-H beta) coupling constants in polypeptides. *J Biomol NMR.* **39**(4), pp.259-263.

Bartholomeusz, C., Gonzalez-Angulo, A.M., Liu, P., Hayashi, N., Lluch, A., Ferrer-Lozano, J. and Hortobagyi, G.N. 2012. High ERK protein expression levels correlate with shorter survival in triple-negative breast cancer patients. *Oncologist.* **17**(6), pp.766-774.

Basler, K., Chen, Y., Sasai, N., Ma, G., Yue, T., Jia, J., Briscoe, J. and Jiang, J. 2011. Sonic Hedgehog Dependent Phosphorylation by CK1α and GRK2 Is Required for Ciliary Accumulation and Activation of Smoothened. *PLoS Biology.* **9**(6).

Batchelor M., Dawber, R. S., Wilson, A. J., Bayliss, R.; α-Helix stabilization by co-operative side chain charge-reinforced interactions to phosphoserine in a basic kinase-substrate motif. *Biochem J* 18 March 2022; 479 (5): 687–700.

Bax, A. and Clore, G.M. 2019. Protein NMR: Boundless opportunities. *J Magn Reson.* **306**, pp.187-191.

Bekker, G.J., Araki, M., Oshima, K., Okuno, Y. and Kamiya, N. 2023. Mutual induced-fit mechanism drives binding between intrinsically disordered Bim and cryptic binding site of Bcl-xL. *Commun Biol.* **6**(1), p349.

Bodle, J.C., Rubenstein, C.D., Phillips, M.E., Bernacki, S.H., Qi, J., Banes, A.J. and Loboa, E.G. 2013. Primary cilia: the chemical antenna regulating human adipose-derived stem cell osteogenesis. *PLoS One.* **8**(5), pe62554.

Bonni, A., Brunet, A., West, A.E., Datta, S.R., Takasu, M.A. and Greenberg, M.E. 1999. Cell Survival Promoted by theRas-MAPK Signaling Pathway by Transcription-Dependent and -Independent Mechanisms. *Science.* **286**(5443).

Boutet, N., Bignon, Y.J., Drouin-Garraud, V., Sarda, P., Longy, M., Lacombe, D. and Gorry, P. 2003. Spectrum of PTCH1 mutations in French patients with Gorlin syndrome. *J Invest Dermatol.* **121**(3), pp.478-481.

Briscoe, J., Chen, Y., Jessell, T.M. and Sruhl, G. 2001. A Hedgehog-Insensitive Form of Patched Provides Evidence for Direct Long-Range Morphogen Activity of Sonic Hedgehog in the Neural Tube. *Molecular Cell.* **7**.

Briscoe, J. and Therond, P.P. 2013. The mechanisms of Hedgehog signalling and its roles in development and disease. *Nat Rev Mol Cell Biol.* **14**(7), pp.416-429.

Brown, A. and Zhang, R. 2020. Primary Cilia: A Closer Look at the Antenna of Cells. *Curr Biol.* **30**(24), pp.R1494-R1496.

Bryant, K.L., Stalnecker, C.A., Zeitouni, D., Klomp, J.E., Peng, S., Tikunov, A.P., Gunda, V., Pierobon, M., Waters, A.M., George, S.D., Tomar, G., Papke, B., Hobbs, G.A., Yan, L., Hayes, T.K., Diehl, J.N., Goode, G.D., Chaika, N.V., Wang, Y., Zhang, G.F., Witkiewicz, A.K., Knudsen, E.S., Petricoin, E.F., 3rd, Singh, P.K.,

Macdonald, J.M., Tran, N.L., Lyssiotis, C.A., Ying, H., Kimmelman, A.C., Cox, A.D. and Der, C.J. 2019. Combination of ERK and autophagy inhibition as a treatment approach for pancreatic cancer. *Nat Med.* **25**(4), pp.628-640.

Buday, L. and Vas, V. 2020. Novel regulation of Ras proteins by direct tyrosine phosphorylation and dephosphorylation. *Cancer Metastasis Rev.* **39**(4), pp.1067-1073.

Buglino, J.A. and Resh, M.D. 2008. Hhat Is a Palmitoylacyltransferase with Specificity for N-Palmitoylation of Sonic Hedgehog. *Journal of Biological Chemistry.* **283**(32), pp.22076-22088.

Buller, N.V., Rosekrans, S.L., Westerlund, J. and van den Brink, G.R. 2012. Hedgehog signaling and maintenance of homeostasis in the intestinal epithelium. *Physiology (Bethesda).* **27**(3), pp.148-155.

Busca, R., Pouyssegur, J. and Lenormand, P. 2016. ERK1 and ERK2 Map Kinases: Specific Roles or Functional Redundancy? *Front Cell Dev Biol.* **4**, p53.

Byrne, E.F.X., Sircar, R., Miller, P.S., Hedger, G., Luchetti, G., Nachtergaele, S., Tully, M.D., Mydock-McGrane, L., Covey, D.F., Rambo, R.P., Sansom, M.S.P., Newstead, S., Rohatgi, R. and Siebold, C. 2016. Structural basis of Smoothened regulation by its extracellular domains. *Nature.* **535**(7613), pp.517-522.

Caballero-Ruiz, B., Gkotsi, D.S., Ollerton, H., Morales-Alcala, C.C., Bordone, R., Jenkins, G.M.L., Di Magno, L., Canettieri, G. and Riobo-Del Galdo,

N.A. 2023. Partial Truncation of the C-Terminal Domain of PTCH1 in Cancer Enhances Autophagy and Metabolic Adaptability. *Cancers (Basel).* **15**(2).

Cai, E., Zhang, J. and Ge, X. 2022. Control of the Hedgehog pathway by compartmentalized PKA in the primary cilium. *Sci China Life Sci.* **65**(3), pp.500-514.

Camacho, C., Coulouris, G., Avagyan, V., Ma, N., Papadopoulos, J., Bealer, K. and Madden, T.L. 2009. BLAST+: architecture and applications. *BMC Bioinformatics.* **10**, p421.

Carpenter, D., Stone, D.M., Brush, J., Ryan, A., Armanini, M., Frantz, G., Rozenthal, A. and de Sauvage, F.J. 1998. Characterization of two patched receptors for the vertebrate hedgehog protein family. *Cell Biology.* **95**.

Chang, H., Li, Q., Moraes, R.C., Lewis, M.T. and Hamel, P.A. 2010. Activation of Erk by sonic hedgehog independent of canonical hedgehog signalling. *Int J Biochem Cell Biol.* **42**(9), pp.1462-1471.

Chapouly, C., Guimbal, S., Hollier, P.L. and Renault, M.A. 2019. Role of Hedgehog Signaling in Vasculature Development, Differentiation, and Maintenance. *Int J Mol Sci.* **20**(12).

Cheerathodi, M.R. and Meckes, D.G., 2020. BioID combined with mass spectrometry to study herpesvirus protein–protein interaction networks. *Herpes Simplex Virus: Methods and Protocols*, pp.327-341.

Chen, H., Wang, J., Yang, H., Chen, D. and Li, P. 2016. Association between FOXM1 and hedgehog signaling pathway in human cervical carcinoma by tissue microarray analysis. *Oncology Letters.* **12**(4), pp.2664-2673.

Chen, X., Morales-Alcala, C.C. and Riobo-Del Galdo, N.A. 2018. Autophagic Flux Is Regulated by Interaction Between the C-terminal Domain of PATCHED1 and ATG101. *Mol Cancer Res.* **16**(5), pp.909-919.

Chen, X.L., Chinchilla, P., Fombonne, J., Ho, L., Guix, C., Keen, J.H., Mehlen, P. and Riobo, N.A. 2014. Patched-1 proapoptotic activity is downregulated by modification of K1413 by the E3 ubiquitin-protein ligase Itchy homolog. *Mol Cell Biol.* **34**(20), pp.3855-3866.

Chiang, C., Litingtung, Y., Harris, M.P., Simandl, B.K., Li, Y., Beachy, P.A. and Fallon, J.F. 2001. Manifestation of the limb prepattern: limb development in the absence of sonic hedgehog function. *Dev Biol.* **236**(2), pp.421-435.

Chong, Z.X., Yeap, S.K. and Ho, W.Y., 2021. Transfection types, methods and strategies: a technical review. *PeerJ*, *9*, p.e11165.

Christensen, S.T., Pedersen, L.B., Schneider, L. and Satir, P. 2007. Sensory cilia and integration of signal transduction in human health and disease. *Traffic.* **8**(2), pp.97-109.

Chung, S.Y. and Subbiah, S., 1996. A structural explanation for the twilight zone of protein sequence homology. *Structure*, *4*(10), pp.1123-1127

Cohen, M.M., Jr. 2010. Hedgehog signaling update. *Am J Med Genet A.* **152A**(8), pp.1875-1914.

Cohn, G.M., Liefwalker, D.F., Langer, E.M. and Sears, R.C. 2020. PIN1 Provides Dynamic Control of MYC in Response to Extrinsic Signals. *Front Cell Dev Biol.* **8**, p224.

Conibear, A.C., Rosengren, K.J., Becker, C.F. and Kaehlig, H., 2019. Random coil shifts of posttranslationally modified amino acids. *Journal of Biomolecular NMR*, *73*(10), pp.587-599.

Cook, F.A. and Cook, S.J. 2021. Inhibition of RAF dimers: it takes two to tango. *Biochem Soc Trans.* **49**(1), pp.237-251.

Costantino, S., Paneni, F., Lüscher, T.F. and Cosentino, F., 2016. Pin1 inhibitor Juglone prevents diabetic vascular dysfunction. *International journal of cardiology*, *203*, pp.702-707.

Delaglio, F., Grzesiek, S., Vuister, G.W., Zhu, G., Pfeifer, J. and Bax, A. 1995. NMRPipe: A multidimensional spectral processing system based on UNIX pipes. *J-Bio NMR.* **305**.

Di Mauro, C., Rosa, R., D'Amato, V., Ciciola, P., Servetto, A., Marciano, R., Orsini, R.C., Formisano, L., De Falco, S., Cicatiello, V., Di Bonito, M., Cantile, M., Collina, F., Chambery, A., Veneziani, B.M., De Placido, S. and Bianco, R. 2017.

Hedgehog signalling pathway orchestrates angiogenesis in triple-negative breast cancers. *Br J Cancer.* **116**(11), pp.1425-1435.

Dunaeva, M., Michelson, P., Kogerman, P. and Toftgard, R. 2003. Characterization of the physical interaction of Gli proteins with SUFU proteins. *J Biol Chem.* **278**(7), pp.5116-5122.

Dyson, H.J. and Wright, P.E., 2021. NMR illuminates intrinsic disorder. *Current opinion in structural biology*, *70*, pp.44-52.

Epstein, E.H. 2008. Basal cell carcinomas: attack of the hedgehog. *Nat Rev Cancer.* **8**(10), pp.743-754.

Esipova, N.G. and Tumanyan, V.G. 2017. Omnipresence of the polyproline II helix in fibrous and globular proteins. *Curr Opin Struct Biol.* **42**, pp.41-49.

Fleet, A.J. and Hamel, P.A. 2018. The protein-specific activities of the transmembrane modules of Ptch1 and Ptch2 are determined by their adjacent protein domains. *J Biol Chem.* **293**(43), pp.16583-16595.

Fracchiolla, D., Chang, C., Hurley, J.H. and Martens, S. 2020. A PI3K-WIPI2 positive feedback loop allosterically activates LC3 lipidation in autophagy. *J Cell Biol.* **219**(7).

Franz-Wachtel, M., Eisler, S.A., Krug, K., Wahl, S., Carpy, A., Nordheim, A., Pfizenmaier, K., Hausser, A. and Macek, B. 2012. Global detection of protein

kinase D-dependent phosphorylation events in nocodazole-treated human cells. *Mol Cell Proteomics.* **11**(5), pp.160-170.

Fry, A.M., Leaper, M.J. and Bayliss, R. 2014. The primary cilium: guardian of organ development and homeostasis. *Organogenesis.* **10**(1), pp.62-68.

Fu, W., Wang, L., Kim, S., Li, J. and Dynlacht, B.D. 2016. Role for the IFT-A Complex in Selective Transport to the Primary Cilium. *Cell Rep.* **17**(6), pp.1505-1517.

Fuchs, Y.F., Eisler, S.A., Link, G., Schlicker, O., Bunt, G., Pfizenmaier, K. and Hausser, A. 2009. A Golgi PKD activity reporter reveals a crucial role of PKD in nocodazole-induced Golgi dispersal. *Traffic.* **10**(7), pp.858-867.

Garcia, B.A., Shabanowitz, J. and Hunt, D.F., 2005. Analysis of protein phosphorylation by mass spectrometry. *Methods*, *35*(3), pp.256-264.

Gibbs, E.B., Cook, E.C. and Showalter, S.A., 2017. Application of NMR to studies of intrinsically disordered proteins. *Archives of biochemistry and biophysics*, *628*, pp.57-70.

Gong, X., Qian, H., Cao, P., Zhao, X., Zhou, Q., Lei, J. and Yan, N. 2018. Structural basis for the recognition of Sonic Hedgehog by human Patched1. *Science.* **361**(6402).

Gonzalez-Hormazabal, P., Musleh, M., Bustamante, M., Stambuk, J., Pisano, R., Valladares, H., Lanzarini, E., Chiong, H., Rojas, J., Suazo, J., Castro,

V.G., Jara, L. and Berger, Z. 2018. Polymorphisms in RAS/RAF/MEK/ERK Pathway Are Associated with Gastric Cancer. *Genes (Basel).* **10**(1).

Griffey, C.J. and Yamamoto, A. 2022. Macroautophagy in CNS health and disease. *Nat Rev Neurosci.* **23**(7), pp.411-427.

Guo, Y.J., Pan, W.W., Liu, S.B., Shen, Z.F., Xu, Y. and Hu, L.L. 2020. ERK/MAPK signalling pathway and tumorigenesis. *Exp Ther Med.* **19**(3), pp.1997-2007.

Guo, Y.Y., Zhang, J.Y., Li, X.F., Luo, H.Y., Chen, F. and Li, T.J. 2013. PTCH1 gene mutations in Keratocystic odontogenic tumors: a study of 43 Chinese patients and a systematic review. *PLoS One.* **8**(10), pe77305.

Hall, E.T., Cleverdon, E.R. and Ogden, S.K. 2019. Dispatching Sonic Hedgehog: Molecular Mechanisms Controlling Deployment. *Trends Cell Biol.* **29**(5), pp.385-395.

Han, Y., Wang, B., Cho, Y.S., Zhu, J., Wu, J., Chen, Y. and Jiang, J. 2019. Phosphorylation of Ci/Gli by Fused Family Kinases Promotes Hedgehog Signaling. *Developmental Cell.* **50**(5), pp.610-626.e614.

Hanna, A. and Shevde, L.A. 2016. Hedgehog signaling: modulation of cancer properies and tumor mircroenvironment. *Mol Cancer.* **15**, p24.

Happ, J.T., Arveseth, C.D., Bruystens, J., Bertinetti, D., Nelson, I.B., Olivieri, C., Zhang, J., Hedeen, D.S., Zhu, J.F., Capener, J.L., Brockel, J.W., Vu, L., King,

C.C., Ruiz-Perez, V.L., Ge, X., Veglia, G., Herberg, F.W., Taylor, S.S. and Myers, B.R. 2022. A PKA inhibitor motif within SMOOTHENED controls Hedgehog signal transduction. *Nat Struct Mol Biol.* **29**(10), pp.990-999.

He, M., Subramanian, R., Bangs, F., Omelchenko, T., Liem, K.F., Jr., Kapoor, T.M. and Anderson, K.V. 2014. The kinesin-4 protein Kif7 regulates mammalian Hedgehog signalling by organizing the cilium tip compartment. *Nat Cell Biol.* **16**(7), pp.663-672.

Higgins, M., Obaidi, I. and McMorrow, T. 2019. Primary cilia and their role in cancer. *Oncol Lett.* **17**(3), pp.3041-3047.

Ho, E.K. and Stearns, T. 2021. Hedgehog signaling and the primary cilium: implications for spatial and temporal constraints on signaling. *Development.* **148**(9).

Hoey, D.A., Downs, M.E. and Jacobs, C.R. 2012. The mechanics of the primary cilium: an intricate structure with complex function. *J Biomech.* **45**(1), pp.17-26.

Holtz, A.M., Peterson, K.A., Nishi, Y., Morin, S., Song, J.Y., Charron, F., McMahon, A.P. and Allen, B.L. 2013. Essential role for ligand-dependent feedback antagonism of vertebrate hedgehog signaling by PTCH1, PTCH2 and HHIP1 during neural patterning. *Development.* **140**(16), pp.3423-3434.

Howard, M.J., 1998. Protein NMR spectroscopy. *Current biology*, *8*(10), pp.R331-R333.

Hu, Y., Cheng, K., He, L., Zhang, X., Jiang, B., Jiang, L., Li, C., Wang, G., Yang, Y. and Liu, M., 2021. NMR-based methods for protein analysis. *Analytical chemistry*, *93*(4), pp.1866-1879.

Huang, W.Y.C., Alvarez, S., Kondo, Y., Kuriyan, J. and Groves, J.T. 2021. Relating cellular signaling timescales to single-molecule kinetics: A first-passage time analysis of Ras activation by SOS. *Proc Natl Acad Sci U S A.* **118**(45).

Hui, C.C. and Angers, S. 2011. Gli proteins in development and disease. *Annu Rev Cell Dev Biol.* **27**, pp.513-537.

Humke, E.W., Dorn, K.V., Milenkovic, L., Scott, M.P. and Rohatgi, R. 2010. The output of Hedgehog signaling is controlled by the dynamic association between Suppressor of Fused and the Gli proteins. *Genes Dev.* **24**(7), pp.670-682.

Hwang, S.H., Somatilaka, B.N., White, K. and Mukhopadhyay, S. 2021. Ciliary and extraciliary Gpr161 pools repress hedgehog signaling in a tissue-specific manner. *Elife.* **10**.

Islam, M.A., Sooro, M.A. and Zhang, P. 2018. Autophagic Regulation of p62 is Critical for Cancer Therapy. *Int J Mol Sci.* **19**(5).

Itakura, E. and Mizushima, N. 2010. Characterization of autophagosome formation site by a hierarchical analysis of mammalian Atg proteins. *Autophagy.* **6**(6), pp.764-776.

Jacobs, D.M., Saxena, K., Vogtherr, M., Bernado, P., Pons, M. and Fiebig, K.M. 2003. Peptide binding induces large scale changes in inter-domain mobility in human Pin1. *J Biol Chem.* **278**(28), pp.26174-26182.

Jagannadham, M.V. and Nagaraj, R., 2008. Detecting the site of phosphorylation in phosphopeptides without loss of phosphate group using MALDI TOF mass spectrometry. *Analytical Chemistry Insights*, *3*, pp.ACI-S497.

Jenkins, D. 2009. Hedgehog signalling: emerging evidence for non-canonical pathways. *Cell Signal.* **21**(7), pp.1023-1034.

Jia, J., Amanai, K., Wang, G., Tang, J., Wang, B. and Jiang, J., 2002. Shaggy/GSK3 antagonizes Hedgehog signalling by regulating Cubitus interruptus. *Nature*, *416*(6880), pp.548-552.

Jiang, J. and Struhl, G. 1995. Protein Kinase A and Hedgehog Signaling in Drosophila Limb Development. *Cell.* **85**.

Johnson, G.L. and Lapadat, R. 2002. Mitogen-Activated Protein Kinase Pathways Mediated by ERK, JNK, and p38 Protein Kinases. *Science.* **298**.

Kahn, S.D. 2011. On the future of genomic data. *Science.* **331**(6018), pp.728-729.

Kawamura, S., Hervold, K., Ramirez-Weber, F.A. and Kornberg, T.B. 2008. Two patched protein subtypes and a conserved domain of group I proteins that regulates turnover. *J Biol Chem.* **283**(45), pp.30964-30969.

Kiesel, P., Alvarez Viar, G., Tsoy, N., Maraspini, R., Gorilak, P., Varga, V., Honigmann, A. and Pigino, G. 2020. The molecular structure of mammalian primary cilia revealed by cryo-electron tomography. *Nat Struct Mol Biol.* **27**(12), pp.1115-1124.

Kim, J., Hsia, E.Y., Brigui, A., Plessis, A., Beachy, P.A. and Zheng, X. 2015. The role of ciliary trafficking in Hedgehog receptor signaling. *Sci Signal.* **8**(379), pra55.

Kinnebrew, M., Luchetti, G., Sircar, R., Frigui, S., Viti, L.V., Naito, T., Beckert, F., Saheki, Y., Siebold, C., Radhakrishnan, A. and Rohatgi, R. 2021. Patched 1 reduces the accessibility of cholesterol in the outer leaflet of membranes. *Elife.* **10**.

Kiprilov, E.N., Awan, A., Desprat, R., Velho, M., Clement, C.A., Byskov, A.G., Andersen, C.Y., Satir, P., Bouhassira, E.E., Christensen, S.T. and Hirsch, R.E. 2008. Human embryonic stem cells in culture possess primary cilia with hedgehog signaling machinery. *J Cell Biol.* **180**(5), pp.897-904.

Kma, L. and Baruah, T.J. 2022. The interplay of ROS and the PI3K/Akt pathway in autophagy regulation. *Biotechnol Appl Biochem.* **69**(1), pp.248-264.

Komatsu, M., Kageyama, S. and Ichimura, Y. 2012. p62/SQSTM1/A170: physiology and pathology. *Pharmacol Res.* **66**(6), pp.457-462.

Kowatsch, C., Woolley, R.E., Kinnebrew, M., Rohatgi, R. and Siebold, C. 2019. Structures of vertebrate Patched and Smoothened reveal intimate links between cholesterol and Hedgehog signalling. *Curr Opin Struct Biol.* **57**, pp.204-214.

Kulkarni, P., Jolly, M.K., Jia, D., Mooney, S.M., Bhargava, A., Kagohara, L.T., Chen, Y., Hao, P., He, Y., Veltri, R.W., Grishaev, A., Weninger, K., Levine, H. and Orban, J. 2017. Phosphorylation-induced conformational dynamics in an intrinsically disordered protein and potential role in phenotypic heterogeneity. *Proc Natl Acad Sci U S A.* **114**(13), pp.E2644-E2653.

Kuwabara, P.E., Lee, M.H., Schedl, T. and Jefferis, G.S.X.E. 2000. A C. elegans patched gene, ptc-1, functions

in germ-line cytokinesis. *Genes and Development.* **14**.

Lake, D., Correa, S.A. and Muller, J. 2016. Negative feedback regulation of the ERK1/2 MAPK pathway. *Cell Mol Life Sci.* **73**(23), pp.4397-4413.

Lavoie, H., Gagnon, J. and Therrien, M. 2020. ERK signalling: a master regulator of cell behaviour, life and fate. *Nat Rev Mol Cell Biol.* **21**(10), pp.607-632.

Lee, Y., Miller, H.L., Russell, H.R., Boyd, K., Curran, T. and McKinnon, P.J. 2006. Patched2 modulates tumorigenesis in patched1 heterozygous mice. *Cancer Res.* **66**(14), pp.6964-6971.

Lee, Y.M. and Liou, Y.C. 2018. Gears-In-Motion: The Interplay of WW and PPIase Domains in Pin1. *Front Oncol.* **8**, p469.

Lenton, S., Grimaldo, M., Roosen-Runge, F., Schreiber, F., Nylander, T., Clegg, R., Holt, C., Hartlein, M., Garcia Sakai, V., Seydel, T. and Marujo Teixeira, S.C. 2017. Effect of Phosphorylation on a Human-like Osteopontin Peptide. *Biophys J.* **112**(8), pp.1586-1596.

Li, D., Jin, L., Alesi, G.N., Kim, Y.M., Fan, J., Seo, J.H., Wang, D., Tucker, M., Gu, T.L., Lee, B.H., Taunton, J., Magliocca, K.R., Chen, Z.G., Shin, D.M., Khuri, F.R. and Kang, S. 2013. The prometastatic ribosomal S6 kinase 2-cAMP response element-binding protein (RSK2-CREB) signaling pathway up-regulates the actin-binding protein fascin-1 to promote tumor metastasis. *J Biol Chem.* **288**(45), pp.32528-32538.

Li, J., Wang, C., Wu, C., Cao, T., Xu, G., Meng, Q. and Wang, B. 2017. PKA-mediated Gli2 and Gli3 phosphorylation is inhibited by Hedgehog signaling in cilia and reduced in Talpid3 mutant. *Dev Biol.* **429**(1), pp.147-157.

Li, Q., Chen, M., Liu, H., Yang, L., Yang, T., Yang, G. and He, G. 2014. The dual role of ERK signaling in the apoptosis of neurons. *Frontiers in Bioscience.* **19**.

Li, X., He, S. and Ma, B. 2020. Autophagy and autophagy-related proteins in cancer. *Mol Cancer.* **19**(1), p12.

Li, X., Wang, J., Coutavas, E., Shi, H., Hao, Q. and Blobel, G. 2016. Structure of human Niemann–Pick C1 protein. *Proceedings of the National Academy of Sciences.* **113**(29), pp.8212-8217.

Liao, G., Yao, Y., Liu, J., Yu, Z., Cheung, S., Xie, A., Liang, X. and Bi, X. 2007. Cholesterol accumulation is associated with lysosomal dysfunction and autophagic stress in Npc1 -/- mouse brain. *Am J Pathol.* **171**(3), pp.962-975.

Liem, K.F., Jr., He, M., Ocbina, P.J. and Anderson, K.V. 2009. Mouse Kif7/Costal2 is a cilia-associated protein that regulates Sonic hedgehog signaling. *Proc Natl Acad Sci U S A.* **106**(32), pp.13377-13382.

Lim, C.H., Sun, Q., Ratti, K., Lee, S.H., Zheng, Y., Takeo, M., Lee, W., Rabbani, P., Plikus, M.V., Cain, J.E., Wang, D.H., Watkins, D.N., Millar, S., Taketo, M.M., Myung, P., Cotsarelis, G. and Ito, M. 2018. Hedgehog stimulates hair follicle neogenesis by creating inductive dermis during murine skin wound healing. *Nat Commun.* **9**(1), p4903.

Linhares, N.D., Svartman, M., Salgado, M.I., Rodrigues, T.C., da Costa, S.S., Rosenberg, C. and Valadares, E.R. 2014. Dental developmental abnormalities in a patient with subtelomeric 7q36 deletion syndrome may confirm a novel role for the SHH gene. *Meta Gene.* **2**, pp.16-24.

Lo Muzio, L. 2008. Nevoid basal cell carcinoma syndrome (Gorlin syndrome). *Orphanet J Rare Dis.* **3**, p32.

Lu, K.P. 2003. Prolyl isomerase Pin1 as a molecular target for cancer diagnostics and therapeutics

. *Cancer Cell.* **4**.

Lu, K.P., Liou, Y.C. and Zhou, X.C. 2002. Pinning down proline-directed phosphorylation signaling. *Trends in Cell Biology.* **12**(4).

Lu, X., Liu, S. and Kornberg, T.B. 2006. The C-terminal tail of the Hedgehog receptor Patched regulates both localization and turnover. *Genes Dev.* **20**(18), pp.2539-2551.

Lu, Z. and Hunter, T. 2014. Prolyl isomerase Pin1 in cancer. *Cell Res.* **24**(9), pp.1033-1049.

Luchetti, G., Sircar, R., Kong, J.H., Nachtergaele, S., Sagner, A., Byrne, E.F., Covey, D.F., Siebold, C. and Rohatgi, R. 2016. Cholesterol activates the G-protein coupled receptor Smoothened to promote Hedgehog signaling. *Elife.* **5**.

Mahoney, B.J., Zhang, M., Zintsmaster, J.S. and Peng, J.W. 2018. Extended Impact of Pin1 Catalytic Loop Phosphorylation Revealed by S71E Phosphomimetic. *J Mol Biol.* **430**(5), pp.710-721.

Makino, S., Masuya, H., Ishijima, J., Yada, Y. and Shiroishi, T. 2001. A spontaneous mouse mutation, mesenchymal dysplasia (mes), is caused by a

deletion of the most C-terminal cytoplasmic domain of patched (ptc). *Dev Biol.* **239**(1), pp.95-106.

Marigo, V., Davey, R.A., Zuo, Y., Cunningham, J.M. and Tabin, C.J. 1996. Biochemical Evidence that Pacthed is the Hedgehog Receptor. *Nature.* **384**.

Marion, D., Driscoll, P.C., Kay, L.E., Wingfield, P.T., Bax, A., Gronenborn, A.M. and Clore, G.M., 1989. Overcoming the overlap problem in the assignment of proton NMR spectra of larger proteins by use of three-dimensional heteronuclear proton-nitrogen-15 Hartmann-Hahn-multiple quantum coherence and nuclear Overhauser-multiple quantum coherence spectroscopy: application to interleukin 1. beta. *Biochemistry*, *28*(15), pp.6150-6156.

Marion, D. 2013. An introduction to biological NMR spectroscopy. *Mol Cell Proteomics.* **12**(11), pp.3006-3025.

Martinez, M.F., Romano, M.V., Martinez, A.P., Gonzalez, A., Muchnik, C., Stengel, F.M., Mazzuoccolo, L.D. and Azurmendi, P.J. 2019. Nevoid Basal Cell Carcinoma Syndrome: PTCH1 Mutation Profile and Expression of Genes Involved in the Hedgehog Pathway in Argentinian Patients. *Cells.* **8**(2).

Mastrangelo, E. and Milani, M. 2018. Role and inhibition of GLI1 protein in cancer. *Lung Cancer (Auckl).* **9**, pp.35-43.

Matena, A., Rehic, E., Honig, D., Kamba, B. and Bayer, P. 2018. Structure and function of the human parvulins Pin1 and Par14/17. *Biol Chem.* **399**(2), pp.101-125.

Matsuura, I., Chiang, K.N., Lai, C.Y., He, D., Wang, G., Ramkumar, R., Uchida, T., Ryo, A., Lu, K. and Liu, F. 2010. Pin1 promotes transforming growth factor-beta-induced migration and invasion. *J Biol Chem.* **285**(3), pp.1754-1764.

McIntyre, P.J., Collins, P.M., Vrzal, L., Birchall, K., Arnold, L.H., Mpamhanga, C., Coombs, P.J., Burgess, S.G., Richards, M.W., Winter, A. and Veverka, V., 2017. Characterization of three druggable hot-spots in the Aurora-A/TPX2 interaction using biochemical, biophysical, and fragment-based approaches. *ACS chemical biology*, *12*(11), pp.2906-2914

McLachlin, D.T. and Chait, B.T., 2001. Analysis of phosphorylated proteins and peptides by mass spectrometry. *Current opinion in chemical biology*, *5*(5), pp.591-602.

Mehta, P., Singh, P., Gupta, N.J., Sankhwar, S.N., Chakravarty, B., Thangaraj, K. and Rajender, S. 2021. Mutations in the desert hedgehog (DHH) gene in the disorders of sexual differentiation and male infertility. *J Assist Reprod Genet.* **38**(7), pp.1871-1878.

Meirson, T., Bomze, D., Kahlon, L., Gil-Henn, H. and Samson, A.O. 2020. A helical lock and key model of polyproline II conformation with SH3. *Bioinformatics.* **36**(1), pp.154-159.

Mielke, S.P. and Krishnan, V.V., 2009. Characterization of protein secondary structure from NMR chemical shifts. *Progress in nuclear magnetic resonance spectroscopy*, *54*(3-4), pp.141-165.

Mizushima, N. 2010. The role of the Atg1/ULK1 complex in autophagy regulation. *Curr Opin Cell Biol.* **22**(2), pp.132-139.

Mizushima, N., Yoshimori, T. and Ohsumi, Y. 2011. The role of Atg proteins in autophagosome formation. *Annu Rev Cell Dev Biol.* **27**, pp.107-132.

Moon, H. and Ro, S.W. 2021. MAPK/ERK Signaling Pathway in Hepatocellular Carcinoma. *Cancers (Basel).* **13**(12).

Myers, B.R., Neahring, L., Zhang, Y., Roberts, K.J. and Beachy, P.A. 2017. Rapid, direct activity assays for Smoothened reveal Hedgehog pathway regulation by membrane cholesterol and extracellular sodium. *Proc Natl Acad Sci U S A.* **114**(52), pp.E11141-E11150.

Nakatsu, Y., Yamamotoya, T., Ueda, K., Ono, H., Inoue, M.K., Matsunaga, Y., Kushiyama, A., Sakoda, H., Fujishiro, M., Matsubara, A. and Asano, T. 2020. Prolyl isomerase Pin1 in metabolic reprogramming of cancer cells. *Cancer Lett.* **470**, pp.106-114.

Narwani, T.J., Santuz, H., Shinada, N., Melarkode Vattekatte, A., Ghouzam, Y., Srinivasan, N., Gelly, J.C. and de Brevern, A.G. 2017. Recent advances on polyproline II. *Amino Acids.* **49**(4), pp.705-713.

Newcombe, E.A., Delaforge, E., Hartmann-Petersen, R., Skriver, K. and Kragelund, B.B. 2022. How phosphorylation impacts intrinsically disordered proteins and their function. *Essays Biochem.* **66**(7), pp.901-913.

Nieuwenhuis, E., Barnfield, P.C., Makino, S. and Hui, C.C. 2007. Epidermal hyperplasia and expansion of the interfollicular stem cell compartment in mutant mice with a C-terminal truncation of Patched1. *Dev Biol.* **308**(2), pp.547-560.

Nieuwenhuis, E., Motoyama, J., Barnfield, P.C., Yoshikawa, Y., Zhang, X., Mo, R., Crackower, M.A. and Hui, C.C. 2006. Mice with a targeted mutation of patched2 are viable but develop alopecia and epidermal hyperplasia. *Mol Cell Biol.* **26**(17), pp.6609-6622.

Niewiadomski, P., Kong, J.H., Ahrends, R., Ma, Y., Humke, E.W., Khan, S., Teruel, M.N., Novitch, B.G. and Rohatgi, R. 2014. Gli protein activity is controlled by multisite phosphorylation in vertebrate Hedgehog signaling. *Cell Rep.* **6**(1), pp.168-181.

O'Connell, M.R., Gamsjaeger, R. and Mackay, J.P. 2009. The structural analysis of protein-protein interactions by NMR spectroscopy. *Proteomics.* **9**(23), pp.5224-5232.

Oberoi, J., Richards, M.W., Crumpler, S., Brown, N., Blagg, J. and Bayliss, R., 2010. Structural basis of poly (ADP-ribose) recognition by the multizinc binding domain of checkpoint with forkhead-associated and RING Domains (CHFR). *Journal of Biological Chemistry*, *285*(50), pp.39348-39358.

Ochoa, D., Jarnuczak, A.F., Vieitez, C., Gehre, M., Soucheray, M., Mateus, A., Kleefeldt, A.A., Hill, A., Garcia-Alonso, L., Stein, F., Krogan, N.J., Savitski, M.M., Swaney, D.L., Vizcaino, J.A., Noh, K.M. and Beltrao, P. 2020. The functional landscape of the human phosphoproteome. *Nat Biotechnol.* **38**(3), pp.365-373.

Pan, Y., Bai, C.B., Joyner, A.L. and Wang, B. 2006. Sonic hedgehog Signaling Regulates Gli2 Transcriptional Activity by Suppressing Its Processing and Degradation. *Molecular and Cellular Biology.* **26**(9), pp.3365-3377.

Pasca di Magliano, M. and Hebrok, M. 2003. Hedgehog signalling in cancer formation and maintenance. *Nat Rev Cancer.* **3**(12), pp.903-911.

Pearse, R. V., Vogan, K.J. and Tabin, C.J. 2001. Ptc1 and Ptc2 transcripts provide distinct readouts of Hedgehog signaling activity during chick embryogenesis. *Developmental Biology*. **239**(1), pp.15–29.

Pearson, W.R. (2014). BLAST and FASTA Similarity Searching for Multiple Sequence Alignment. In: Russell, D. (eds) Multiple Sequence Alignment Methods. Methods in Molecular Biology, vol 1079. Humana Press, Totowa, NJ. https://doi.org/10.1007/978-1-62703-646-7_5

Peart, J.R., Lu, R., Sadanandom, A., Malcuit, I., Moffett, P., Brice, D.C., Schauser, L., Jaggard, D.A., Xiao, S., Coleman, M.J., Dow, M., Jones, J.D., Shirasu, K. and Baulcombe, D.C. 2002. Ubiquitin ligase-associated protein SGT1 is required for host and nonhost disease resistance in plants. *Proc Natl Acad Sci U S A.* **99**(16), pp.10865-10869.

Pedersen, L.B., Mogensen, J.B. and Christensen, S.T. 2016. Endocytic Control of Cellular Signaling at the Primary Cilium. *Trends Biochem Sci.* **41**(9), pp.784-797.

Petrov, K., de Almeida Magalhaes, T. and Salic, A. 2021. Mechanism and ultrasensitivity in Hedgehog signaling revealed by Patched1 disease mutations. *Proc Natl Acad Sci U S A.* **118**(6).

Pfeffer, S.R. 2019. NPC intracellular cholesterol transporter 1 (NPC1)-mediated cholesterol export from lysosomes. *J Biol Chem.* **294**(5), pp.1706-1709.

Pietrobono, S., Gagliardi, S. and Stecca, B. 2019. Non-canonical Hedgehog Signaling Pathway in Cancer: Activation of GLI Transcription Factors Beyond Smoothened. *Front Genet.* **10**, p556.

Plotnikova, O.V., Pugacheva, E.N. and Golemis, E.A. 2009. Primary cilia and the cell cycle. *Methods Cell Biol.* **94**, pp.137-160.

Porter, J.A., Young, K.E. and Beachy, P.A. 1996. Cholesterol Modification of Hedgehog Signaling Proteins in Animal Development. *Science.* **274**.

Qi, C., Di Minin, G., Vercellino, I., Wutz, A. and Khorkov, V.M. 2019. Structural basis of sterol recognition by human hedgehog receptor PTCH1. *Sci Adv.* **5**.

Qi, X., Schmiege, P., Coutavas, E., Wang, J. and Li, X. 2018. Structures of human Patched and its complex with native palmitoylated sonic hedgehog. *Nature.* **560**(7716), pp.128-132.

Qian, H., Cao, P., Hu, M., Gao, S., Yan, N. and Gong, X. 2019. Inhibition of tetrameric Patched1 by Sonic Hedgehog through an asymmetric paradigm. *Nat Commun.* **10**(1), p2320.

Qin, H., Diener, D.R., Geimer, S., Cole, D.G. and Rosenbaum, J.L. 2004. Intraflagellar transport (IFT) cargo. *The Journal of Cell Biology.* **164**(2), pp.255-266.

Qu, J., Yu, F., Hong, Y., Guo, Y., Sun, L., Li, X., Zhang, J., Zhang, H., Shi, R., Chen, F. and Li, T. 2015. Underestimated PTCH1 mutation rate in sporadic keratocystic odontogenic tumors. *Oral Oncol.* **51**(1), pp.40-45.

Radhakrishnan, A., Rohatgi, R. and Siebold, C. 2020. Cholesterol access in cellular membranes controls Hedgehog signaling. *Nat Chem Biol.* **16**(12), pp.1303-1313.

Raffel, C., Jenkins, R.B., Frederick, L., Hebrink, D., Aldrete, B., Fults, D.W. and James, C.D. 1997. Sporadic Medulloblastomas Contain PTCH Mutations. *Cancer Research.* **57**.

Ramaswamy, B., Lu, Y., Teng, K.Y., Nuovo, G., Li, X., Shapiro, C.L. and Majumder, S. 2012. Hedgehog signaling is a novel therapeutic target in

tamoxifen-resistant breast cancer aberrantly activated by PI3K/AKT pathway. *Cancer Res.* **72**(19), pp.5048-5059.

Ramsbottom, S.A. and Pownall, M.E. 2016. Regulation of Hedgehog Signalling Inside and Outside the Cell. *J Dev Biol.* **4**(3), p23.

Reggiori, F. and Tooze, S.A. 2012. Autophagy regulation through Atg9 traffic. *J Cell Biol.* **198**(2), pp.151-153.

Rezaei-Ghaleh, N., Blackledge, M. and Zweckstetter, M. 2012. Intrinsically disordered proteins: from sequence and conformational properties toward drug discovery. *Chembiochem.* **13**(7), pp.930-950.

Ribeiro, I., Marcão, A., Amaral, O., Sá Miranda, M., Vanier, M.T. and Millat, G. 2001. Niemann-Pick type C disease: NPC1 mutations associated with severe and mild cellular cholesterol trafficking alterations. *Human Genetics.* **109**(1), pp.24-32.

Riobo, N.A., Lu, K., Ai, X., Haines, G.M. and Emerson, C.P., Jr. 2006. Phosphoinositide 3-kinase and Akt are essential for Sonic Hedgehog signaling. *Proc Natl Acad Sci U S A.* **103**(12), pp.4505-4510.

Riobo-Del Galdo, N.A., Lara Montero, A. and Wertheimer, E.V. 2019. Role of Hedgehog Signaling in Breast Cancer: Pathogenesis and Therapeutics. *Cells.* **8**(4).

Roldós, V., Cañada, F.J. and Jiménez-Barbero, J., 2011. Carbohydrate–protein interactions: a 3D view by NMR. *ChemBioChem*, *12*(7), pp.990-1005.

Roskoski Jr, R., 2010. RAF protein-serine/threonine kinases: structure and regulation. *Biochemical and biophysical research communications*, *399*(3), pp.313-317

Rost, B. 1999. Twilight zone of protein sequence alignments. *Protein Engineering.* **12**(2), pp.85-94.

Roux, K.J., Kim, D.I., Burke, B. and May, D.G., 2018. BioID: a screen for protein-protein interactions. *Current protocols in protein science*, *91*(1), pp.19-23.

Roux, P.P., Shahbazian, D., Vu, H., Holz, M.K., Cohen, M.S., Taunton, J., Sonenberg, N. and Blenis, J. 2007. RAS/ERK signaling promotes site-specific ribosomal protein S6 phosphorylation via RSK and stimulates cap-dependent translation. *J Biol Chem.* **282**(19), pp.14056-14064.

Rozengurt, E. 2011. Protein kinase D signaling: multiple biological functions in health and disease. *Physiology (Bethesda).* **26**(1), pp.23-33.

Rubin, L.L. and de Sauvage, F.J. 2006. Targeting the Hedgehog pathway in cancer. *Nat Rev Drug Discov.* **5**(12), pp.1026-1033.

Rudolf, A.F., Kinnebrew, M., Kowatsch, C., Ansell, T.B., El Omari, K., Bishop, B., Pardon, E., Schwab, R.A., Malinauskas, T., Qian, M., Duman, R., Covey, D.F., Steyaert, J., Wagner, A., Sansom, M.S.P., Rohatgi, R. and Siebold, C. 2019. The

morphogen Sonic hedgehog inhibits its receptor Patched by a pincer grasp mechanism. *Nat Chem Biol.* **15**(10), pp.975-982.

Sabol, M., Trnski, D., Musani, V., Ozretic, P. and Levanat, S. 2018. Role of GLI Transcription Factors in Pathogenesis and Their Potential as New Therapeutic Targets. *Int J Mol Sci.* **19**(9).

Sahu, D., Bastidas, M. and Showalter, S.A. 2014. Generating NMR chemical shift assignments of intrinsically disordered proteins using carbon-detected NMR methods. *Anal Biochem.* **449**, pp.17-25.

Saito, T., Mitomi, H., Imamhasan, A., Hayashi, T., Kurisaki-Arakawa, A., Mitani, K., Takahashi, M., Kajiyama, Y. and Yao, T. 2015. PTCH1 mutation is a frequent event in oesophageal basaloid squamous cell carcinoma. *Mutagenesis.* **30**(2), pp.297-301.

Samatar, A.A. and Poulikakos, P.I. 2014. Targeting RAS-ERK signalling in cancer: promises and challenges. *Nat Rev Drug Discov.* **13**(12), pp.928-942.

Sánchez, C., Tompa, P., Szücs, K., Friedrich, P. and Avila, J. (1996), Phosphorylation and Dephosphorylation in the Proline-Rich C-Terminal Domain of Microtubule-Associated Protein 2. European Journal of Biochemistry, 241: 765-771.

Schnoes, A.M., Brown, S.D., Dodevski, I. and Babbitt, P.C. 2009. Annotation error in public databases: misannotation of molecular function in enzyme superfamilies. *PLoS Comput Biol.* **5**(12), pe1000605.

Selenko, P., Frueh, D.P., Elsaesser, S.J., Haas, W., Gygi, S.P. and Wagner, G., 2008. In situ observation of protein phosphorylation by high-resolution NMR spectroscopy. *Nature structural & molecular biology*, *15*(3), pp.321-329.

Shin, K., Lee, J., Guo, N., Kim, J., Lim, A., Qu, L., Mysorekar, I.U. and Beachy, P.A. 2011. Hedgehog/Wnt feedback supports regenerative proliferation of epithelial stem cells in bladder. *Nature.* **472**(7341), pp.110-114.

Shiromizu, T., Adachi, J., Watanabe, S., Murakami, T., Kuga, T., Muraoka, S. and Tomonaga, T. 2013. Identification of missing proteins in the neXtProt database and unregistered phosphopeptides in the PhosphoSitePlus database as part of the Chromosome-centric Human Proteome Project. *J Proteome Res.* **12**(6), pp.2414-2421.

Singh, B.N., Koyano-Nakagawa, N., Donaldson, A., Weaver, C.V., Garry, M.G. and Garry, D.J., 2015. Hedgehog signaling during appendage development and regeneration. *Genes*, *6*(2), pp.417-435

Skoda, A.M., Simovic, D., Karin, V., Kardum, V., Vranic, S. and Serman, L. 2018. The role of the Hedgehog signaling pathway in cancer: A comprehensive review. *Bosn J Basic Med Sci.* **18**(1), pp.8-20.

Sorrentino, G., Comel, A., Mantovani, F. and Del Sal, G. 2014. Regulation of mitochondrial apoptosis by Pin1 in cancer and neurodegeneration. *Mitochondrion.* **19 Pt A**, pp.88-96.

Spadari, F., Pulicari, F., Pellegrini, M., Scribante, A. and Garagiola, U. 2022. Multidisciplinary approach to Gorlin-Goltz syndrome: from diagnosis to surgical treatment of jawbones. *Maxillofac Plast Reconstr Surg.* **44**(1), p25.

Stewart, D.P., Marada, S., Bodeen, W.J., Truong, A., Sakurada, S.M., Pandit, T., Pruett-Miller, S.M. and Ogden, S.K. 2018. Cleavage activates dispatched for Sonic Hedgehog ligand release. *Elife.* **7**.

Suizu, F., Ryo, A., Wulf, G., Lim, J. and Lu, K.P. 2006. Pin1 regulates centrosome duplication, and its overexpression induces centrosome amplification, chromosome instability, and oncogenesis. *Mol Cell Biol.* **26**(4), pp.1463-1479.

Szczepny, A., Rogers, S., Jayasekara, W.S.N., Park, K., McCloy, R.A., Cochrane, C.R., Ganju, V., Cooper, W.A., Sage, J., Peacock, C.D., Cain, J.E., Burgess, A. and Watkins, D.N. 2017. The role of canonical and non-canonical Hedgehog signaling in tumor progression in a mouse model of small cell lung cancer. *Oncogene.* **36**(39), pp.5544-5550.

Tan, X., Zhou, F., Wan, J., Hang, J., Chen, Z., Li, B., Zhang, C., Shao, K., Jiang, P., Shi, S., Feng, X., Lv, N., Wang, Z., Ling, Y., Zhao, X., Ding, D., Sun, J., Xiong, M. and He, J. 2010. Pin1 expression contributes to lung cancer: Prognosis and carcinogenesis. *Cancer Biol Ther.* **9**(2), pp.111-119.

Tang, J.Y., Aszterbaum, M., Athar, M., Barsanti, F., Cappola, C., Estevez, N., Hebert, J., Hwang, J., Khaimskiy, Y., Kim, A., Lu, Y., So, P.L., Tang, X., Kohn, M.A., McCulloch, C.E., Kopelovich, L., Bickers, D.R. and Epstein, E.H., Jr. 2010.

Basal cell carcinoma chemoprevention with nonsteroidal anti-inflammatory drugs in genetically predisposed PTCH1+/- humans and mice. *Cancer Prev Res (Phila).* **3**(1), pp.25-34.

Tanimura, S. and Takeda, K. 2017. ERK signalling as a regulator of cell motility. *J Biochem.* **162**(3), pp.145-154.

Tempé, D., Casas, M., Karaz, S., Blanchet-Tournier, M.-F. and Concordet, J.-P. 2006. Multisite Protein Kinase A and Glycogen Synthase Kinase 3β Phosphorylation Leads to Gli3 Ubiquitination by SCFβTrCP. *Molecular and Cellular Biology.* **26**(11), pp.4316-4326.

Timmis, A.J. 2021. *Structure-function relationship of the Patched family of proteins*. Doctor of Philosophy thesis, University of Leeds.

Timmis, A.J., Cross, F., Gkotsi, D.S., Ollerton, H., Johnson, C.A. and Galdo, N.A.R.-D. 2023.

Tukachinsky, H., Petrov, K., Watanabe, M. and Salic, A. 2016. Mechanism of inhibition of the tumor suppressor Patched by Sonic Hedgehog. *Proc Natl Acad Sci U S A.* **113**(40), pp.E5866-E5875.

Ullah, R., Yin, Q., Snell, A.H. and Wan, L. 2022. RAF-MEK-ERK pathway in cancer evolution and treatment. *Semin Cancer Biol.* **85**, pp.123-154.

van Geuns, R.J.M., Wielopolski, P.A., de Bruin, H.G., Rensing, B.J., van Ooijen, P.M.A., Hulshoff, M., Oudkerk, M. and de Feyter, P.J. 1999. Basic

Principles of Magnetic Resonance Imaging. *Progress in Cardiovascular Diseases.* **42**(2).

Vranken, W.F., Boucher, W., Stevens, T.J., Fogh, R.H., Pajon, A., Llinas, M., Ulrich, E.L., Markley, J.L., Ionides, J. and Laue, E.D. 2005. The CCPN data model for NMR spectroscopy: development of a software pipeline. *Proteins.* **59**(4), pp.687-696.

Wang, C.Y., Chang, Y.C., Kuo, Y.L., Lee, K.T., Chen, P.S., Cheung, C.H.A., Chang, C.P., Phan, N.N., Shen, M.R. and Hsu, H.P. 2019. Mutation of the PTCH1 gene predicts recurrence of breast cancer. *Sci Rep.* **9**(1), p16359.

Wang, L., Klionsky, D.J. and Shen, H.M. 2023. The emerging mechanisms and functions of microautophagy. *Nat Rev Mol Cell Biol.* **24**(3), pp.186-203.

Wang, W., Jack, B.M., Wang, H.H., Kavanaugh, M.A., Maser, R.L. and Tran, P.V. 2021. Intraflagellar Transport Proteins as Regulators of Primary Cilia Length. *Front Cell Dev Biol.* **9**, p661350.

Wei, R., Lv, M., Li, F., Cheng, T., Zhang, Z., Jiang, G., Zhou, Y., Gao, R., Wei, X., Lou, J. and Wu, X., 2017. Human CAFs promote lymphangiogenesis in ovarian cancer via the Hh-VEGF-C signaling axis. *Oncotarget*, *8*(40), p.67315.

Wheway, G., Nazlamova, L. and Hancock, J.T. 2018. Signaling through the Primary Cilium. *Front Cell Dev Biol.* **6**, p8.

Wicking, C., Shanley, S., Smyth, I., Gillies, S., Negus, K., Graham, S., Suthers, G., Haites, N., Edwards, M., Wainwright, B. and Chenevix-Trench, G. 1997. *Most Germ-Line Mutations in the Nevoid Basal Cell Carcinoma Syndrome Lead to a Premature Termination of the PATCHED Protein, and No Genotype-Phenotype Correlations Are Evident*

Wintjens, R., Wieruszeski, J.M., Drobecq, H., Rousselot-Pailley, P., Buee, L., Lippens, G. and Landrieu, I. 2001. 1H NMR study on the binding of Pin1 Trp-Trp domain with phosphothreonine peptides. *J Biol Chem.* **276**(27), pp.25150-25156.

Wishart, D.S. and Sykes, B.D. 1993. The 13C Chemical-Shift Index: A simple method for the identification of protein secondary structure using 13C chemical-shift data. *Journal of Biomolecular NMR.*

Wu, M., Li, Y., Chang, Q., Zhao, X., Chen, Q. 2018. Total synthesis and modification of proline-rich cyclopeptides Phakellistatins 17 and 18 isolated from marine sponge, *Tetrahedron Letters*,**59**, (45), pp. 4011-4014

Wu, X., Yan, R., Cao, P., Qian, H. and Yan, N. 2022. Structural advances in sterol-sensing domain-containing proteins. *Trends Biochem Sci.* **47**(4), pp.289-300.

Xia, T., Zhang, H., Zhang, L., Yang, X., Sun, G., Chen, J., Xu, D. and Zhao, C. 2019. Comparative and evolutionary analysis of the reptilian hedgehog gene family (Shh, Dhh, and Ihh). *PeerJ.* **7**, pe7613.

Ren, X.D. and Schwartz, M.A., 2000. Determination of GTP loading on Rho. In *Methods in enzymology* (Vol. 325, pp. 264-272). Academic Press.

Xu, Y.X., Hirose, Y., Zhou, X.Z., Lu, K.P. and Manley, J.L. 2003. Pin1 modulates the structure and function of human RNA polymerase II. *Genes Dev.* **17**(22), pp.2765-2776.

Yadav, S.S. and Miller, W.T. 2007. Cooperative activation of Src family kinases by SH3 and SH2 ligands. *Cancer Lett.* **257**(1).

Yang, C., Qi, Y. and Sun, Z. 2021. The Role of Sonic Hedgehog Pathway in the Development of the Central Nervous System and Aging-Related Neurodegenerative Diseases. *Front Mol Biosci.* **8**, p711710.

Yang, J., Andre, P., Ye, L. and Yang, Y.Z. 2015. The Hedgehog signalling pathway in bone formation. *Int J Oral Sci.* **7**(2), pp.73-79.

Yeh, E.S. and Means, A.R. 2007. PIN1, the cell cycle and cancer. *Nat Rev Cancer.* **7**(5), pp.381-388.

Ying, J., Delaglio, F., Torchia, D.A. and Bax, A. 2017. Sparse multidimensional iterative lineshape-enhanced (SMILE) reconstruction of both non-uniformly sampled and conventional NMR data. *J Biomol NMR.* **68**(2), pp.101-118.

Yu, F.Y., Hong, Y.Y., Qu, J.F., Chen, F. and Li, T.J. 2014. The large intracellular loop of ptch1 mediates the non-canonical Hedgehog pathway

through cyclin B1 in nevoid basal cell carcinoma syndrome. *Int J Mol Med.* **34**(2), pp.507-512.

Yu, J.H., Im, C.Y. and Min, S.H. 2020. Function of PIN1 in Cancer Development and Its Inhibitors as Cancer Therapeutics. *Front Cell Dev Biol.* **8**, p120.

Yue, S., Tang, L.Y., Tang, Y., Tang, Y., Shen, Q.H., Ding, J., Chen, Y., Zhang, Z., Yu, T.T., Zhang, Y.E. and Cheng, S.Y. 2014. Requirement of Smurf-mediated endocytosis of Patched1 in sonic hedgehog signal reception. *Elife.* **3**.

Yuksel-Apak, M., Bogershausen, N., Pawlik, B., Li, Y., Apak, S., Uyguner, O., Milz, E., Nurnberg, G., Karaman, B., Gulgoren, A., Grzeschik, K.H., Nurnberg, P., Kayserili, H. and Wollnik, B. 2012. A large duplication involving the IHH locus mimics acrocallosal syndrome. *Eur J Hum Genet.* **20**(6), pp.639-644.

Zamora-Olivares, D., Kaoud, T.S., Zeng, L., Pridgen, J.R., Zhuang, D.L., Ekpo, Y.E., Nye, J.R., Telles, M., Anslyn, E.V. and Dalby, K.N., 2019. Quantification of ERK kinase activity in biological samples using differential sensing. *ACS chemical biology*, *15*(1), pp.83-92.

Zarrinpar, A., Bhattacharyya, R.P. and Lim, W.A. 2003. The Structure and Function of Proline Recognition Domains. *Science.* **2003**(179).

Zhang, T., Chen, M., Lu, Y., Xing, Q. and Chen, W. 2011. A novel mutation of the PTCH1 gene activates the Shh/Gli signaling pathway in a Chinese family

with nevoid basal cell carcinoma syndrome. *Biochem Biophys Res Commun.* **409**(2), pp.166-170.

Zhang, Y. and Beachy, P.A. 2023. Cellular and molecular mechanisms of Hedgehog signalling. *Nat Rev Mol Cell Biol.*

Zhang, Y., Bulkley, D.P., Xin, Y., Roberts, K.J., Asarnow, D.E., Sharma, A., Myers, B.R., Cho, W., Cheng, Y. and Beachy, P.A. 2018. Structural Basis for Cholesterol Transport-like Activity of the Hedgehog Receptor Patched. *Cell.* **175**(5), pp.1352-1364 e1314.

Zhao, C., Chen, A., Jamieson, C.H., Fereshteh, M., Abrahamsson, A., Blum, J., Kwon, H.Y., Kim, J., Chute, J.P., Rizzieri, D., Munchhof, M., VanArsdale, T., Beachy, P.A. and Reya, T. 2009. Hedgehog signalling is essential for maintenance of cancer stem cells in myeloid leukaemia. *Nature.* **458**(7239), pp.776-779.

Zhao, X., Zhu, W., Zhang, R., Zhang, M., Zhao, J., Hou, J. and Zhang, W., 2019. Targeted juglone blocks the invasion and metastasis of HPV-positive cervical cancer cells. *Journal of Pharmacological Sciences*, *140*(3), pp.211-217.

Zhong, C. and Wang, B. 2022. Regulation of Cholesterol Binding to the Receptor Patched1 by its interactions With the Ligand Sonic Hedgehog (Shh). *Front Mol Biosci.* **9**, p831891.

Zhou, J., Zhang, G., Shi, M., Liu, Z., Xiao, M., Fu, S., Gong, X. and Shi, X. 2019. A novel splicing mutation of PTCH1 in a Chinese family with nevoid basal cell carcinoma syndrome. *Med Mol Morphol.* **52**(4), pp.235-237.

Zhulyn, O., Nieuwenhuis, E., Liu, Y.C., Angers, S. and Hui, C.C. 2015. Ptch2 shares overlapping functions with Ptch1 in Smo regulation and limb development. *Dev Biol.* **397**(2), pp.191-202.